WHOI-2014-03

Woods Hole Oceanographic Institution

Ocean Bottom Seismometer Augmentation in the North Pacific (OBSANP) - Cruise Report

by

Stephen, R.A*., Worcester, P.F.**, Udovydchenkov, I.A.*, Aaron, E.**, Bolmer, S.T.*, Carey, S**., McPeak, S.P.***, Swift, S.A.*, and Dzieciuch, M.A.**

*Woods Hole Oceanographic Institution
Woods Hole, MA 02543
**Scripps Institution of Oceanography
San Diego, CA 92152
***Applied Physics Laboratory
University of Washington, Seattle, WA 98105

December 2014

Technical Report

Funding was provided by the Office of Naval Research under contract #'s N00014-10-1-0987 and N00014-10-1-0510

WHOI-2014-03

Ocean Bottom Seismometer Augmentation in the North Pacific (OBSANP) - Cruise Report

by

Stephen, R.A., Worcester, P.F., Udovydchenkov, I.A., Aaron, E., Bolmer, S.T., Carey, S., McPeak, S.P., Swift, S.A., and Dzieciuch, M.A.

Woods Hole Oceanographic Institution
Woods Hole, Massachusetts 02543

December 2014

Technical Report

Funding was provided by the Office of Naval Research under contract #'s N00014-10-1-0987 and N00014-10-1-0510

Approved for public release; distribution unlimited.

Approved for Distribution:

Kelly J. Sewart for DMc

Dan McCorkle, Chair

Department of Geology and Geophysics

Ocean Bottom Seismometer Augmentation in the North Pacific (OBSANP) - Cruise Report

Stephen, R.A.*, Worcester, P.F., Udovydchenkov, I.A.*, Aaron, E.**, Bolmer, S.T.*, Carey, S.**, McPeak, S.P.***, Swift, S.A*, and Dzieciuch, M.A.****

Technical Report

*** Woods Hole Oceanographic Institution**
Woods Hole, MA. 02543

****Scripps Institution of Oceanography**
San Diego, CA. 92152

***** Applied Physics Laboratory**
University of Washington
Seattle, WA. 98105

Abstract

The Ocean Bottom Seismometer Augmentation in the North Pacific Experiment (OBSANP, June-July, 2013, R/V Melville) addresses the coherence and depth dependence of deep-water ambient noise and signals. During the 2004 NPAL Experiment in the North Pacific Ocean, in addition to predicted ocean acoustic arrivals and deep shadow zone arrivals, we observed "deep seafloor arrivals" (DSFA) that were dominant on the seafloor Ocean Bottom Seismometer (OBS) (at about 5000m depth) but were absent or very weak on the Distributed Vertical Line Array (DVLA) (above 4250m depth). At least a subset of these arrivals correspond to bottom-diffracted surface-reflected (BDSR) paths from an out-of-plane seamount. BDSR arrivals are present throughout the water column, but at depths above the conjugate depth are obscured by ambient noise and PE predicted arrivals. On the 2004 NPAL/LOAPEX experiment BDSR paths yielded the largest amplitude seafloor arrivals for ranges from 500 to 3200km. The OBSANP experiment tests the hypothesis that BDSR paths contribute to the arrival structure on the deep seafloor even at short ranges (from near zero to 4-1/2CZ). The OBSANP cruise had three major research goals: a) identification and analysis of DSFA and BDSR arrivals occurring at short (1/2CZ) ranges in the 50 to 400Hz band, b) analysis of deep sea ambient noise in the band 0.03 to 80Hz, and c) analysis of the frequency dependence of BR and SRBR paths. On OBSANP we deployed a 32 element VLA from 12 to 1000m above the seafloor, eight short-period OBSs and four long-period OBSs and carried out a 15day transmission program using a J15-3 acoustic source.

Cruise Synopsis

Cruise: R/V Melville MV1308

Departed: San Diego, CA, 0800L (1500Z) on June 12 (JD 163), 2013
Arrived: Seattle, WA, 1100L (1800Z) on July 11 (JD192), 2013

Science Party

Ernie Aaron	SIO	OBSIP Development Technician
Tom Bolmer	WHOI	Data Manager
Scott Carey	SIO	Hydrophone Module Development Technician
Mary Huey	SIO	Computer Technician
Sean McPeak	APL-UW	Senior Engineer
Matthew Norenberg	SIO	Senior Marine Mechanician
Jim Ryder	WHOI	Senior Engineering Assistant II
Keith Shadle	SIO	Resident Technician
Dr. Ralph Stephen	WHOI	Co-Principle Investigator
Dr. Stephen Swift	WHOI	Marine Geologist, OBSIP Technician
Dr. Ilya Udovydchenkov	WHOI	Guest Scientist
Dr. Peter Worcester (Chief Scientist)	SIO	Co-Principle Investigator

Science Objectives

1) Study the coherence and depth dependence of deep-water ambient noise and signals.
2) Study the relationship between seafloor pressure and seafloor particle motion for both ambient noise and short- and long-range signals.
3) Study the contribution of Deep Seafloor Arrivals (DSFAs) and Bottom-Diffracted Surface-Reflected (BDSR) paths of the arrival structure at receivers on the deep seafloor.

Itinerary

Load Ship	JD161-162	(10-11 June)
OBSANP cruise departed San Diego	JD163/1500Z	(12 June, 0800L)
Arrive at DVLA site	JD167/1745Z	(16 June, 1045L)
Deployed and surveyed DVLA and 12 OBSs	JD169/1330Z	(18 June, 0630L)
End the J15-3 transmission program	JD184/2345Z	(03 July, 1645L)
Recover 12 OBSs, the near-seafloor DVLA and four transponders	JD187/0200Z	(05 July, 1900L)
Depart DVLA site	JD187/1630Z	(06 July, 0930L)
Arrive Seattle	JD192/1800Z	(11 July, 1100L)
Offload Ship	JD193	(12 July)

Table of Contents

Index of Figures

Index of Tables

1 Introduction

The Ocean Bottom Seismometer Augmentation in the North Pacific Experiment (OBSANP, June 12 - July 11, 2013, San Diego - Seattle, R/V Melville, Figure 1.1) was the second of two cruises that studied the coherence and depth dependence of deep-water ambient noise and signals. Seafloor signals were studied in the band from 50-350Hz and seafloor ambient noise was studied in the band from 0.03-700Hz. The first cruise was the OBSAPS cruise in the Philippine Sea (Stephen *et al.*, 2011). Both cruises focused on elucidating the physics and characteristics of Deep Seafloor Arrivals (DSFA) and Bottom-Diffracted Surface-Reflected (BDSR) arrivals (Stephen *et al.*, 2009; Stephen *et al.*, 2013).

During the 2004 NPAL Experiment in the North Pacific Ocean, in addition to predicted ocean acoustic arrivals and deep shadow zone arrivals, we observed "deep seafloor arrivals" that were dominant on the seafloor Ocean Bottom Seismometer (OBS) (at about 5000m depth) but were absent or very weak on the Distributed Vertical Line Array (DVLA) (above 4250m depth). At least a subset of these arrivals correspond to bottom-diffracted surface-reflected (BDSR) paths from an out-of-plane seamount. BDSR arrivals are present throughout the water column, but at depths above the conjugate depth are obscured by ambient noise and PE predicted arrivals. On the 2004 NPAL/LOAPEX experiment BDSR paths yielded the largest amplitude seafloor arrivals for ranges from 500 to 3200km.

The OBSANP experiment tests the hypothesis that BDSR paths contribute to the arrival structure on the deep seafloor even at short ranges (from near zero to 4-1/2CZ). The OBSANP cruise had three major research goals: a) identification and analysis of DSFA and BDSR arrivals occurring at short (1/2CZ) ranges in the 50 to 400Hz band, b) analysis of deep sea ambient noise in the band 0.03 to 80Hz, and c) analysis of the frequency dependence of BR and SRBR paths. On OBSANP we deployed a 32 element VLA from 12 to 1000m above the seafloor, eight short-period OBSs and four long-period OBSs and carried out a 15day transmission program using a J15-3 acoustic source.

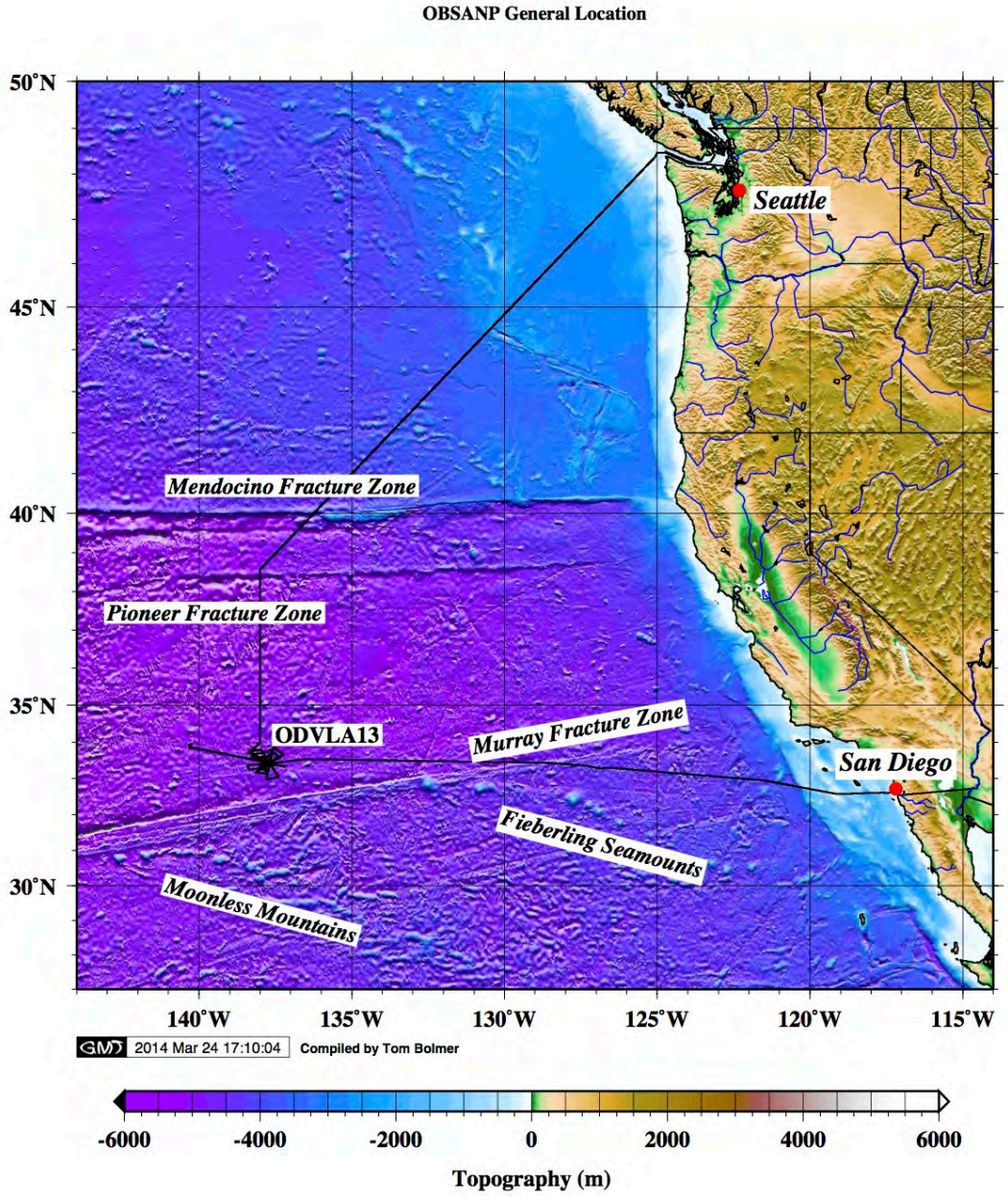

Figure 1.1: OBSANP Cruise Track

OBSANP was carried out at the same location as the NPAL04/LOAPEX receiver site. This shows the location of the OBSANP experiment. The black line shows the MV1308 cruise track. The experiment was conducted around the ODVLA13 site.

2 Scientific Objectives

On NPAL04 we observed a new class of arrivals in long-range ocean acoustic propagation that we call Deep Seafloor Arrivals (DSFAs) because they are the dominant arrivals on ocean bottom seismometers (Mercer *et al.*, 2009; Stephen *et al.*, 2009; Stephen *et al.*, 2008). They either were undetected or very weak on the deepest DVLA hydrophone located near the conjugate depth about 750m above the seafloor (Stephen *et al.*, 2011). It appears that at least some of the DSFAs corresponded to long-range guided wave energy that diffracted from a small seamount near the receivers and reflected back down from the sea surface (Stephen *et al.*, 2013). Part of the path for DSFAs is through or on the seafloor perhaps as an interface wave (`Figure 2.1`, `Figure 2.2`, and `Figure 2.3`). This work is relevant to the Navy because it seeks to quantify and understand the signal propagation and noise floors that are necessary to evaluate and exploit seismo-acoustics for operational ASW systems.

By returning to the NPAL04 site with more OBSs, a deep DVLA extending from the seafloor to 1000m above the seafloor, and a towable, controlled source (J15-3) we aimed to further define the characteristics of DSFAs, to understand the conditions under which they are excited and to understand how they propagate. The long-term objective here is to understand the relationship between seafloor pressure and seafloor particle motion for both ambient noise and short- and long-range signals. What is the relationship between the seismic (ground motion) noise on the seafloor and the acoustic noise in the water column?

In addition to studying DSFAs we acquired ambient noise data over a 21day period. Although it has been recognized for a long time that acoustic noise in the 0.1 to 30Hz band is a function of surface gravity wave conditions (McCreery *et al.*, 1993; Webb and Cox, 1986), recent studies indicate that seafloor ambient noise in deep water (~5,000m) in the 1-30Hz band carries significant information about even very short ocean surface waves (wavelengths from 6m to a centimeter) (Duennebier *et al.*, 2012; Farrell and Munk, 2008; 2010; 2013). Since our ship will be in the vicinity of the seafloor sensors during the whole recording period we will have direct observations of sea surface conditions to compare with the seafloor ambient noise data.

There are two specific goals of this project:
1) Quantitatively compare the signal and noise levels in the 50-350Hz band on the hydrophones and geophones at the seafloor to the hydrophones suspended up to 1 kilometer above the seafloor, for ranges from near zero to 250km. By comparing the particle velocity from the geophone to the pressure from the hydrophone we can infer the role of rigidity in the propagation process of both signals and noise. For a plane wave in a uniform acoustic medium the ratio of pressure to velocity is simply the acoustic impedance (density times phase velocity) (Jensen *et al.*, 1994). For interface waves at the seafloor, however, the relationship between pressure and particle velocity is more complicated and involves phase shifts depending on the type of interface waves (Rauch, 1980; Sutton and Barstow, 1990).
2) Study the characteristics of ambient noise in the 1-30Hz band at and just above the deep seafloor. Ambient noise in this band has been postulated by Farrell and Munk to be very sensitive to surface wind speed and surface gravity and capillary wave conditions. Much of their work has been based on seafloor measurements taken at the H2O observatory (Figure 2.2). We

will make similar measurements at the seafloor in a similar environment, but we will also have a DVLA to observe the near-seafloor depth dependence of the phenomena.

Specific questions to be addressed include:

1. Can we excite Deep Seafloor Arrivals from Seamount B (Figure 2.3) at short ranges and a variety of azimuths?
2. What is the frequency dependence of the deep arrival structure from 50-350Hz?
3. What is the range dependence of the deep arrival structure out to 250km?
4. What is the azimuth dependence of the deep arrival structure?
5. What are the relative SNRs of arrivals on vertical and horizontal geophones, co-located seafloor hydrophones and moored hydrophones (from 12m to 1000m off the bottom - 30 hydrophones at about 30m separation)?
6. What are the phase relationships between pressure and vertical and horizontal particle motion for deep seafloor arrivals and ambient noise?
7. What is the relationship between the observed deep arrival structure and the PE predicted arrival structure?
8. How far above the seafloor does the Deep Seafloor Arrival structure extend?
9. What is the depth dependence of ambient noise between the conjugate depth and the deep seafloor?

Before OBSANP the only definitive observation of DSFAs had been at the NPAL04 site. During the LOAPEX/NPAL04 experiment sources, centered near 68 and 75Hz, were deployed at two depths, 350m and 800m, and at seven ranges, 50km, 250km, 500km, 1000km, 1600km, 2300km and 3200km. All of the source stations were intentionally located along the same geodesic. Oddly DSFAs were only observed at 500km range and greater. The DSFAs were observed on the vertical channel of ocean bottom seismometers but were only weakly observed on the deepest hydrophone (750m above the seafloor) deployed in that experiment. We returned to the site to fill-in these gaps:

a) extend the frequency range to cover M-sequences from 77.5 to 310Hz,
b) include hydrophones and three component geophones on the seafloor and a DVLA extending from the seafloor to 1000m above the seafloor,
c) have continuous tows and station stops for a controlled source in the upper 100m
d) source tows would include radial lines at a variety of azimuths as well as arcs and circles around the receivers and around Seamount B.

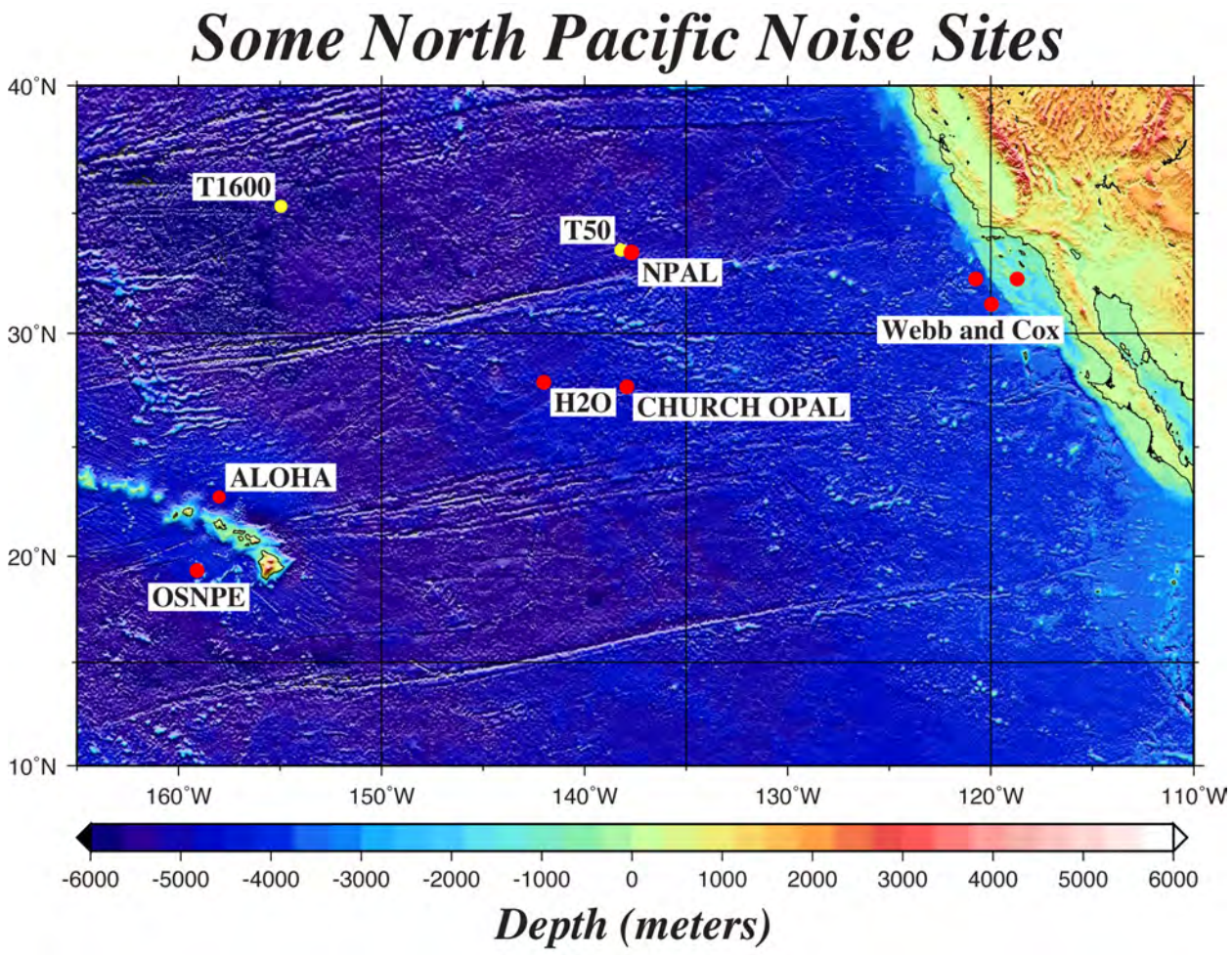

Figure 2.1: Ambient Noise Sites
Location diagram for some useful seafloor ambient noise studies in the Northeast Pacific.

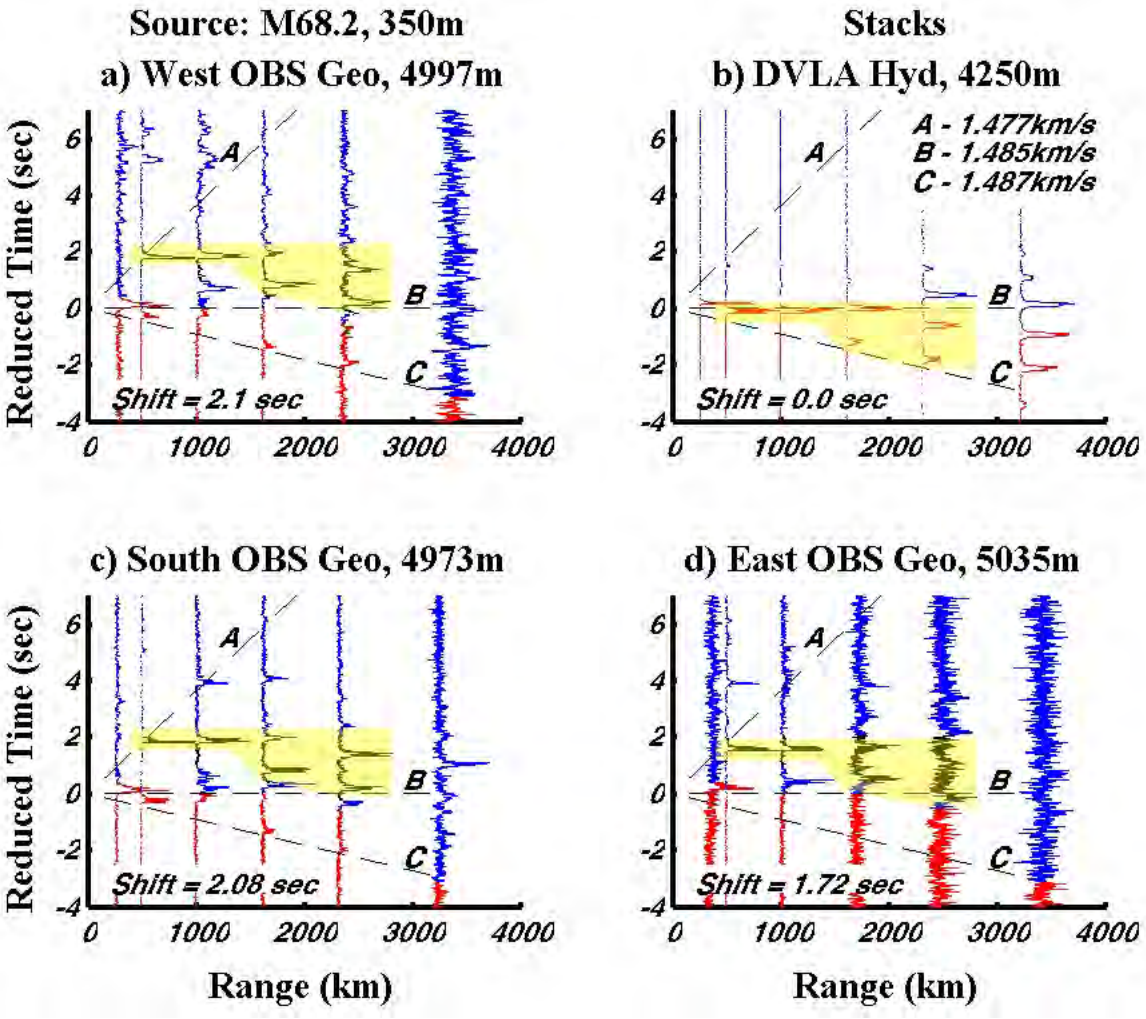

Figure 2.2: NPAL04 Seafloor Arrivals
The seafloor arrivals shown in the highlighted yellow regions have a distinctive pattern for all three OBSs deployed on NPAL04. The arrival pattern appears to be a delayed version, by about 2sec, of the pattern on the deepest element of the DVLA. The shifts of these arrivals with respect to the PE arrivals on the DVLA are a constant regardless of range. It is remarkable how robust and simple this pattern is. Deep seafloor arrivals are "not" random!

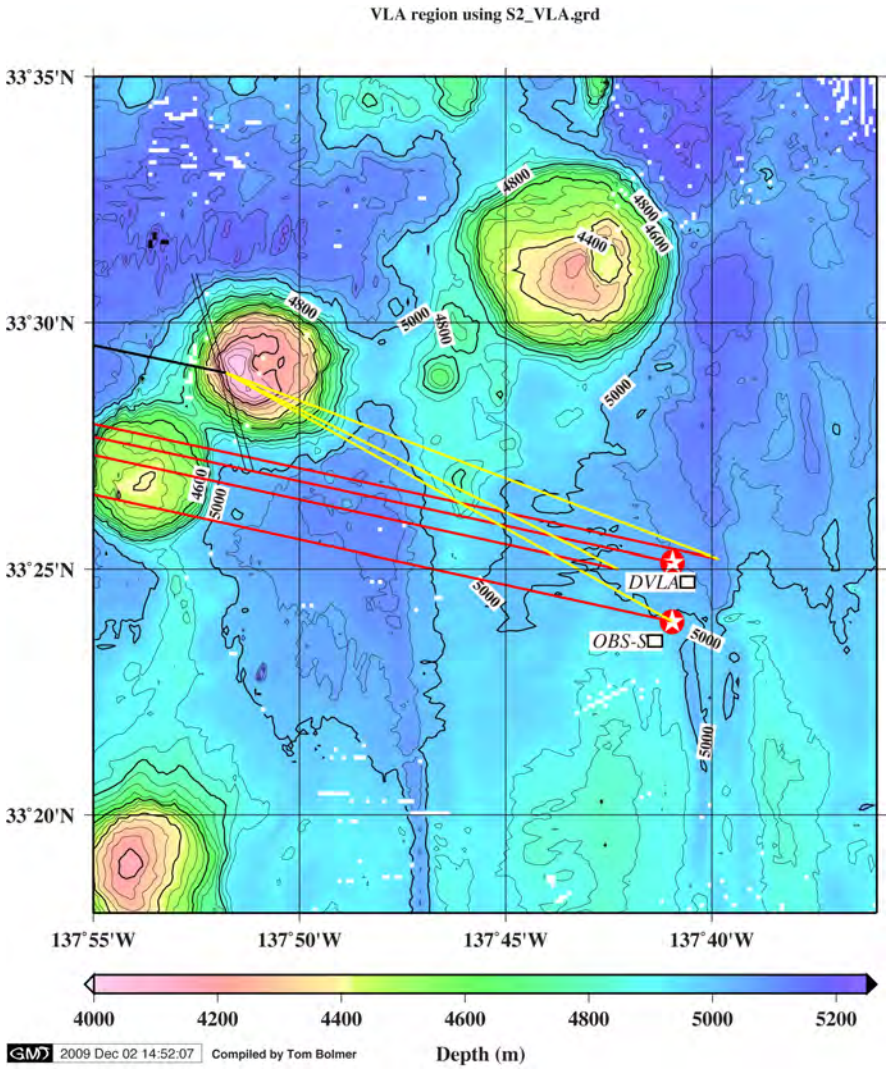

Figure 2.3: Deep Seafloor Arrival Pattern and Propagation Paths
The deep seafloor arrival pattern highlighted in yellow in Figure 2.2 is consistent with the following propagation path. From all sources from T500 toT2300 the sound travels through the sound channel to seamount B (black line). The sound is then coherently scattered (diffracted) from seamount B up to the sea surface and back down to the seafloor receivers (yellow lines). This would explain why the seafloor arrivals are not observed on the DVLA.

3 Technical Approach

During OBSANP, we returned to the Deep VLA site (Figure 1.1 and Figure 2.1, Lat: 33° 25.135'N, Lon: 137° 40.948'W, Depth - multi-beam: 5045m) with a near-seafloor Distributed Vertical Line Array (DVLA) receiver that extended upward 1000 m from the seafloor and 12 OBSs (eight short period and four long period) (Figure 3.1 and Figure 3.2). Once the instruments were installed, we transmitted to them from 18 June through 3 July with a J15-3 acoustic source suspended from shipboard.

In addition to studying DSFAs, ambient noise data were acquired. Ultra-Low-Noise hydrophones developed by SAIC (ULN-SAIC) were integrated into two of the long-period OBSs.

All instruments (OBSs, DVLA, and the acoustic transponders used to measure the motion of the near-seafloor DVLA mooring) were successfully recovered prior to the end of the OBSANP cruise.

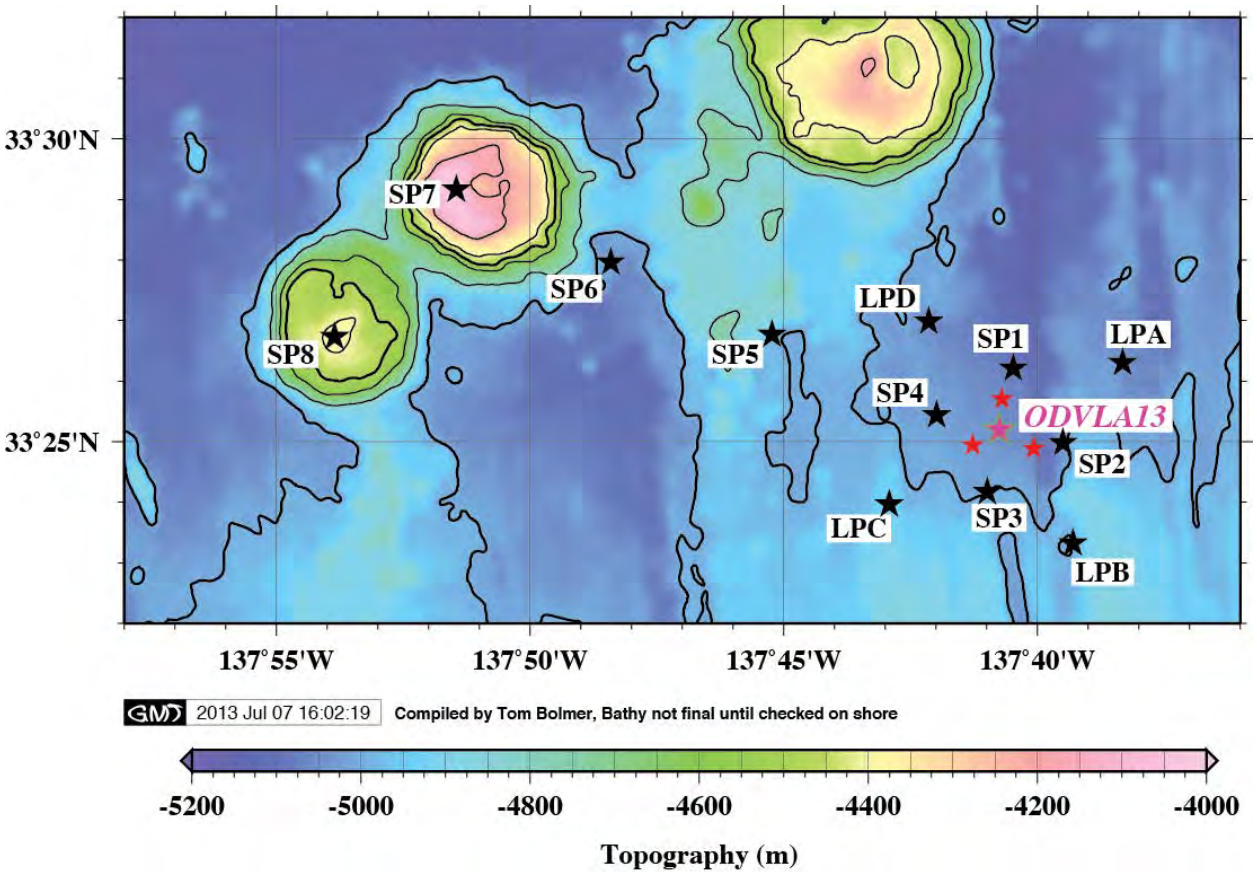

Figure 3.1: OBSANP Instrument Locations
Locations of the eight short period OBSs (SP*), the four long period OBSs (LP*), and the OBSANP DVLA (ODVLA13) with respect to the bathymetric relief. The three red stars around ODVLA13 are the acoustic transponders used to measure mooring motion.

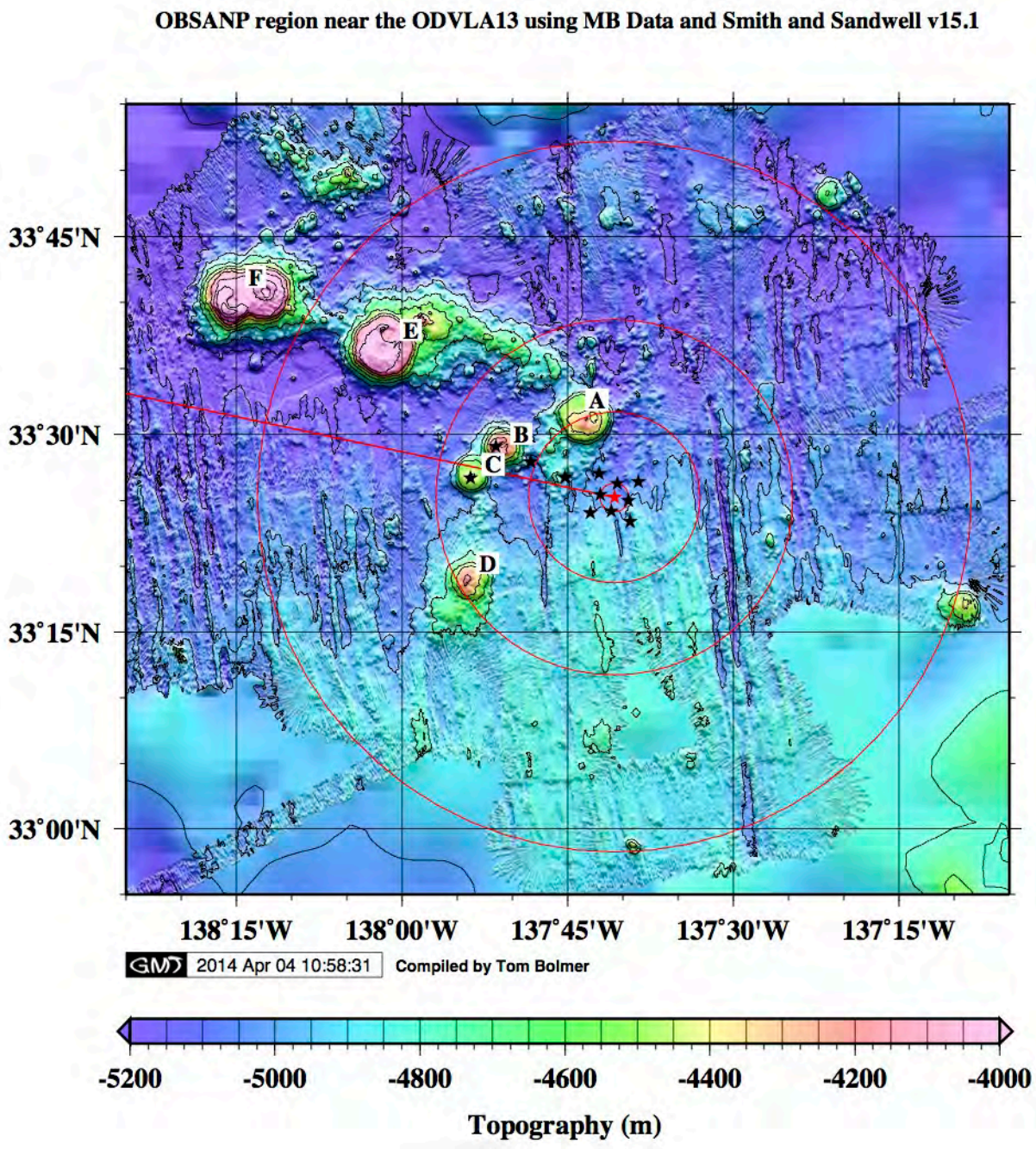

Figure 3.2: OBSANP Regional Bathymetry
This shows the bathymetry around the ODVLA13 (red star). The black stars the locations of the OBSs. The red line is the 2004 LOAPEX geodesic. The red circles are ranges from the ODVLA13 of 2, 12, 25, and 50 kilometers. The letters designate Seamounts of interest.

3.1 Moored DVLA Receiver

The near-seafloor DVLA, referred to as the OBSANP-DVLA (O-DVLA) consisted of one 1000-m array with a D-STAR controller located at the top of the array and 32 Hydrophone Modules (HM) distributed along it (Figure 3.3). The deepest HM on the O-DVLA was 12 m above the seafloor, which is as close to the seafloor as an HM can conveniently be placed. Preliminary indications are that 27 of the HM worked properly, but for reasons that are not understood, five (5) HM apparently never started recording. Further investigation of the failures was done after the HMs were returned to San Diego.

The O-DVLA was navigated using the long-baseline navigation system in the D-STAR and three Benthos TR-6001-17 recoverable acoustic transponders on the seafloor. The transponders functioned properly throughout the experiment.

A Nortek Aquadopp 6000-m acoustic current meter was located just above the acoustic releases on the O-DVLA. It appears to have functioned properly.

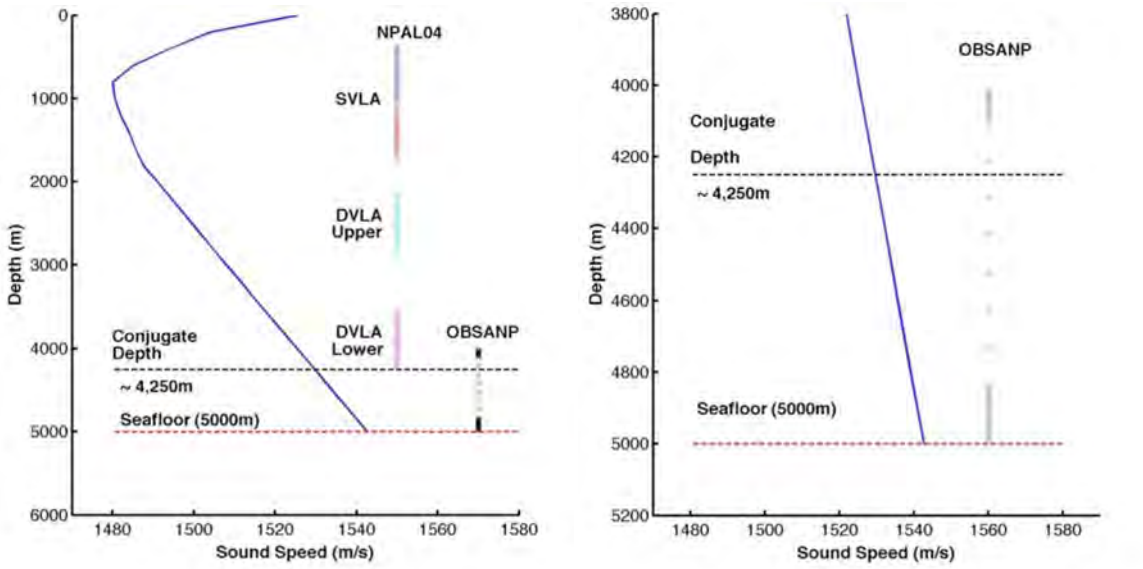

Figure 3.3: OBSANP ODVLA13 Element Locations
(left) The OBSANP DVLA has 16 elements at 10 m spacing ($\lambda/2$ at 75 Hz) at the bottom, and ten elements at 10 m spacing at the top. The two mini-arrays are separated by six elements at 105 m spacing. The Shallow and Deep VLAs deployed for NPAL04 (SVLA and DVLA) are shown for comparison. A nominal sound speed profile from NPAL04 is shown. (right) An expanded view of the OBSANP DVLA.

3.2 Ocean Bottom Seismometers

The SIO OBSIP group provided eight (8) short-period and four (4) long-period OBSs. Four of the short-period OBSs (SP1-SP4) were installed about 2000 m from the O-DVLA. The four long-period OBSs (LPA-LPD) were installed about 4000 m from the O-DVLA. These eight instruments were aligned with respect to the LOAPEX source geodesic. Two short period OBSs

(SP7 and SP8) were located as close as possible to the tops of Seamounts B and C, respectively, to measure the incident field at these features. The final two short period OBSs (SP5 and SP6) are on a line between Seamount B and the O-DVLA.

The short-period OBSs have three-component Mark Products L22 28-Hz geophones and an HTI-90-U hydrophone. The long-period OBS have broadband, three-component Trillium 240 seismometers and a Differential Pressure Gauge (DPG). The long period OBSs provided seafloor ambient noise data for comparison with other deep-water, broadband data sets in the Pacific such as OBSAPS (Stephen *et al.*, 2011), H2O (Duennebier *et al.*, 2002; Stephen *et al.*, 2006) and the OSNPE (Stephen *et al.*, 2003). SAIC Ultra-Low-Noise hydrophones (ULN-SAIC) were integrated into two of the long-period OBSs (LPA and LPC). These specifically targeted the very low ambient noise levels that are observed in the 4-20Hz band about 5% of the time (Duennebier *et al.*, 2012; Farrell and Munk, 2008; 2010; 2013). All OBS sampled at 1000 Hz. All OBSs functioned normally.

Hydrophone Modules originally developed for the DVLA were attached to six of the short period OBSs (SP1-SP4, SP7, and SP8) to supplement the hydrophones included in the short period instruments. Preliminary indications are that all of these HMs functioned correctly.

The locations and water depths of all the receivers are given in Table 4-4 and the OBSIP deployment information is given in Table 4-5. A summary of all the data channels is given in Table 4-6.

4 J15-3 Acoustic Source Program

J15-3 operations were quite successful with no downtime due to equipment failure and essentially two weeks of scheduled transmissions. We transmitted primarily m-sequences at various frequencies spanning 20 to 310 Hz with the source at depths from 60 m to 100 m. The m-sequences fall into four categories: (1) multi-frequency, short range (< 1/2 CZ) tows at 77.5, 155, and 310 Hz; (2) single frequency, long range (up to 250 km, ~ 4-1/2 CZ) tows at 77.5 Hz; (3) multi-frequency station stops at 1/2, 1-1/2, 2-1/2, and 3-1/2 CZ at 77.5, 102.3, 155, 204.6, and 310 Hz; and (4) low frequency transmissions (19.375, 25.575, 38.75, and 51.15 Hz) at short ranges (< 1/2 CZ) to provide field data for modeling with SPECFEM3D. We also tested Minimum Shift Keying (MSK) format m-sequences, which are an alternative to our usual phase shift keying (PSK) format and could potentially have improved properties for some applications.

The convergence zone ranges were determined using PE transmission loss computations based on the first CTD cast on the cruise (Figure 4.1, Figure 4.2, and Figure 4.3). At the depth of top of Seamount B (~4250m), the strongest arrivals occur at 1/2CZ, 1-1/2CZ, 2-1/2CZ and 3-1/2CZ ranges, that is 22-35km, 79-91km, 136-146km, and 192-205km. Since both the top of Seamount B and the DVLA are below the conjugate depth of 3670m, we used the same ranges for the convergent zones to both sites. To allow for error we used three station stops per convergent zone spanning 10km.

In the first phase of the transmission program, we carried out a “pin cushion” pattern of station stops spanning 1/2CZ ranges to the O-DVLA and Seamount B (Figure 4.4). This pattern was designed to insonify Seamount B at a variety of sagittal and azimuthal angles and to distinguish bottom diffracted from bottom-reflected energy. All station stops are labeled 'Q*' and the positions are given in Table 4-1.

The closest three Q-stops on each line are 23, 28 and 33km from ODVLA. These ranges span the predicted 1/2CZ distance to the ODVLA. The furthest three Q-stops on each line are 38, 43 and 48km from ODVLA. Since Seamounts B and C are about 16 and 20km from the ODVLA respectively, the three furthest Q-stops essentially insonify the tops of the seamounts at 1/2CZ. Seamounts B and C are about 4km across at the top.

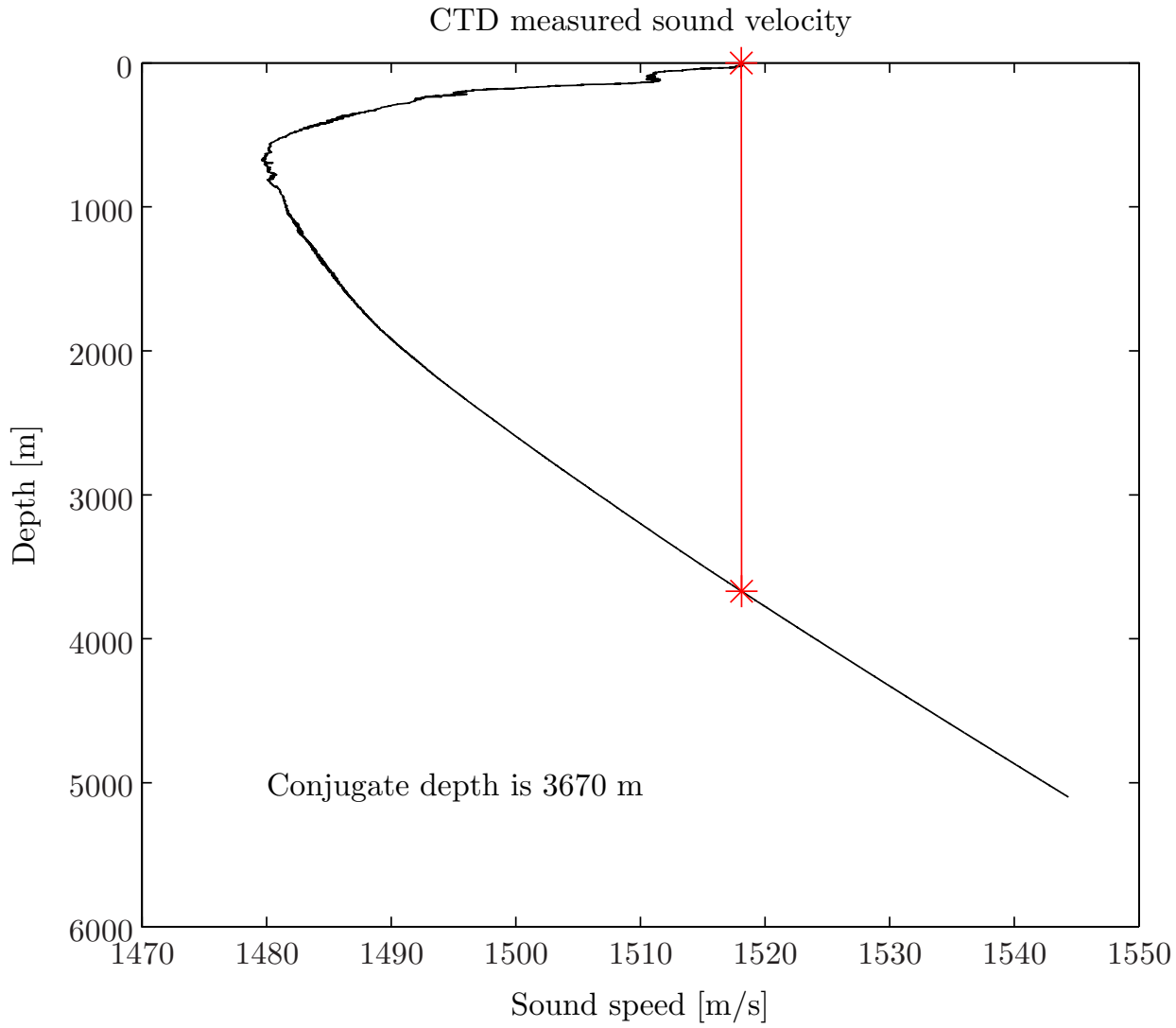

Figure 4.1: Sound Speed Profile
Estimate of the conjugate depth using the first CTD cast.

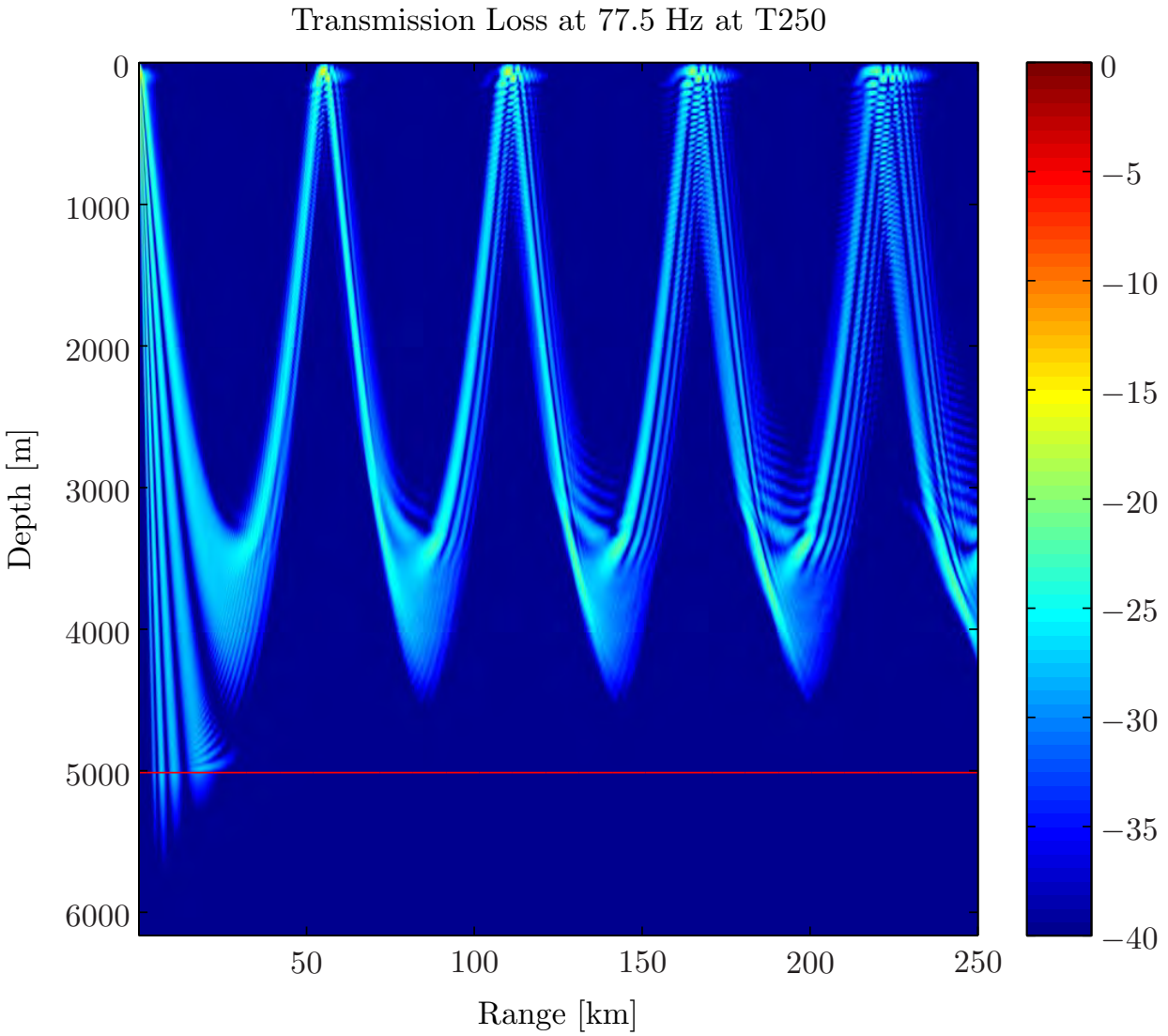

Figure 4.2: Example of Transmission Loss Calculation
Example of transmission loss calculation (based on the first CTD cast) that was used to estimate ranges for station stops. (See Appendix C.)

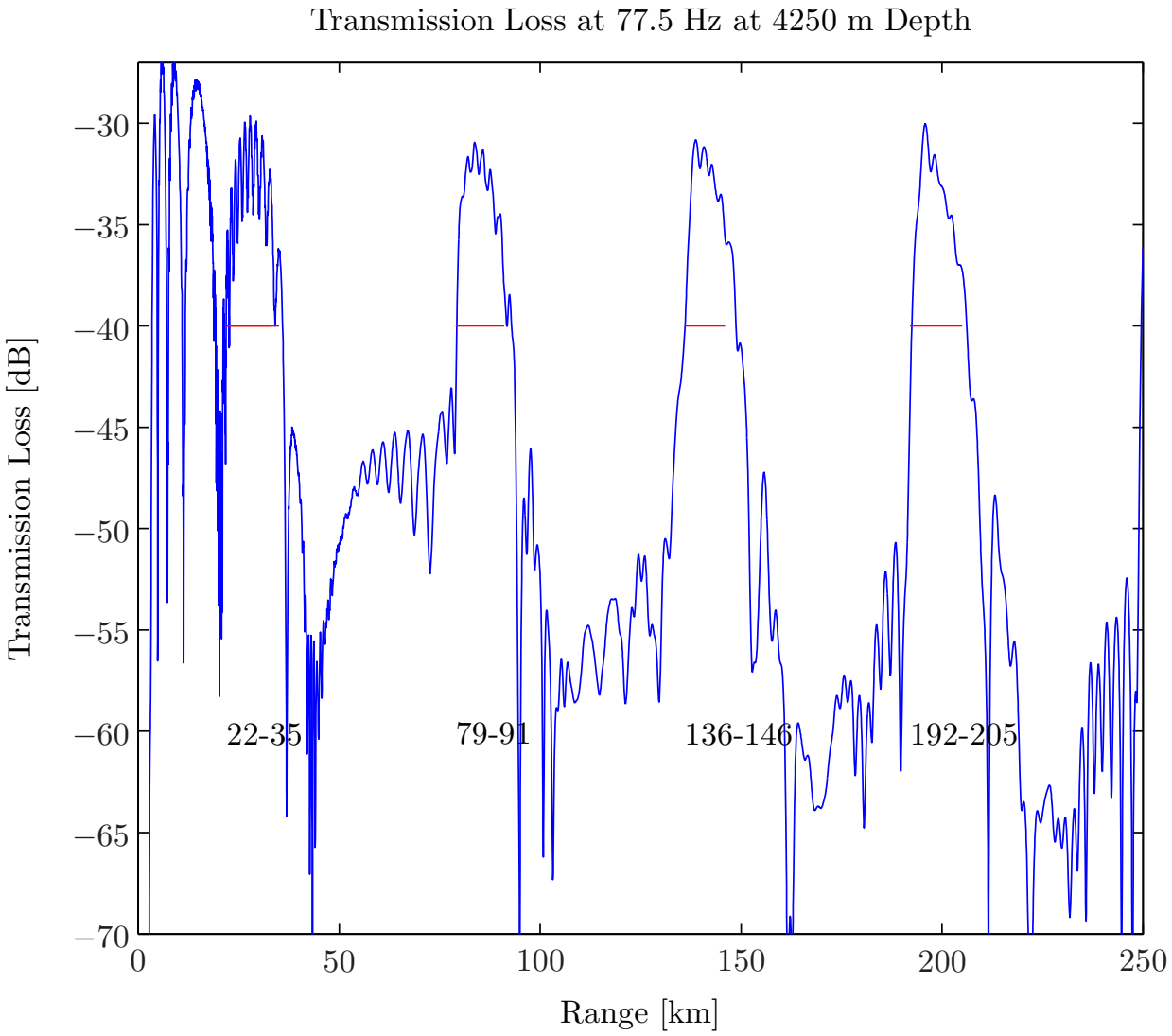

Figure 4.3: Transmission Loss Curve for 4250m
Transmission loss curve for 4250m, the depth of Seamount B, and ranges for the convergent zone arrivals.

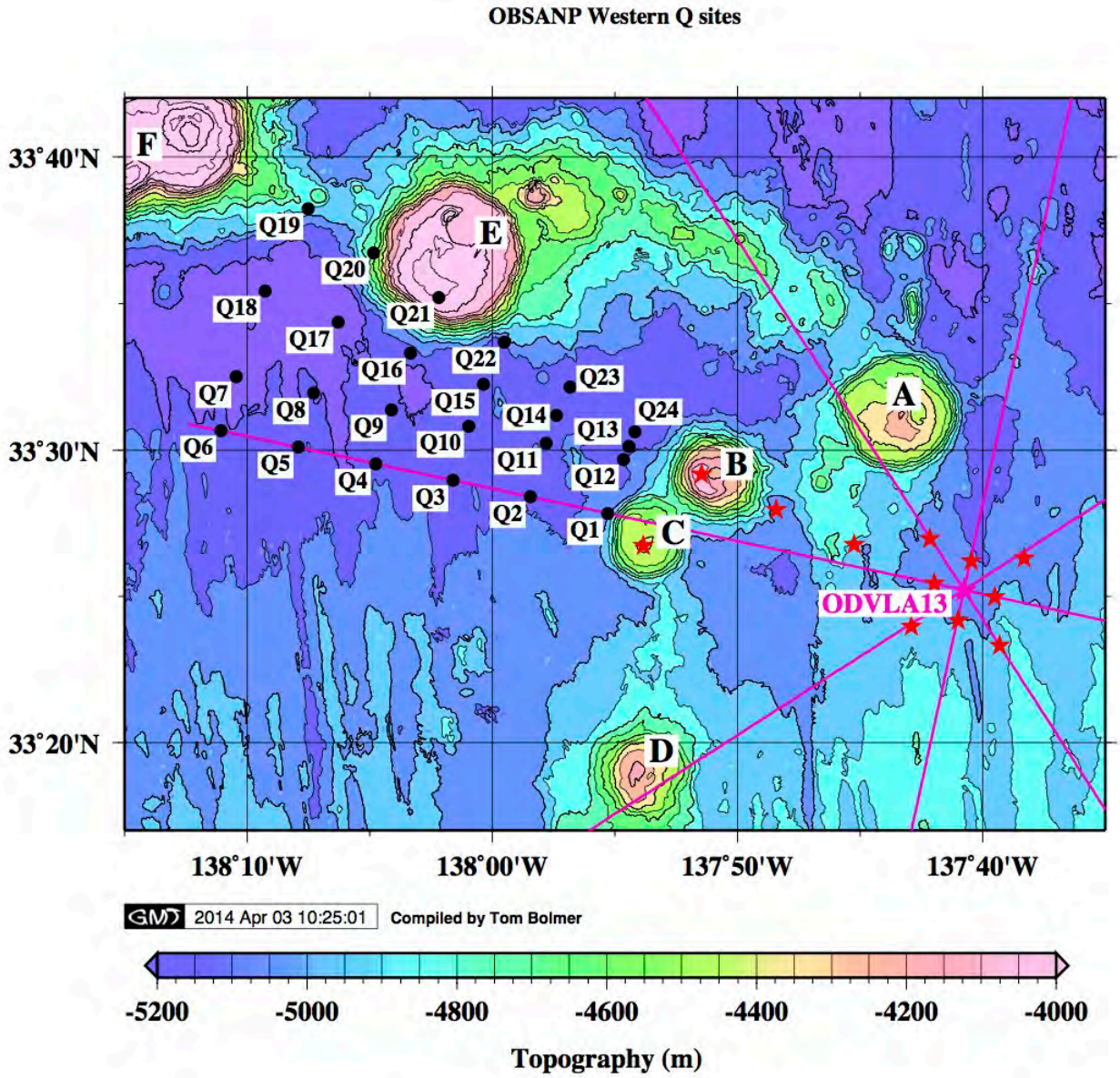

Figure 4.4: "Pin Cushion" of Station Stops
A "pin cushion" of station stops was designed to ensonify Seamounts B and C at a variety of sagittal and azimuthal angles. The stations span 1/2 CZ from the O-DVLA and the seamounts. Q1 to Q6 (Event #1) are on the LOAPEX geodesic. Q13 to Q18 (Event #3) are collinear with Seamount B and the O-DVLA. Q7 to Q12 (Event #2) and Q19 to Q24 (Event #4&9) are aligned with Seamount B but are oblique to the ODVLA13 transmission path. The red stars are the locations of the OBSs. The magenta lines show the locations of the short-range tows.

We attempted to replicate the LOAPEX results as closely as possible by carrying out a series of long- and short-range tows and station stops along the LOAPEX geodesic out to 250 km range (Figure 4.5). During LOAPEX, DSFAs were observed using the HX-554 source at ranges of 500 km and greater, so we could not duplicate the 2004 results directly. These transmissions will, however, fill in the long-range propagation story for short ranges along the same path.

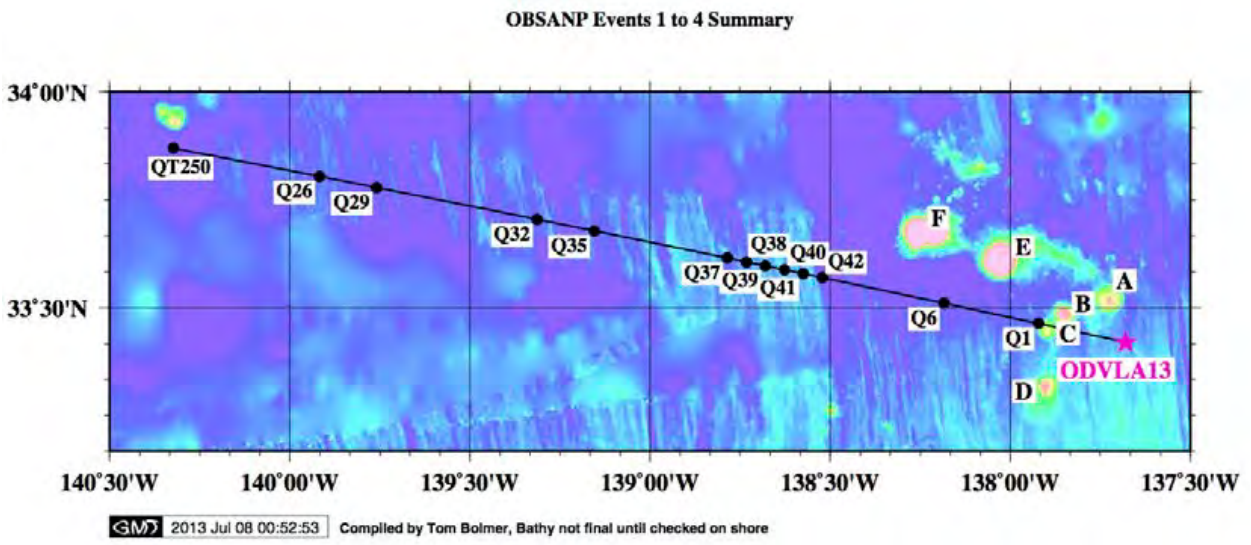

Figure 4.5: Long Line and Station Stops

In an attempt to replicate the 2004 LOAPEX results, we transmitted continuously out to 250 km range on the LOAPEX geodesic (Event #5) and then occupied station stops at 1-1/2, 2-1/2 and 3-1/2 CZ's from the O-DVLA (Event #6-8). Stations between Q1 and Q6 are shown in Figure 4.4.

In order to obtain a comprehensive view of propagation and scattering within 1/2 CZ to receivers on and near the seafloor, we carried out a series of radial line tows out to 50 km range at eight azimuths and half of a "Star of David" pattern over the seamounts across 1/2 CZ ranges (Figure 4.6) This pattern is similar to the OBSAPS experiment in the Philippine Sea in 2011, so propagation and scattering characteristics at the two sites can be compared. The way points for the radial lines, 'T*', and the Star of David, 'R*' are given in Table 4-2.

In the fourth phase, we occupied two station stops within 1/2 CZ of both the O-DVLA and Seamounts B and C in order to carry out source tests that will be useful in subsequent experiments (Figure 4.7). We transmitted identical m-sequences in both MSK and PSK formats. We had not done MSK format transmissions in the past, but they have smoother phase than the PSK format, which could be an advantage for some types of sources.

Also, although the J15-3 is not recommended for use below 100 Hz, we tested the source with CW and m-sequence transmissions down to 20 Hz. Source levels are quite low at these frequencies, but we are at very short ranges from the receivers and are optimistic that we will see useful returns. Full three dimensional bottom-interaction problems with shear, that can be studied using codes like SPECFEM3D, are more tractable at these low frequencies.

A summary of the whole J15-3 acoustic transmission program is given in Table 4-3.

4.1 Other Measurements

Five CTD and 92 XBT casts were made during the cruise. Extensive multibeam (Kongsberg Simrad EM122) and sub-bottom profiler (Knudsen 3260 3.5 kHz) measurements were made in the experimental area. The WaMoS system routinely provided information on the surface waves in the vicinity of the ship. AIS information was logged to provide information on other ships in the vicinity. Finally, routine shipboard data were collected throughout the cruise.

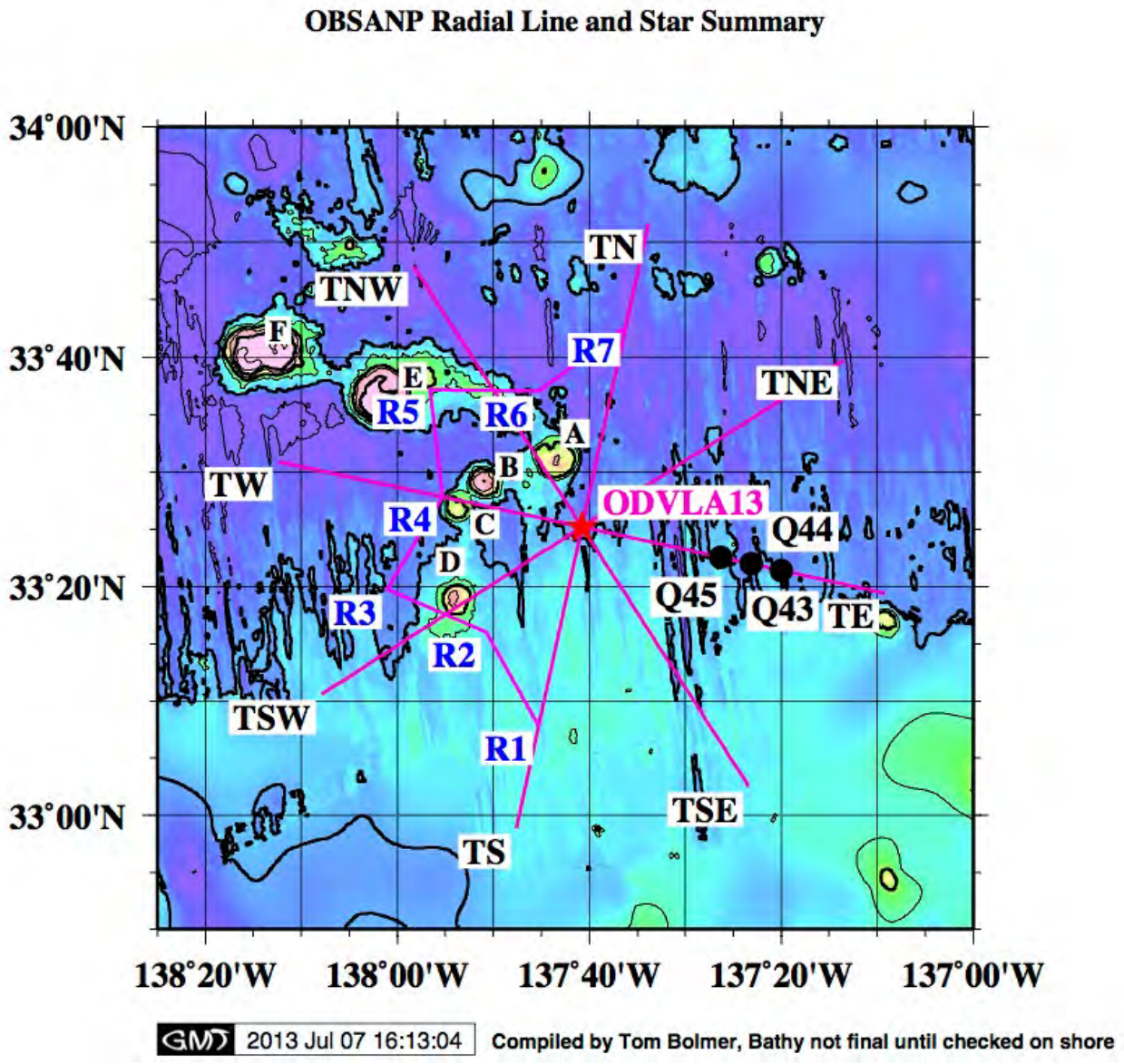

Figure 4.6: Radial Lines and Star of David
Phase 3 of the transmission program carried out a comprehensive survey (out to 50 km) around the DVLA. Black dots are the locations of three station stops, Q43-Q45 (Event#10), east of the ODVLA. The magenta lines show the short-range, radial tows with end points labeled TN, TNE, etc (Event # 11-14). The blue labels, 'R*', are the way points for the Star of David (Event #15).

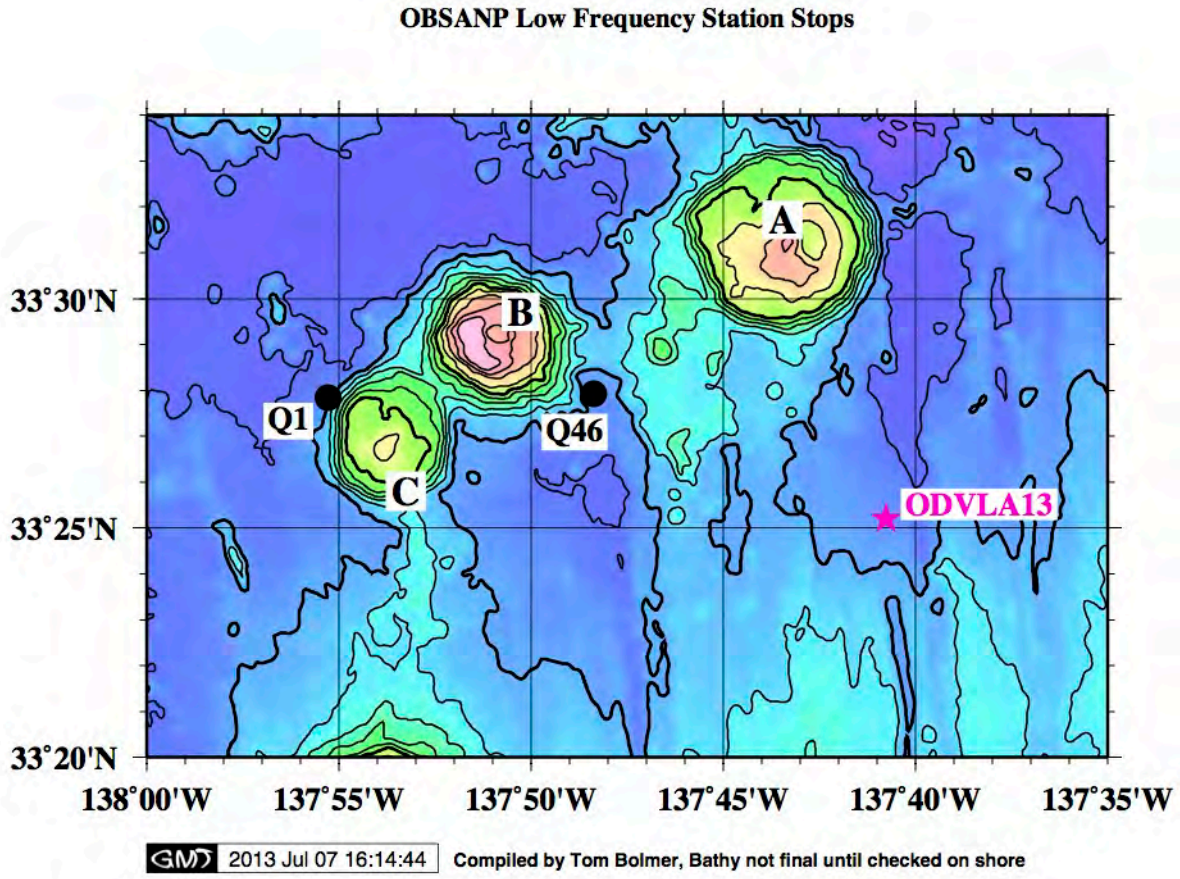

Figure 4.7: OBSANP MSK and Low frequency Test Locations
Q1 and Q46 were the locations of the MSK and low frequency tests (Event #16). The black dots are the Q station stops. The letters designate Seamounts of interest. [OBSANP_Ralph_Q1_Q46.jpg]

Table 4-1 Q Station Locations

Latitude	*Longitude*	*Q Station*
33.46401	-137.9213	Q1
33.47344	-137.9739	Q2
33.48285	-138.0265	Q3
33.50159	-138.1318	Q5
33.49223	-138.0791	Q4
33.51093	-138.1844	Q6
33.54184	-138.174	Q7
33.53242	-138.1214	Q8
33.52298	-138.0687	Q9
33.51352	-138.0161	Q10
33.50404	-137.9635	Q11
33.49453	-137.9109	Q12
33.5021	-137.9069	Q13
33.51981	-137.9563	Q14
33.53751	-138.0058	Q15
33.55518	-138.0554	Q16
33.57284	-138.1049	Q17
33.59047	-138.1545	Q18
33.63734	-138.1253	Q19
33.61199	-138.0807	Q20
33.58663	-138.0362	Q21
33.56124	-137.9917	Q22
33.53584	-137.9472	Q23
33.51043	-137.9028	Q24
33.80478	-139.9173	Q26
33.77892	-139.7583	Q29
33.70541	-139.3137	Q32
33.67877	-139.1551	Q35
33.61581	-138.7853	Q37
33.60673	-138.7326	Q38
33.59763	-138.6798	Q39
33.5885	-138.6271	Q40
33.57935	-138.5743	Q41
33.57017	-138.5216	Q42
33.35691	-137.333	Q43
33.36658	-137.3854	Q44
33.37624	-137.4379	Q45
33.46546	-137.8062	Q46
33.86978	-140.32299	QT250

Table 4-2 Way Points for Tows

Longitude	*Latitude*	*Way Point*
-137.1536	33.32366	TE
-138.2065	33.51482	TW
-138.1314	33.17643	TSW
-137.225	33.66263	TNE
-137.5644	33.85968	TN
-137.7934	32.98091	TS
-137.3895	33.04174	TSE
-137.972	33.79829	TNW
-137.7548	33.13034	R1
-137.8459	33.26719	R2
-138.0178	33.32953	R3
-137.9218	33.46408	R4
-137.9432	33.6197	R5
-137.7551	33.61735	R6
-137.6036	33.71032	R7

Table 4-3 Timeline for the Transmission Programs

This table is from the logbook kept in the lab. There are some errors in this. Generally, this is accurate and reliable. All transmissions used J15-3 serial number 11. The folders listed contain the DAQ data files and the NMEA navigation from the transmission/recording program.

Day in the year	*Start time*	*End time*	*Station or Line Name*	*Program*	*Folder Name*	*Ship Speed (kts)*	*DAC Gain*	*Depth (m)*	*Calendar date*
169	15:54:00	16:00:00	Q1	ambient	JD169_Q1_ambient	0	0	60	18-Jun
169	16:16:00	16:33:47	Q1	CW_1_4k	JD169_Q1_CW_gain_0p05_60m	0	0.05	60	18-Jun
169	16:43:00	16:49:40	Q1	CW_1_4k	JD169_Q1_CW_gain_0p25_60m	0	0.75	60	18-Jun
169	16:57:00	17:03:22	Q1	CW_1_4k	JD169_Q1_CW_gain_1p0_60m	0	1	60	18-Jun
169	17:07:00	17:23:20	Q1	CW_1_4k	JD169_Q1_CW_gain_1p25_60m	0	1.25	60	18-Jun
169	17:29:00	17:34:45	Q1	CW_1_4k	JD169_Q1_CW_gain_1p50_60m	0	1.5	60	18-Jun
169	17:37:00	17:42:06	Q1	CW_1_4k	JD169_Q1_CW_gain_1p75_60m	0	1.75	60	18-Jun
169	17:47:00	17:52:05	Q1	CW_1_4k	JD169_Q1_CW_gain_2p.00_60m	0	2	60	18-Jun
169	17:55:00	17:01:10	Q1	04_4k	JD169_Q1_Primry_04_4K_gain_2p00_60m	0	2	60	18-Jun
169	18:06:00	18:23:06	Q1	06a_4k	JD169_Q1_6a_gain_2p00_60m	0	2	60	18-Jun
169	18:25:00	18:38:11	Q1	06b_4k	JD169_Q1_6b_gain_2p00_60m	0	2	60	18-Jun
169	19:04:00	19:23:00	Q1	06c_4k	JD169_Q1_6c_gain_2p00_60m_run1	0	2	60	18-Jun
169	19:27:00	19:44:00	Q1	06a_4k	JD169_Q1_6a_gain_2p00_60m_run2	0	2	60	18-Jun
169	19:51:00		Q1		misfired; timing error	0	0	0	18-Jun
169	19:55:00	20:08:00	Q1	06b_4k		0	2	60	18-Jun
169	20:10:00		Q1	06c_4k		0	2	60	18-Jun
169	21:52:00	21:58:00	Q2	06T	JD169_Q2_6t_gain2p00_60m_run1	0	2	62.15	18-Jun
169	22:53:00	23:42:00	Q2	06T	JD169_Q2_6t_gain2p00_60m_run2	0	2	61.91	18-Jun
169	22:00:00	39:00:00	Q3	6a	JD170_Q3_6a_gain2p00_60m_run1	0	2	62.06	18-Jun
170	01:42:00	01:55:00	Q3	6b	JD170_Q3_6b_gain2p00_60m_run1	0	2	62	18-Jun
170	01:58:00	02:47:00	Q3	6t	JD170_Q3_6t_gain2p00_60m_run1	0	2	62	18-Jun
170	02:58:00	03:47:00	Q3	6t	JD170_Q3_6t_gain2p00_60m_run2	0	2	62	18-Jun
170	06:03:00	00:00:00	Q4		JD170_Q4_6t_gain2p00_60m_run1_lostdata	0	0	0	19-Jun
170	07:32:00	00:00:00	Q4	6c	JD170_Q4_6c_gain2p00_60m_run1_testrun	0	2	62	19-Jun
170	07:58:00	08:46:45	Q4	6t	JD170_Q4_6t_gain2p00_60m_run1	0	2	62	19-Jun
170	08:58:00	09:46:45	Q4	6t	JD170_Q4_6t_gain2p00_60m_run2	0	2	62	19-Jun
170	11:15:00	11:28:15	Q5	6b	JD170_Q5_6b_gain2p00_60m_run1	0	2	62	19-Jun
170	11:29:00	11:47:43	Q5	6c	JD170_Q5_6c_gain2p00_60m_run1	0	2	62	19-Jun

Day in the year	*Start time*	*End time*	*Station or Line Name*	*Program*	*Folder Name*	*Ship Speed (kts)*	*DAC Gain*	*Depth (m)*	*Calendar date*
170	11:58:00	12:00:00	Q5	6t	JD170_Q5_6t_gain2p00_60m_run1	0	2	62	19-Jun
170	14:35:00	00:00:00	Q6	6b	JD170_Q6_6b_gain2p00_60m_run1	0	2	62	19-Jun
170	14:59:00	15:47:00	Q6	6t	JD170_Q6_6t_gain2p00_60m_run1	0	2	62	19-Jun
170	16:04:00	16:23:00	Q6	6c	JD170_Q6_6c_gain2p00_60m_run1	0	2	62	19-Jun
170	16:26:00	16:43:00	Q6	6a	JD170_Q6_6a_gain2p00_60m_run1	0	2	62	19-Jun
170	18:00:00	18:48:00	Q7	6t	JD170_Q7_6t_gain2p00_60m_run1	0	2	62	19-Jun
170	19:00:00	19:48:00	Q7	6t	JD170_Q7_6t_gain2p00_60m_run2	0	2	62	19-Jun
170	21:35:00	21:47:00	Q8	6b	JD170_Q8_6b_gain2p00_60m_run1	0	2	62	19-Jun
170	21:53:00	00:00:00	Q8	6c	File size error	0	2	62	19-Jun
170	22:00:00	22:48:00	Q8	6t	JD170_Q8_6t_gain2p00_60m_run1	0	2	62	19-Jun
170	23:01;00	23:20:00	Q8	6c	JD170_Q8_6c_gain2p00_60m_run1	0	2	62	19-Jun
170	23:27:00	23:49:00	Q8	6a	JD170_Q8_6ta_gain2p00_60m_run1	0	2	62	19-Jun
171	01:35:00	01:43:00	Q9	6b	JD171_Q9_6b_gain2p00_60m_run1	0	2	62	19-Jun
171	02:00:00	02:42:00	Q9	6t	JD171_Q9_6t_gain2p00_60m_run1	0	2	62	19-Jun
171	03:15:00	03:22:00	Q9	6a	JD171_Q9_6t_gain2p00_60m_run1	0	2	62	19-Jun
171	03:35:00	03:48:00	Q9	6b	JD171_Q9_6b_gain2p00_60m_run1	0	2	62	19-Jun
171	03:53:00	04:11:30	Q9	6c	JD171_Q9_6c_gain2p00_60m_run2	0	2	62	19-Jun
171	06:00:00	06:50:00	Q10	6t	JD171_Q10_6t_gain2p00_60m_run1	0	2	62	19-Jun
171	07:00:00	08:10:00	Q10	6t	JD171_Q10_6t_gain2p00_60m_run2	0	2	62	19-Jun
171	09:15:00	09:34:00	Q11	6a	JD171_Q11_6a_gain2p00_60m_run1	0	2	62	20-Jun
171	09:36:00	09:49:00	Q11	6b	JD171_Q11_6b_gain2p00_60m_run1	0	2	62	20-Jun
171	09:53:00	10:41:00	Q11	6t	JD171_Q11_6t_gain2p00_60m_run1	0	2	62	20-Jun
171	10:55:00	11:13:00	Q11	6a	JD171_Q11_6c_gain2p00_60m_run2	0	2	62	20-Jun
171	12:32:00	12:43:00	Q12	6b	JD171_Q12_6b_gain2p00_60m_run1	0	2	62	20-Jun
171	12:53:00	13:41:00	Q12	6t	JD171_Q12_6t_gain2p00_60m_run1	0	2	62	20-Jun
171	13:51:00	14:13:00	Q12	6a	JD171_Q12_6a_gain2p00_60m_run2	0	2	62	20-Jun
171	14:16:00	14:34:00	Q12	6c	JD171_Q12_6c_gain2p00_60m_run2	0	2	62	20-Jun
171	15:00:00	15:48:00	Q13	6t	JD171_Q13_6t_gain2p00_60m_run1	0	2	62	20-Jun
171	16:00:00	16:48:00	Q13	6t	JD171_Q13_6t_gain2p00_60m_run2	0	2	62	20-Jun
171	18:15:00	18:31:00	Q14	6a	JD171_Q14_6a_gain2p00_60m_run1	0	2	62	20-Jun
171	19:00:00	19:48:00	Q14	6t	JD171_Q14_6t_gain2p00_60m_run1	0	2	62	20-Jun
171	19:53:00	20:11:00	Q14	6a	JD171_Q14_6c_gain2p00_60m_run1	0	2	62	20-Jun
171	20:18:00	20:30:00	Q14	6b	JD171_Q14_6b_gain2p00_60m_run1	0	2	62	20-Jun
171	21:52:00	23:51:00	Q15	6tx	JD171_Q15_6tx_gain2p00_60m	0	2	62	20-Jun
172	23:51:00	01:08:00	Q16		JD172_Q15_to_Q16_padisabled_60m	2	0	61	20-Jun

Day in the year	*Start time*	*End time*	*Station or Line Name*	*Program*	*Folder Name*	*Ship Speed (kts)*	*DAC Gain*	*Depth (m)*	*Calendar date*
172	01:08:00	03:09:00	Q16	6tx	JD172_Q16_6tx_gain2p00_60m	0	2	62	20-Jun
172	03:09:00	04:21:00	Q17		JD172_Q16_to_Q17_pa_disabled_60m	2	0	62	20-Jun
172	04:22:00	06:21:00	Q17	6tx	JD172_Q17_6tx_gain2p00_60m	0	2	60	20-Jun
172	06:22:00	07:39:00	Transit		JD172_Q17_to_Q18_pa_disabled_60m	2	0	62	20-Jun
172	07:39:00	09:43:00	Q18	6tx	JD172_Q18_6tx_gain2p00_60m	0	2	60	21-Jun
172	09:43:00	11:18:00	Q18-Q19	6tx	JD172_Q18_to_Q19_pa_disabled_60m	2	2	0	21-Jun
172	11:20:00	13:25:00	Q19	6tx	JD172_Q19_6tx_gain2p00_60m	0	2	62	21-Jun
172	13:25:00	14:49:00	Q19-Q20	6tx	JD172_Q19_to_Q20_pa_disabled_60m	2	2	0	21-Jun
172	14:49:00	16:41:00	Q20	6tx	JD172_Q4_6tx_gain2p00_60m	0	2	62	21-Jun
172	19:17:00	20:16:00	Q6-T250	5	JD172_Q6_to_T250_gain2p00_64m_01	4	2	60	21-Jun
172	20:17:00	21:16:00	Q6-T250	5	JD172_Q6_to_T250_gain2p00_64m_02	4	2	60	21-Jun
172	21:17:00	22:16:00	Q6-T250	5	JD172_Q6_to_T250_gain2p00_64m_03	4	2	60	21-Jun
172	22:17:00	23:16:00	Q6-T250	5	JD172_Q6_to_T250_gain2p00_64m_04	4	2	60	21-Jun
172	23:17:00	00:16:00	Q6-T250	5	JD172_Q6_to_T250_gain2p00_64m_05	4	2	60	21-Jun
173	00:17:00	01:16:00	Q6-T250	5	JD173_Q6_to_T250_gain2p00_64m_01	4	2	60	22-Jun
173	01:17:00	02:16:00	Q6-T250	5	JD173_Q6_to_T250_gain2p00_64m_02	4	2	60	22-Jun
173	02:17:00	03:16:00	Q6-T250	5	JD173_Q6_to_T250_gain2p00_64m_03	4	2	60	22-Jun
173	03:17:00	04:16:00	Q6-T250	5	JD173_Q6_to_T250_gain2p00_64m_04	4	2	60	22-Jun
173	04:17:00	05:16:00	Q6-T250	5	JD173_Q6_to_T250_gain2p00_64m_05	4	2	60	22-Jun
173	05:17:00	06:16:00	Q6-T250	5	JD173_Q6_to_T250_gain2p00_64m_06	4	2	60	22-Jun
173	06:17:00	07:16:00	Q6-T250	5	JD173_Q6_to_T250_gain2p00_64m_07	4	2	60	22-Jun
173	07:17:00	08:16:00	Q6-T250	5	JD173_Q6_to_T250_gain2p00_64m_08	4	2	60	22-Jun
173	08:17:00	09:16:00	Q6-T250	5	JD173_Q6_to_T250_gain2p00_64m_09	4	2	60	22-Jun
173	09:17:00	10:16:00	Q6-T250	5	JD173_Q6_to_T250_gain2p00_64m_10	4	2	67	22-Jun
173	10:17:00	11:16:00	Q6-T250	5	JD173_Q6_to_T250_gain2p00_64m_11	4	2	70	22-Jun
173	11:17:00	12:16:00	Q6-T250	5	JD173_Q6_to_T250_gain2p00_64m_12	4	2	68	22-Jun
173	12:17:00	13:16:00	Q6-T250	5	JD173_Q6_to_T250_gain2p00_64m_13	4	2	68	22-Jun
173	13:17:00	14:16:00	Q6-T250	5	JD173_Q6_to_T250_gain2p00_64m_14	4	2	69	22-Jun
173	14:17:00	15:16:00	Q6-T250	5	JD173_Q6_to_T250_gain2p00_64m_15	4	2	68	22-Jun
173	15:17:00	16:16:00	Q6-T250	5	JD173_Q6_to_T250_gain2p00_64m_16	4	2	68	22-Jun
173	16:17:00	17:16:00	Q6-T250	5	JD173_Q6_to_T250_gain2p00_64m_17	4	2	68	22-Jun
173	17:17:00	18:16:00	Q6-T250	5	JD173_Q6_to_T250_gain2p00_64m_18	4	2	67	22-Jun
173	18:17:00	19:16:00	Q6-T250	5	JD173_Q6_to_T250_gain2p00_64m_19	4	2	73	22-Jun
173	19:17:00	20:02:00	Q6-T250	5	JD173_Q6_to_T250_gain2p00_64m_20	5	2	65	22-Jun
174	01:52:00	03:41:00	T250	6XT	JD174_T250_6TX_gain2p00_60m *	0	2	60	23-Jun

Day in the year	*Start time*	*End time*	*Station or Line Name*	*Program*	*Folder Name*	*Ship Speed (kts)*	*DAC Gain*	*Depth (m)*	*Calendar date*
174	08:15:00	10:20:00	Q26	6XT	JD174_Q26_6TX_gain2p00_60m	0	2	60	23-Jun
174	12:19:00	10:23:00	Q29	6XT	JD174_Q29_6TX_gain2p00_60m	0	2	61	23-Jun
174	19:09:00	21:08:00	Q32	6XT	JD174_Q32_6TX_gain2p00_60m	0	2	62	23-Jun
174	21:09:00	23:21:00	Q32 to Q35		JD174_Q32_to_Q35_NoChroma	6	2	60	23-Jun
175	23:22:00	01:21:00	Q35	6XT	JD174_Q35_6TX_gain2p00_60m	0	2	60	24-Jun
175	01:22:00	05:41:00	Q35 to Q37		JD175_Q35_to_Q37_NoChroma	6	2	60	24-Jun
175	05:42:00	07:49:00	Q37	6XT	JD175_Q37_6TX_gain2p00_60m	0	2	60	24-Jun
175	07:49:00	09:08:00	Q37 to Q38		JD175_Q37_to_Q38_NoChroma	5	2	52	24-Jun
175	09:08:00	11:09:00	Q38	6XT	JD175_Q38_6TX_gain2p00_60m	0	2	61	24-Jun
175	11:09:00	12:05:00	Q38 to Q39		JD175_Q38_to_Q39_NoChroma	5	2	0	24-Jun
175	12:05:00	12:09:00	Q39	6XT	JD175_Q39_6TX_gain2p00_60m	0	2	61	24-Jun
175	12:10:00	16:51:00	Q39 to Q42		JD175_Q39_to_Q42_NoChroma	0	0	0	24-Jun
175	16:52:00	18:40:00	Q42	6XT	JD175_Q42_6TX_gain2p00_60m	0	2	62	24-Jun
175	18:41:00	19:51:00	Q42 to Q41		JD175_Q42_to_Q41_NoChroma	0	0	0	24-Jun
175	19:52:00	21:40:00	Q41	6XT	JD175_Q41_6TX_gain2p00_60m	0	2	62	24-Jun
175	21:41:00	22:51:00	Q41 to Q40		JD175_Q41_to_Q40_NoChroma	0	0	0	24-Jun
175	22:52:00	00:41:00	Q40	6XT	JD175_Q40_6TX_gain2p00_60m	0	2	62	24-Jun
176	05:09:00	07:09:00	Q24	6XT	JD176_Q24_6TX_gain2p00_60m	0	2	62	25-Jun
176	07:09:00	08:04:00	Q24 to Q23		JD175_Q24_to_Q23_NoChroma	5	2	0	25-Jun
176	08:04:00	10:09:00	Q23	6XT	JD176_Q23_6TX_gain2p00_60m	0	2	61	25-Jun
176	10:09:00	10:56:00	Q23 to Q22		JD175_Q23_to_Q22_NoChroma	5	0	0	25-Jun
176	10:56:00	13:10:00	Q22	6XT	JD176_Q22_6TX_gain2p00_60m	0	2	62	25-Jun
176	13:10:00	13:57:00	Q22 to Q21		JD175_Q22_to_Q21_NoChroma	0	0	0	25-Jun
176	13:57:00	16:08:00	Q21	6XT	JD176_Q21_6TX_gain2p00_60m	0	2	62	25-Jun
176					JD176_177_on_deck_junk	0	0	0	6/25-6/26
177	15:22:00	7:21:00	Q43	6XT	JD177_Q43_6TX_gain2p00_60m	0	2	61	26-Jun
177	17:22:00	18:21:00	Q43 to Q44		JD177_Q43_to_Q44_NoChroma	0	0	0	26-Jun
177	18:22:00	20:21:00	Q44	6XT	JD177_Q44_6TX_gain2p00_60m	0	2	62	26-Jun
177	20:22:00	21:21:00	Q44 to Q45		JD177_Q44_to_Q45_NoChroma	0	0	0	26-Jun
177	21:22:00	23:21:00	Q45	6XT	JD177_Q45_6TX_gain2p00_60m	0	2	62	26-Jun
177	23:22:00		Q45	6XT	JD177_Q45_lowering_J15-3_junk	0	2	62	26-Jun
178	02:00:00	02:59:00	TE-W	4	JD178_TE_TW_4_75m_0200_0300Z	2	2	75	27-Jun
178	03:00:00	03:59:00	TE-W	4	JD178_TE_TW_4_75m_0300_0400Z	2	2	75	27-Jun
178	04:00:00	04:59:00	TE-TW	4	JD178_TE_TW_4_75m_0400_0500Z	2	2	75	27-Jun
178	05:00:00	05:59:00	TE-TW	4	JD178_TE_TW_4_75m_0200_0300Z	2	2	75	27-Jun

Day in the year	*Start time*	*End time*	*Station or Line Name*	*Program*	*Folder Name*	*Ship Speed (kts)*	*DAC Gain*	*Depth (m)*	*Calendar date*
178	06:00:00	06:59:00	TE-TW	4	JD178_TE_TW_4_75m_0600_0700Z	2	2	75	27-Jun
178	07:00:00	07:59:00	TE-TW	4	JD178_TE_TW_4_75m_0700_0800Z	2	2	75	27-Jun
178	08:00:00	08:59:00	TE-TW	4	JD178_TE_TW_4_75m_0800_0900Z	2	2	75	27-Jun
178	09:00:00	09:59:00	TE-TW	4	JD178_TE_TW_4_75m_0900_1000Z	2	2	75	27-Jun
178	10:00:00	10:59:00	TE-TW	4	JD178_TE_TW_4_75m_1000_1100Z	2	2	75	27-Jun
178	11:00:00	11:59:00	TE-TW	4	JD178_TE_TW_4_75m_1100_1200Z	2	2	75	27-Jun
178	12:00:00	12:59:00	TE-TW	4	JD178_TE_TW_4_75m_1200_1300Z	2	2	75	27-Jun
178	13:00:00	13:59:00	TE-TW	4	JD178_TE_TW_4_75m_1300_1400Z	2	2	75	27-Jun
178	14:00:00	14:59:00	TE-TW	4	JD178_TE_TW_4_75m_1400_1500Z	2	2	75	27-Jun
178	15:00:00	15:59:00	TE-TW	4	JD178_TE_TW_4_75m_1500_1600Z	2	2	75	27-Jun
178	16:00:00	16:59:00	TE-TW	4	JD178_TE_TW_4_75m_1600_1700Z	2	2	75	27-Jun
178	17:00:00	17:59:00	TE-TW	4	JD178_TE_TW_4_75m_1700_1800Z	2	2	75	27-Jun
178	18:00:00	18:59:00	TE-TW	4	JD178_TE_TW_4_75m_1800_1900Z	2	2	75	27-Jun
178	19:00:00	19:59:00	TE-TW	4	JD178_TE_TW_4_75m_1900_2000Z	2	2	75	27-Jun
178	20:00:00	20:59:00	TE-TW	4	JD178_TE_TW_4_75m_2000_2100Z	2	2	75	27-Jun
178	21:00:00	21:59:00	TE-TW	4	JD178_TE_TW_4_75m_2100_2200Z	2	2	75	27-Jun
178	22:00:00	22:59:00	TE-TW	4	JD178_TE_TW_4_75m_2200_2300Z	2	2	75	27-Jun
178	23:00:00	23:59:00	TE-TW	4	JD178_TE_TW_4_75m_2300_0000Z	2	2	75	27-Jun
179	00:00:00	00:59:00	TE-TW	4	JD179_TE_TW_4_75m_0000_0100Z	2	2	75	28-Jun
179	01:00:00	01:59:00	TE-TW	4	JD179_TE_TW_4_75m_0100_0200Z	2	2	75	28-Jun
179	02:00:00	02:59:00	TE-TW	4	JD179_TE_TW_4_75m_0200_0300Z	2	2	75	28-Jun
179	03:00:00	03:59:00	TE-TW	4	JD179_TE_TW_4_75m_0300_0400Z	2	2	75	28-Jun
179	04:00:00	04:59:00	TE-TW	4	JD179_TE_TW_4_75m_0400_0500Z	2	2	75	28-Jun
179	05:00:00	05:59:00	TE-TW	4	JD179_TE_TW_4_75m_0500_0600Z	2	2	75	28-Jun
179	06:00:00	06:56:00	TE-TW	4	JD179_TE_TW_4_75m_0600_recover	2	2	75	28-Jun
179	13:55:00	13:59:00	TNW-TSE	OBSAWP	JD179_TNW_TSE_4_60m_1355_1400Z	2	2	60	28-Jun
179	14:00:00	14:59:00	TNW-TSE	sea_04.sio	JD179_TNW_TSE_4_60m_1400_1500Z	2	2	60	28-Jun
179	15:00:00	15:59:00	TNW-TSE	sea_04.sio	JD179_TNW_TSE_4_60m_1500_1600Z	2	2	60	28-Jun
179	16:00:00	16:59:00	TNW-TSE	sea_04.sio	JD179_TNW_TSE_4_60m_1600_1700Z	2	2	60	28-Jun
179	17:00:00	17:59:00	TNW-TSE	4	JD179_TNW_TSE_4_60m_1700_1800Z	2	2	60	28-Jun
179	18:00:00	18:59:00	TNW-TSE	4	JD179_TNW_TSE_4_60m_1800_1900Z	2	2	60	28-Jun
179	19:00:00	19:59:00	TNW-TSE	4	JD179_TNW_TSE_4_60m_1900_2000Z	2	2	60	28-Jun
179	20:00:00	20:59:00	TNW-TSE	4	JD179_TNW_TSE_4_60m_2000_2100Z	2	2	60	28-Jun
179	21:00:00	21:59:00	TNW-TSE	4	JD179_TNW_TSE_4_60m_2100_2200Z	2	2	60	28-Jun
179	22:00:00	22:59:00	TNW-TSE	4	JD179_TNW_TSE_4_60m_2200_2300Z	2	2	60	28-Jun

Day in the year	*Start time*	*End time*	*Station or Line Name*	*Program*	*Folder Name*	*Ship Speed (kts)*	*DAC Gain*	*Depth (m)*	*Calendar date*
179	23:00:00	23:59:00	TNW-TSE	4	JD179_TNW_TSE_4_60m_2300_2400Z	2	2	60	28-Jun
180	00:00:00	00:59:00	TNW-TSE	4	JD180_TNW_TSE_4_60m_0000_0100Z	2	2	60	29-Jun
180	01:00:00	01:59:00	TNW-TSE	4	JD180_TNW_TSE_4_60m_0100_0200Z	2	2	60	29-Jun
180	02:00:00	02:59:00	TNW-TSE	4	JD180_TNW_TSE_4_60m_0200_0300Z	2	2	60	29-Jun
180	03:00:00	03:59:00	TNW-TSE	4	JD180_TNW_TSE_4_60m_0300_0400Z	2	2	60	29-Jun
180	04:00:00	04:59:00	NW-TSE	4	JD180_TNW_TSE_4_60m_0400_0500Z	2	2	60	29-Jun
180	05:00:00	05:59:00	TNW-TSE	4	JD180_TNW_TSE_4_60m_0500_0600Z	2	2	60	29-Jun
180	06:00:00	06:59:00	NW-TSE	4	JD180_TNW_TSE_4_60m_0600_0700Z	2	2	60	29-Jun
180	07:00:00	07:59:00	TNW-TSE	4	JD180_TNW_TSE_4_60m_0700_0800Z	2	2	60	29-Jun
180	08:00:00	08:59:00	TNW-TSE	4	JD180_TNW_TSE_4_60m_8000_0900Z	2	2	60	29-Jun
180	09:00:00	09:59:00	TNW-TSE	4	JD180_TNW_TSE_4_60m_0900_1000Z	2	2	60	29-Jun
180	10:00:00	10:59:00	TNW-TSE	4	JD180_TNW_TSE_4_60m_1000_1100Z	2	2	60	29-Jun
180	11:00:00	11:59:00	TNW-TSE	4	JD180_TNW_TSE_4_60m_1100_1200Z	2	2	60	29-Jun
180	12:00:00	12:59:00	TNW-TSE	4	JD180_TNW_TSE_4_60m_1200_1300Z	2	2	60	29-Jun
180	13:00:00	3:59:00	TNW-TSE	4	JD180_TNW_TSE_4_60m_1300_1400Z	2	2	60	29-Jun
180	14:00:00	14:59:00	TNW-TSE	4	JD180_TNW_TSE_4_60m_1400_1500Z	2	2	60	29-Jun
180	15:00:00	15:59:00	TNW-TSE	4	JD180_TNW_TSE_4_60m_1500_1600Z	2	2	60	29-Jun
180	16:00:00	16:39:00	TNW-TSE	4	JD180_TNW_TSE_4_60m_1600_1640Z	2	2	60	29-Jun
180	16:40:00	20:29:00	TSE-TS	TSE to TS transit	JD180_TSE_TS_1640_2030Z_NoChroma	0	0	0	29-Jun
180	20:30:00	20:59:00	TS-TN	4	JD180_TS_TN_4_60m_2030_2100Z	2	2	60	29-Jun
180	21:00:00	21:59:00	TS-TN	4	JD180_TS_TN_4_60m_2100_2200Z	2	2	60	29-Jun
180	22:00:00	22:59:00	TS-TN	4	JD180_TS_TN_4_60m_2200_2300Z	2	2	60	29-Jun
180	23:00:00	23:59:00	TS-TN	4	JD180_TS_TN_4_60m_2300_2400Z	2	2	60	29-Jun
181	00:00:00	00:59:00	TS-TN	4	JD181_TS_TN_4_60m_0000_0100Z	2	2	60	30-Jun
181	01:00:00	01:59:00	TS-TN	4	JD181_TS_TN_4_60m_0100_0200Z	2	2	60	30-Jun
181	02:00:00	02:59:00	TS-TN	4	JD181_TS_TN_4_60m_0200_0300Z	2	2	60	30-Jun
181	03:00:00	03:59:00	TS-TN	4	JD181_TS_TN_4_60m_0300_0400Z	2	2	60	30-Jun
181	04:00:00	04:59:00	TS-TN	4	JD181_TS_TN_4_60m_0400_0500Z	2	2	60	30-Jun
181	05:00:00	05:59:00	TS-TN	4	JD181_TS_TN_4_60m_0500_0600Z	2	2	60	30-Jun
181	06:00:00	06:59:00	TS-TN	4	JD181_TS_TN_4_60m_0600_0700Z	2	2	60	30-Jun
181	07:00:00	07:59:00	TS-TN	4	JD181_TS_TN_4_60m_0700_0800Z	2	2	60	30-Jun
181	08:00:00	08:59:00	TS-TN	4	JD181_TS_TN_4_60m_0800_0900Z	2	2	60	30-Jun
181	09:00:00	09:59:00	TS-TN	4	JD181_TS_TN_4_60m_0900_1000Z	2	2	60	30-Jun
181	10:00:00	10:59:00	TS-TN	4	JD181_TS_TN_4_60m_1000_1100Z	2	2	60	30-Jun

Day in the year	*Start time*	*End time*	*Station or Line Name*	*Program*	*Folder Name*	*Ship Speed (kts)*	*DAC Gain*	*Depth (m)*	*Calendar date*
181	11:00:00	11:59:00	TS-TN	4	JD181_TS_TN_4_60m_1100_1200Z	2	2	60	30-Jun
181	12:00:00	12:59:00	TS-TN	4	JD181_TS_TN_4_60m_1200_1300Z	2	2	60	30-Jun
181	13:00:00	13:59:00	TS-TN	4	JD181_TS_TN_4_60m_1300_1400Z	2	2	60	30-Jun
181	14:00:00	14:59:00	TS-TN	4	JD181_TS_TN_4_60m_1400_1500Z	2	2	60	30-Jun
181	15:00:00	15:59:00	TS-TN	4	JD181_TS_TN_4_60m_1500_1600Z	2	2	60	30-Jun
181	16:00:00	16:59:00	TS-TN	4	JD181_TS_TN_4_60m_1600_1700Z	2	2	60	30-Jun
181	17:00:00	17:59:00	TS-TN	4	JD181_TS_TN_4_60m_1700_1800Z	2	2	60	30-Jun
181	18:00:00	18:59:00	TS-TN	4	JD181_TS_TN_4_60m_1800_1900Z	2	2	60	30-Jun
181	19:00:00	19:59:00	TS-TN	4	JD181_TS_TN_4_60m_1900_2000Z	2	2	60	30-Jun
181	20:00:00	20:59:00	TS-TN	4	JD181_TS_TN_4_60m_2000_2100Z	2	2	60	30-Jun
181	21:00:00	21:59:00	TS-TN	4	JD181_TS_TN_4_60m_2100_2200Z	2	2	60	30-Jun
181	22:00:00	22:59:00	TS-TN	4	JD181_TS_TN_4_60m_2200_2300Z	2	2	60	30-Jun
181	23:00:00	23:59:00	TS-TN	4	JD181_TS_TN_4_60m_2300_2400Z	2	2	60	30-Jun
182	00:00:00	03:59:00	TN-TNE		JD182_TN_TNE_NoChroma_0000_0400Z	6	0	60	1-Jul
182	04:00:00	04:59:00	TNE-TSW	4	JD182_TNE_TSW_4_60m_0400_0500Z	2	2	60	1-Jul
182	05:00:00	05:59:00	TNE-TSW	4	JD182_TNE_TSW_4_60m_0500_0600Z	2	2	60	1-Jul
182	06:00:00	06:59:00	TNE-TSW	4	JD182_TNE_TSW_4_60m_0600_0700Z	2	2	60	1-Jul
182	07:00:00	07:59:00	TNE-TSW	4	JD182_TNE_TSW_4_60m_0700_0800Z	2	2	60	1-Jul
182	08:00:00	08:59:00	TNE-TSW	4	JD182_TNE_TSW_4_60m_0800_0900Z	2	2	60	1-Jul
182	09:00:00	09:59:00	TNE-TSW	4	JD182_TNE_TSW_4_60m_0900_1000Z	2	2	60	1-Jul
182	10:00:00	10:59:00	TNE-TSW	4	JD182_TNE_TSW_4_60m_1000_1100Z	2	2	60	1-Jul
182	11:00:00	11:59:00	TNE-TSW	4	JD182_TNE_TSW_4_60m_1100_1200Z	2	2	60	1-Jul
182	12:00:00	12:59:00	TNE-TSW	4	JD182_TNE_TSW_4_60m_1200_1300Z	2	2	60	1-Jul
182	13:00:00	13:59:00	TNE-TSW	4	JD182_TNE_TSW_4_60m_1300_1400Z	2	2	60	1-Jul
182	14:00:00	14:59:00	TNE-TSW	4	JD182_TNE_TSW_4_60m_1400_1500Z	2	2	60	1-Jul
182	15:00:00	15:59:00	TNE-TSW	4	JD182_TNE_TSW_4_60m_1500_1600Z	2	2	60	1-Jul
182	16:00:00	16:59:00	TNE-TSW	4	JD182_TNE_TSW_4_60m_1600_1700Z	2	2	60	1-Jul
182	17:00:00	17:59:00	TNE-TSW	4	JD182_TNE_TSW_4_60m_1700_1800Z	2	2	60	1-Jul
182	18:00:00	18:59:00	TNE-TSW	4	JD182_TNE_TSW_4_60m_1800_1900Z	2	2	60	1-Jul
182	19:00:00	19:59:00	TNE-TSW	4	JD182_TNE_TSW_4_60m_1900_2000Z	2	2	60	1-Jul
182	20:00:00	20:59:00	TNE-TSW	4	JD182_TNE_TSW_4_60m_2000_2100Z	2	2	60	1-Jul
182	21:00:00	21:59:00	TNE-TSW	4	JD182_TNE_TSW_4_60m_2100_2200Z	2	2	60	1-Jul
182	22:00:00	22:59:00	TNE-TSW	4	JD182_TNE_TSW_4_60m_2200_2300Z	2	2	60	1-Jul
182	23:00:00	23:59:00	TNE-TSW	4	JD182_TNE_TSW_4_60m_2300_2400Z	2	2	60	1-Jul
183	00:00:00	00:59:00	TNE-TSW	4	JD183_TNE_TSW_4_60m_0000_0100Z	2	2	60	2-Jul

Day in the year	*Start time*	*End time*	*Station or Line Name*	*Program*	*Folder Name*	*Ship Speed (kts)*	*DAC Gain*	*Depth (m)*	*Calendar date*
183	01:00:00	01:59:00	TNE-TSW	4	JD183_TNE_TSW_4_60m_0100_0200Z	2	2	60	2-Jul
183	02:00:00	02:59:00	TNE-TSW	4	JD183_TNE_TSW_4_60m_0200_0300Z	2	2	60	2-Jul
183	03:00:00	03:59:00	TNE-TSW	4	JD183_TNE_TSW_4_60m_0300_0400Z	2	2	60	2-Jul
183	04:00:00	04:59:00	TNE-TSW	4	JD183_TNE_TSW_4_60m_0400_0500Z	2	2	60	2-Jul
183	05:00:00	05:59:00	TNE-TSW	4	JD183_TNE_TSW_4_60m_0500_0600Z	2	2	60	2-Jul
183	06:00:00	06:59:00	TNE-TSW	4	JD183_TNE_TSW_4_60m_0600_0700Z	2	2	60	2-Jul
183	07:00:00	07:19:00	TNE-TSW	4	JD183_TNE_TSW_4_60m_0700_0719Z	2	2	60	2-Jul
183	07:19:00	11:24:00	TSW-R1	4	JD183_TSW_R1_4_65m_0719_1124Z	6	2	65	2-Jul
183	11:24:00	11:59:00	R1-R2	4	JD183_R1_R2_4_65m_1124_1200Z	5	2	65	2-Jul
183	12:00:00	12:59:00	R1-R2	4	JD183_R1_R2_4_65m_1200_1300Z	4	2	65	2-Jul
183	13:00:00	13:29:00	R1-R2	4	JD183_R1_R2_4_65m_1300_1330Z	4	2	65	2-Jul
183	13:30:00	13:59:00	R2-R3	4	JD183_R2_R3_4_65m_1330_1400Z	4	2	65	2-Jul
183	14:00:00	14:59:00	R2-R3	4	JD183_R2_R3_4_65m_1400_1500Z	4	2	65	2-Jul
183	15:00:00	15:25:00	R2-R3	4	JD183_R2_R3_4_65m_1500_1525Z	4	2	65	2-Jul
183	15:25:00	15:59:00	R3-R4	4	JD183_R3_R4_4_65m_1525_1600Z	4	2	65	2-Jul
183	16:00:00	16:59:00	R3-R4	4	JD183_R3_R4_4_65m_1600_1700Z	4	2	65	2-Jul
183	17:00:00	17:40:00	R3-R4	4	JD183_R3_R4_4_65m_1700_1740Z	4	2	65	2-Jul
183	17:40:00	17:59:00	R4-R5	4	JD183_R4_R5_4_65m_1740_1800Z	4	2	65	2-Jul
183	18:00:00	18:59:00	R4-R5	4	JD183_R4_R5_4_65m_1800_1900Z	4	2	65	2-Jul
183	19:00:00	19:30:00	R4-R5	4	JD183_R4_R5_4_65m_1900_1930Z	4	2	65	2-Jul
183	19:30:00	20:00:00	R5-R6	4	JD183_R5_R6_4_65m_1930_2000Z	4	2	65	2-Jul
183	20:00:00	21:00:00	R5-R6	4	JD183_R5_R6_4_65m_2000_2100Z	4	2	65	2-Jul
183	21:00:00	21:30:00	R5-R6	4	JD183_R5_R6_4_65m_2100_2130Z	4	2	65	2-Jul
183	21:30:00	22:00:00	R5-R6	4	JD183_R5_R6_4_65m_2130_2200Z	4	2	65	2-Jul
183	22:00:00	22:59:00	R6-R7	4	JD183_R6_R7_4_65m_2200_2300Z	4	2	65	2-Jul
183	23:00:00	23:59:00	R6-R7	4	JD183_R6_R7_4_65m_2300_2400Z	4	2	65	2-Jul
184	00:00:00	00:59:00	R7-Q1		JD184_R7_Q1_NoChroma_0000_0100Z	6	2	60	3-Jul
184	01:00:00	01:59:00	R7-Q1		JD184_R7_Q1_NoChroma_0100_0200Z	6	2	60	3-Jul
184	02:00:00	02:59:00	R7-Q1		JD184_R7_Q1_NoChroma_0200_0300Z	6	2	60	3-Jul
184	03:52:00	04:21:00	Q1	7	Program7/JD184_Q1_100m_NoChroma	0	2	103	3-Jul
184	04:22:00	05:41:00	Q1	6TX	Program7/JD184_Q1_6tx_gain2p00_100m_run1	0	0	0	3-Jul
184	05:52:00	06:41:00	Q1	6TX_msk	Program7/JD184_Q1_6tx_msk_gain2p00_100m	0	0	0	3-Jul
184	06:52:00	07:21:00	Q1	6TX	Program7/JD184_Q1_6tx_gain2p00_100m_run2	0	0	2	3-Jul
184	07:25:00	07:41:00	Q1	CW_51	Program7/Tests_to_determine_sc_ampl_gain/Phase_I_adjusting_gains/Test1_CW_51_15	0	0	2	3-Jul

Day in the year	*Start time*	*End time*	*Station or Line Name*	*Program*	*Folder Name*	*Ship Speed (kts)*	*DAC Gain*	*Depth (m)*	*Calendar date*
184	07:45:00	07:58:00	Q1	CW_38	Program7/Tests_to_determine_sc_ampl_gain/Phase_I_adjusting_gains/Test1_CW_38_75	0	0	2	3-Jul
184	08:02:00	08:19:00	Q1	CW_25	Program7/Tests_to_determine_sc_ampl_gain/Phase_I_adjusting_gains/Test1_CW_25_575	0	0	2	3-Jul
184	08:22:00	08:30:00	Q1	CW_19	Program7/Tests_to_determine_sc_ampl_gain/Phase_I_adjusting_gains/Test1_CW_19_375	0	0	2	3-Jul
184	08:37:00	09:05:00	Q1	CW_19	Program7/Tests_to_determine_sc_ampl_gain/Phase_II_initial_data_collection/CW/19_375	0	0	2	3-Jul
184	08:37:00	09:05:00	Q1	CW_25	Program7/Tests_to_determine_sc_ampl_gain/Phase_II_initial_data_collection/CW/25_575	0	0	2	3-Jul
184	08:37:00	09:05:00	Q1	CW_38	Program7/Tests_to_determine_sc_ampl_gain/Phase_II_initial_data_collection/CW/38_75	0	0	2	3-Jul
184	08:37:00	09:05:00	Q1	CW_51	Program7/Tests_to_determine_sc_ampl_gain/Phase_II_initial_data_collection/CW/51_15	0	0	2	3-Jul
184	08:37:00	09:05:00	Q1	CW_19	Program7/Tests_to_determine_sc_ampl_gain/Phase_II_initial_data_collection/MSEQ/19_375	0	0	2	3-Jul
184	08:37:00	09:05:00	Q1	CW_25	Program7/Tests_to_determine_sc_ampl_gain/Phase_II_initial_data_collection/MSEQ/25_575	0	0	2	3-Jul
184	08:37:00	09:05:00	Q1	CW_38	Program7/Tests_to_determine_sc_ampl_gain/Phase_II_initial_data_collection/MSEQ/38_75	0	0	2	3-Jul
184	08:37:00	09:05:00	Q1	CW_51	Program7/Tests_to_determine_sc_ampl_gain/Phase_II_initial_data_collection/MSEQ/51_15	0	0	2	3-Jul
184	10:24:00	10:30:00	Q1	CW_51	Program7/Tests_to_determine_sc_ampl_gain/Phase_IIa_visual_inspection_CW_51_15_Hz_timing_error	0	0	2	3-Jul
184	10:52:00	11:18:00	Q1	7a	Program7/Transmissions/JD184_Q1_7a	0	0	2	3-Jul
184	11:20:00	11:44:00	Q1	7aMSK	Program7/Transmissions/JD184_Q1_7aMSK	0	0	2	3-Jul
184	11:52:00	12:41:00	Q1	7c	Program7/Transmissions/Low_gain/25_575_MSEQ	0	0	2	3-Jul
184	12:52:00	13:24:00	Q1	7b	Program7/Transmissions/JD184_Q1_7b	0	0	2	3-Jul
184	13:28:00	13:32:00	Q1	CW_25	Program7/Tests_to_determine_sc_ampl_gain/Phase_IIb_visual_inspection_CW_25_575_Hz	0	0	2	3-Jul
184	13:45:00	13:48:00	Q1	CW_19	Program7/Tests_to_determine_sc_ampl_gain/Phase_IIc_visual_inspection_CW_19_375_Hz	0	0	2	3-Jul
184	13:35:00		Q1	CW_25	Program7/Tests_to_determine_sc_ampl_gain/Phase_IId_more_data_collection_to_up_gain/Test5_CW_25_575	0	0	2	3-Jul
184	13:39:00	13:41:00	Q1	MSEQ_25	Program7/Tests_to_determine_sc_ampl_gain/Phase_IId_more_data_collection_to_up_gain/Test5_MSEQ_25_575	0	0	2	3-Jul

OBSANP - Cruise Report

Day in the year	*Start time*	*End time*	*Station or Line Name*	*Program*	*Folder Name*	*Ship Speed (kts)*	*DAC Gain*	*Depth (m)*	*Calendar date*
184	13:53:00		Q1	CW_19	Program7/Tests_to_determine_sc_ampl_gain/Phase_IId_more_data_collection_to_up_gain/Test5_CW_19_375	0	0	2	3-Jul
184	13:56:00	13:59:00	Q1	MSEQ_19	Program7/Tests_to_determine_sc_ampl_gain/Phase_IId_more_data_collection_to_up_gain/Test5_MSEQ_19_375	0	0	2	3-Jul
184	14:10:00	15:16:00	Q1	7d	Program7/Transmissions/JD184_Q1_7d	0	0	2	3-Jul
184	15:18:00	15:51:00	Q1	7b_MSK	Program7/Transmissions/JD184_Q1_7b_MSK	0	0	2	3-Jul
184	15:53:00	16:41:00	Q1	7c_MSK	Program7/Transmissions/JD184_Q1_7c_MSK	0	0	2	3-Jul
184	16:45:00	17:50:00	Q1	7d_MSK	Program7/Transmissions/JD184_Q1_7d_MSK	0	0	2	3-Jul
184	17:52:00	18:42:00	Q1	7c	Program7/Transmissions/JD184_Q1_7c	0	0	2	3-Jul

Table 4-4 Instrument Locations and Depths

This table shows the depths on the seafloor of the Instruments. These depths were derived from the Latitude and Longitude of the sites after being surveyed in. The depths are derived from a bathymetry grid created October 31, 2013.

Instrument	*Latitude*	*Longitude*	*Depth from Grid*	*MB Depth at time of Deployment*	*Difference of Depths*	*Notes*
ODVLA13	33.4200	-137.6793	5047.87	5035.5	-12.37	
LPA	33.4384	-137.6387	5049.12	5033	-16.12	
LPB	33.3887	-137.6550	4995.74	5002	06.26	SAIC-AOG1
LPC	33.3995	-137.7153	4933.4	4922	-11.40	
LPD	33.4497	-137.7025	5046.57	5048	01.43	SAIC-AOG2
SP1	33.4368	-137.6746	5076.43	5084	07.57	HM150
SP2	33.4163	-137.6584	5023.05	5036	12.95	HM151
SP3	33.4029	-137.6832	5004.24	5017	12.76	HM152
SP4	33.4240	-137.6998	5018.24	5023	04.76	HM153
SP5	33.4462	-137.7539	4955.63	4896	-59.63	
SP6	33.4661	-137.8069	5018.23	5003	-15.23	
SP7	33.4861	-137.8576	4024.41	4003	-21.41	HM154
SP8	33.4455	-137.8975	4391.58	4385	-06.58	HM155
11.0kHz	33.4285	-137.6783	5058.15	5051	-07.15	transponder
11.5kHz	33.4149	-137.6679	5069.87	5050.7	-19.17	transponder
12.0kHz	33.4158	-137.6879	5027.24	5014	-13.24	transponder

All depths to seafloor.

Table 4-5 OBS Deployment Specifications.

This Table was provided by Ernie Aaron at sea.

corrected LON	*corrected LAT*	*site*	*depth (m)*	*acoustic*	*logger*	*sensor*	*PS tag time (deployment)*	*corrected LAT*	*corrected LON*	*depth (m)*	*sound velocity*	*survey*	*comment*
-137.63870	33.43840	LPA	5033	24	LP98	10-T240	2013:168:02:38:00.0000016	33.43840	-137.63870	5033	1504	Y	
-137.65500	33.38870	LPB	5002	14	LP82	44-T240	2013:168:03:30:00.0000011	33.38870	-137.65500	5002	1504	Y	SAIC-AOG1
-137.71530	33.39950	LPC	4922	25	LP101	57-T240	2013:168:05:13:59.9999999	33.39950	-137.71530	4922	1503	Y	
-137.70250	33.44970	LPD	5048	23	LP110	36-T240	2013:168:06:00:00.0000012	33.44970	-137.70250	5048	1504	Y	SAIC-AOG2
-137.67460	33.43680	SP1	5084	108	13040	GP42	2013:168:07:55:00.0009095	33.43680	-137.67460	5084	1504	Y	HM150
-137.65840	33.41630	SP2	5036	95	13041	GP47	2013:168:17:54:59.9999050	33.41630	-137.65840	5036	1504	Y	HM151
-137.68320	33.40290	SP3	5017	87	13037	GP36	2013:168:19:20:00.0000538	33.40290	-137.68320	5017	1504	Y	HM152
-137.69980	33.42400	SP4	5023	40	13039	GP01	2013:168:20:45:59.9999770	33.42400	-137.69980	5023	1504	Y	HM153
-137.75390	33.44620	SP5	4896	11	13038	GP24	2013:168:21:35:59.9999714	33.44620	-137.75390	4896	1503	Y	
-137.80690	33.46610	SP6	5003	85	13042	GP40	2013:168:21:59:59.9999787	33.46610	-137.80690	5003	1504	Y	
-137.85760	33.48610	SP7	4003	28	13043	GP57	2013:168:22:39:00.0000022	33.48610	-137.85760	4003	1497	Y	HM154
-137.89750	33.44550	SP8	4385	33	13044	GP51	2013:168:23:19:59.9999241	33.44550	-137.89750	4385	1499	Y	HM155

Table 4-6 Data Channels Summary.

HM Channels

overall channel #	*Serial #*	*Instrument*	*Height above Bottom*	*Depth in meters*	*comments*
1	73	HM, DVLA	987	4061	Shallowest HM on ODVLA13
2	74	HM, DVLA	977	4071	
3	75	HM, DVLA	967	4081	
4	76	HM, DVLA	957	4091	
5	77	HM, DVLA	947	4101	
6	78	HM, DVLA	937	4111	
7	79	HM, DVLA	927	4121	
8	98	HM, DVLA	582	4466	
9	99	HM, DVLA	477	4571	
10	101	HM, DVLA	372	4676	
11	102	HM, DVLA	267	4781	
12	103	HM, DVLA	162	4886	
13	104	HM, DVLA	152	4896	
14	105	HM, DVLA	142	4906	
15	107	HM, DVLA	132	4916	
16	108	HM, DVLA	122	4926	
17	136	HM, DVLA	112	4936	
18	138	HM, DVLA	102	4946	
19	139	HM, DVLA	92	4956	
20	141	HM, DVLA	82	4966	
21	142	HM, DVLA	72	4976	
22	143	HM, DVLA	62	4986	
23	144	HM, DVLA	52	4996	
24	145	HM, DVLA	42	5006	
25	146	HM, DVLA	32	5016	
26	147	HM	22	5026	
27	148	HM	12	5036	Deepest HM on ODVLA13
			Site		
28	150	HM	OBS SP1	5076	
29	151	HM	OBS SP2	5023	
30	152	HM	OBS SP3	5004	
31	153	HM	OBS SP4	5018	
32	154	HM	OBS SP7	4024	
33	155	HM	OBS SP8	4392	
All HMs are processed with PhilSea Transfer Function using the OBSAPS code					

HM_TF_Fix. This adjusts the TF below 2Hz so spectra agree with the OBS hydrophones. There is also a ~2dB difference between HMs and OBS hydrophones

Long Period OBS Channels

overall channel #	*Site*	*Instrument*	*Channel*	*Depth in meters*	*Type*	*comments*
34	LPA	OBS	FH1	5049	Trillium-240	
35	LPA	OBS	FH2	5049	Trillium-240	
36	LPA	OBS	FHZ	5049	Trillium-240	
37	LPA	OBS	EDH	5049	DPG	labeled GDH
38	LPB	OBS	FH1	4996	Trillium-240	
39	LPB	OBS	FH2	4996	Trillium-240	
40	LPB	OBS	FHZ	4996	Trillium-240	
41	LPB	OBS	GDH	4996	DPG	Low by 40dB
42	LPB	OBS	SAIC	4996		
43	LPC	OBS	FH1	4933	Trillium-240	
44	LPC	OBS	FH2	4933	Trillium-240	
45	LPC	OBS	FHZ	4933	Trillium-240	
46	LPC	OBS	GDH	4933	DPG	
47	LPD	OBS	FH1	5047	Trillium-240	
48	LPD	OBS	FH2	5047	Trillium-240	
49	LPD	OBS	FHZ	5047	Trillium-240	
50	LPD	OBS	EDH	5047	DPG	all one number
51	LPD	OBS	SAIC	5047		

Trillium 240s should be processed with the Phil Sea TF at 1000sps. DPGs should be processed with the PhilSea TF at 1000sps. SAICs should be processed with SAIC_TF_new at 1000sps and plotted with code SAIC_TF.Fix. The SAIC hydrophone is supposed to have a flat response from 0.05Hz to 7.5KHz. There seems to be a low cut filter at 5Hz. Curves were adjusted so that SAIC hydrophone data agreed with OBS hydrophone data on a typically noisy day.

Short Period OBS Channels

overall channel #	*Site*	*Instrument*	*Channel*	*Depth in meters*	*Type*	*comments*
52	SP1	OBS	GH1	5076	Sercel L-28	Bad timing????
53	SP1	OBS	GH2	5076	Sercel L-28	Bad timing????
54	SP1	OBS	GHZ	5076	Sercel L-28	Bad timing????
55	SP1	OBS	GDH	5076	HTI-90-U hydrophone	Bad timing????
56	SP2	OBS	GH1	5023	Sercel L-28	
57	SP2	OBS	GH2	5023	Sercel L-28	
58	SP2	OBS	GHZ	5023	Sercel L-28	
59	SP2	OBS	GDH	5023	HTI-90-U hyd	spikes in the ambient noise but time compresses OK
60	SP3	OBS	GH1	5004	Sercel L-28	
61	SP3	OBS	GH2	5004	Sercel L-28	
62	SP3	OBS	GHZ	5004	Sercel L-28	
63	SP3	OBS	GDH	5004	HTI-90-U hyd	
64	SP4	OBS	GH1	5018	Sercel L-28	
65	SP4	OBS	GH2	5018	Sercel L-28	
66	SP4	OBS	GHZ	5018	Sercel L-28	
67	SP4	OBS	GDH	5018	HTI-90-U hyd	
68	SP5	OBS	GH1	4956	Sercel L-28	
69	SP5	OBS	GH2	4956	Sercel L-28	
70	SP5	OBS	GHZ	4956	Sercel L-28	
71	SP5	OBS	GDH	4956	HTI-90-U hyd	
72	SP6	OBS	GH1	5018	Sercel L-28	
73	SP6	OBS	GH2	5018	Sercel L-28	
74	SP6	OBS	GHZ	5018	Sercel L-28	
75	SP6	OBS	GDH	5018	HTI-90-U hyd	
76	SP7	OBS	GH1	4024	Sercel L-28	Partial records for only 2 days
77	SP7	OBS	GH2	4024	Sercel L-28	
78	SP7	OBS	GHZ	4024	Sercel L-28	
79	SP7	OBS	GDH	4024	HTI-90-U hyd	
80	SP8	OBS	GH1	4392	Sercel L-28	
81	SP8	OBS	GH2	4392	Sercel L-28	
82	SP8	OBS	GHZ	4392	Sercel L-28	
83	SP8	OBS	GDH	4392	HTI-90-U hyd	
Sercel L-28s and HTI-90-Us should be processed with the Phil Sea TF						

5 Note on Depths

See Section 5 of the OBSAPS cruise report (Stephen *et al.*, 2011) for a discussion of some of the issues involved in determining the depth of sensors. Based on input from Peter Worcester, we assume that the "best" depths are those determined from an amalgamation of multi beam data (from previous cruises as well as our own) that has been edited for "glitches" by Tom Bolmer (see Section 8.6). The latitude and longitude of the DVLA and OBSs is determined by acoustic surveying. Then the "best " depth is given by Tom's multibeam map for that location.

The depths of all of the receivers are given in Table 4-6 based on the multi-beam map dated October 31, 2013. The seafloor depth at the DVLA based on the October 2013 multibeam is 5048m. (The seafloor depth of the DVLA in Table 12-1 was a pre-cruise estimate.) Depths in the OBS deployment section (Table 4-5 and Section 20.5.8) are values read from the multi-beam when the OBSs were dropped. These depths were used to compute the OBS locations from an OBSIP algorithm.

Depth profiles along the radial lines (spokes) are given in Figure 5.1 and Figure 5.2, depth profiles under the four Q-station lines are given in Figure 5.3, and the depth profile under the 250km long line is given in Figure 5.4.

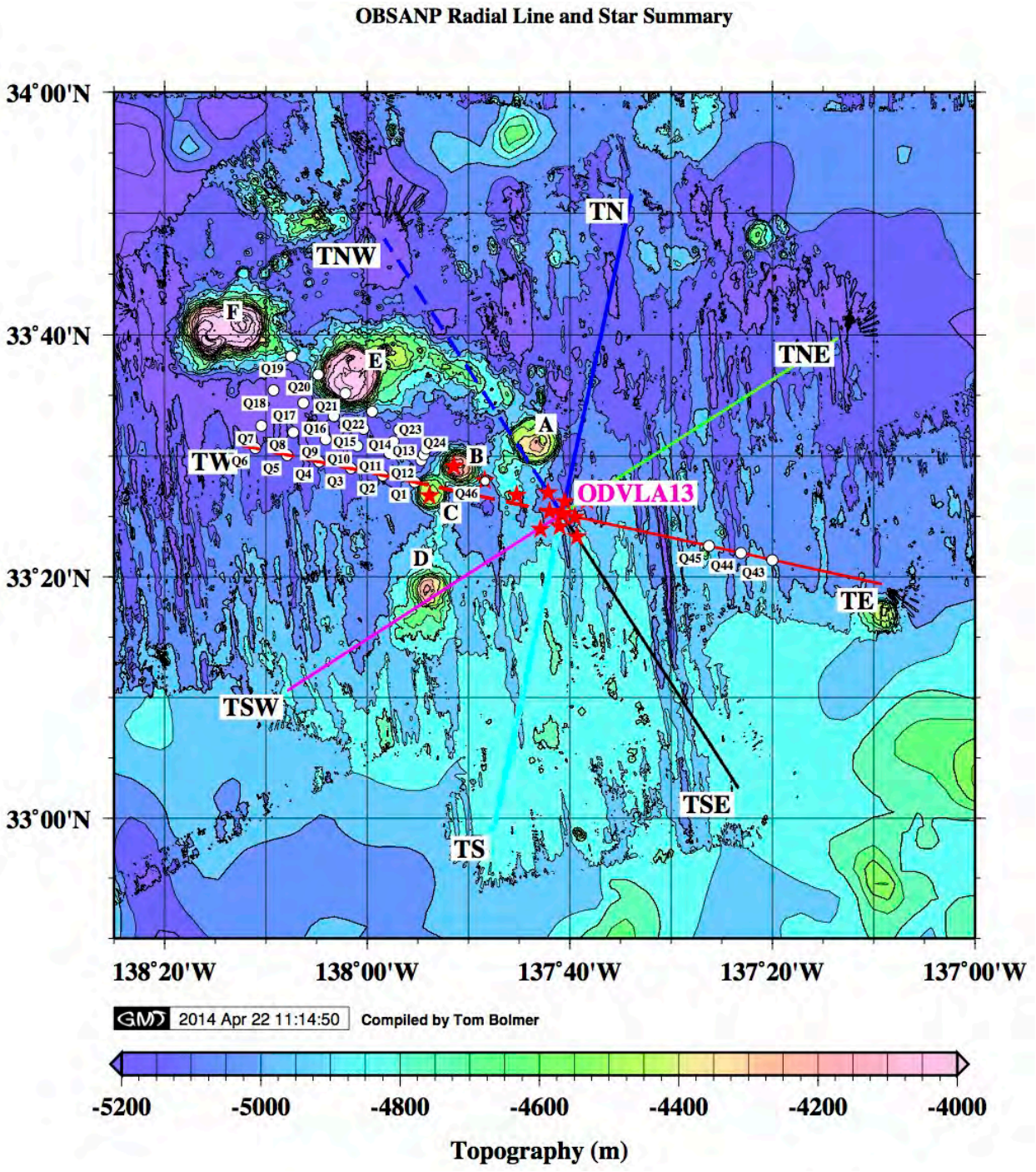

Figure 5.1: Location of Spoke Profiles
The location of the profiles below are shown above with the color of the profiles the same in both figures. The S line has a very faint and hard to see light blue color.

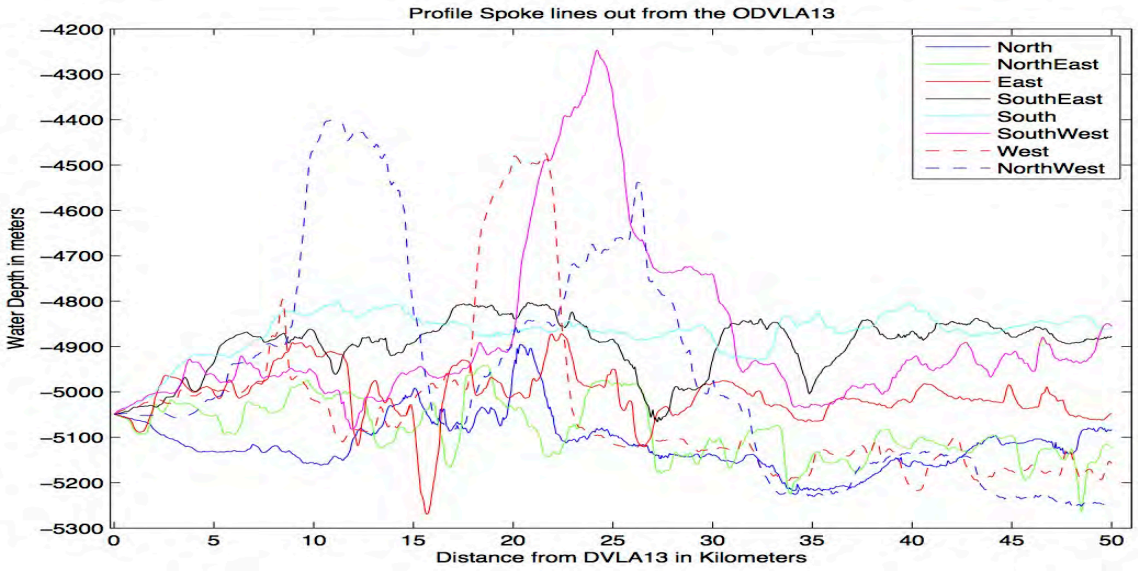

Figure 5.2: Profiles of the Spoke Lines
This shows the profiles of the 8 Spoke lines. The color key as the same for both figures.

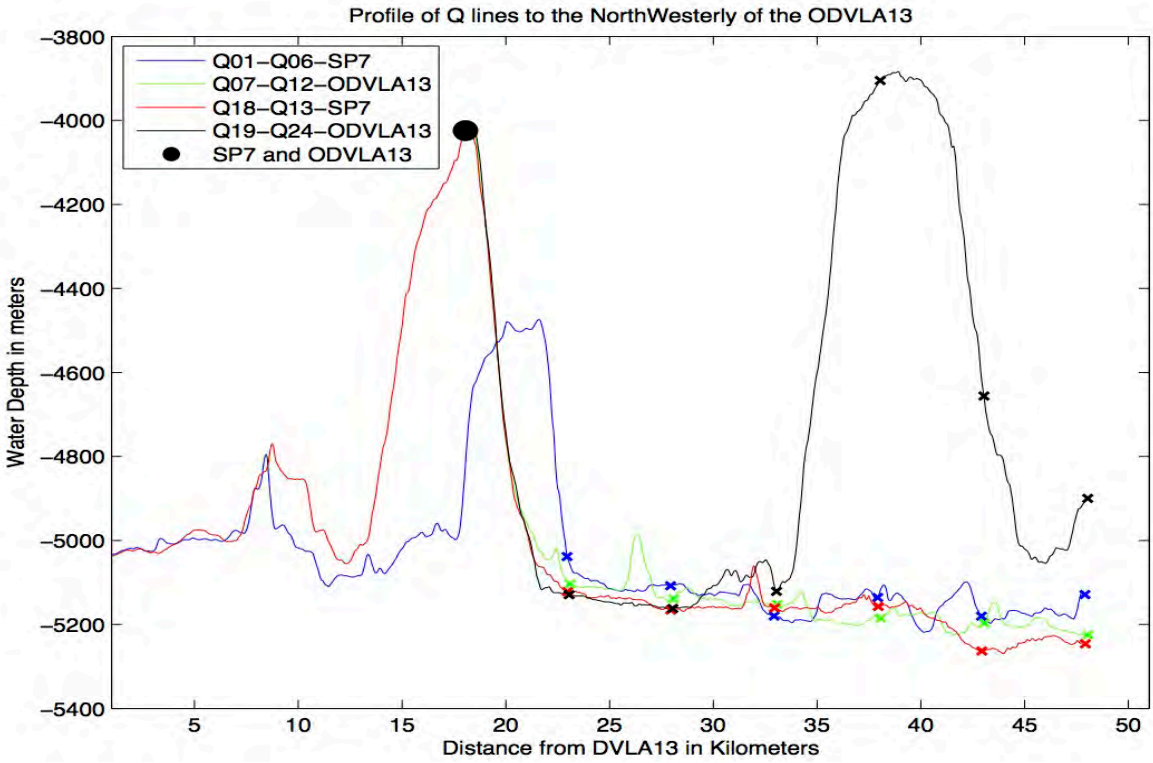

Figure 5.3: Profile of 4 Q station stop lines
This shows the profiles of the 4 Western Q station stop lines. The profiles are from the ODVLA13 or OBS SP6. Q station locations are shown as Xs.

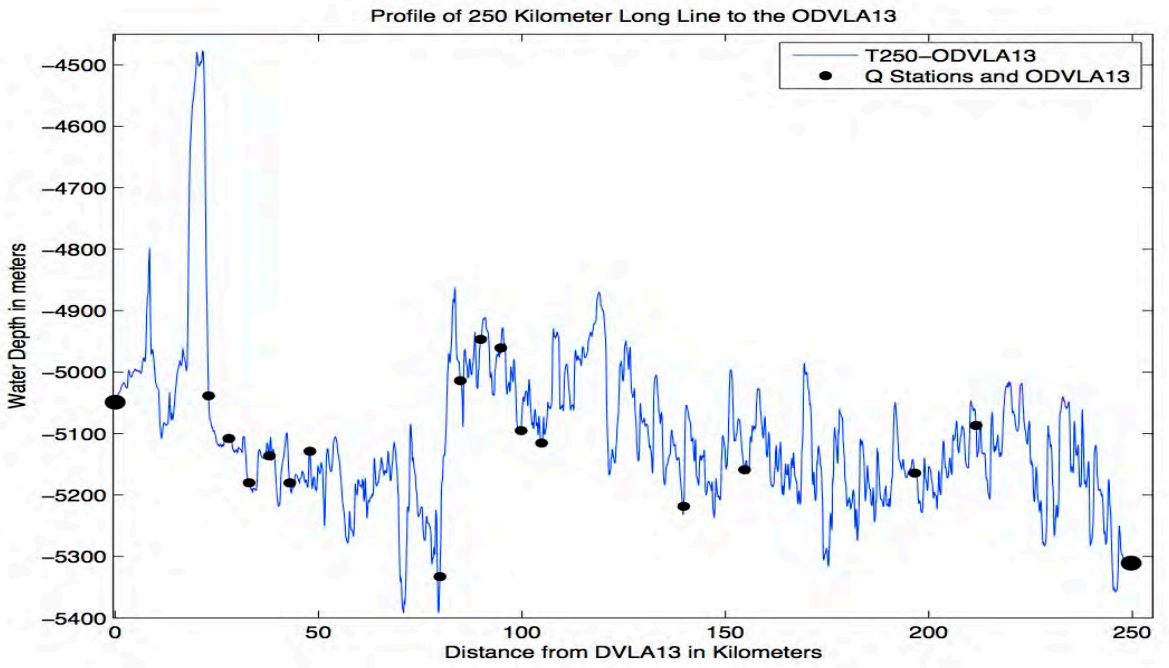

Figure 5.4: Profile of the 250 Km Line
This shows the profile from the ODVLA13 out 250 kilometers to Q station T250. The Q station locations are shown as the smaller dots.

6 OBSANP Signal Menu

Table 6-1 Transmission Signal Characteristics

Program Name	*Cycles per Digit*	*Periods per transmission*	*Carrier Freq*	*Samples per cycle*	*Sampling Freq*	*Digits per Period*	*Samples per digit*	*Samples per period*	*Period duration (sec)*	*Transmission duration (sec)*	*gap (sec)*	*Total Duration (min)*	*Program Number*
4	2	4	77.5	4	310	1023	8	8184	26.4	105.6	14.4	2.0	1
4	4	4	155	4	620	1023	16	16368	26.4	105.6	14.4	2.0	2
4	4	4	310	4	1240	1023	16	16368	13.2	52.8	7.2	1.0	3
5	2	25	77.5	4	310	1023	8	8184	26.4	660.0	0.0	11.0	4
6a	2	37	77.5	4	310	1023	8	8184	26.4	976.8	43.2	17.0	5
6b	2	37	155	4	620	1023	8	8184	13.2	488.4	21.6	8.5	6
6b	2	37	310	4	1240	1023	8	8184	6.6	244.2	25.8	4.5	7
6c	2	37	102.3	4	409.2	1023	8	8184	20.0	740.0	10.0	12.5	8
6c	2	37	204.6	4	818.4	1023	8	8184	10.0	370.0	20.0	6.5	9
7a	2	37	51.15	4	204.6	1023	8	8184	40	1480	0	24.67	10
7b	2	37	38.75	4	155	1023	8	8184	52.8	1953.6	0	32.56	11
7c	2	37	25.575	4	102.3	1023	8	8184	80	2960	0	49.33	12
7d	2	37	19.375	4	77.5	1023	8	8184	105.6	3907.2	0	65.12	13

freq_A2D	1953.125	For HMs	Time series are always downsampled from freq_A2D to Sampling Freq
	1000	For OBSs	

NN_rcvx equals the duration plus some padding, the whole thing delayed for the flight time.

* - Note: Program 7 had MSK formats as well as M-sequences. There was also a 6Tx MSK format. Tom should not try to time compress these.

7 Quick Look Analysis.

7.1 Spectra of Ambient Noise

7.1.1 Spectrograms

Examples of spectrograms are shown in Figure 7.1. Days 170-173 were extremely calm conditions, flat seas with essentially no wind, and this is reflected in the grams. Day 181 was another quiet day. The bar on the right of each gram shows the range from the ODVLA of the Melville (red) and passing ships (blue, from the AIS). On Day 182 a Chinese freighter passed almost directly over the ODVLA and changed course slightly to avoid the Melville. Melville noise seems to be dominantly in the 20-100Hz band. Red bands in the 0.01-0.1Hz band on the SAIC hydrophone are earthquakes.

7.1.2 Percentile Summaries

Summaries of the spectra percentiles are shown in Figure 7.2 through Figure 7.7. Figure 7.2, Figure 7.3 and Figure 7.4 show 50%, 5% and 95% curves for all of the hydrophone elements. Figure 7.5, Figure 7.6 and Figure 7.7 show 50%, 5% and 95% curves for the vertical component of all of the geophone elements.

At the 5th percentile level the SAIC hydrophones were up to 10dB quieter than the OBS hydrophones (OBSIP, Babcock) and OBS hydrophone modules (HMs, Worcester) from 3Hz to 15Hz (Figure 7.3). At the beginning of the deployment we did have a few days of extremely quiet sea state. In the 15Hz to 300Hz band, however, the SAIC hydrophones are up to 10dB “noisier" than the quietest OBS hydrophones and HMs. In this band there seem to be two populations of sensors: a quiet group of some OBS hydrophones and HMs and a noisy group of some OBS hydrophones and HMs plus the SAIC hydrophones. There might be something about the location of the sensors that explains the two different noise fields in this band.

7.2 Transfer Functions

The OBSANP spectra in Section 7.1 have some ad hoc adjustments to the transfer functions in order for the results to make sense. Here is a brief overview:

1) The HM transfer function is based on the transfer function that we used for the Phil Sea data (our codes are called RAS_Test_TF.m, spectra_prctile_plot_2_RAS.m and HM_TF_Fix.mat, created September 20, 2013). This uses the HM transfer function that Matt sent us for the Philippine Sea above 2Hz. The HM spectra below 2Hz have been adjusted to agree with the OBS hydrophones. Above 2Hz there is ~2dB difference between the HMs and the OBS hydrophones. Using the distributed transfer functions from Matt and Jeff, the OBS hydrophone spectra are quieter than the HM spectra by about 2dB at frequencies above 40Hz. It looks like the OBS hydrophones have included the desensitivity of the HTI-90-U's with depth (~5000m) and the HMs did not.

2) The values for the DPG on LPB are ~40dB quieter than the values for the DPG on LPA and LPC. We just added 40dB to the LPB spectra. The values for the DPG on LPD are all the same number (i.e. N/G). DPGs were processed with the same transfer function (from Jeff) that was used for the Philippine Sea data but the sampling rate was adjusted (1000sps).

3) The Trillium 240's were processed with the same transfer function (from Jeff) that was used for the Philippine Sea data but the sampling rate was adjusted (1000sps).

4) The SAIC hydrophone response is supposed to be flat from 0.05Hz to 7.5Hz, but there seems to be a low cut filter at 5Hz. The SAIC transfer function was adjusted so that spectra agreed with the OBS hydrophone data on a typically noisy day. (Our codes are called RAS_Test_SAIC_TF.m, TFOBSANP_SAIC.m and SAIC_TF_Fix.mat)

5) We have had trouble with timing on SP1.

6) The OBS hydrophone on SP2 has spikes in the time series but time compressions seem to work OK.

7) SP7 only returned a couple of days of data.

8) The Sercel L-28's (the geophones on the SP OBSs) and the HTI-90-U's (OBS hydrophones) were processed with the same transfer functions as the Philippine Sea data (from Jeff).

Subsequent to the preparation of these figures (around April 2014) revised transfer function information was received for the OBSs and Hydrophone Modules. This information is in Appendix L and Appendix M, respectively.

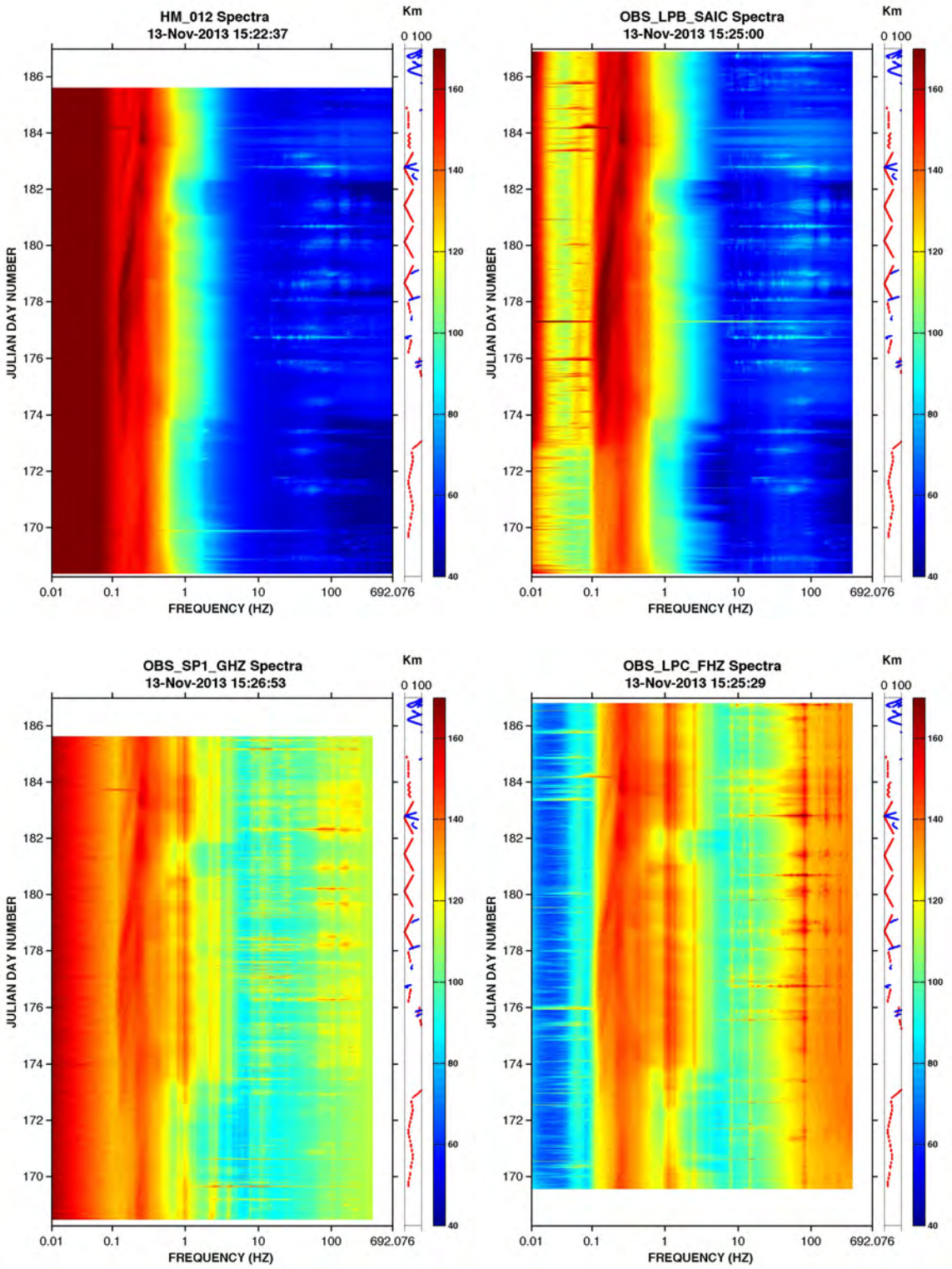

Figure 7.1: Samples of OBSANP Spectrograms
Upper left: ODVLA Hydrophone module 12m above the seafloor [HM_012_Long_spectra.jpg], Upper right: SAIC Hydrophone [OBS_LPB_SAIC_spectra.jpg], Lower left: Short period vertical component [OBS_SP1_GHZ_spectra.jpg], Lower right: Long period vertical component [OBS_LPD_FHZ_spectra.jpg].

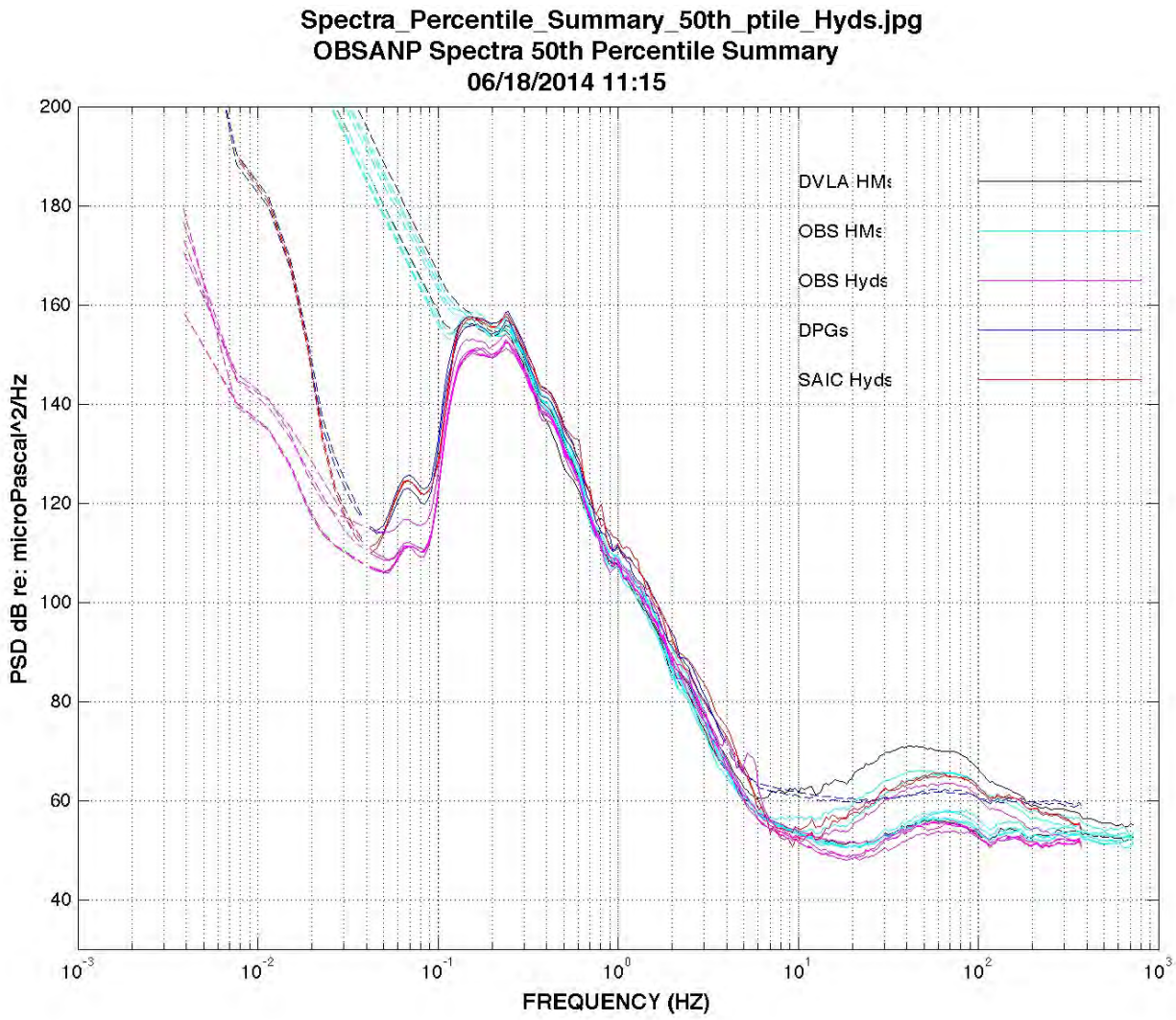

Figure 7.2: Hydrophone Spectra at 50th P-tile
Dashed segments indicate where the spectra are unreliable.

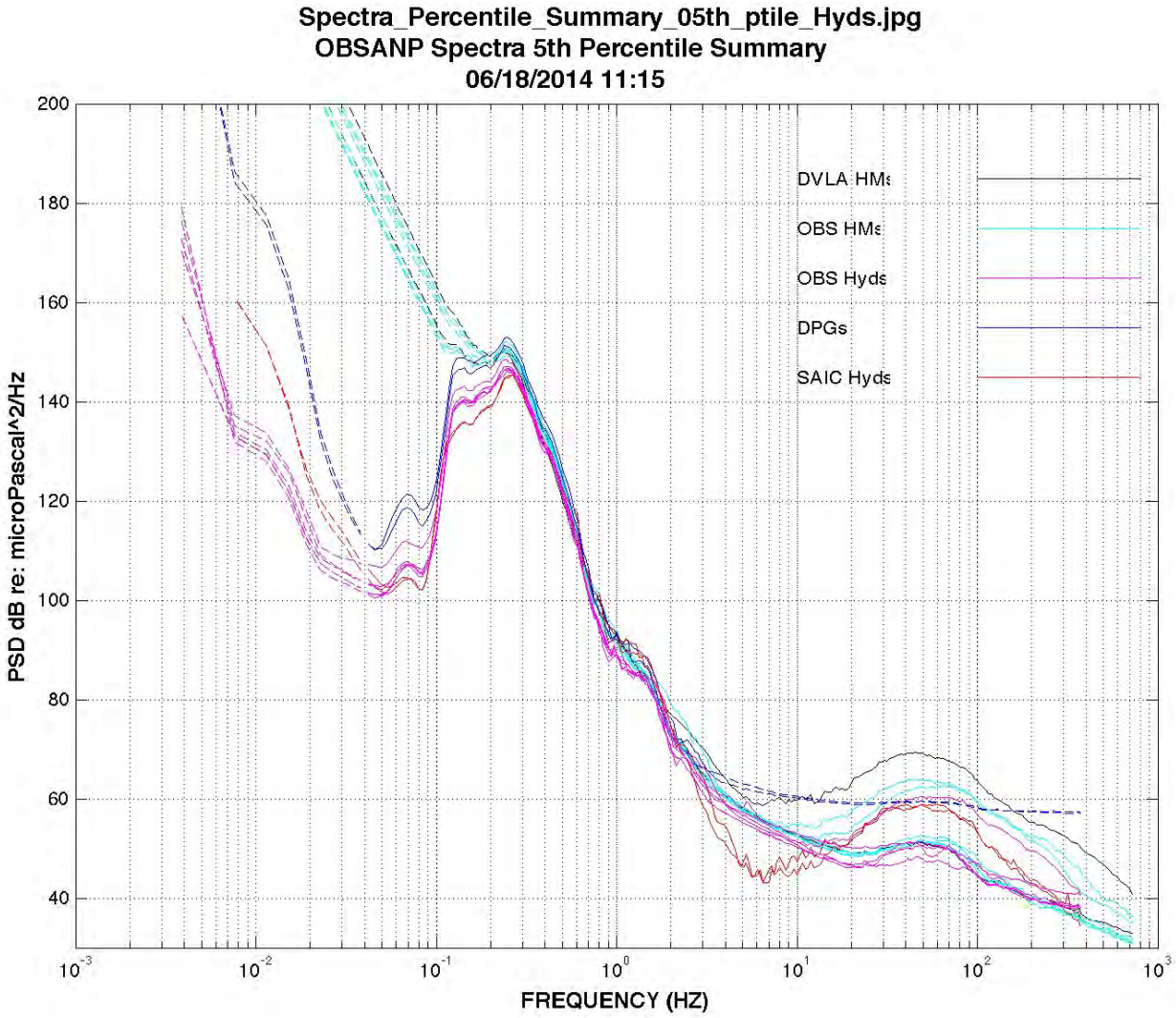

Figure 7.3: Hydrophone Spectra at 5th P-tile

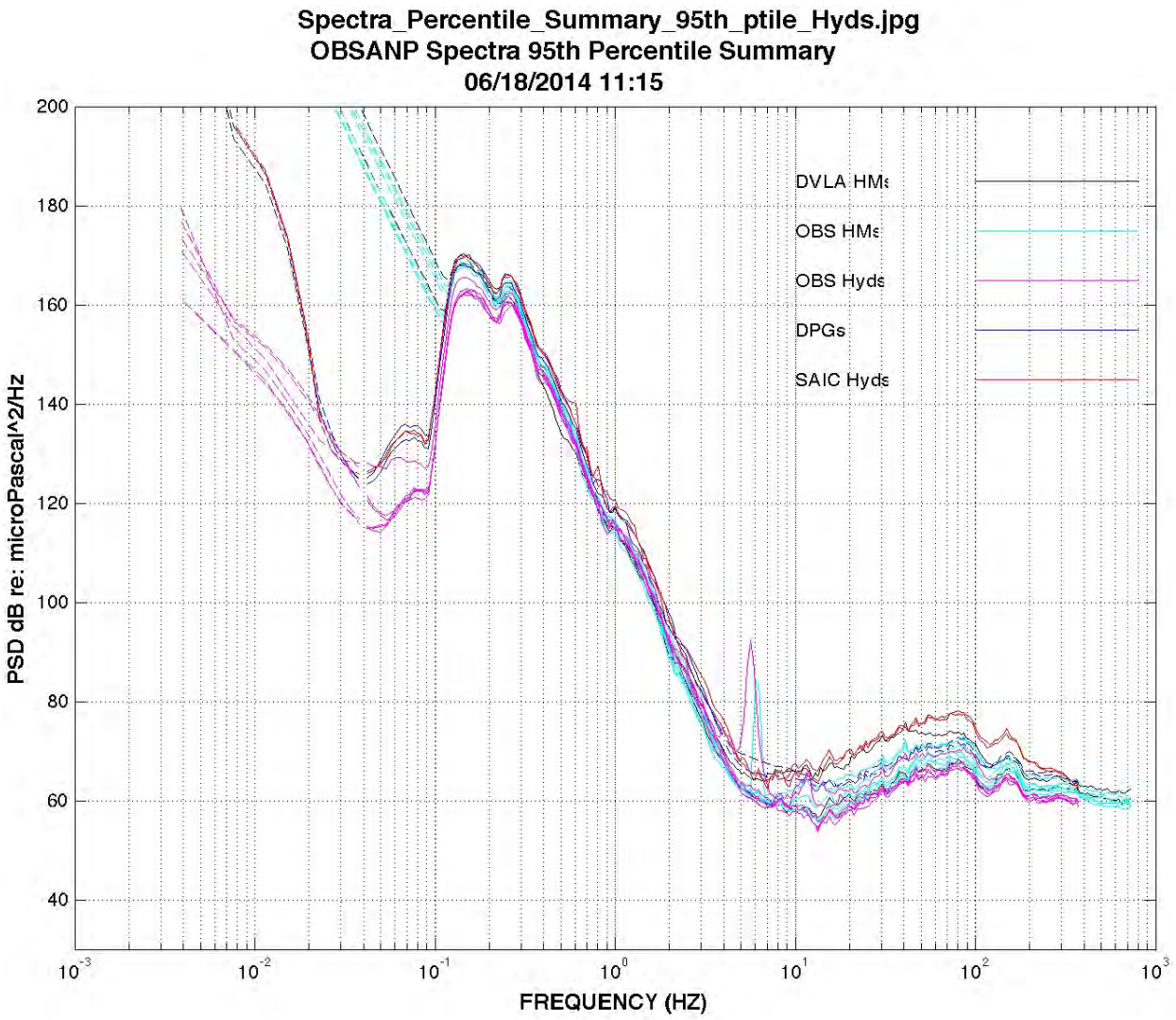

Figure 7.4: Hydrophone Spectra at 95th P-tile

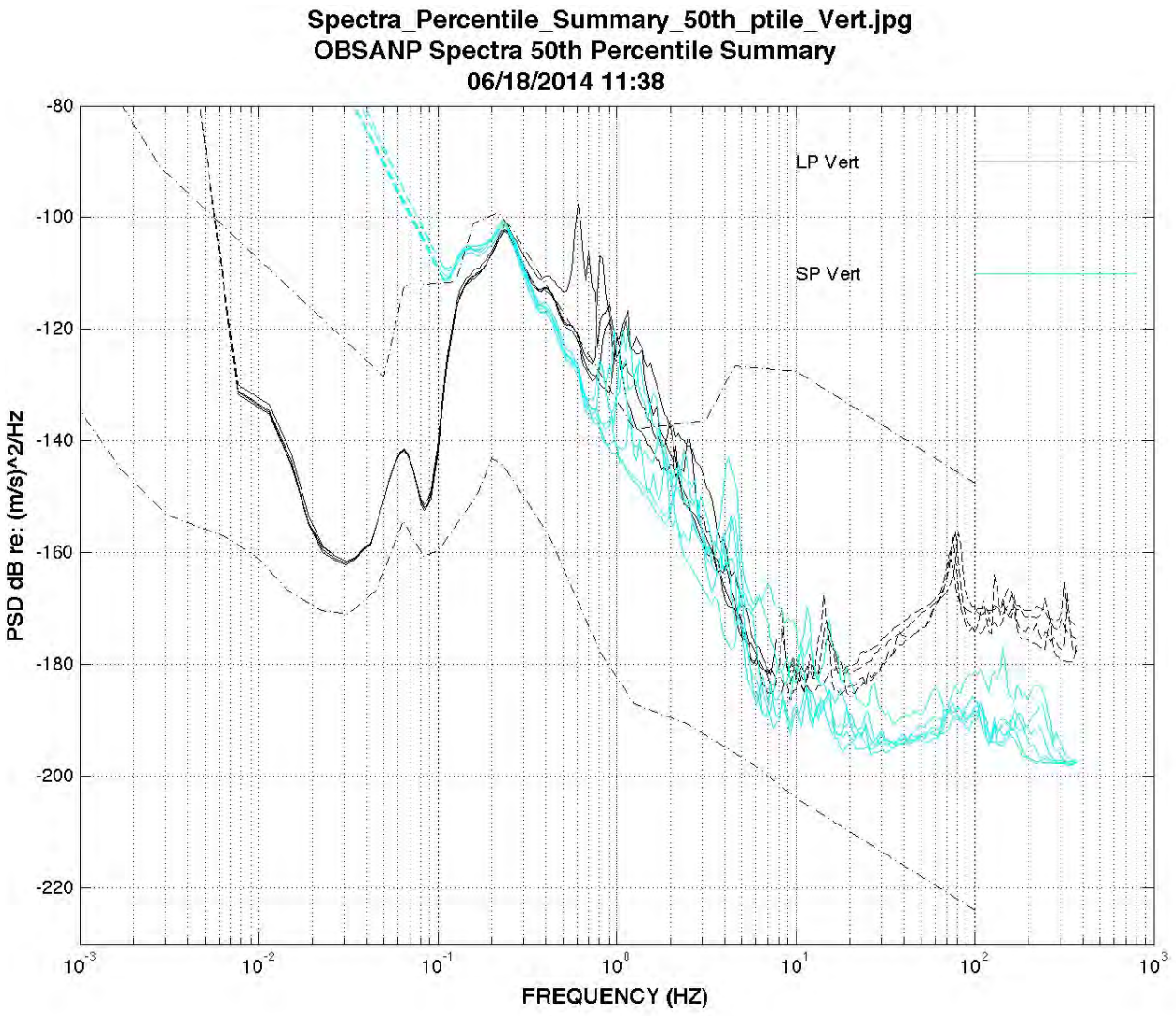

Figure 7.5: Vertical Seismometer Spectra at 50th P-tile

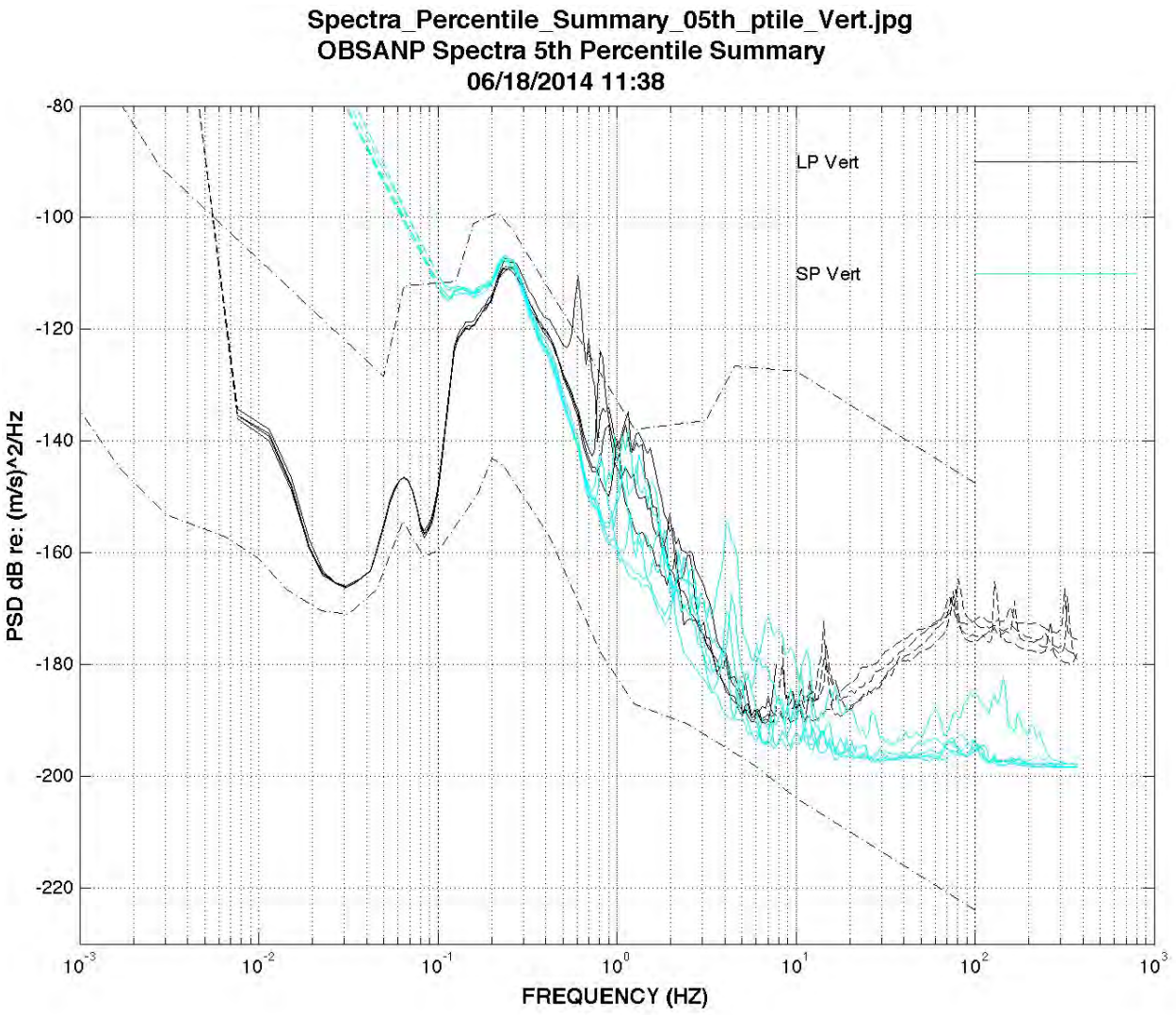

Figure 7.6: Vertical Seismometer Spectra at 5th P-tile

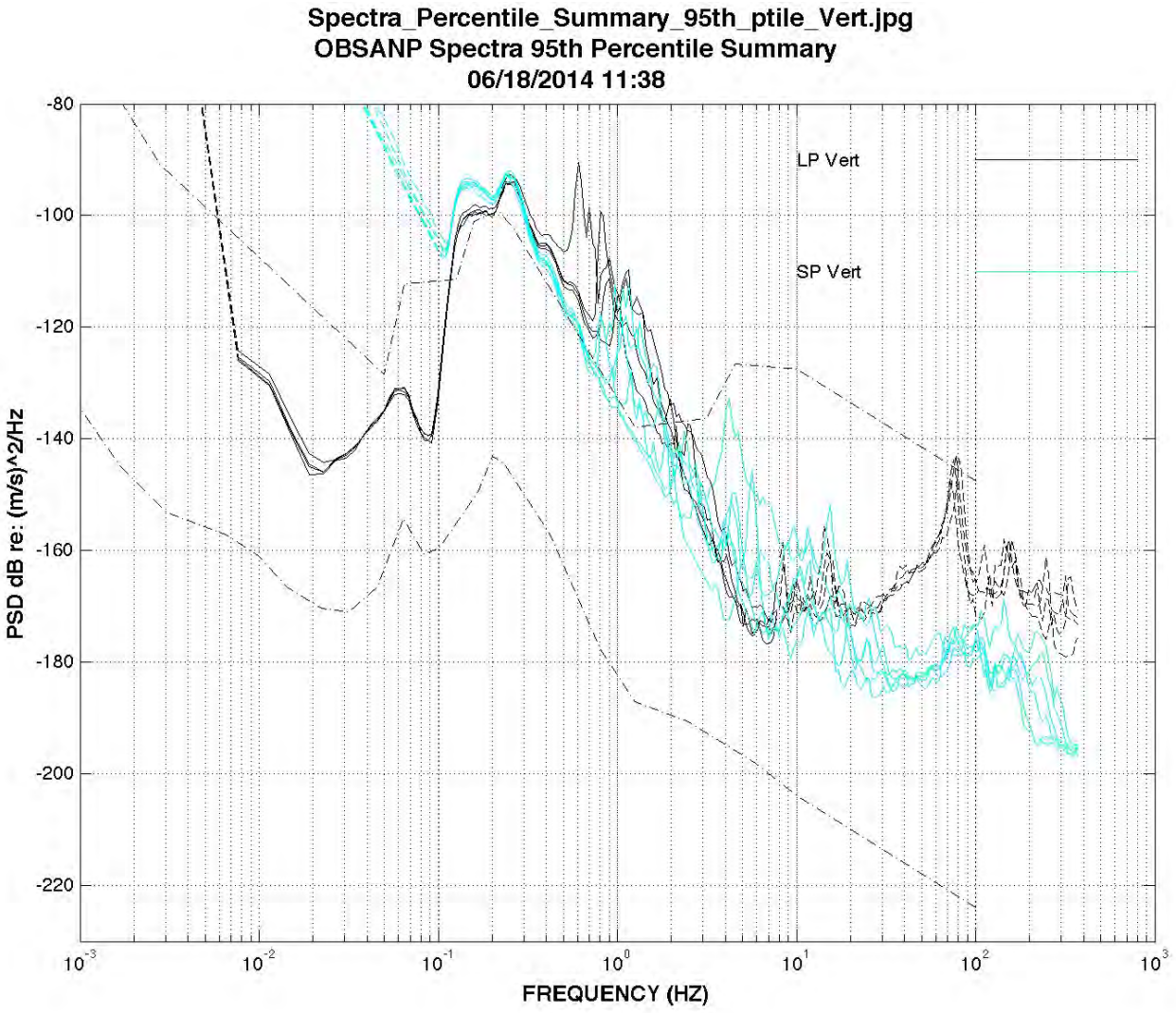

Figure 7.7: Vertical Seismometer Spectra at 95th P-tile

7.3 Controlled Source Transmissions

7.3.1 Pin Cushion

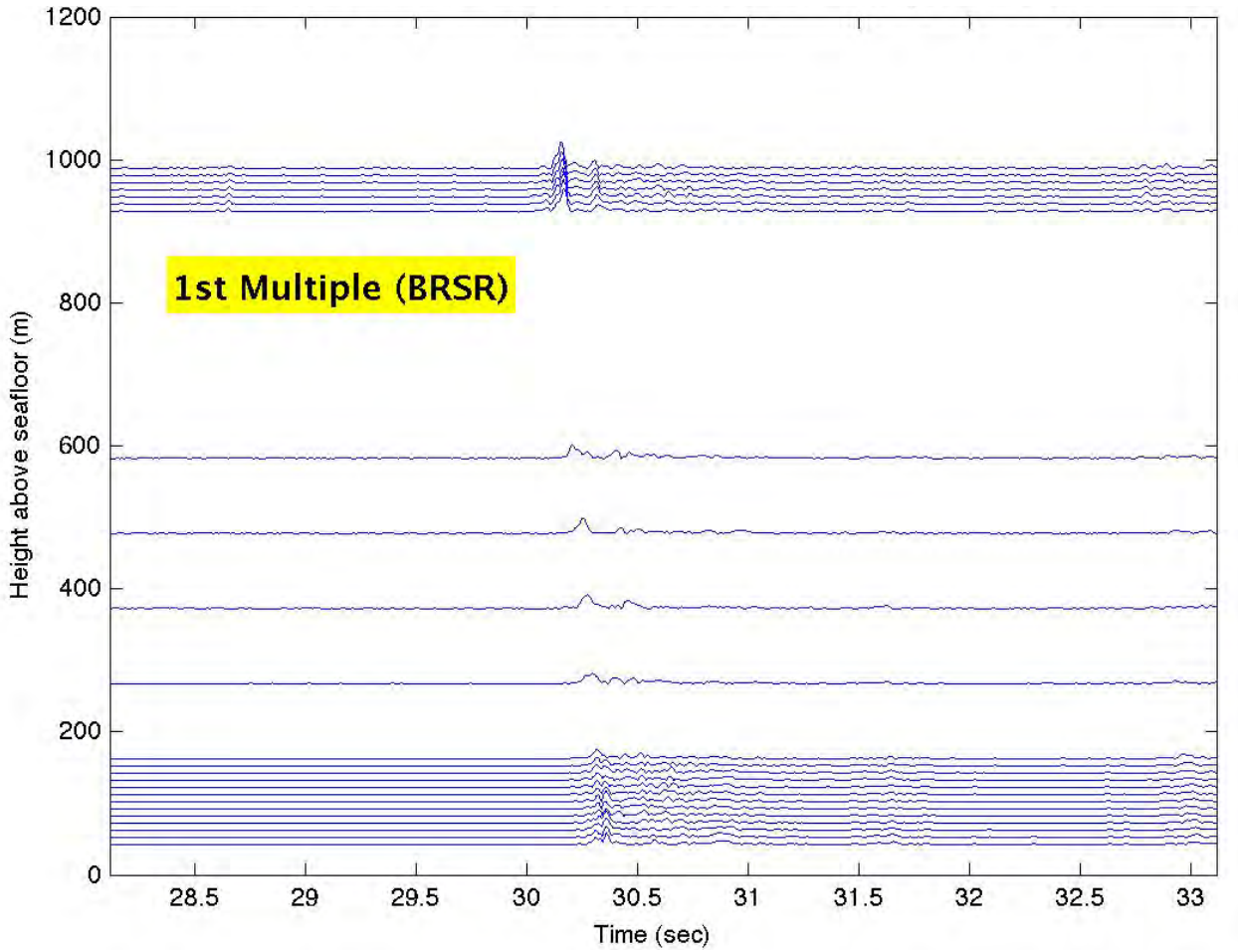

Figure 7.8: DVLA Traces at 43km Range on NPAL04 Geodesic
This example of arrivals on the DVLA for the Station Stop at 43km range along the NPAL04 geodesic shows primarily the BRSR arrival. [ODVLA13_2k_Q05_TS.jpg]

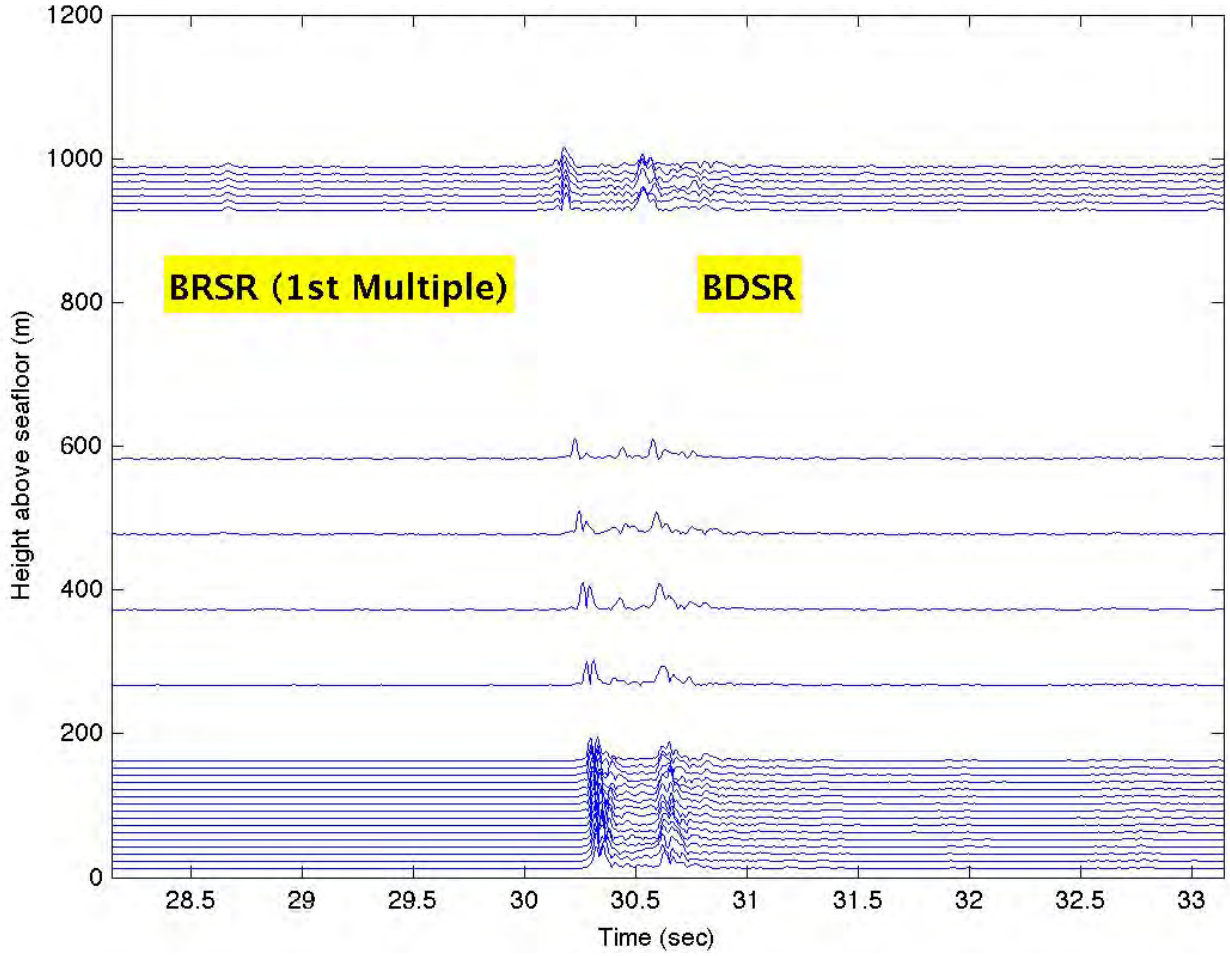

Figure 7.9: DVLA Traces at 43km Range in-line with Seamount B
This example of arrivals on the DVLA for the Station Stop at 43km range in-line with Seamount B shows both BRSR and BDSR arrivals. [ODVLA13_1k_Q17_TS.jpg]

7.3.2 Long Line

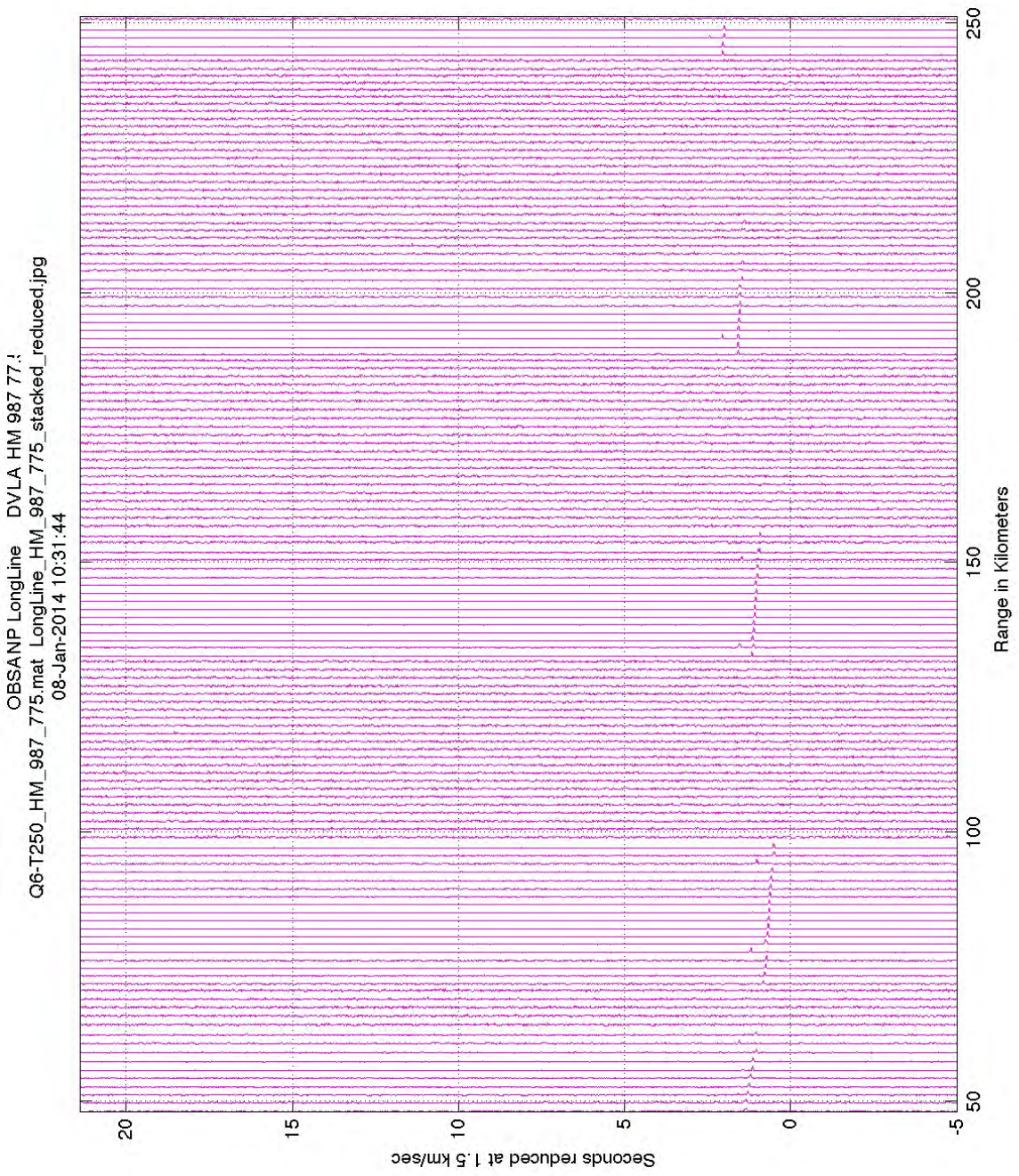

Figure 7.10: Long-line to shallowest HM on DVLA
This figure shows the 77.5Hz time compressed traces as a function of range and reduced time (time-range/1.5) for the long line tow at the shallowest hydrophone module on the DVLA (987m above the seafloor). Transmissions were received above the ambient noise at ranges from 1-1/2CZ (~50-100km), 2-1/2CZ (~140-150km), 3-1/2CZ (190-200km) and 4-1/2CZ (beyond 240km).

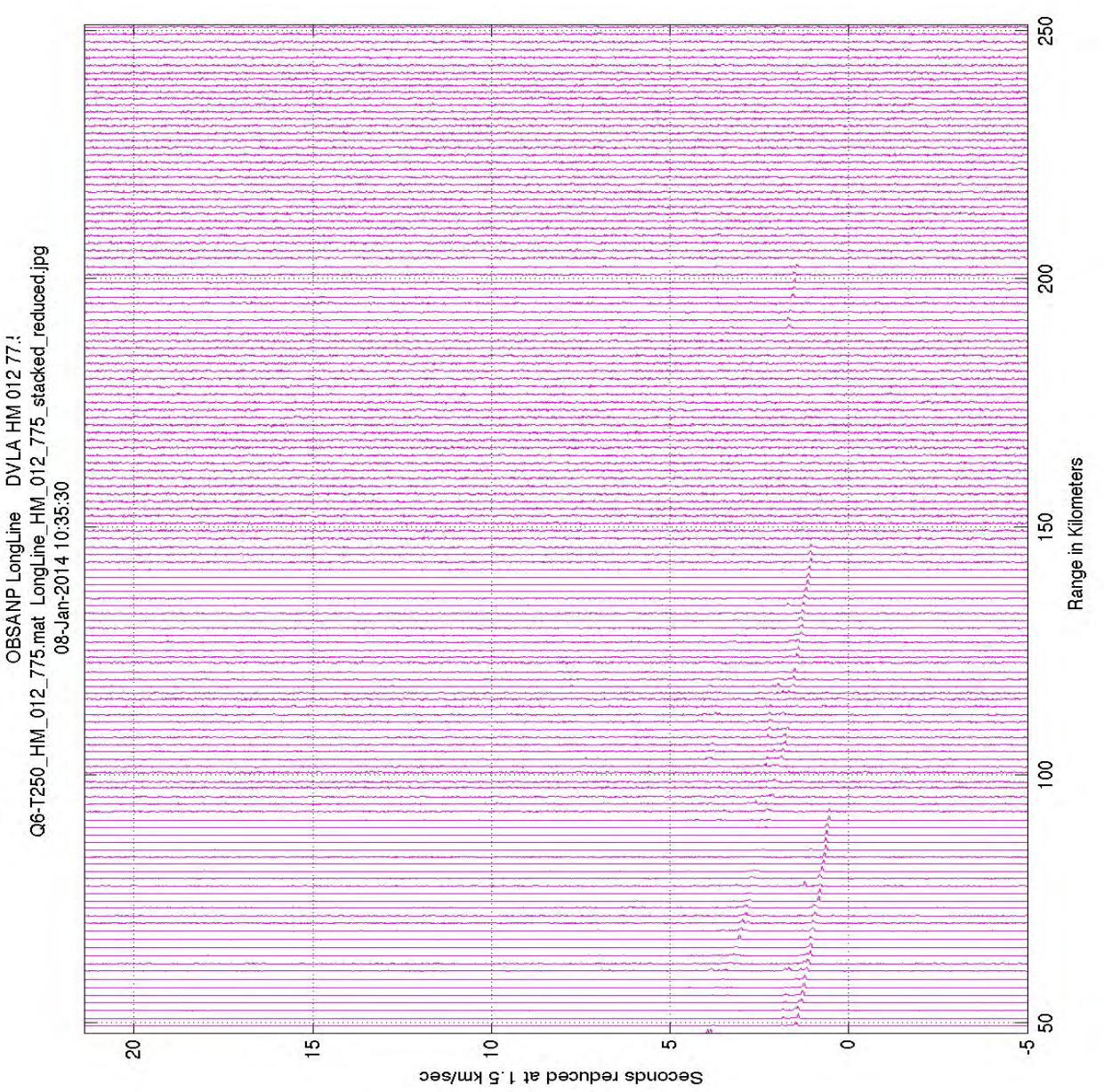

Figure 7.11: Long-line to deepest HM on DVLA
This figure shows the 77.5Hz time compressed traces as a function of range and reduced time (time-range/1.5) for the long line tow at the deepest hydrophone module on the DVLA (12m above the seafloor). Transmissions were received at ranges out to 3-1/2CZ (190-200km).

7.3.3 Radial Line Example

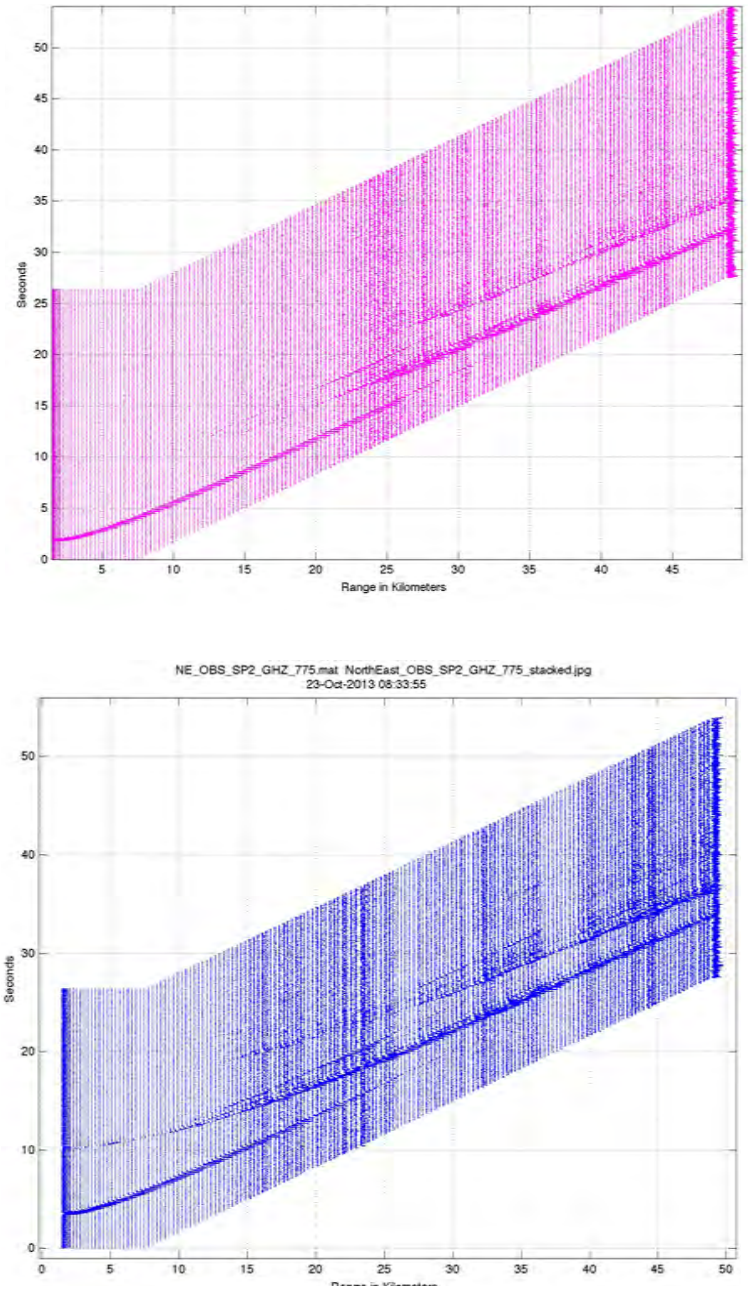

Figure 7.12: 77.5Hz Time Compressions for Northeast Radial Line
Example of 77.5Hz time compressions for transmissions on the Northeast radial line to the hydrophone module (magenta) and vertical geophone (blue) on SP2. Good signal-to-noise is obtained for transmissions out to 50km range. The vertical geophone signals have more structure in the late arrivals than the HM signals. [NE_HM_OBS_SP2_775_stacked.jpg and NorthEast_OBS_SP2_GHZ_775_stacked.jpg]

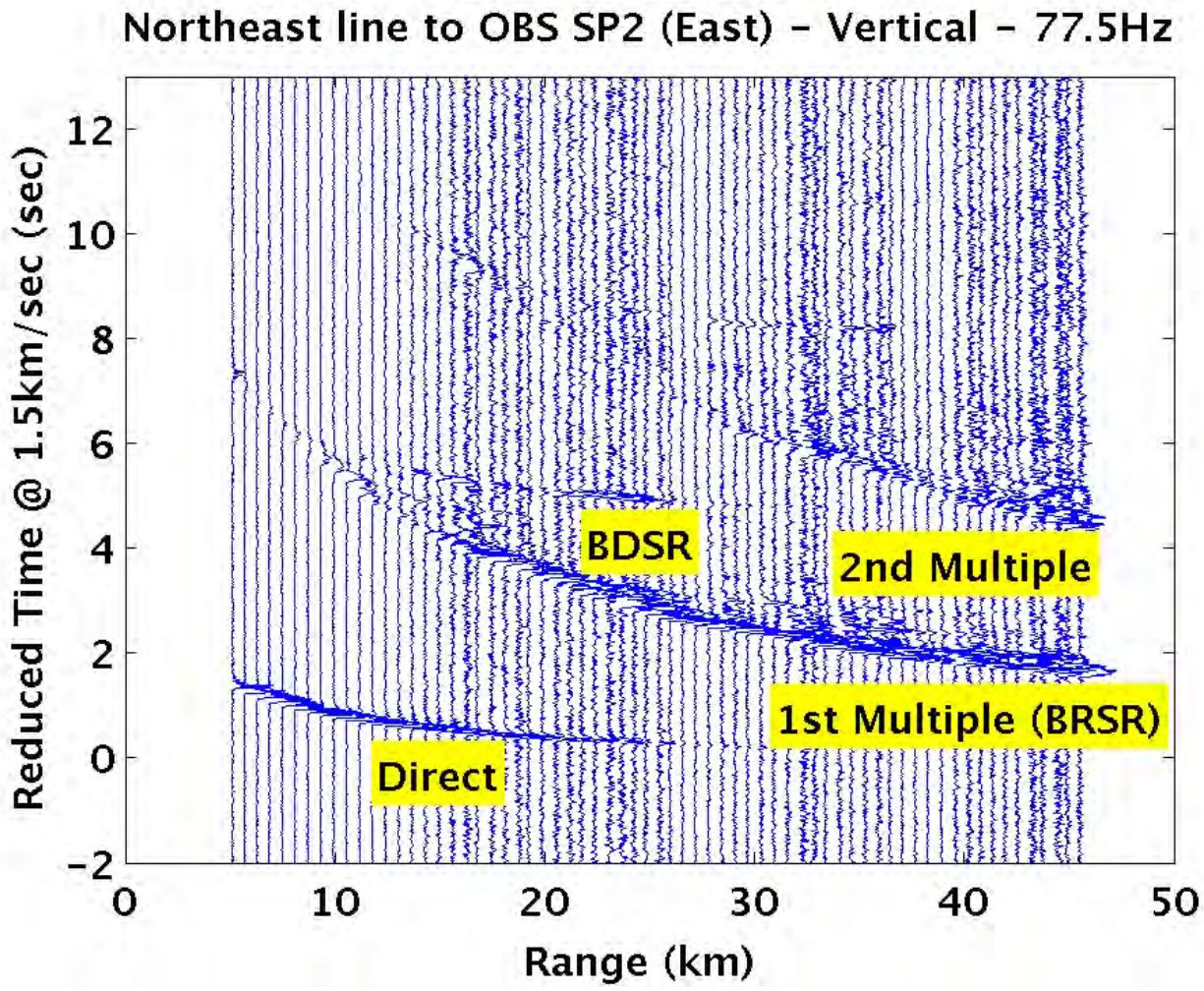

Figure 7.13: Example of 77.5Hz time compressions on the Northeast radial line
Example of 77.5Hz time compressions for transmissions on the Northeast radial line to the vertical geophone on the East OBS (SP2). There is a clear bottom-diffracted surface-reflected (BDSR) arrival occurring after the first multiple and at ranges from 12 to 25km. [NorPac_RT_14_1_SP2_E__1.jpg]

7.3.4 MSK and Low Frequency Tests

Figure 7.14 to Figure 7.17 show examples of receptions at the DVLA from Q1 at frequencies of 19.375, 25.575, 38.75, and 51.15Hz, respectively. The MSK and Low Frequency Tests are described in more detail in Appendices 15 and 16.

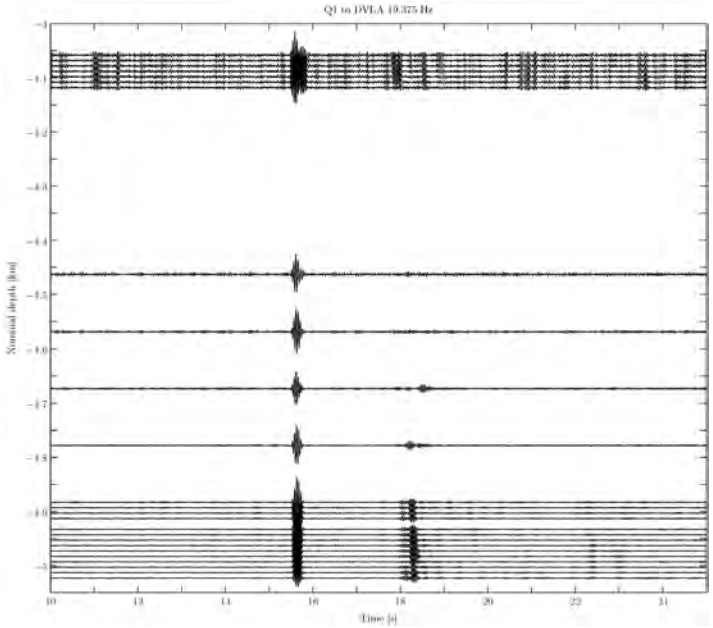

Figure 7.14: Q1 to DVLA at 19.375Hz.
[fig1_Q1_to_DVLA_19_375_Hz.pdf]

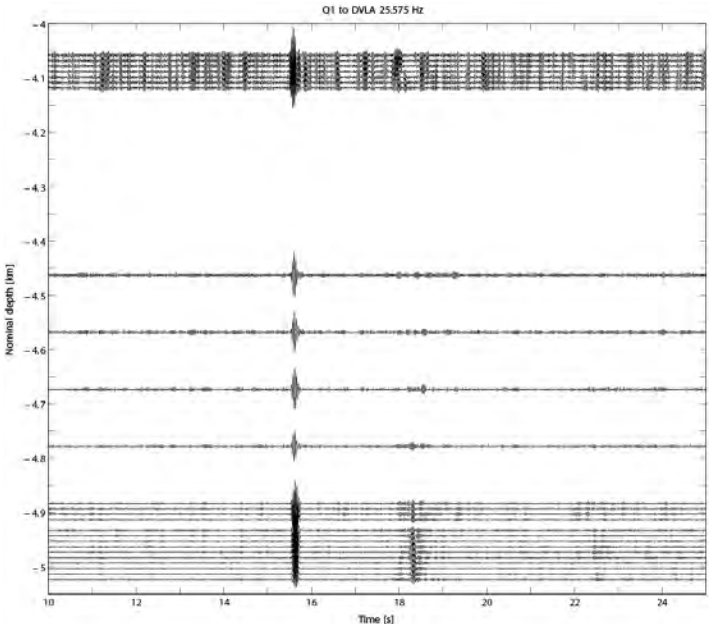

Figure 7.15: Q1 to DVLA at 25.575Hz.
[fig1a_Q1_to_DVLA_25_575_Hz.pdf]

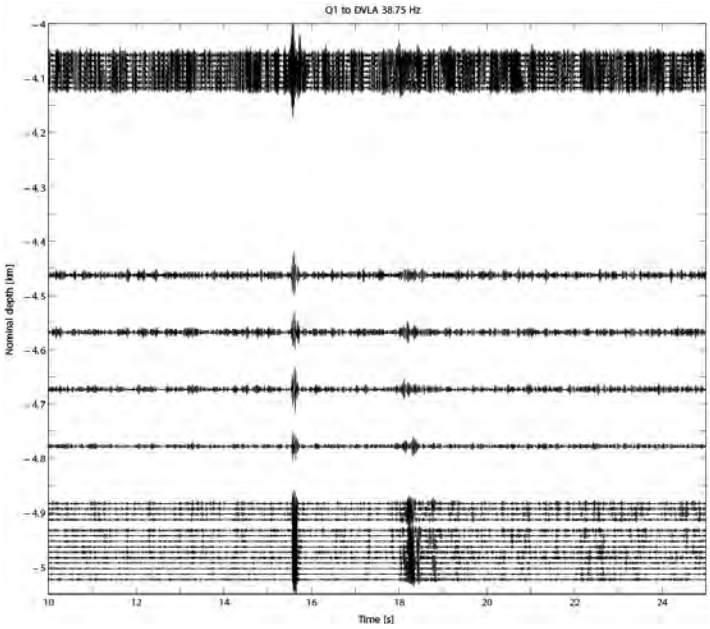

Figure 7.16: Q1 to DVLA at 38.75Hz.
[fig1b_Q1_to_DVLA_38_75_Hz.pdf]

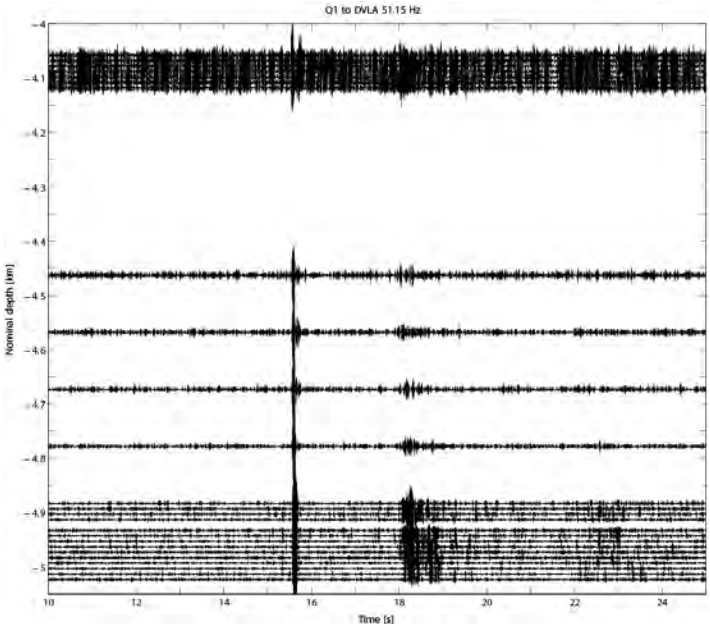

Figure 7.17: Q1 to DVLA at 51.15Hz.
[fig1c_Q1_to_DVLA_51_15_Hz.pdf]

7.3.5 High-Frequency Station Stops

The geophones in the short period OBSs are typically used in the band 5-100Hz for seismic reflection and seismic refraction experiments in the earth's crust. This section shows some examples of time compressed traces from Q1 to the vertical geophone at SP2 with M-sequences from 77.5Hz up to 310Hz (Figure 7.18 to Figure 7.22).

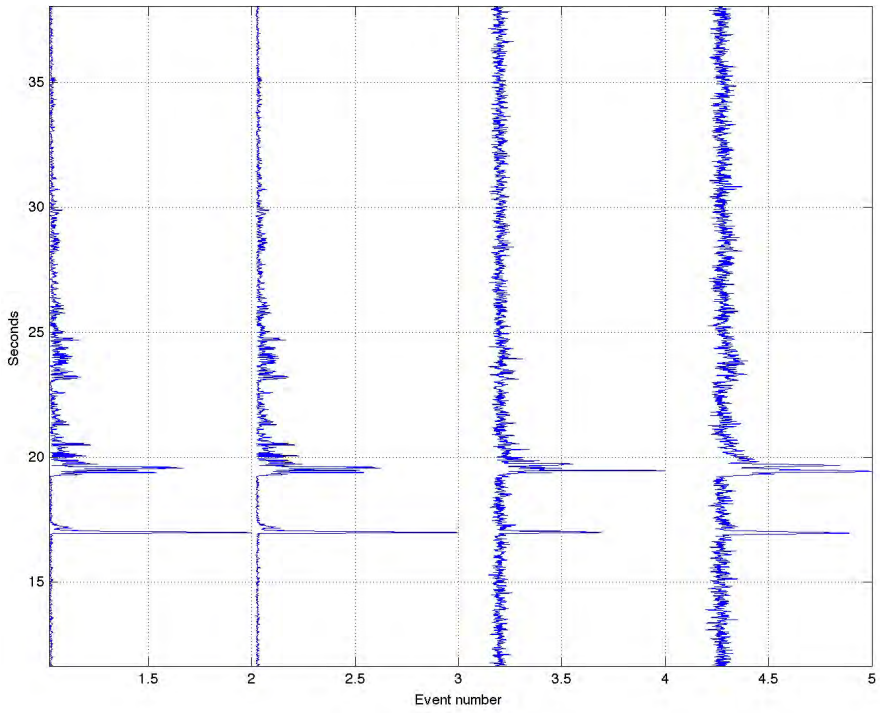

Figure 7.18: Time compressed traces for Q1 to SP2 (vertical component) at 77.5Hz.

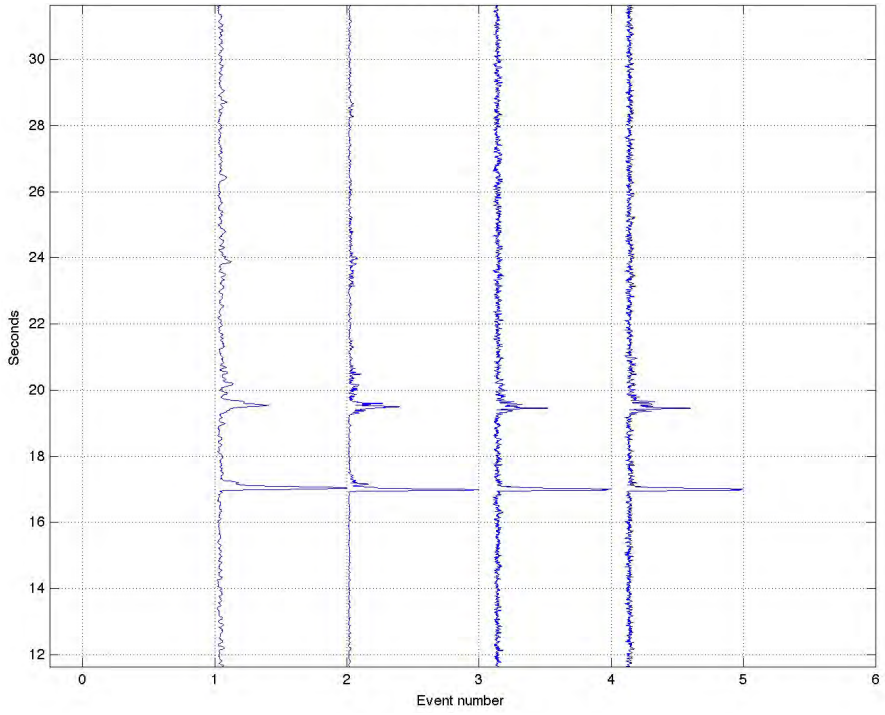

Figure 7.19: Time compressed traces for Q1 to SP2 (vertical component) at 102Hz.

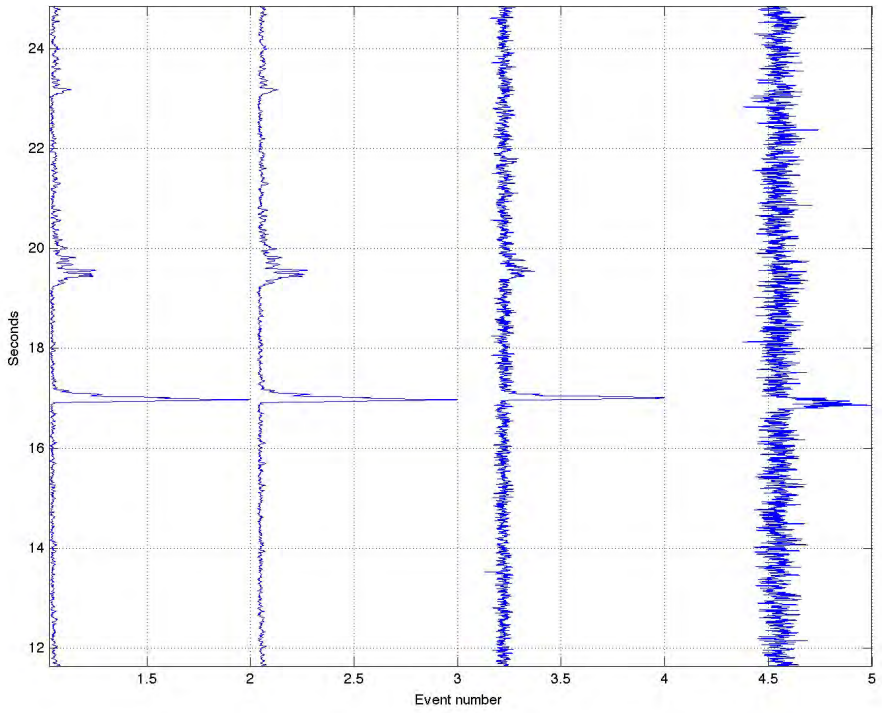

Figure 7.20: Time compressed traces for Q1 to SP2 (vertical component) at 155Hz.

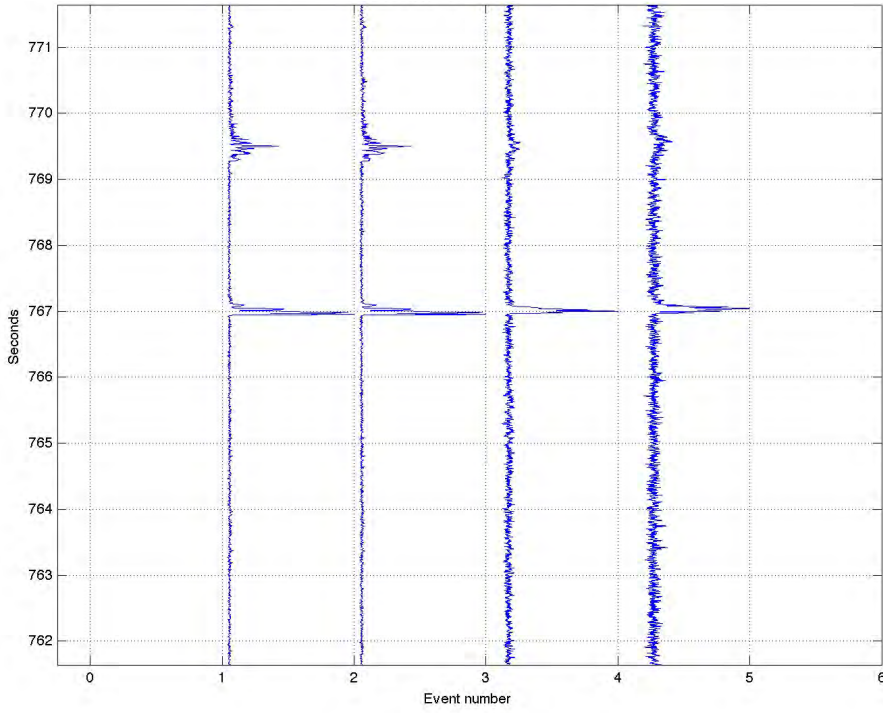

Figure 7.21: Time compressed traces for Q1 to SP2 (vertical component) at 204Hz.

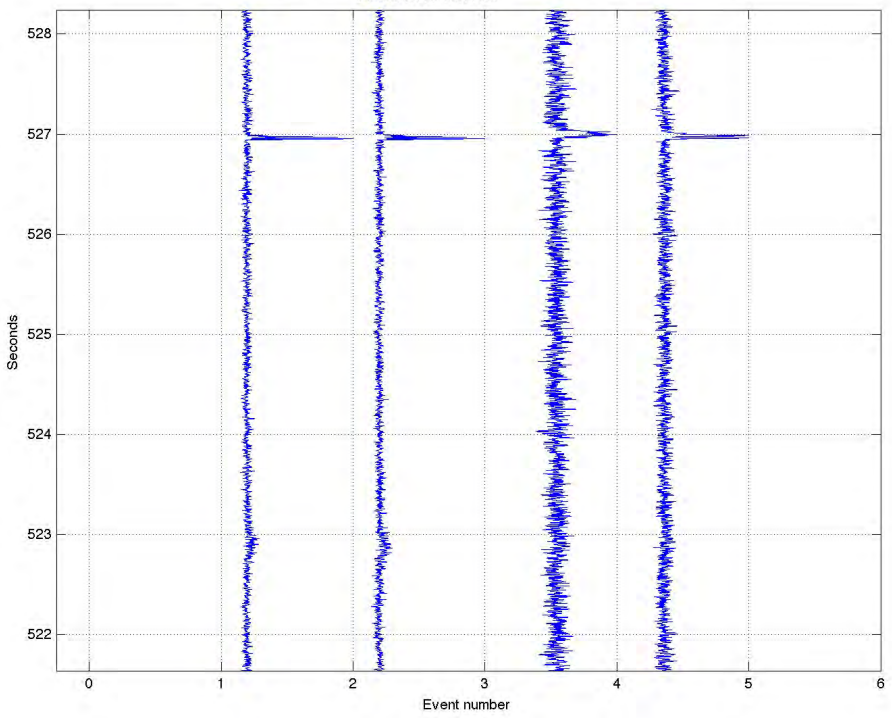

Figure 7.22: Time compressed traces for Q1 to SP2 (vertical component) at 310Hz.

7.3.6 High Frequency Radial Lines

Examples of time-compressed traces for the Northeast radial line to the hydrophone module and vertical component on SP2 and 155Hz and 310Hz M-sequences are shown in Figure 7.23 and Figure 7.24. These are higher frequency versions of Figure 7.12.

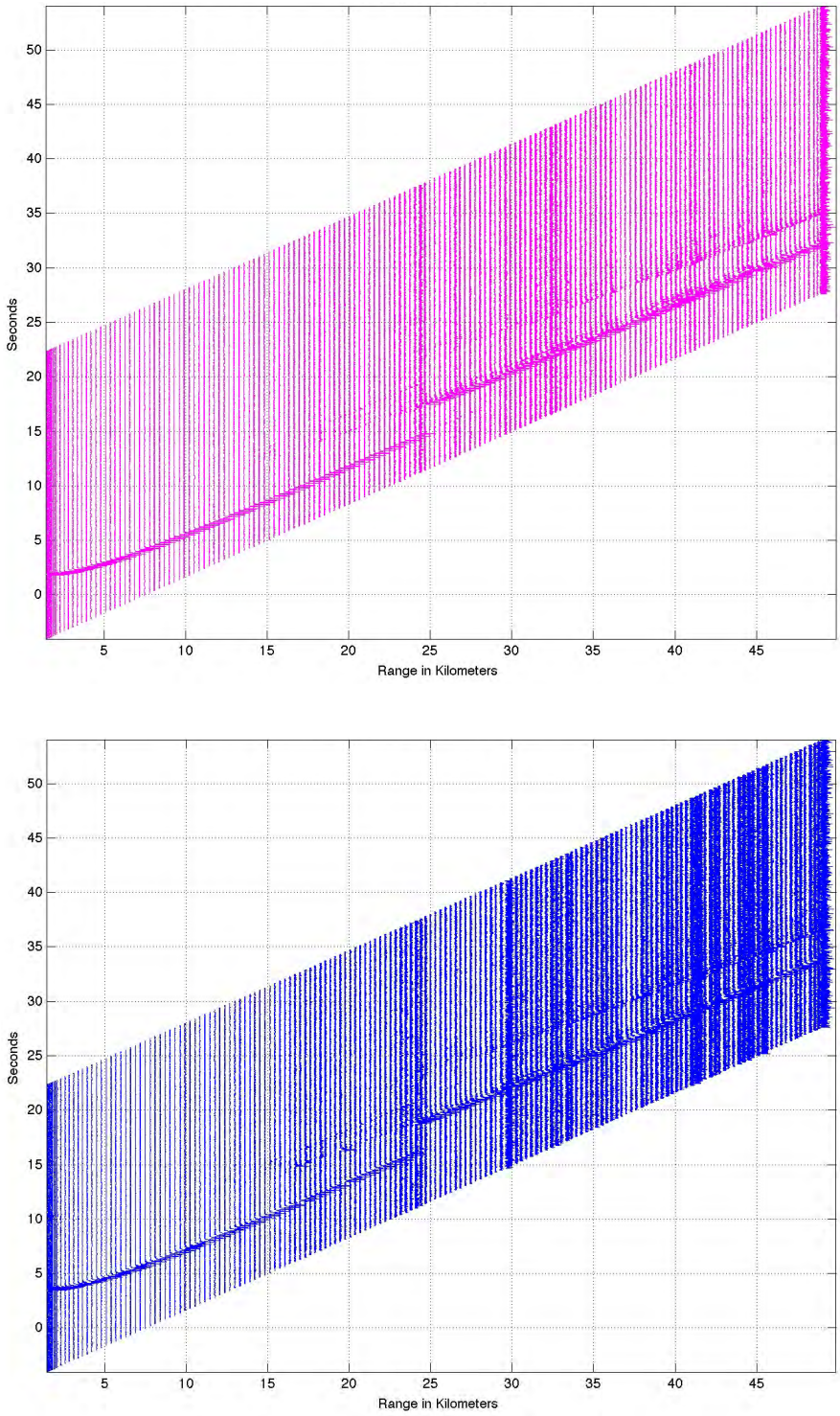

Figure 7.23: 155Hz Time Compressions for Northeast Radial Line
Example of 155Hz time compressions for transmissions on the Northeast radial line to the hydrophone module (magenta) and the vertical geophone (blue) on SP2. Good signal-to-noise is obtained for transmissions out to 50km range.

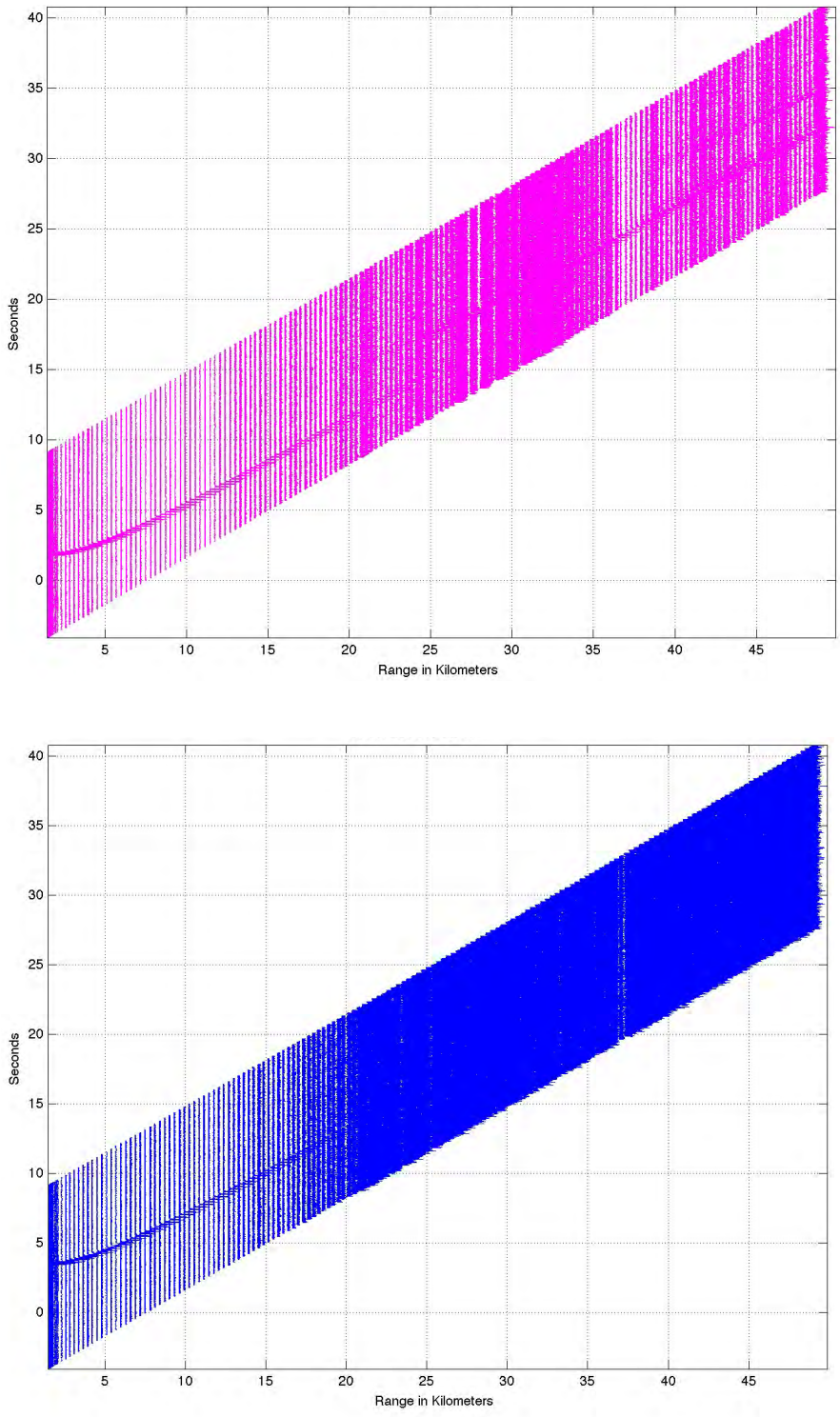

Figure 7.24: 310Hz Time Compressions for Northeast Radial Line
Example of 310Hz time compressions for transmissions on the Northeast radial line to the hydrophone module (magenta) and the vertical geophone (blue) on SP2. Signal-to-noise is not as good as at 77.5 and 155Hz.

8 Auxilliary Data.

8.1 CTD

Table 8-1 CTD cast locations

Cast #	*Date*			*Time*	*Lon*	*Lat*
	Month	*Day*	*Year*	*hh:mm:ss*	*Decimal Degrees*	
01	Jun	17	2013	15:45:35	-137.667	33.4672
02	Jun	22	2013	21:41:40	-140.328	33.8705
03	Jun	26	2013	03:49:31	-137.679	33.3838
04	Jun	28	2013	10:01:08	-137.972	33.7982
05	Jul	06	2013	02:54:04	-137.678	33.4285

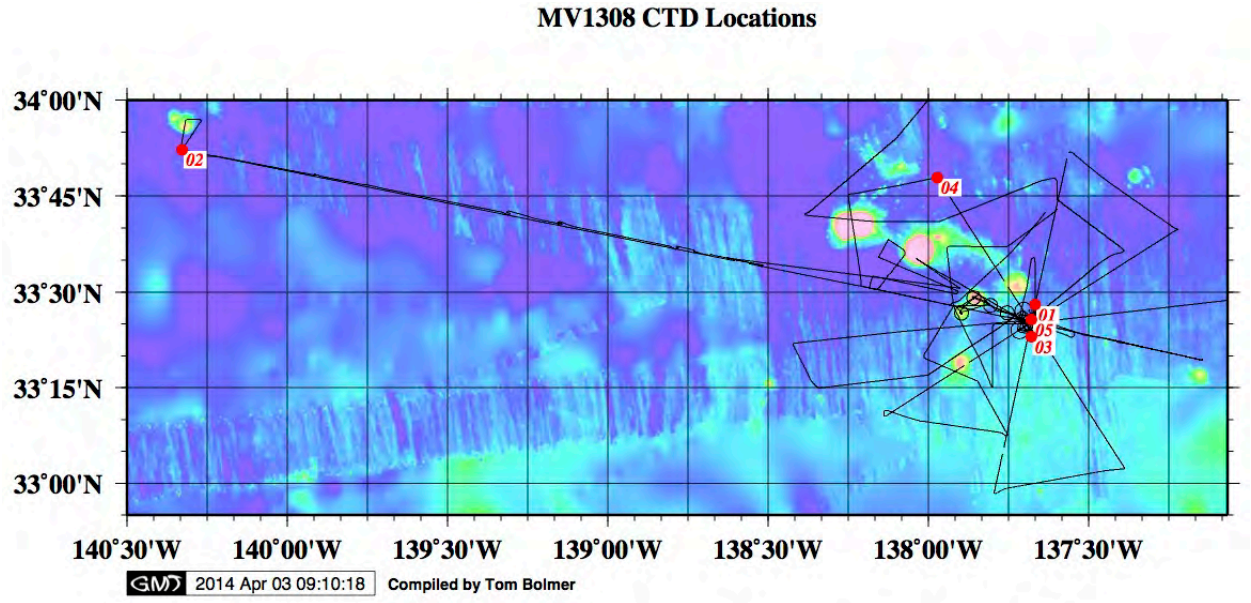

Figure 8.1: OBSANP CTD locations
This shows the locations of the 5 CTD Casts done on MV1308. Cast locations are shown with red dots.

8.2 XBTs

Table 8-2 all XBTs used on MV1308.

Drop #	Time hh:mm:ss	Date mm/dd 2013	Lat	Long	Max Depth meters	Type of XBT	Serial #	Comments Post drop
			dec. degrees					
1	18:24:59	06/13	33.06	-123.13	1100	FastDeep	14116	
2	16:28:31	06/14	33.4	-127.99	1100	FastDeep	14117	
3	02:46:47	06/16	33.5	-134.21	1100	FastDeep	14120	
4	03:31:55	06/17	33.43	-137.65	1100	FastDeep	12744	
5	23:56:39	06/17	33.45	-137.89	1100	FastDeep	12743	
6	20:53:26	06/18	33.47	-137.93	1100	FastDeep	12742	
7	04:07:21	06/19	33.48	-138.04	2200	T5	341635	
8	10:30:16	06/19	33.5	-138.1	420	T5	341636	
8	10:30:16	06/19	33.5	221.9	420	T5	341636	Dud Doing another one
9	10:38:48	06/19	33.5	-138.11	2200	T5	341634	
10	16:58:39	06/19	33.51	-138.18	333	FastDeep	12741	
11	17:03:49	06/19	33.52	-138.18	1100	FastDeep	12745	
12	20:16:32	06/19	33.54	-138.16	1100	T5	341633	
13	00:44:05	06/20	33.53	-138.09	2200	T5	341632	
14	08:33:14	06/20	33.51	-137.99	2216	T5	341629	
15	17:05:40	06/20	33.51	-137.92	1100	FastDeep	12746	
16	20:51:27	06/20	33.52	-137.97	2202	T5	341631	
17	03:29:36	06/21	33.56	-138.07	150	T5	341627	
18	03:39:35	06/21	33.56	-138.08	2031	T5	341630	
19	10:07:00	06/21	33.59	-138.15	2248	T5	341626	
19	10:07:00	06/21	33.59	221.85	2248	T5	341626	
20	17:35:41	06/21	33.59	-138.08	1100	FastDeep	12747	
21	23:03:19	06/21	33.57	-138.52	1824	T5	341628	
22	03:24:29	06/22	33.63	-138.9	2088	T5	341625	
23	07:40:50	06/22	33.69	-139.26	285	T5	341507	
24	07:47:01	06/22	33.69	-139.27	2202	T5	341506	
25	11:54:00	06/22	33.75	-139.63	44	T5	341505	QC: Premature wire break detected
26	11:59:46	06/22	33.76	-139.64	2194	T5	341508	
27	15:51:29	06/22	33.81	-139.98	2197	T5	341509	
28	18:59:11	06/22	33.85	-140.23	2217	T5	341510	
29	04:46:34	06/23	33.85	-140.26	1100	FastDeep	12748	
30	10:49:42	06/23	33.81	-139.91	2211	T5	341513	
31	15:09:12	06/23	33.77	-139.7	2189	T5	341514	

Drop	Time	Date	Lat	Long	Max	Type	Serial	Comments
32	21:38:33	06/23/	33.71	-139.29	2183	T5	341511	
33	03:12:20	06/24	33.65	-138.98	2190	T5	341515	
34	08:05:04	06/24	33.62	-138.77	2189	T5	341512	
35	14:27:14	06/24	33.59	-138.66	8	T5	341516	No valid drop data QC: Premature wire break detected
36	14:33:18	06/24	33.59	-138.65	2222	T5	349185	
37	19:13:16	06/24	33.58	-138.55	2232	T5	349184	
38	21:57:06	06/24	33.58	-138.59	2233	T5	349177	
39	04:04:03	06/25	33.52	-137.99	1100	FastDeep	12749	
40	10:17:42	06/25	33.54	-137.95	2219	T5	349186	
41	19:26:05	06/25	33.44	-137.68	2157	T5	349183	
42	10:54:23	06/26	33.43	-137.72	2190	T5	349178	
43	17:39:08	06/26	33.36	-137.35	622	T5	349179	
44	17:43:44	06/26	33.36	-137.36	2213	T5	349182	
45	20:47:47	06/26	33.37	-137.42	2210	T5	349187	
46	02:06:16	06/27	33.33	-137.18	1100	FastDeep	12750	
47	07:09:41	06/27	33.36	-137.32	2215	T5	349188	
48	11:09:26	06/27	33.38	-137.48	2218	T5	349181	
48	11:09:26	06/27	33.38	222.52	2218	T5	349181	
49	15:10:21	06/27	33.41	-137.64	230	T5	349180	Bad drop
50	15:17:24	06/27	33.41	-137.64	2173	T5	351520	
51	19:15:47	06/27	33.44	-137.79	2208	T5	351524	
52	22:48:35	06/27	33.47	-137.93	2214	T5	351528	
53	03:14:47	06/28	33.49	-138.08	2220	T5	351527	
54	18:11:13	06/28	33.68	-137.88	2188	T5	351526	
55	22:05:34	06/28	33.57	-137.79	1100	FastDeep	12751	
56	02:20:04	06/29	33.45	-137.7	2194	T5	351525	
57	07:20:01	06/29	33.3	-137.59	2197	T5	351523	
58	11:12:51	06/29	33.19	-137.5	2224	T5	351522	
59	15:20:41	06/29	33.08	-137.42	2156	T5	351521	
60	19:28:59	06/29	33	-137.7	1100	FastDeep	14182	
61	23:52:15	06/29	33.09	-137.77	2250	T5	351519	
62	04:19:11	06/30	33.23	-137.73	2202	T5	351518	
63	08:26:12	06/30	33.36	-137.7	649	T5	351517	
64	08:34:34	06/30	33.36	-137.69	555	T5	363624	
64	08:34:34	06/30	33.36	222.31	555	T5	363624	dud
65	13:13:29	06/30	33.51	-137.66	2236	T5	363263	

Drop	Time	Date	Lat	Long	Max	Type	Serial	Comments
66	17:22:53	06/30	33.65	-137.62	63	T5	363620	QC: Premature wire break detected
67	17:26:42	06/30	33.65	-137.62	2229	T5	363622	
68	21:15:21	06/30	33.77	-137.59	2162	T5	363621	
69	21:27:11	06/30	33.78	-137.59	2144	T5	363619	
70	01:03:43	07/01	33.81	-137.47	1100	FastDeep	14183	
71	01:20:19	07/01	33.79	-137.45	1100	FastDeep	14184	
72	05:29:22	07/01	33.64	-137.27	1004	T5	363613	
73	05:37:19	07/01	33.64	-137.27	2206	T5	363614	
74	09:40:18	07/01	33.57	-137.41	1017	T5	363617	
74	09:40:18	07/01	33.57	222.59	1017	T5	363617	got to 100 then ended. I suspect it blew into the ship. I accept this since it got 1000.
75	13:29:09	07/01	33.5	-137.54	2259	T5	363618	
76	19:12:19	07/01	33.39	-137.73	331	T5	363615	
77	19:16:00	07/01	33.39	-137.73	2242	T5	363616	
78	23:23:32	07/01	33.32	-137.87	2219	T5	363625	
79	04:27:25	07/02	33.23	-138.04	654	T5	363626	
80	04:33:34	07/02	33.23	-138.04	1272	T5	363627	
81	07:32:06	07/02	33.18	-138.14	2162	T5	363628	
82	11:47:59	07/02	33.16	-137.77	1998	T5	363629	
83	17:21:05	07/02	33.45	-137.93	2172	T5	363633	
84	17:38:45	07/02	33.47	-137.92	2180	T5	363630	
84	17:38:45	07/02	33.47	222.08	2180	T5	363630	25 knot winds, sea state 6, profile unrealistic
85	22:11:07	07/02	33.65	-137.7	1820	T5	363634	
86	23:53:51	07/02	33.72	-137.63	1100	FastDeep	14185	
87	02:10:03	07/03	33.56	-137.79	1100	FastDeep	14186	
88	18:58:50	07/03	33.46	-137.91	2256	T5	363631	
89	08:59:38	07/05	33.4	-137.98	1429	T5	363635	
90	21:59:56	07/06	34.85	-138	1100	FastDeep	14187	
91	22:47:34	07/07	39.03	-137.44	1100	FastDeep	14188	
92	23:12:23	07/08	42.08	-133.62	1100	FastDeep	14189	
93	23:32:08	07/09	45.26	-129.42	1100	FastDeep	14190	

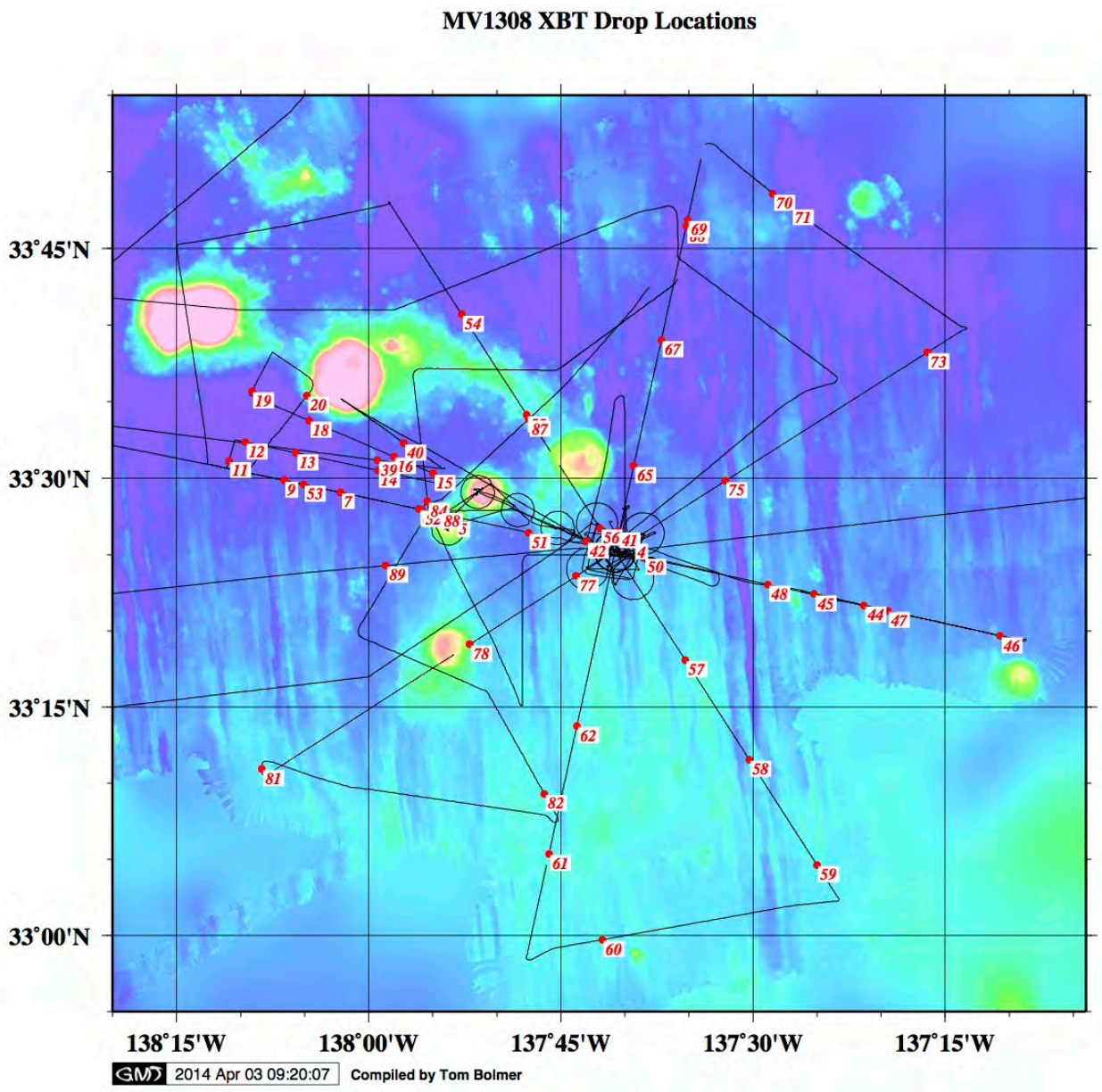

Figure 8.2: OBSANP XBT locations near ODVLA13
This shows the locations of the XBT drops done on MV1308 in the 50 kilometer range of the ODVLA13. Drop locations are shown with red dots.

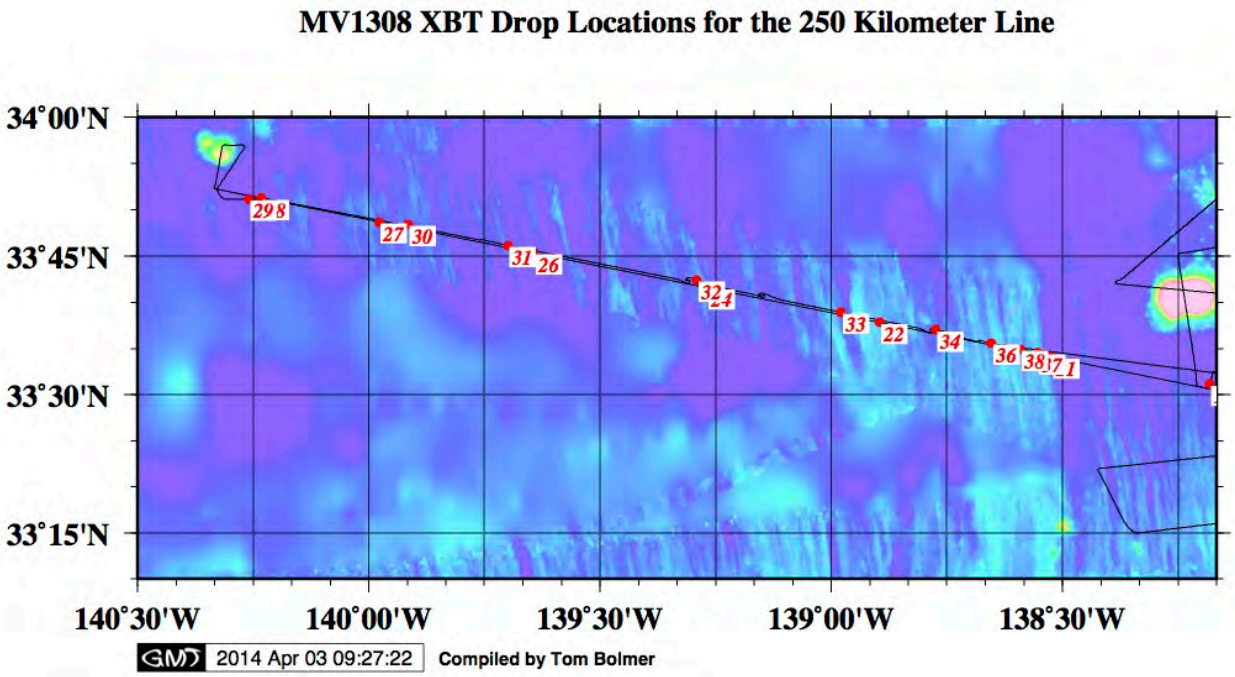

Figure 8.3: OBSANP XBT Locations on long Westerly line
This shows the locations of the XBT drops done on MV1308 on the Long 250 kilometer line from the ODVLA13. Drop locations are shown with red dots.

8.3 Current Meter

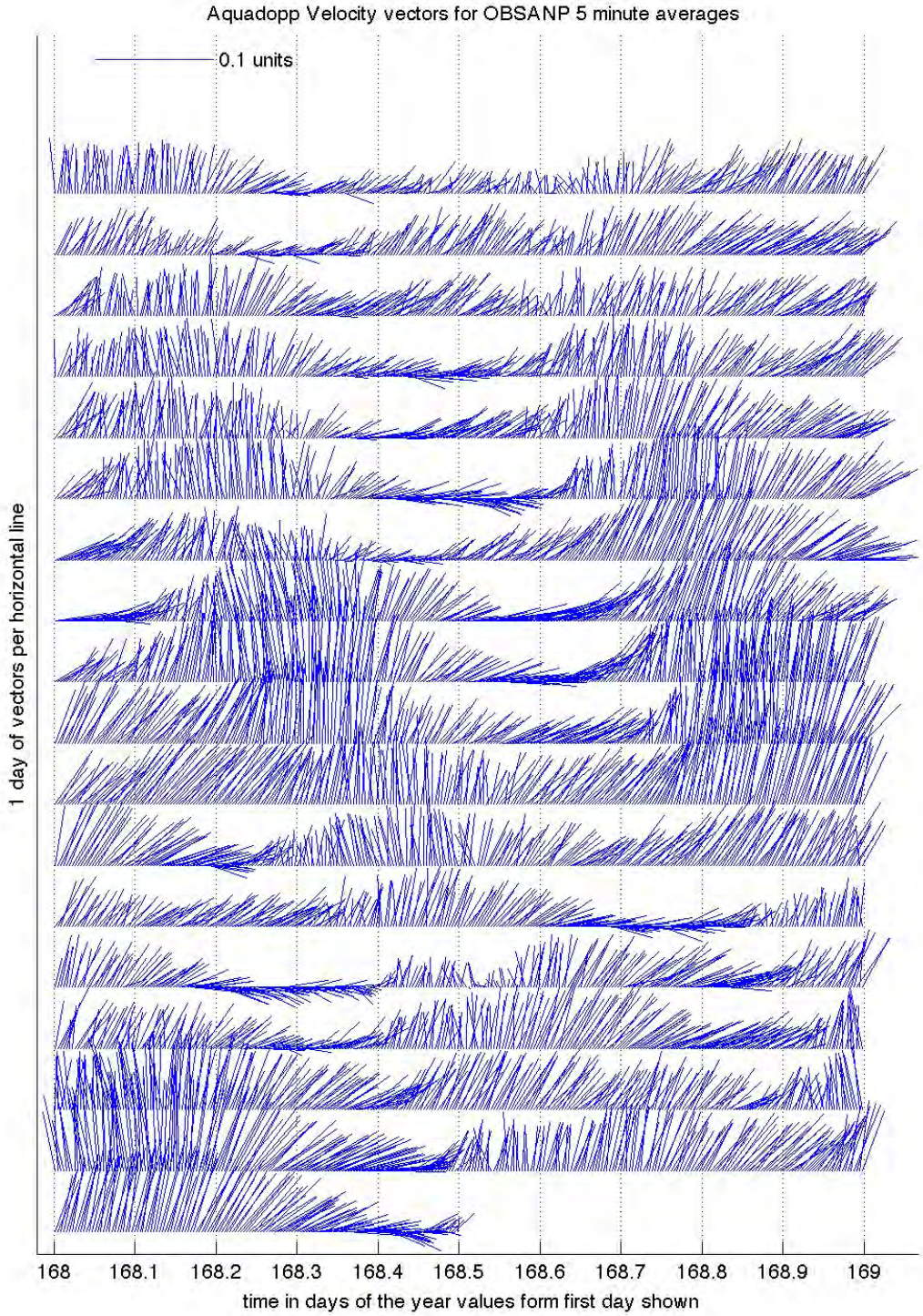

Figure 8.4: OBSANP Current Meter vectors plotted
This shows the vectors of the currents for full deployment of the ODVLA13. The bottom axis shows the day in 1/10 of a day length for just day 169. The data increases with time from the top left to the bottom right. Data is shown as 1 unit being 1 Meter/Second.

8.4 Seabird Depth and Temperature

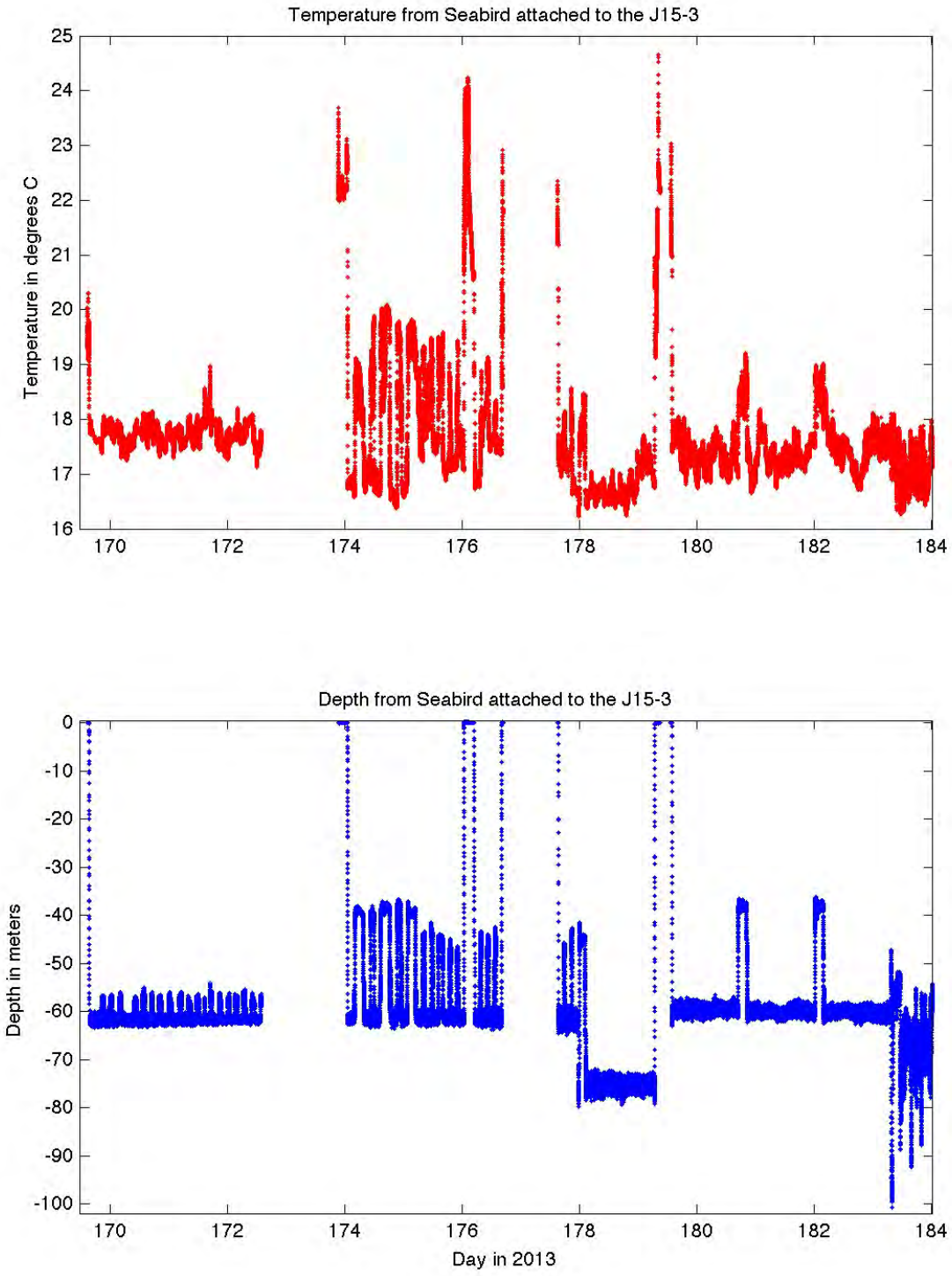

Figure 8.5: Seabird on J15 Temperature and Depth

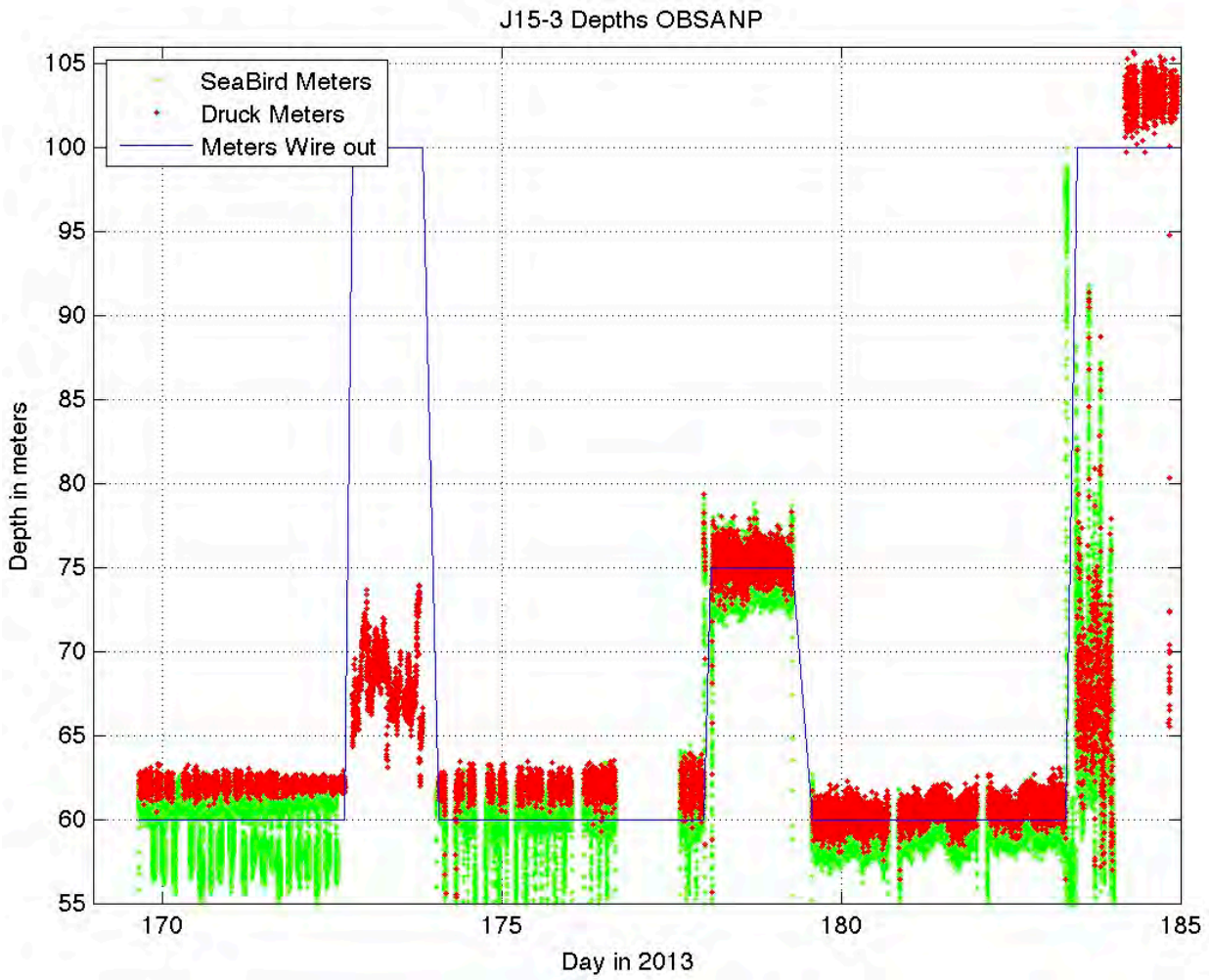

Figure 8.6: Seabird and Druck Depths with wireout
This compares the depths recorded by the Seabird and Druck depth sensors. The estimated amount of J15-3 tow wire is plotted here for comparison purposes.

8.5 Automatic Identification System (AIS) Data

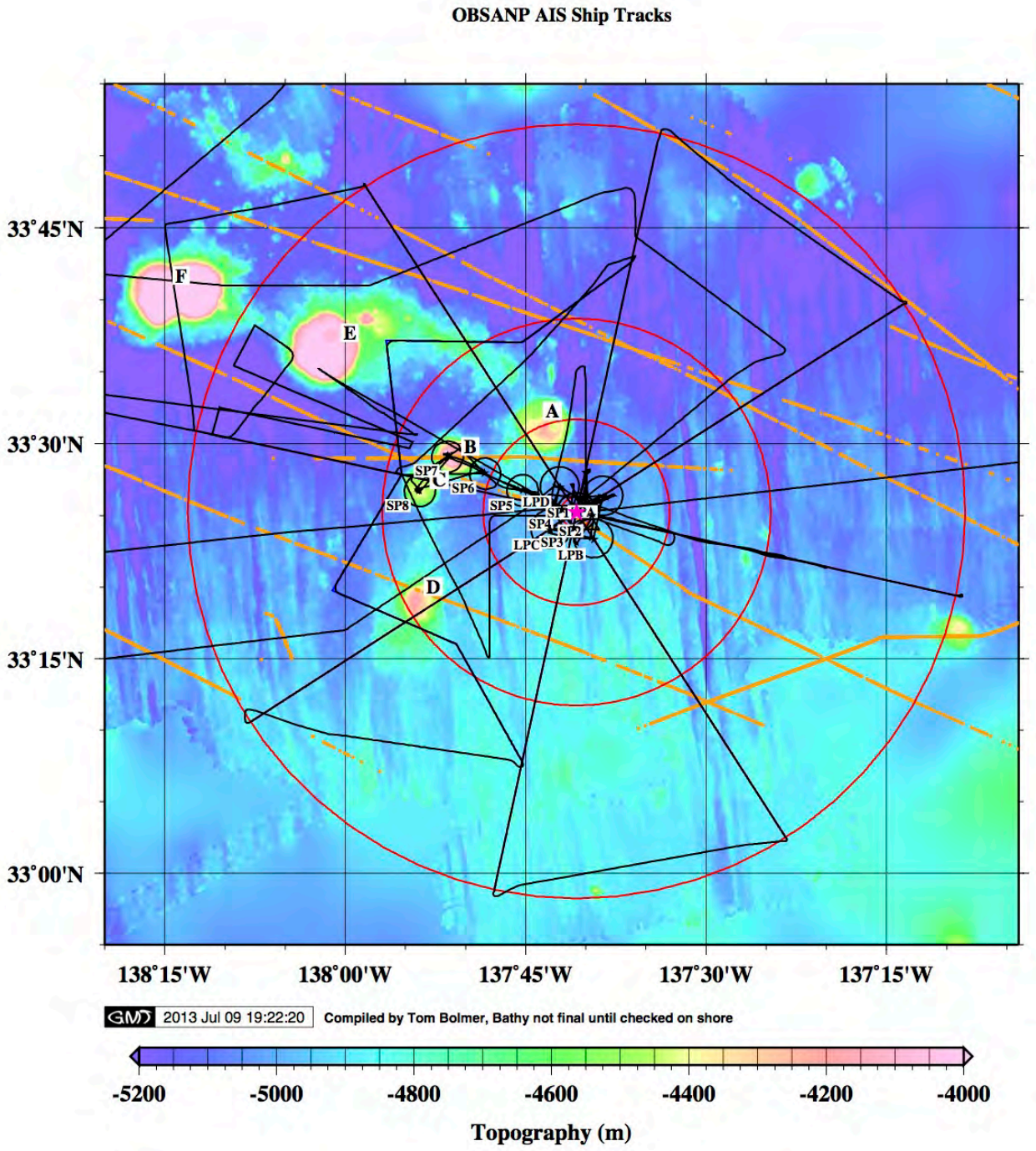

Figure 8.7: OBSANP AIS ship tracks
This figure shows tracks of other ships that passed near the ODVLA13. The orange tracks are ship tracks as recorded on the AIS. The black track is the Melville. The red circles are 12, 25 and 50 kilometer distance form the ODVLA13.

Automatic Identification System (AIS) Data were recorded during the cruise. This data was recorded both by the science party's antenna and logging software. Partway through the cruise this data was also recorded by the logging the data as seen by the ship's AIS antenna. The ship's data covered a larger distance away, since it was higher up on the ship. These data were all recorded on the ship and thus do not cover all of the ship's that may have passed near the ODVLA13 and the nearby OBSs.

8.6 OBSANP MultiBeam Processing Summary - Tom Bolmer

OBSANP MultiBeam Processing Summary

Tom Bolmer

7/8/13

This is a brief a brief description of the EM122 (MultiBeam) (MB) processing done for MV1308 from June 12, 2013, to July 11, 2013, from San Diego to Seattle. This cruise transited directly to the OBSANP working area centered at about 137deg 40' W and 33deg 25'N. The MB data were broken up into three survey groups by the computer tech on the EM122 SIS computer. The first section MV1308 was from San Diego to the work site. The second survey was MV1308a at the work site. The third survey was MC1308b, which is from the work site to Seattle.

All of the processing done on these data was done using the MB-System software package on my Apple Laptop running OSX 10.8. The original EM122 data were rsynced to my computer. On this disk these original *.all files were mbcopied from the original mb file format #58 to mb file format #59, so that they could be ping edited. This rsync and mbopying was all done using Linux sh shell scripts. After these data were mbcopied to format 59 they were run through the program mbclean to remove the 2 outermost beams from each end of the file's swaths. Then the file was processed using mbprocess to make files that can be plotted and manipulated.

After this initial step the data were ping edited in format 59 to remove erroneous beams form the data. The files then rerun through mbprocess to apply the ping edits.

The first survey, MV1308 ,was ping edited from file *0000_20130612_192913_melville.mb59* to file *0085_20130614_130407_melville.mb59*. Then, I stopped ping editing until we neared the working site. I resumed ping editing on file *0179_20130616_114222_melville.mb59* and continued to the end of the survey.

In the second survey, MV1308a, all of the data files were ping edited. The cruise went over many previous swaths from the cruise and sat on stations for long time periods. Since the watch standers could not be relied upon to turn the EM122 back on to pinging and logging, I had them leave the EM122 continually running. This made for much overlap of data and many sections on station of really horrible data. When I ping edited these data I was very aggressive in what I removed since it was generally covered by other files of data.

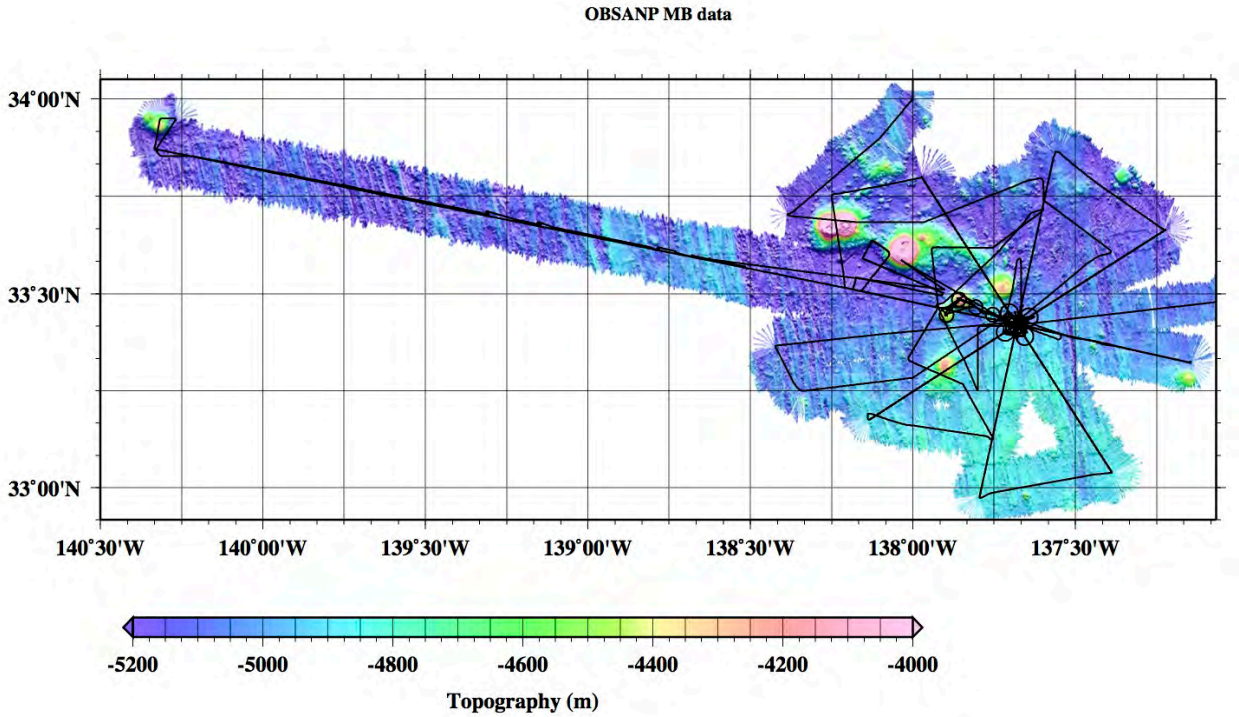

Figure 8.8: Bathymetry from MV1308 Multibeam data.
This figure shows the extent of the data from Survey MV1308a. These data were ping edited and then gridded at a 75 meter grid spacing. The cruise track is shown in black.

In this second survey area were several past cruises that acquired MB data. These data were found by a web search. These cruise are named in the below table

Table 8-3 Data used in Bathymetry Grid

Cruise Name	Year	Ship
RNDB01WT	1988	Thomas Washington
RNDB03WT	1988	Thomas Washington
RNDB18WT	1989	Thomas Washington
EW9506	1995	Ewing
NECR02RR	2000	Roger Revelle
KRUS01RR	2004	Roger Revelle
LFEX01MV	2004	Melville

These cruises can be used to work up a map of the OBSANP region if desired. Generally the MV1308 data covered the previous MB data in our working area.

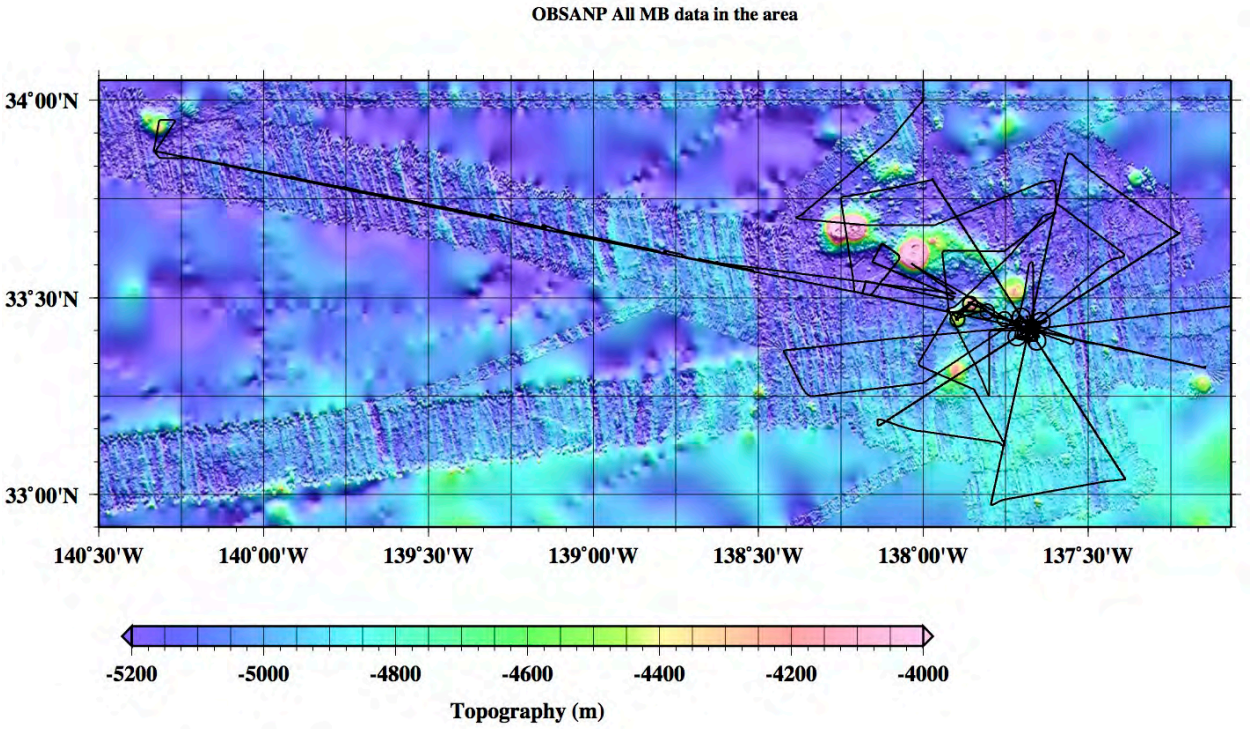

Figure 8.9: Bathymetry from MV1308 and other data sources.
This figure shows same area as in the figure above. This includes the previous MB cruises listed above and uses Smith & Sandwell's world topography data version 15.1 as a background. The cruise track is shown in black.

The final survey MV1308b starts at 34 degrees North and runs to the end of the cruise in Seattle. None of these data were processed at all. Looking at the tracks in Smith & Sandwell these data cover new areas for MB data and could be of use to anyone interested in this region's Bathymetry.

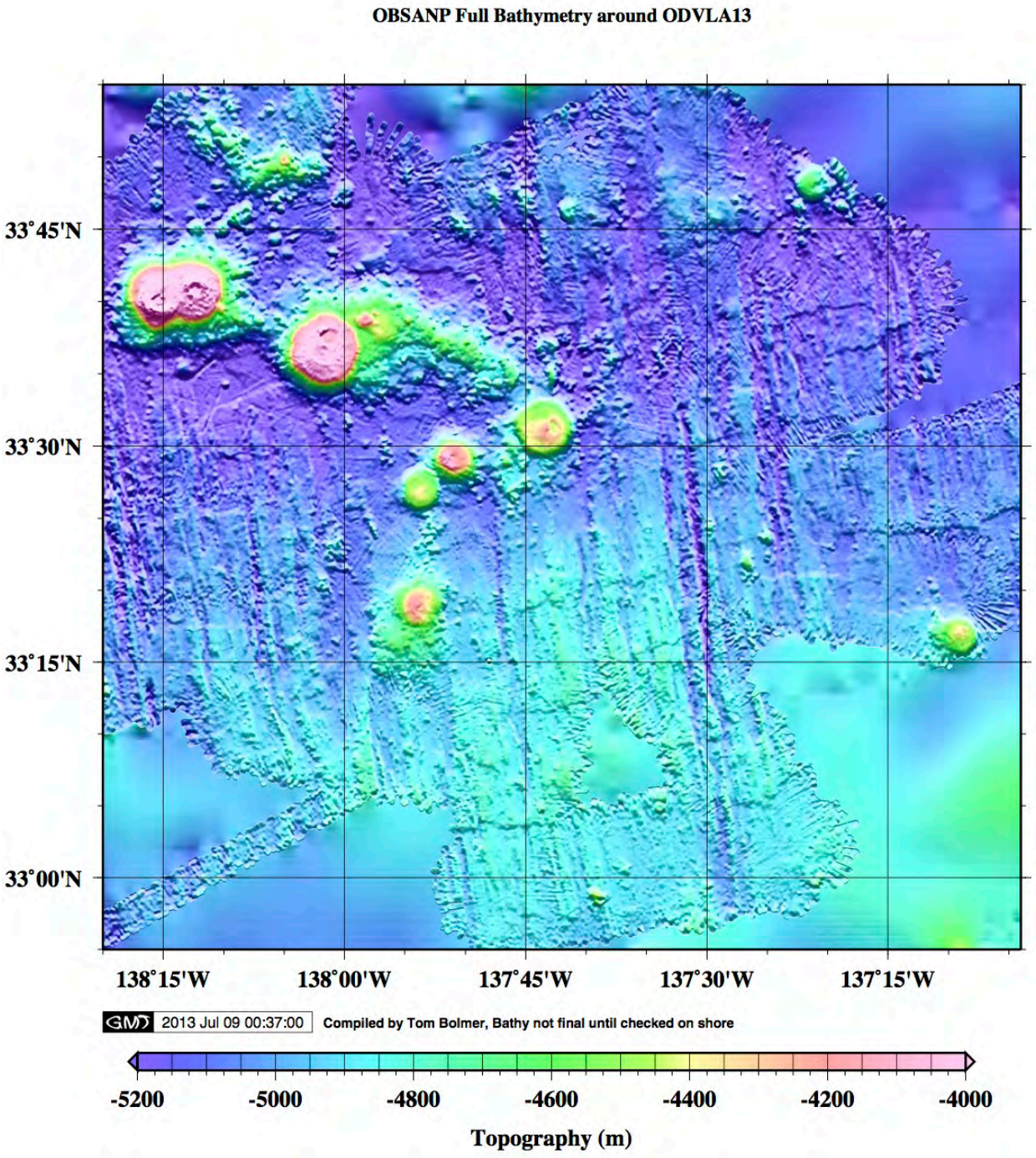

Figure 8.10: Bathymetry Grid created at Sea

This is the grid that was created at sea from the cruise MV1308, small sections of previous MB cruises, and Smith & Sandwell's version 15.1 world topography data set.

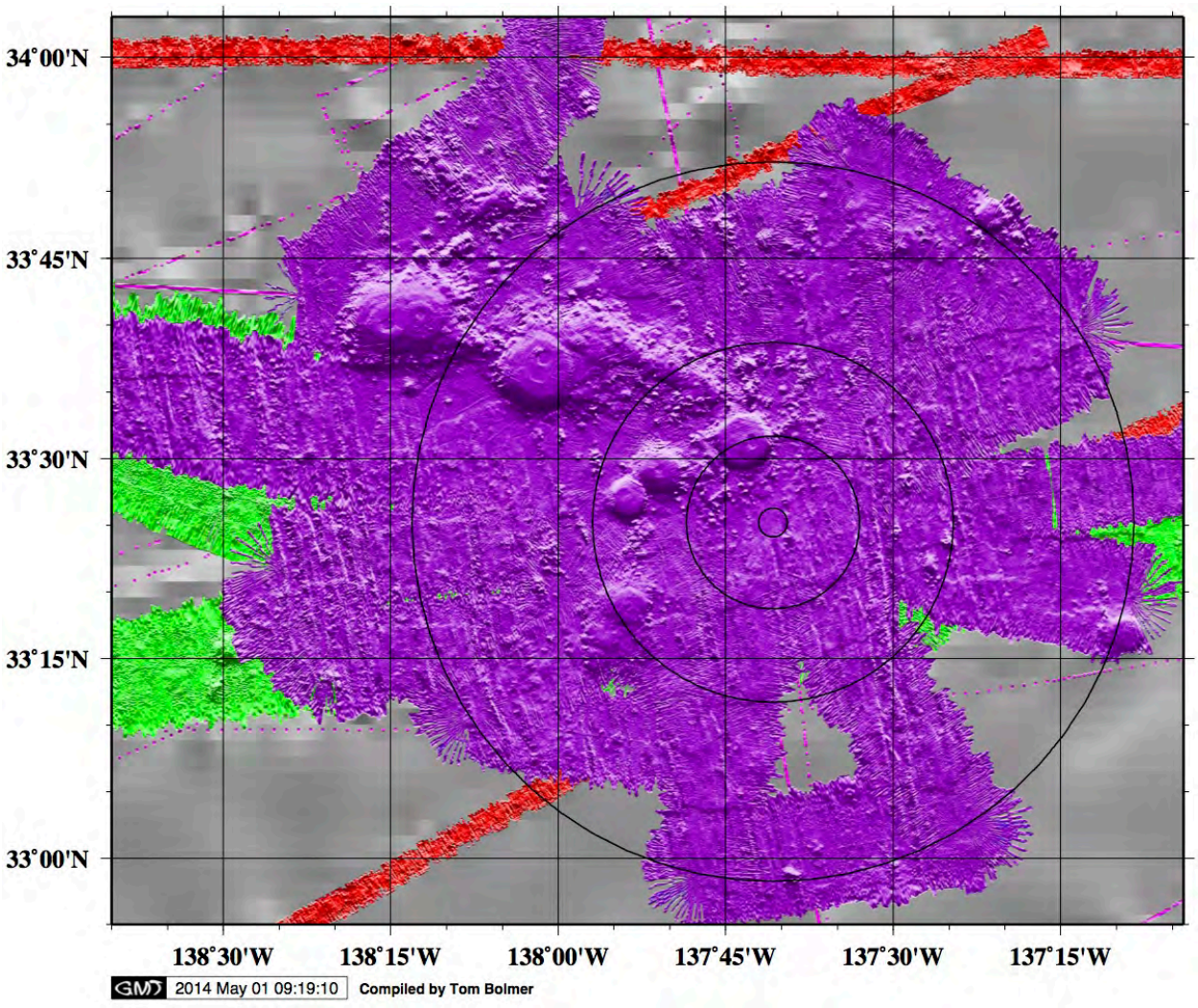

Figure 8.11: The sources of Bathymetry data used.
The colors show the areas where these data were used and not according to the methods mentioned above. The Purple color is for MV1308, Green for previous wide swath cruises, Red is for older, narrower swath, Multibeam systems, and Maroon dots are for NGDC echo sounder track line points from NGDC.

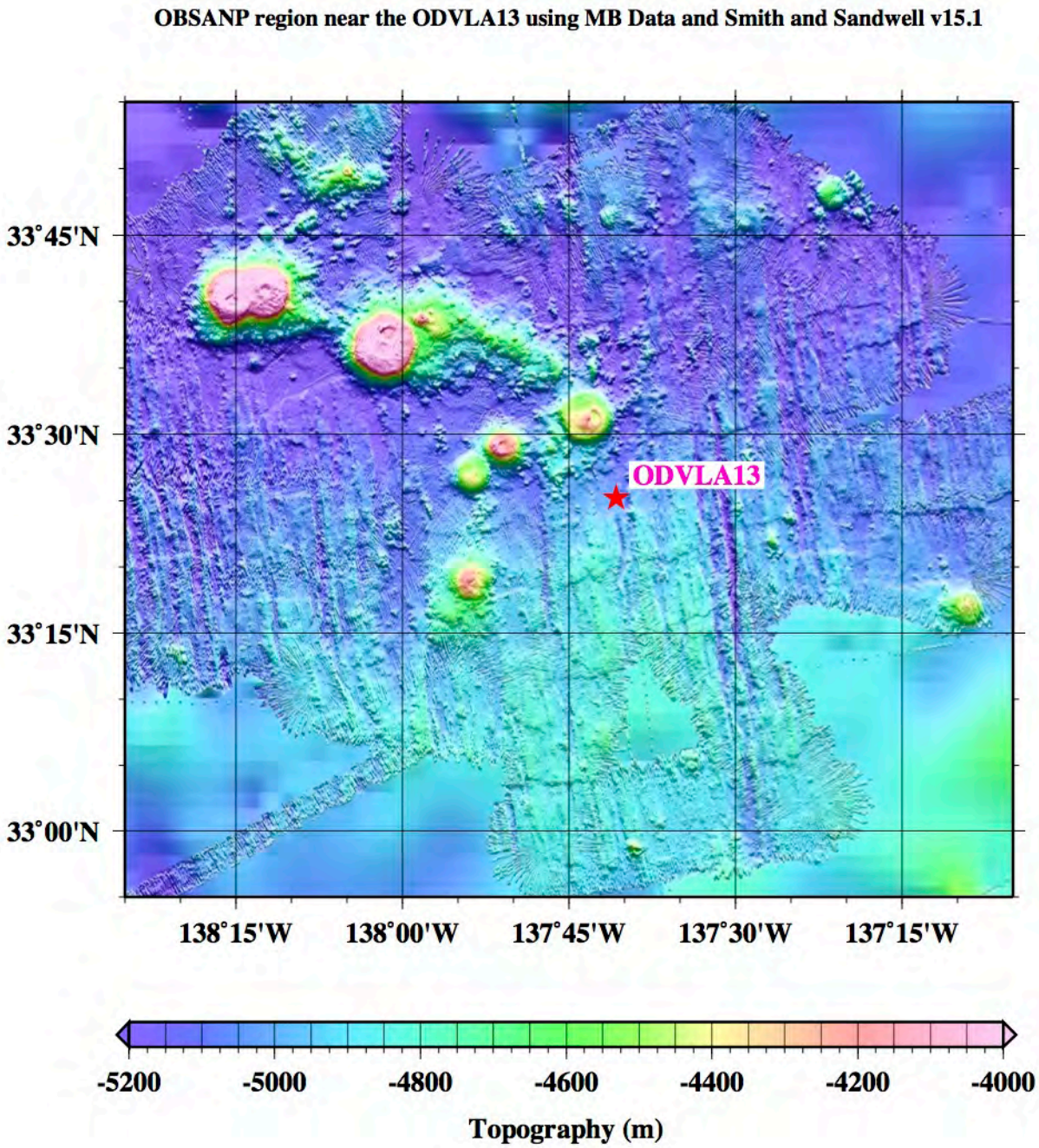

Figure 8.12: Final Bathymetry grid created for the OBSANP Region

This grid was created using all of the MultiBeam data available and Smith & Sandwell's version 15.1 world topography data set on October 31, 2013. This is a grid created at 50 meter spacing. All of the Multibeam used has been edited as best to remove data that does not fit in with the rest. This is the grid that is being used as the final bathymetry data set.

8.7 Weather

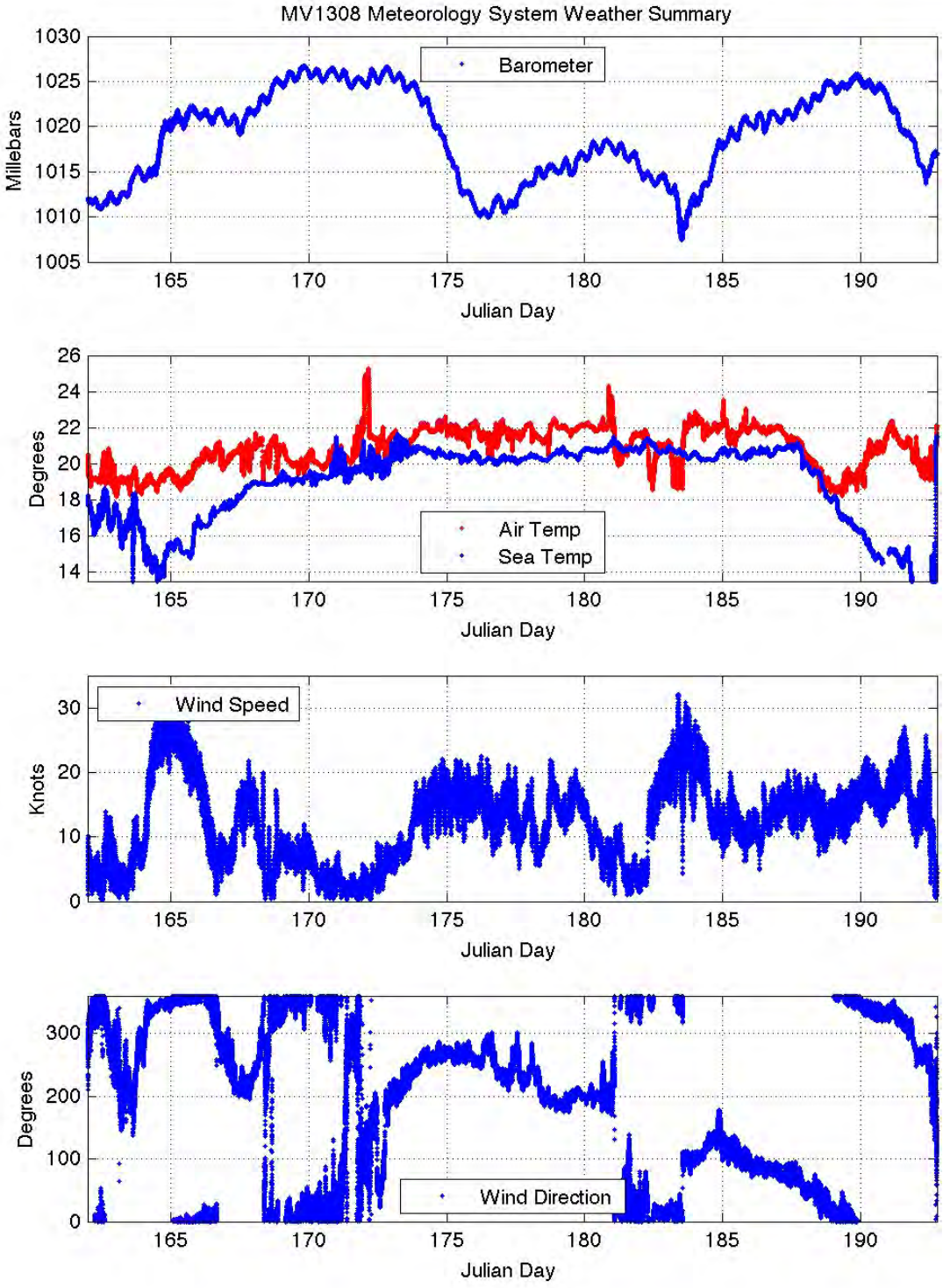

Figure 8.13: Summary of the weather recorded by the ship during MV1308.

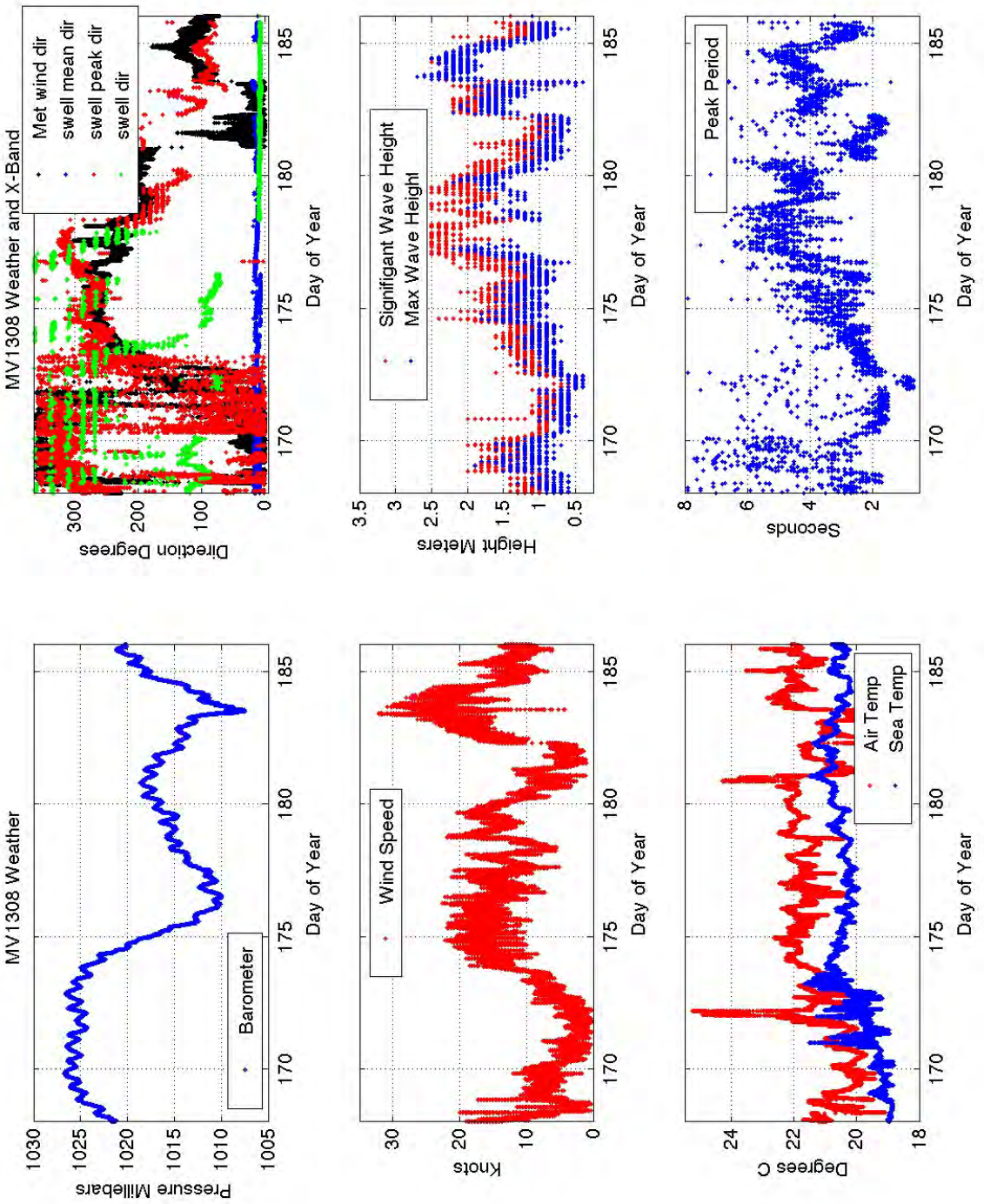

Figure 8.14: Summary of MV1308 including Wave Analysis Radar Data.
This includes some of the data from the wave analysis radar system on the ship. These data are a brief quick look at the wave data relative to the Meteorology data recorded by the Melville.

9 Hydrophone Modules.

HM Serial Numbers 080, 081, 082, 083 and 084 at mooring locations H7 through H11 and distances from the lower cable eye of 906, 896, 886, 781, and 676m, respectively, returned no data.

Deployment details for the Hydrophone Modules (HMs) used on OBSANP are given in Table 4-6. Examples of ambient noise spectra and time compressions on the HMs are given in Section 7 on Quick Look Analysis.

Figure 9.1 to Figure 9.3 show examples of higher resolution spectrograms for Hydrophone Module HM150 that was attached to OBS SP1 (about 2km North of the DVLA). (These were prepared by Matt Dzieciuch in June 2014.) These spectra were corrected for loss of sensitivity at high pressure and for the low-frequency roll-off of the pre-amp, etc.

Figure 9.4 shows a lower resolution spectrogram of the same data for the whole experiment along with the range of the Melville (red) and passing ships (blue). Figure 9.5 is a percentile summary of the same spectrogram. The spectra were computed using a transfer function with the same caveats as described in Section 7.2.

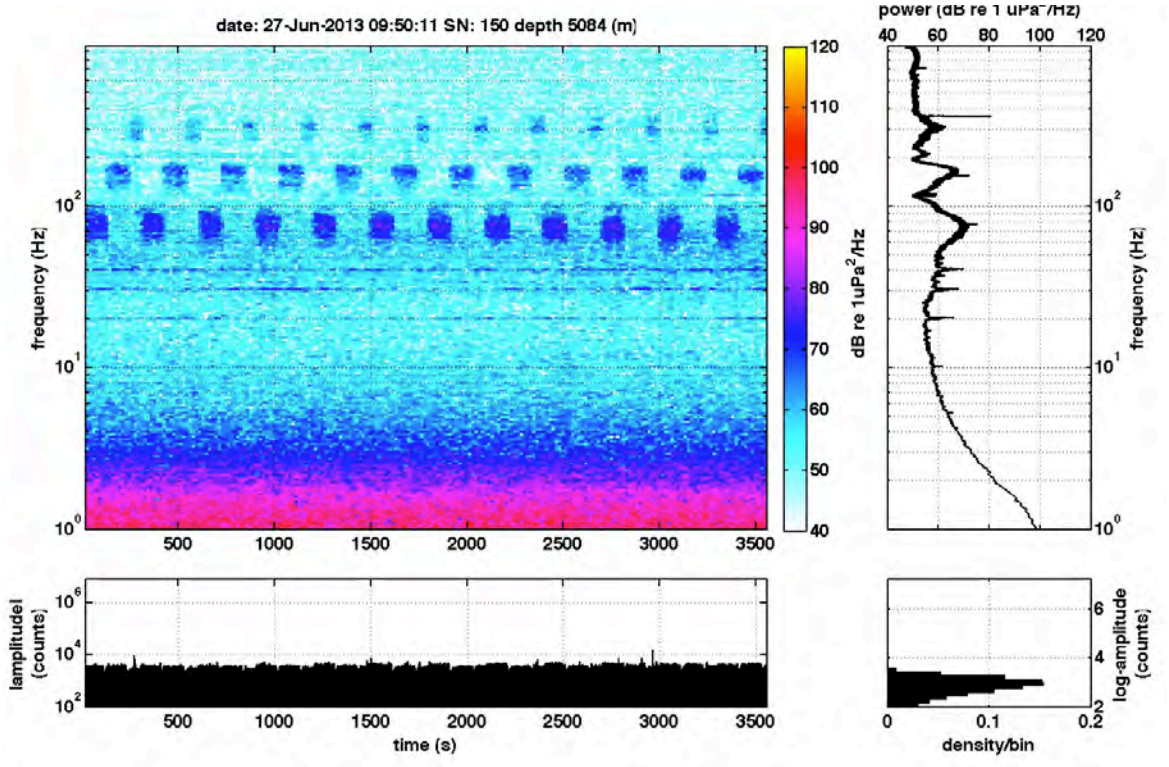

Figure 9.1: Spectrogram of J15-3 Transmissions
The blocky pattern is the J15-3 transmissions as we steamed radial lines over the DVLA. This is Program 4, 2min of 77.5Hz, 2min of 155Hz and 1min of 310Hz M-sequences, repeated continuously. [J15_3_Transmission_Program_4.jpg]

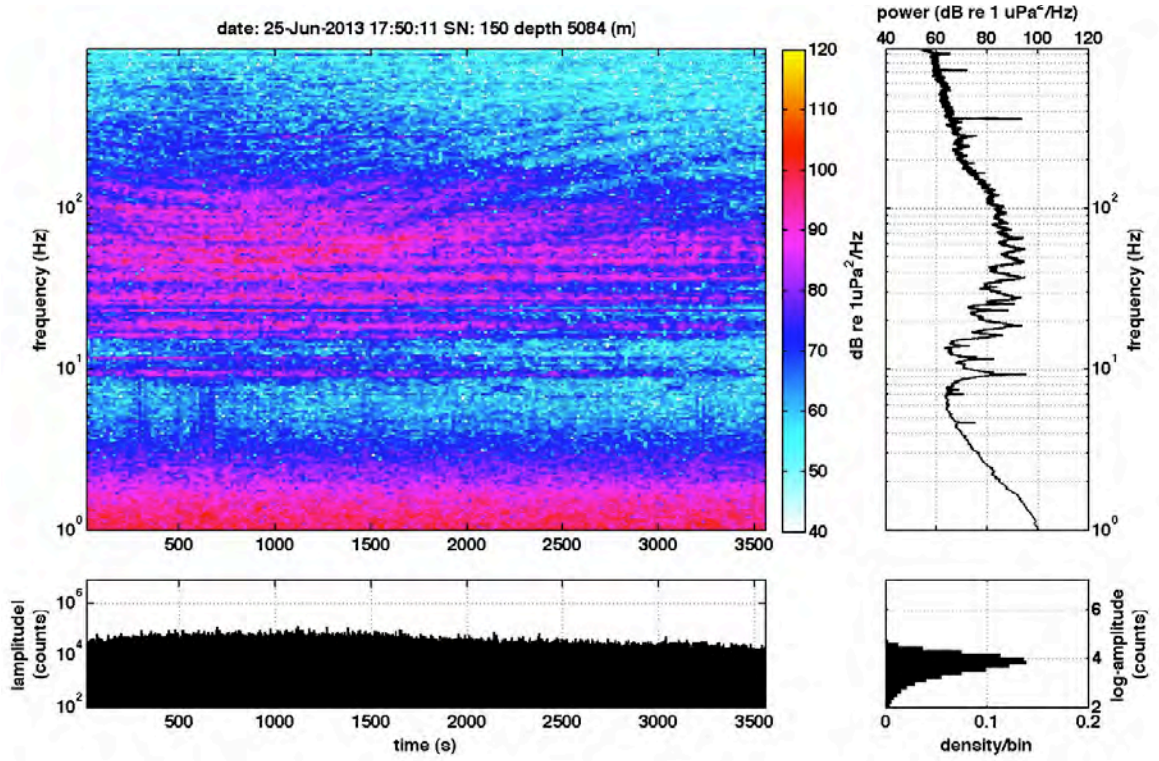

Figure 9.2: Spectrogram of Passing Ship
[Passing_ship.jpg]

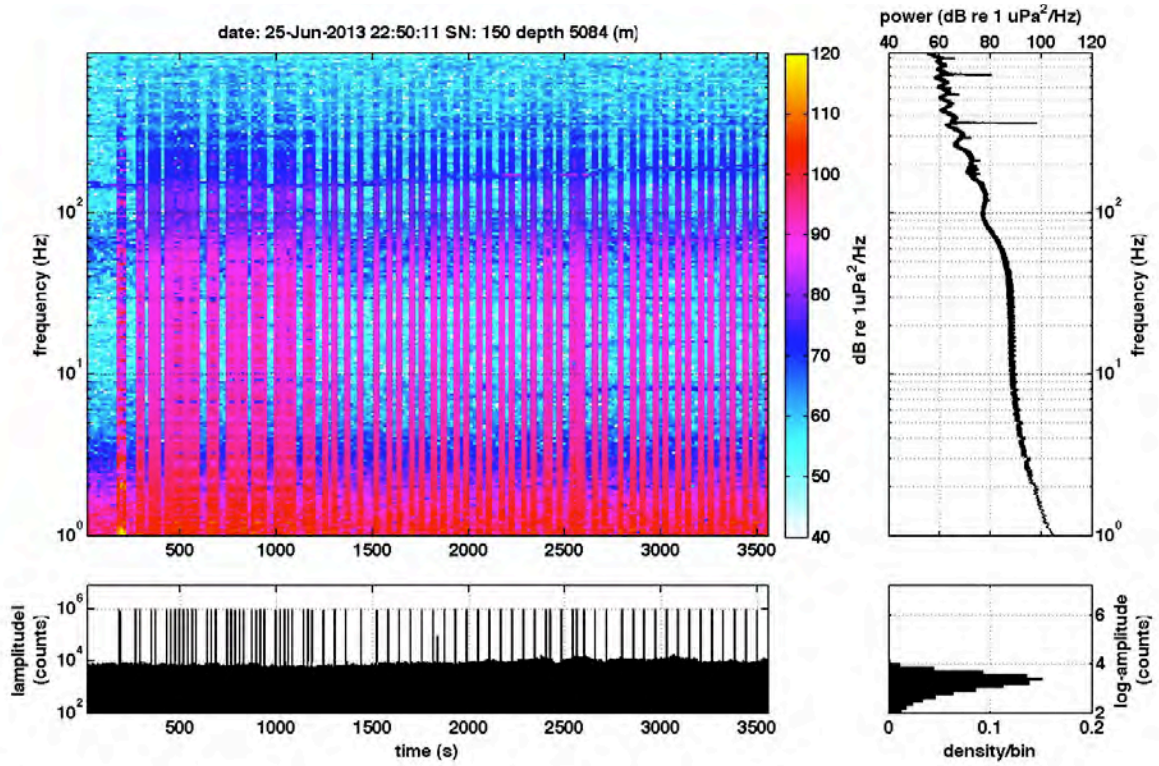

Figure 9.3: An hour of pulses
[Coded_pulses???.jpg]

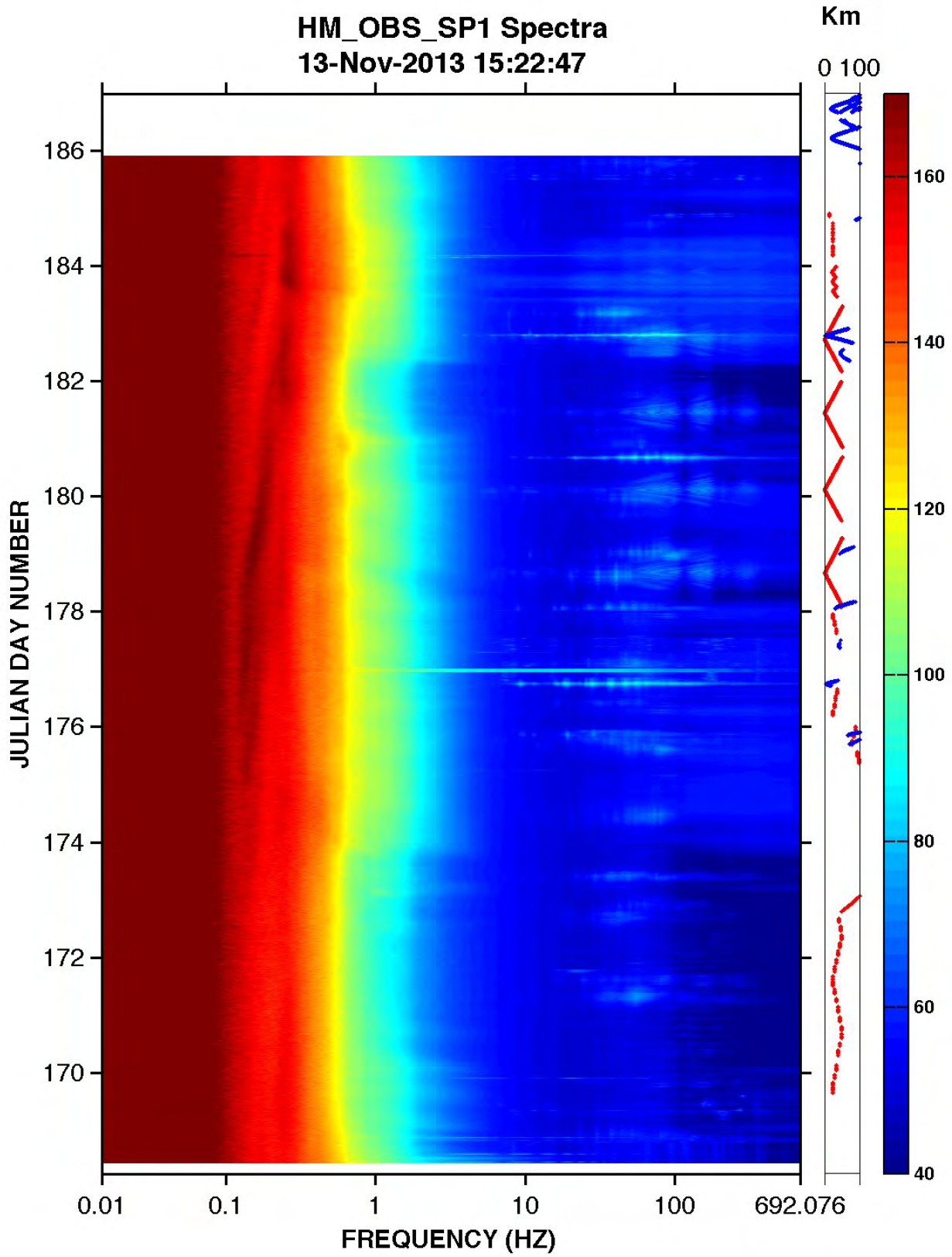

Figure 9.4: Spectrogram for HM on OBS SP1.
[HM_OBS_SP1_Long_spectra.jpg]

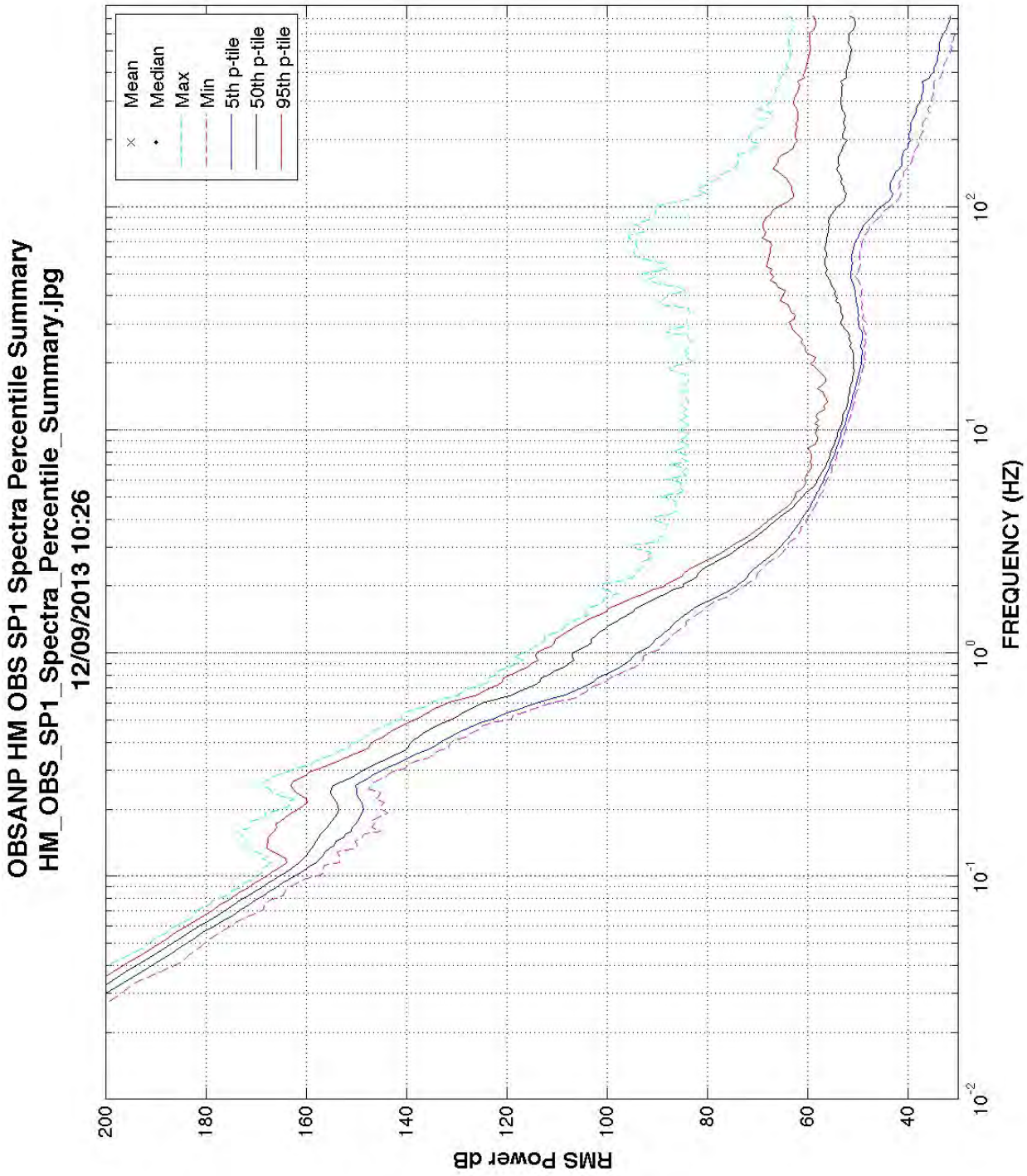

Figure 9.5: Percentile Summary of the HM on OBS SP1.
[HM_OBS_SP1_Spectra_Percentile_Summary.jpg]

10 Acknowledgments.

The OBSANP experiment was conducted jointly by the Scripps Institution of Oceanography (Worcester) and Woods Hole Oceanographic Institution (Stephen). SIO (Worcester) was responsible for the DVLA. WHOI (Stephen) was responsible for J15-3 operations and was lead PI on the OBSIP effort. The SIO OBSIP group provided the OBS; Aaron (SIO) was responsible for OBS operations. We greatly appreciate the support from Captain Curl, the officers, and crew of the R/V Melville, who helped to make the cruise such a success. The experiment was funded by the ONR Ocean Acoustics Program (Code 322 OA) under grants N00014-10-1-0987 and N00014-10-1-0510.

.

Many figures were prepared using the Generic Mapping Tool (http://gmt.soest.hawaii.edu/) (Wessel and Smith, 1998). The multi-beam data was processed using the MB-System (Caress and Chayes, 1996). The OBS data used in this research was provided by instruments from the Ocean Bottom Seismograph Instrument Pool (www.obsip.org), which is funded by the National Science Foundation. OBSIP data is archived at the IRIS Data Management Center. (www.iris.edu)

11 References.

Caress, D. W., and Chayes, D. N. (**1996**). "Improved Processing of Hydrosweep DS Multibeam Data on the R/V *Maurice Ewing*," Mar. Geophys. Res. **18**, 631-650.

Duennebier , F. K., Harris, D. W., Jolly, J., Babinec, J., Copson, D., and Stiffel, K. (**2002**). "The Hawaii-2 observatory seismic system," IEEE J. Ocean. Eng. **27**, 212-217.

Duennebier , F. K., Lukas, R., Nosal, E.-N., Aucan, J., and Weller, R. A. (**2012**). "Wind, waves, and acoustic background levels at Station ALOHA," J. Geophys. Res. **117**. doi:10.1029/2011JC007267.

Farrell, W. E., and Munk, W. (**2008**). "What do deep sea pressure fluctuations tell about short surface waves?," Geophys. Res. Lett. **35**, doi:10.1029/2008GL035008. doi:10.1029/2008GL035008.

Farrell, W. E., and Munk, W. (**2010**). "Booms and busts in the deep," Journal of Physical Oceanography **40**, 2159-2169. 10.1175/2010JPO4440.1.

Farrell, W. E., and Munk, W. (**2013**). "Surface gravity waves and their acoustic signatures, 1-30Hz, on the mid-Pacific seafloor," J. Acoust. Soc. Am. **134**, 3134-3143. 10.1121/1.4818780.

Jensen, F. B., Kuperman, W. A., Porter, M. B., and Schmidt, H. (**1994**). *Computational ocean acoustics*, (American Institute of Physics, New York), pp. 612.

McCreery, C. S., Duennebier, F. K., and Sutton, G. H. (**1993**). "Correlation of deep ocean noise (0.4 to 30 Hz) with wind, and the Holu Spectrum - A worldwide constant," J. Acoust. Soc. Am. **93**, 2639-2648.

Mercer, J. A., Colosi, J. A., Howe, B. M., Dzieciuch, M. A., Stephen, R., and Worcester, P. F. (**2009**). "LOAPEX: The long-range ocean acoustic propagation experiment," IEEE J. Ocean. Eng. **34**, 1-11.

Rauch, D. (**1980**). *Seismic interface waves in coastal waters: A review*, (SACLANT ASW Research Center, San Bartolomeo (SP), Italy), pp.

Stephen, R. A., Bolmer, S. T., Dzieciuch, M. A., Worcester, P. F., Andrew, R. K., Buck, L. J., Mercer, J. A., Colosi, J. A., and Howe, B. M. (**2009**). "Deep seafloor arrivals: An unexplained set of arrivals in long-range ocean acoustic propagation," J. Acoust. Soc. Am. **126**, 599-606. 10.1121/1.3158826.

Stephen, R. A., Bolmer, S. T., Udovydchenkov, I., Worcester, P. F., Dzieciuch, M. A., Van Uffelen, L., Mercer, J. A., Andrew, R. K., Buck, L. J., Colosi, J. A., and Howe, B. M. (**2008**), NPAL04 OBS data analysis part 1: Kinematics of deep seafloor arrivals, WHOI Technical Report 2008-03, (Woods Hole Oceanographic Institution, Woods Hole, MA).

Stephen, R. A., Bolmer, S. T., Udovydchenkov, I. A., Dzieciuch, M. A., Worcester, P. F., Andrew, R. K., Mercer, J. A., Colosi, J. A., and Howe, B. M. (**2013**). "Deep seafloor arrivals in long range ocean acoustic propagation," J. Acoust. Soc. Am. **134**, 3307-3317. 10.1121/1.4818845.

Stephen, R. A., Duennebier, F. K., Harris, D., Jolly, J., Bolmer, S. T., and Bromirski, P. D. (**2006**). "Data Report: Broadband Seismic Observations at the Hawaii-2 Observatory, ODP Leg 200," in *Proceedings of the Ocean Drilling Program, (Scientific Results)*, edited by Kasahara, J., Stephen, R. A., Acton, G. D. and Frey, F. A.,200[Online]), Available from World Wide Web: <http://www-odp.tamu.edu/publications/200_SR/003/003.htm>. [Cited 2006-2006-2027].

Stephen, R. A., Kemp, J., McPeak, S. P., Bolmer, S. T., Carey, S., Aaron, E., Campbell, R., Moskovitz, B., Calderwood, J., Cohen, B., Worcester, P. F., and Dzieciuch, M. A. (**2011**), Ocean Bottom Seismometer Augmentation of the Philippine Sea Experiment (OBSAPS) Cruise Report, WHOI Technical Report 2011-04, (Woods Hole Oceanographic Institution, Woods Hole, MA).

Stephen, R. A., Spiess, F. N., Collins, J. A., Hildebrand, J. A., Orcutt, J. A., Peal, K. R., Vernon, F. L., and Wooding, F. B. (**2003**). "Ocean seismic network pilot experiment," Geochem. Geophys. Geosys. **4**. doi: 10.1029/2002GC000485.

Sutton, G. H., and Barstow, N. (**1990**). "Ocean-bottom ultra low-frequency (ULF) seismo-acoustic ambient noise: 0.002 to 0.4 Hz," J. Acoust. Soc. Am. **87**, 2005-2012.

Webb, S. C., and Cox, C. S. (**1986**). "Observations and modeling of seafloor microseisms," J. Geophys. Res. **91**, 7343-7358.

Wessel, P., and Smith, W. H. F. (**1998**). "New, improved version of generic mapping tools released," EOS, Transactions of the American Geophysical Union **79**, 579.

12 Appendix A. Ocean Bottom Seismometer Augmentation in the North Pacific (OBSANP) SIO Experiment Plan

Version 1.1
May 27, 2013
Peter Worcester

A new class of acoustic arrivals was observed on ocean bottom seismometers (OBSs) during the 2004 Long-range Ocean Acoustic Propagation Experiment (LOAPEX). During this experiment an HX-554 acoustic source suspended from shipboard transmitted broadband 75-Hz signals from a variety of ranges to a Deep Vertical Line Array (Deep VLA) receiver surrounded by four OBSs. The arrivals were called Deep Seafloor Arrivals (DSFAs), because they were the dominant arrivals on the OBSs, but were either undetected or very weak on the bottom hydrophone of the Deep VLA, located about 750 m above the seafloor. It was subsequently found that at least some DSFAs corresponded to energy that scattered from an off-axis seamount and subsequently reflected from the sea surface before arriving at the OBSs.

During the Ocean Bottom Seismometer Augmentation in the North Pacific (OBSANP) experiment, we are returning to the Deep VLA site with 12 OBSs (eight short period and four long period), a near-seafloor Distributed Vertical Line Array (DVLA) receiver extending upward 1000 m from the seafloor, and a J15-3 source in order to further define the characteristics of DSFAs and to understand the conditions under which they are excited and propagate. Hydrophone Modules originally developed for the DVLA will be attached to six of the short-period OBS to supplement the hydrophones included in the OBS instruments. In addition, Ultra-Low-Noise hydrophones developed by SAIC (ULN-SAIC) will be integrated into two of the long-period OBS. The J15-3 transmissions will mostly be within 50 km of the DVLA, but there will be one long line to about 250-km range. In addition to studying DSFAs, ambient noise data will also be acquired.

All instrumentation (OBSs, DVLA, and the acoustic transponders used to measure the motion of the near-seafloor DVLA mooring) will be recovered prior to the end of the OBSANP cruise.

The OBSANP experiment is being conducted jointly by the Scripps Institution of Oceanography (Worcester) and Woods Hole Oceanographic Institution (Stephen). SIO (Worcester) is responsible for the DVLA. The SIO OBSIP group will provide the OBS. WHOI (Stephen) is responsible for J15-3 operations. The experiment is funded by the ONR Ocean Acoustics Program (Code 322 OA).

12.1 Geometry

12.1.1 Moored DVLA receiver

The near-seafloor DVLA, referred to as the OBSANP-DVLA (O-DVLA), will be deployed at 33° 25.1348'N, 137° 40.9475'W, which is the location of the Deep VLA deployed for the SPICEX and LOAPEX experiments (Figure 12.1). The water depth at the Deep VLA location is 5045 m (corrected). The O-DVLA will consist of one 1000-m array with 32 Hydrophone Modules. The mooring design is given in Figure 12.2. A D-STAR (DVLA–Simple Tomographic Acoustic Receiver) controller will be located at the top of the array.

D-STAR	**Serial Number**
Primary	104
Spare	107

The locations of the Hydrophone Modules (HM) are given in Table 12-1 and Figure 12.2. They were chosen as follows:

(1) The deepest HM on the O-DVLA will be 12 m above the seafloor, which is as close to the seafloor as it can conveniently be placed.

(2) O-DVLA deep subarray: 16 HM spaced 10 m apart (~ one-half wavelength at 75 Hz) starting with the deepest HM. This array is designed to (i) improve the SNR and determine the vertical arrival angles of the J15-3 transmissions received on the O-DVLA just above the seafloor and (ii) provide information on the angular structure of the low-frequency ambient noise well below the critical depth.

(3) O-DVLA shallow subarray: 10 HM spaced 10 m apart just below the D-STAR located at the top of the O-DVLA. This array is primarily designed to improve the SNR of the J15-3 transmissions received on the O-DVLA near the surface conjugate depth, although it will also provide (limited) information on the vertical arrival angles. The low-frequency ambient noise level is expected to be substantially higher near the surface conjugate depth than just above the seafloor, requiring some gain to improve the SNR and make the DSFAs more visible.

(4) Six (6) HM spaced 105 m apart between the two subarrays to measure the depth dependence of the omnidirectional ambient noise during the OBSANP experiment.

The O-DVLA will be navigated using the long-baseline navigation system in the D-STAR and three Benthos TR-6001-17 recoverable acoustic transponders on the seafloor.

12.1.2 Moored O-DVLA temperature, pressure, and velocity measurements.

The D-STAR controller will measure pressure with an accuracy of ± 3.5 dBars (0.05% of 7000 dBar full scale) at 15-minute intervals throughout the experiment, as well as in conjunction with NAV measurements. The D-STAR temperature sensor is located inside the pressure sensor and therefore does not provide accurate measurements of ocean temperature due to the heat generated by the D-STAR electronics.

The Hydrophone Modules in the O-DVLA will make precision temperature measurements with an accuracy of ± 0.005°C. Temperature measurements will be made at 5-minute intervals during the Continuous schedule (HH:04:00, HH:09:00, HH:14:00, HH:19:00, …, HH:59:00). They will be made at 15-minute intervals, as well as in conjunction with NAV measurements, during the Standby and Recovery schedules.

A Nortek Aquadopp 6000-m acoustic current meter will be deployed above the acoustic releases on the O-DVLA (Figure 12.2).

12.2 Acoustic transmission/reception schedule

12.2.1 J15-3 Transmission Schedule

WHOI (Stephen) is responsible for the J15-3 operations and will specify the detailed transmission locations and signals. Transmissions will typically be in the frequency band 25–400 Hz with the J15-3 at a depth of 60 m. The tentative plan calls for phase-coded m-sequence transmissions that fall into four categories:

(1) multi-frequency, short range (< ½ CZ) tows at 77.5, 155 and 310 Hz;
(2) single frequency, long range (up to 250 km, ~ 3 ½ CZ) tows at 77.5 Hz;
(3) multi-frequency station stops at ½, 1 ½, 2 ½ and 3 ½ CZ at 77.5, 102.3,155, 204.6, and 310 Hz); and
(4) a 38.75-Hz transmission at short ranges (< ½ CZ) that would provide field data for modeling with SPECFEM3D.

12.2.2 O-DVLA Reception Schedule

The DVLA will start the Continuous recording schedule at 08:00:00 UTC on the day following deployment (Table 12-2). During this schedule, the Hydrophone Modules will record continuously except for intervals once per hour to allow for NAV tasks to measure the mooring motion (see below). The DVLA sample rate will be 1953.125 Hz.

The Hydrophone Modules are powered up throughout the Continuous reception period. The HM clock is set once at the beginning of the continuous reception, after allowing the HM oscillator to warm up for 400 s. The D-STARs invoke time latches of the HMs twice an hour (HH:18:05 and HH:48:05) throughout the continuous receptions to allow for post-experiment clock corrections.

Recording in the Hydrophone Modules will be terminated manually following recovery, as the Recovery schedule is not set to begin until after the O-DVLA is recovered.

The data storage and energy budgets for the Hydrophone Modules and the D-STARs are given in Table 12-3, Table 12-4, and Table 12-5. Each Hydrophone Module has a 16-Gbyte Secure Digital card.

12.2.3 Autonomous Hydrophone Module Reception Schedule

The autonomous Hydrophone Modules attached to the short-period OBS will record continuously except for intervals once per hour to allow for NAV tasks during which the Hydrophone Modules will record the NAV interrogation signals transmitted by the D-STAR. The sample rate in the autonomous Hydrophone Modules will be 1953.125 Hz.

The autonomous Hydrophone Modules will be started manually prior to deployment. Recording in the autonomous Hydrophone Modules will be terminated manually following recovery. Manual clock checks will be done after starting sampling and prior to terminating sampling.

12.3 Ambient noise and SNR

A variety of signals will be transmitted by the J15-3 source at a variety of ranges, as noted above. In order to give some feeling for the expected signal-to-noise ratios (SNRs), Table 12-6 gives the predicted signal-to-noise ratios (SNRs) at a range of 100 km for the J15-3 with a source level of 172 dB re 1 μPa at 1 m. As a strawman, the predictions are for 10 periods of an m-sequence transmission with 255 digits at a carrier frequency of 75 Hz and 1023 digits at a carrier frequency of 250 Hz. Each period of the m-sequence signal then has a duration of 10.2000 s at 75 Hz and 12.2760 s at 250 Hz. Both transmissions have three cycles/digit (Q = 3).

At 75 Hz distant ship traffic is the dominant source of ambient noise. The O-DVLA mooring is in intensity zone IV, but close to the boundary between intensity zones IV and V, for ship-generated ambient noise. Zones IV and V have predicted spectral levels of 75.2 dB and 80.0 dB re 1 μPa^2/Hz, respectively (Sadowski, Katz, and McFadden, *Ambient Noise Standards for Acoustic Modeling and Analysis,* Naval Underwater Systems Center, 1984).

At 250 Hz both distant ship traffic and surface processes contribute to the ambient noise. Ambient noise has a predicted spectral level of 66.7 dB re 1 μPa^2/Hz at 250 Hz due to surface processes (Sea state 4) and a predicted spectral level of 63.4 dB re 1 μPa^2/Hz at 250 Hz due to shipping (using shipping density V as a worst case) (Sadowski, Katz, and McFadden, *Ambient Noise Standards for Acoustic Modeling and Analysis,* Naval Underwater Systems Center, 1984). The overall predicted spectral level is then about 68 dB re 1 μPa^2/Hz.

12.4 Long-baseline acoustic navigation system, transponder surveys, and acoustic releases

The O-DVLA will be tracked using three Benthos TR-6001-17 recoverable acoustic transponders deployed approximately1000 m from the O-DVLA in an equilateral triangle centered on the mooring location. The D-STAR will operate in a single-frequency interrogate (9.0 kHz), multiple-frequency reply (11.0, 11.5, 12.0 kHz) mode. The transponders will be positioned as follows with respect to the O-DVLA:

11.0 kHz: 1000 m at 0ºT
11.5 kHz: 1000 m at 120ºT
12.0 kHz: 1000 m at 240ºT

The D-STAR will use 2-ms jitter-reduction precursors (10.0 kHz) preceding 8-ms interrogation pulses (9.0 kHz). The D-STAR will transmit interrogation signals once per hour throughout the experiment and record the transponder replies using a 15-s recording window (`Table 12-7`). The D-STAR will record unprocessed NAV data.

The Hydrophone Modules will record NAV data using a 15-s recording window during the Standby, Continuous, and Recovery schedules. They will begin sampling five (5) seconds prior to the interrogate pulse in order to record both the interrogate pulse and the transponder replies. The recording window is scheduled to begin well before the interrogation pulse in order to allow for the drift of the Hydrophone Module clocks during the long continuous recording period. Low-frequency recording at the Hydrophone Modules during the Continuous schedule will be interrupted once per hour for the Navigation task (`Table 12-8`). The continuous sampling (except for the first sampling period, which is a special case) occurs from HH:(NAV end + 2 s) to HH+1:(NAV start – 2 s). It will be possible to filter and decimate the Navigation receptions at the Hydrophone Modules to make more continuous time series at the lower sample rate, if desired.

The acoustic releases to be used are given below. All releases are rated for two-year operation. SIO will bring a DS-7000 deck unit, which will be used with the ship's 12-kHz hull-mounted transducer. John Kemp will provide a Benthos DS-8000 deck unit as a spare. (Note that the DS-8000 has to be used with a transducer lowered over the side, as it is not compatible with the ship's 12-kHz transducer.

	Release #1			**Release #2**		
	S/N	**RCV (kHz)**	**XMIT (kHz)**	**S/N**	**RCV (kHz)**	**XMIT (kHz)**
DVLA	936	8.5	9.5	590	10.5	11.0
Spares	023	8.5	9.5	024	10.5	11.0

The transponder and mooring locations will be surveyed after deployment.

Recovery aids. The Near-Seafloor DVLA will have an Argos beacon (Cobham Model AS-900A) and radio (Novatech Model RF700A1, 154.585 MHz) supplied by SIO on the Pickup Float.

12.5 Other O-DVLA measurements

D-STAR. Once a day at 01:06:00 UTC a daily task will occur. The outstanding engineering data are written to compact flash at this time, if the buffer holding the engineering data is full.

The frequency of the precision, low-power Q-Tech MCXO QT2002 system oscillator will be compared once per day with the frequency of a Symmetricom X72 Rubidium frequency standard and the difference between the two recorded with a precision of 1 part in 10^{10}. The Rb warmup is started as part of the daily task, and the frequency comparison is completed at 01:14:00 UTC. The low-power oscillator frequency is not adjusted in response to the Rb measurement, and the D-STAR clock will therefore gradually drift. The low-power oscillator is typically set with a precision of about 1 part in 10^{8}, giving a low frequency drift of order 1 ms/day.

12.6 Ocean Bottom Seismometers

The SIO OBSIP group will provide eight (8) short-period and four (4) long-period OBS (Table 12-9 and Figure 12.1). The short-period OBS have three-component Mark Products L22 28-Hz geophones and an HTI-90-U hydrophone. Six of the short-period OBS will have SIO Hydrophone Modules attached to them. The long-period OBS have broadband, three-component Trillium 240 seismometers and a Differential Pressure Gauge (DPG). SAIC Ultra-Low-Noise hydrophones (ULN-SAIC) will be integrated into two of the long-period OBS.

All OBS will sample at 1000 Hz. Each has a 64 GB Compact Flash card. The data will be made available in SEED format following recovery.

The OBS have EdgeTech acoustic release electronics. All of the OBS receive at 11.0 kHz and reply at 13.0 kHz. The pulse duration is 8 ms.

Approximately one hour is need per OBS deployment. A total of 12 hours will therefore be needed to deploy the OBSs. Recovery takes somewhat longer because of the time required for the OBS to reach the surface following release.

12.7 CTD measurements

Deep CTD casts will be made near the O-DVLA when it is deployed and recovered. Additional CTD casts to a depth of 2000 m will be done once per day during J15-3 operations. The SIO Oceanographic Data Facility will provide the CTD (Seabird), as well as a data acquisition system.

12.8 Cruise plan

The cruise schedule is given in Table 12-10. The scientific party is given in Table 12-11.

John Kemp (WHOI) is responsible for preparing the O-DVLA mooring. Jim Ryder (WHOI) will be in charge of the deck for the O-DVLA deployment and recovery. He will provide an electric reel winder and tension cart for use with the SIO TSE mooring winch.

SIO MARFAC will provide the SIO TSE mooring winch, together with the dividers to create two bays on the drum. SIO (Worcester) will NOT provide any air tuggers.

Bathymetry and sub-bottom profiles in the vicinity of the O-DVLA will be measured using the ship's EM-122 multibeam system and Knudsen 3260 echo sounder operating at 3.5 kHz, respectively.

SIO (Worcester) and the SIO OBSIP group will share a truck for transporting equipment from Seattle to San Diego following the cruise.

Table 12-1 Nominal Hydrophone Module depths
The depths do not include the effect of stretch in the wire rope under tension.

Distance From Lower Eye (m)	Depth (m)	Hydrophone Module	Comments	Serial Number	Critical Depth (m)
					Spring: 3480
1000	4034	DSTAR	Upper eye		
976	4058	H0	10-m spacing	073	
966	4068	H1		074	
956	4078	H2		075	
946	4088	H3		076	
936	4098	H4		077	
926	4108	H5		078	
916	4118	H6		079	
906	4128	H7		080	
896	4138	H8		081	
886	4148	H9	105-m spacing	082	
					Summer: 4250
781	4253	H10		083	
676	4358	H11		084	
571	4463	H12		098	
466	4568	H13		099	
361	4673	H14		101	
256	4778	H15		102	
151	4883	H16	10-m spacing	103	
141	4893	H17		104	
131	4903	H18		105	
121	4913	H19		107	
111	4923	H20		108	
101	4933	H21		136	
91	4943	H22		138	
81	4953	H23		139	
71	4963	H24		141	
61	4973	H25		142	
51	4983	H26		143	
41	4993	H27		145	
31	5003	H28		146	
21	5013	H29		147	
11	5023	H30		148	
1	5033	H31		149	
0	5034		Lower eye		
	5045		Seafloor		

The depths are computed assuming that the mooring components below the lower eye of the 1000-m shot of ¼" jacketed Nilspin wire rope of the O-DVLA are (Figure 12.2):

Hardware	0.226
Nortek Aquadopp Current Meter	1
Hardware	0.235
3 Meters 3/8" Mooring Chain	3
Hardware	0.255
Dueled Benthos Releases with 1/2" Trawler Chain	1.945
Hardware	0.26
3 Meters 3/8" Mooring Chain	3
Hardware	0.26
2300 Lb Ww Anchor	0.5
TOTAL	10.68 m

Table 12-2 O-DVLA reception schedule**.**

The DVLA will start the "Continuous" recording schedule at 0800 UTC on the day following deployment. STAR parameter files allowing recording to start on any year day in the range 166–172 (15–21 June 2013) will be available. Year day 1 is 1 January 2013. Hydrophone Module recording will be terminated manually as the Recovery schedule is not set to begin until after the O-DVLA is recovered.

Schedule	**Start Time (UTC)**			**Comments**
	Date	**Year day**	**UTC**	
Standby	spin-up (~16 June 2013)	(~167)		NAV-PT-OSTAR, Rb tasks only
Continuous	15–21 June 2013	166–172	0800	Continuous reception
Recovery	09 July 2013	190	0800	NAV-PT-OSTAR, Rb tasks only

Table 12-3 Hydrophone Module data storage budget, O-DVLA.

Each Hydrophone Module has a 16-Gbyte Secure Digital memory card. There are three bytes per data sample. Each thermistor sample requires 16384 bytes of storage during the Standby and Recovery schedules, but is integrated into the acoustic sampling file during the Continuous schedule. The DVLA engineering data will not be copied to the Hydrophone Modules.

	Sample Rate (Hz)	Data Storage (Gbytes)	Comments
Continuous receptions	1953.125	10.072	20 days (480 hr) @ 3580.9792 s/hr
Navigation	39,062.500	0.844	480 receptions @ 15 s (24 NAV/day x 20 days)
Thermistor		–	Only stored in separate files during the Standby and Recovery schedules
Engineering data		0	
Total		10.916	
SD card capacity		16.0	
Safety margin		5.084	

Table 12-4 D-STAR data storage budget**.**
The D-STAR has two 32-Gbyte Compact Flash cards. Data will be written in parallel to the cards ("Shadowed disks"). There are two bytes per data sample. The navigation data will be unprocessed. The D-STAR will record NAV data once per hour.

	Sample Rate (Hz)	Data Storage (Gbytes)	Comments
Navigation	39,062.500	0.563	480 receptions @ 15 s (24 NAV/day x 20 days)
Engineering data		≤ 0.040	40 Mbyte pre-allocated file
Total		0.603	
Disk capacity		32	Shadowed disks
Safety margin		31.397	

Table 12-5 Hydrophone Module energy budget**.**

Each Hydrophone Module has one Electrochem BCX-TSD lithium battery with a nominal capacity of 40 Ah at 25°C.

	Energy (Ah)	Comments
Continuous receptions	16.94	20 days (480 hr)
Navigation	0.21	480 receptions @ 15 s (24 NAV/day x 20 days)
Thermistor	0	Continuous receptions include thermistor sampling
Sleep	0.05	30-day cruise
Total	17.20	
Battery capacity	33.3	Derated for intermittent operation at 0°C
Safety margin	16.1	48%

Table 12-6 Signal-to-noise ratios for the J15-3

Table of the Signal-to-noise ratios for the J15-3 transmissions at frequencies of 75 and 250 Hz at a range of 100 km. The SNRs at a single hydrophone for a resolved ray arrival are given, conservatively assuming spherical spreading. Attenuation is calculated for the North Pacific Ocean using Lovett (A = 0.055). At 75 Hz the ambient noise level is for shipping density IV; the noise levels would be 4.8 dB higher (and the SNR 4.8 dB lower) for shipping density V. The noise bandwidth assumes three cycles/digit (Q = 3).

	75 Hz	**250 Hz**	
Source level (rms)	172	172	dB re 1 μPa at 1 m
Spreading loss (spherical)	–100.0	–100.0	dB
Attenuation (dB/km) 75 Hz: 0.00042 250 Hz: 0.0043	–0.04	–0.4	dB
Received signal level	72.0	71.6	dB re 1 μPa
Noise (1 Hz band)	75.2	68	dB re 1 μPa^2/ Hz
Bandwidth, Q=3	14.0	19.2	dB re 1 Hz
Total noise level	89.2	87.2	dB re 1 μPa
Broadband SNR (before processing)	–17.2	-15.6	dB
Period averaging gain (10 periods)	10.0	10.0	dB
Pulse compression gain 75 Hz: 255 digits 250 Hz: 1023 digits	24.1	30.1	dB
Total signal processing gain	34.1	40.1	dB
Single hydrophone SNR	16.9	24.5	dB

Table 12-7 Navigation interrogate times, O-DVLA.

	Mooring ID	Transmit Time (UTC)	Interrogate Frequency (kHz)
DVLA	0		9.0
Standby		HH:51:00	
Continuous		HH:50:00	
Recovery		HH:51:00	

Table 12-8 Timing of Hydrophone Module sampling during Continuous receptions.

Bottle ID	NAV sampling (39062.5 Hz)	Sampling (1953.125 Hz)
0	HH:49:55 – HH:50:10	HH:50:12 – HH+1:49:53

Table 12-9 Ocean Bottom Seismometers**.**
The "Range" is the range to the O-DVLA. The "Other Sensors" are the SIO Hydrophone Modules (HM) and the SAIC Ultra-Low-Noise hydrophones (ULN-SAIC).

Instrument	Designation	Location	Range (km)	Other Sensors
Short Period (SP1)	"West"	33.422749ºN, 137.703512ºW	2	HM150
Short Period (SP2)	"North"	33.436485ºN, 137.677859ºW	2	HM151
Short Period (SP3)	"East"	33.415074ºN, 137.661406ºW	2	HM152
Short Period (SP4)	"South"	33.401341ºN, 137.687056ºW	2	HM153
Short Period (SP5)		33.485000ºN, 137.858333ºW		HM154
Short Period (SP6)		33.441002ºN, 137.741139ºW		HM155
Short Period (SP7)		33.455680ºN, 137.780191ºW		
Short Period (SP8)		33.470346ºN, 137.819255ºW		
Long Period (LPA)	"Northwest"	33.449190ºN, 137.705737ºW	4	ULN-SAIC
Long Period (LPB)	"Southeast"	33.388633ºN, 137.659196ºW	4	ULN-SAIC
Long Period (LPC)	"Northeast"	33.438331ºN, 137.646174ºW	4	
Long Period (LPD)	"Southwest"	33.399485ºN, 137.718726ºW	4	

Table 12-10 Field Work Schedule.

***R/V Melville*, San Diego, CA – Seattle, WA**

All times are local (PDT). Chief Scientist: Dr. Peter Worcester

Date		Yearday 2013	Local Time	
07 June	Fri.	158		WHOI shipment arrives MARFAC
08 June	Sat.	159		
09 June	Sun.	160		
10 June	Mon.	161		Load ship/Pre-cruise prep
11 June	Tues.	162		Load ship/Pre-cruise prep
12 June	Wed.	163	0800	Depart San Diego for mooring O-DVLA Transit, San Diego – O-DVLA (1031 nm, 94 hrs @ 11.0 kts)
13–15 June		164–166		Transit Test OBS acoustic systems (~ 4500 m depth): 4 hrs Test O-DVLA releases (and D-STAR ?) (1000 m depth): 2 hrs
16 June	Sun.	167	1200	Arrive O-DVLA Deploy O-DVLA Survey O-DVLA Deploy acoustic transponders (3 each)
17 June	Mon.	168		Deploy OBS
18 June	Tues.	169		Survey transponders & OBS CTD (full ocean depth)
19 June – 3 July		170–184		J15-3 operations, including: CTD once/day (2000 m) XBT every watch
4 July	Thur.	185		Recover O-DVLA Recover transponders (daylight)
5 July	Fri.	186		Recover OBS
6 July	Sat.	187	2100	Recover OBS CTD (full ocean depth) Depart O-DVLA for Seattle: Transit, O-DVLA – Entrance, Strait of Juan de Fuca (1076 nm, 98 hrs @ 11.0 kts) Transit, Entrance, Strait of Juan de Fuca – Seattle (120 nm, 12 hrs)
7–10 July		188–191		Transit
11 July	Thur.	192	1100	Arrive Seattle/Unload ship
12 July	Fri.	193	1800	Unload ship SIO personnel depart Seattle

Notes:

1. Distances are great circle routes.
2. Transit times calculated at 11.0 kts.
3. Nominal positions:

San Diego: 32° 40'N, 117° 14'W

Strait of Juan de Fuca Traffic Separation Lighted Buoy JA: 48.494°N 124.728°W
(48° 29.64' N 124° 43.68' W)

O-DVLA: 33° 25.1348'N, 137° 40.9475'W, 5045 m

Table 12-11 Scientific party.

Personnel	Institution	Title
1. Ernie Aaron	SIO	Development Technician
2. Tom Bolmer	WHOI	Data Manager
3. Scott Carey	SIO	Development Technician
4. Sean McPeak	APL-UW	Sr. Engineer
5. Matthew Norenberg	SIO	Sr. Marine Mechanician
6. Jim Ryder	WHOI	Senior Engineering Assistant II
7. Dr. Ralph Stephen	WHOI	Sr. Scientist
8. Dr. Stephen Swift	WHOI	OBS Technician
9. Dr. Ilya Udovydchenkov	WHOI	Guest Scientist
10. Dr. Peter Worcester (Chief Scientist)	SIO	Research Oceanographer

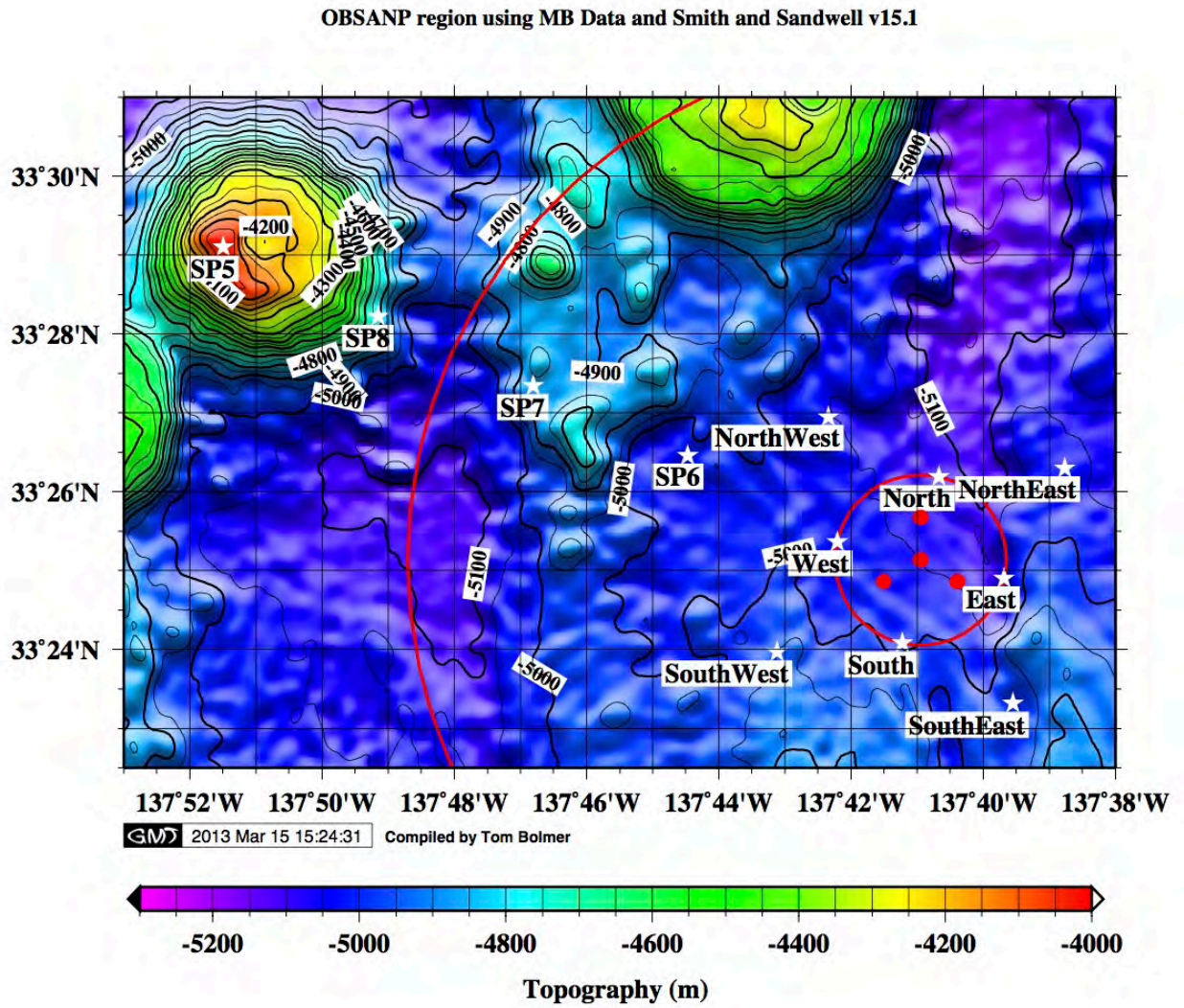

Figure 12.1: OBSANP geometry.
The O-DVLA and three acoustic transponders 1000 m distant are indicated by red dots. The 12 OBSs will be deployed at the locations of the white stars. The J15-3 towed source will be deployed primarily within 50 km range of the O-DVLA. The red circles have radii of 2 and 12 km. The bathymetry is a combination of multibeam data and Smith-Sandwell v15.1.

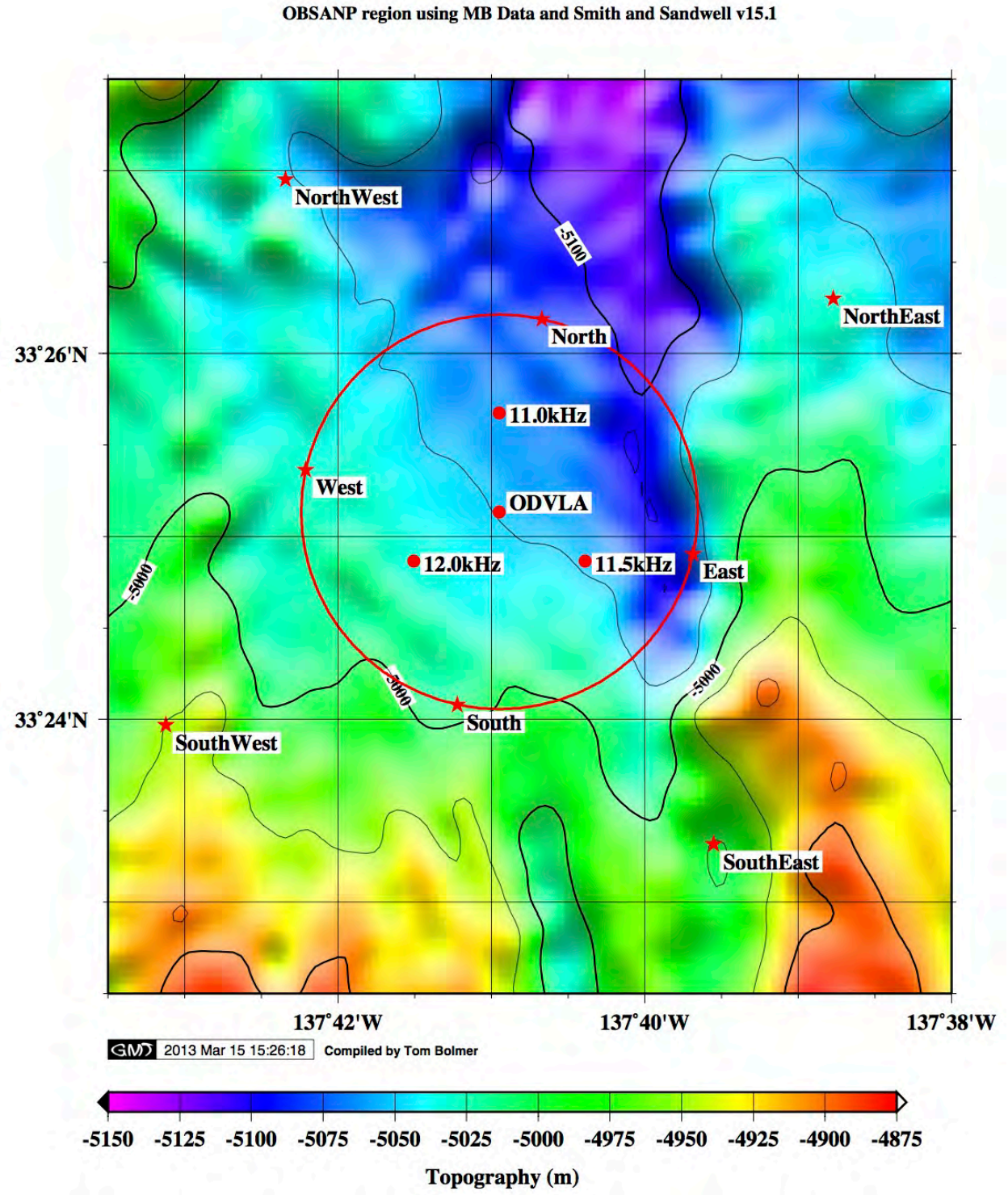

Figure 12.2: Blowup around the O-DVLA
Same as Fig. 12.1, except providing a close-up of the locations of the O-DVLA, acoustic transponders (11.0, 11.5, and 12.0 kHz), and OBSs in the immediate vicinity of the O-DVLA.

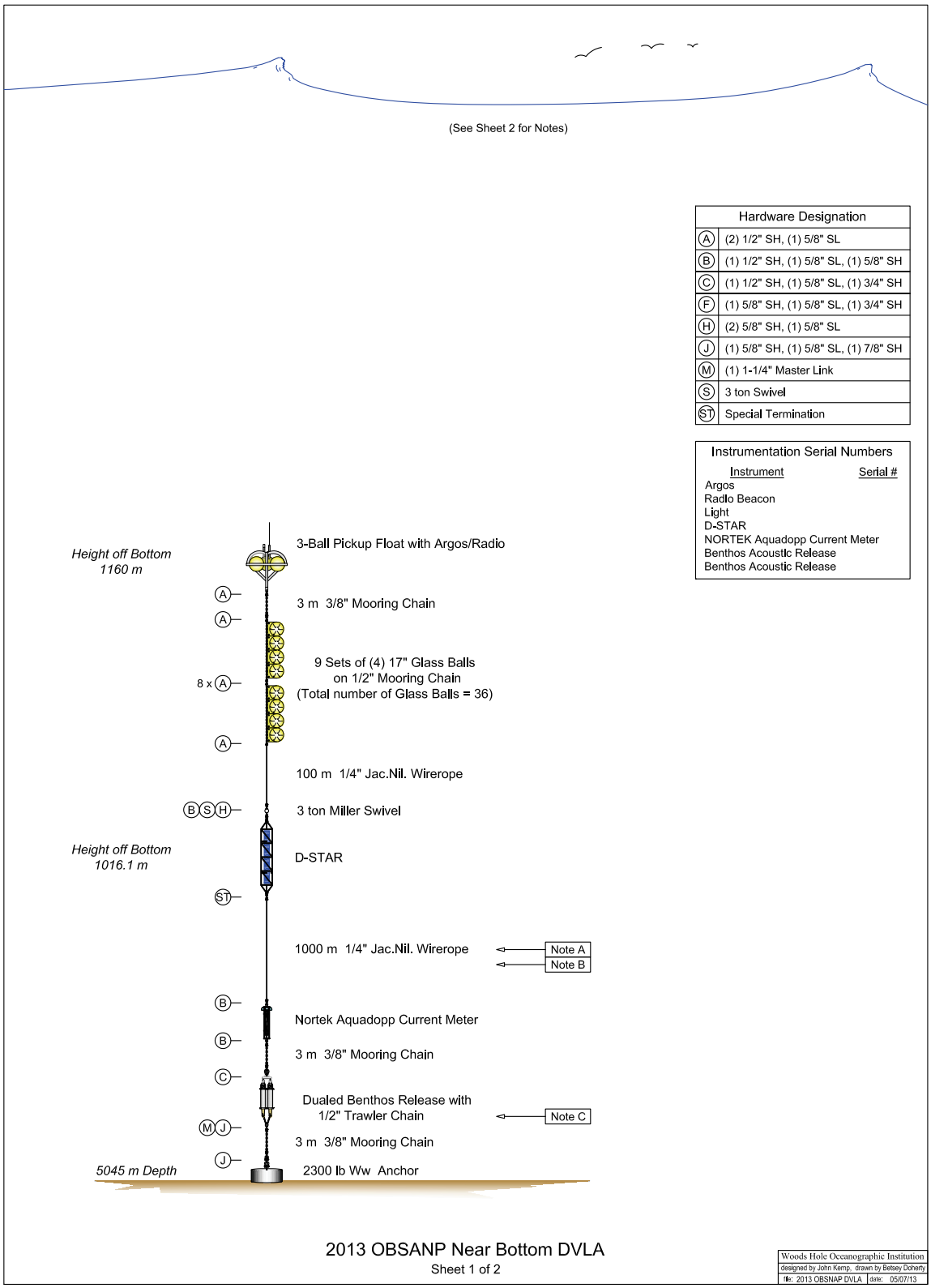

Figure 12.3: Near-seafloor O-DVLA mooring.

Hardware Required (Per Mooring Without Spares)	
Qty	
26	1/2" Anchor Shackles
7	5/8" Anchor Shackles
1	3/4" Anchor Shackles
2	7/8" Anchor Shackles
18	5/8" Sling Links
1	1 -1/4 Master Link
1	3 ton Swivel with Anode

Spares Required	
Qty	
1	1000 m DVLA shot of wire with 32 marks
1	100 m shot of wirerope
1	Set of components below release
1	Anchor
20%	Spares on Remaining Hardware

Note A			
Measure 1/4" IM cable back from lower swage for mounting hydrophone modules			
	Mark as follows:		
Measure	**Label**	**Mount**	**Serial**
1.0	H31	Hydrophone	TBD
11.0	H30	Hydrophone	TBD
21.0	H29	Hydrophone	TBD
31.0	H28	Hydrophone	TBD
41.0	H27	Hydrophone	TBD
51.0	H26	Hydrophone	TBD
61.0	H25	Hydrophone	TBD
71.0	H24	Hydrophone	TBD
81.0	H23	Hydrophone	TBD
91.0	H22	Hydrophone	TBD
101.0	H21	Hydrophone	TBD
111.0	H20	Hydrophone	TBD
121.0	H19	Hydrophone	TBD
131.0	H18	Hydrophone	TBD
141.0	H17	Hydrophone	TBD
151.0	H16	Hydrophone	TBD
256.0	H15	Hydrophone	TBD
361.0	H14	Hydrophone	TBD
466.0	H13	Hydrophone	TBD
571.0	H12	Hydrophone	TBD
676.0	H11	Hydrophone	TBD
781.0	H10	Hydrophone	TBD
886.0	H9	Hydrophone	TBD
896.0	H8	Hydrophone	TBD
906.0	H7	Hydrophone	TBD
916.0	H6	Hydrophone	TBD
926.0	H5	Hydrophone	TBD
936.0	H4	Hydrophone	TBD
946.0	H3	Hydrophone	TBD
956.0	H2	Hydrophone	TBD
966.0	H1	Hydrophone	TBD
976.0	H0	Hydrophone	TBD

Note B
Mooring will be deployed using SIO TSE Winch.

Note C
MOE will supply Benthos Dualing Strongback

2013 OBSANP Near Bottom DVLA
Sheet 2

Figure 12.4: Near-seafloor O-DVLA mooring.

13 Appendix B. Ocean Bottom Seismometer Augmentation in the North Pacific (OBSANP): Cruise Quick-look Report

July 9, 2013
Peter Worcester (SIO) and Ralph Stephen (WHOI)

R/V Melville Cruise MV1308: Peter Worcester, Chief Scientist
San Diego, California – Seattle, Washington
12 June– 11 July 2013

A new class of acoustic arrivals was observed on ocean bottom seismometers (OBSs) during the 2004 Long-range Ocean Acoustic Propagation Experiment (LOAPEX). During this experiment an HX-554 acoustic source suspended from shipboard transmitted from a variety of ranges to a Deep Vertical Line Array (Deep VLA) receiver surrounded by four OBSs. The arrivals were called Deep Seafloor Arrivals (DSFAs), because they were the dominant arrivals on the OBSs, but were either undetected or very weak on the bottom hydrophone of the Deep VLA, located about 750 m above the seafloor. In a paper about to be published in JASA, we attributed some of these arrivals to bottom-diffracted, surface-reflected (BDSR) energy that scattered from a seamount near the Deep VLA and subsequently reflected from the sea surface before arriving at the OBSs.

During the Ocean Bottom Seismometer Augmentation in the North Pacific (OBSANP) experiment, we returned to the Deep VLA site with a near-seafloor Distributed Vertical Line Array (DVLA) receiver that extended upward 1000 m from the seafloor and 12 OBSs (eight short period and four long period) (Figure 13.1). Once the instruments were installed, we transmitted to them from 18 June through 3 July with a J15-3 acoustic source suspended from shipboard. The locations of the DVLA and OBSs and the J15-3 transmission program were designed to test the hypothesis that DSFAs correspond to BDSR energy, to further define the characteristics of the DSFAs, and to understand the conditions under which they are excited and propagate. The J15-3 transmissions were mostly within 50 km of the DVLA, but there was one long line to about 250-km range.

In addition to studying DSFAs, ambient noise data were acquired. Ultra-Low-Noise hydrophones developed by SAIC (ULN-SAIC) were integrated into two of the long-period OBSs.

All instruments (OBSs, DVLA, and the acoustic transponders used to measure the motion of the near-seafloor DVLA mooring) were successfully recovered prior to the end of the OBSANP cruise.

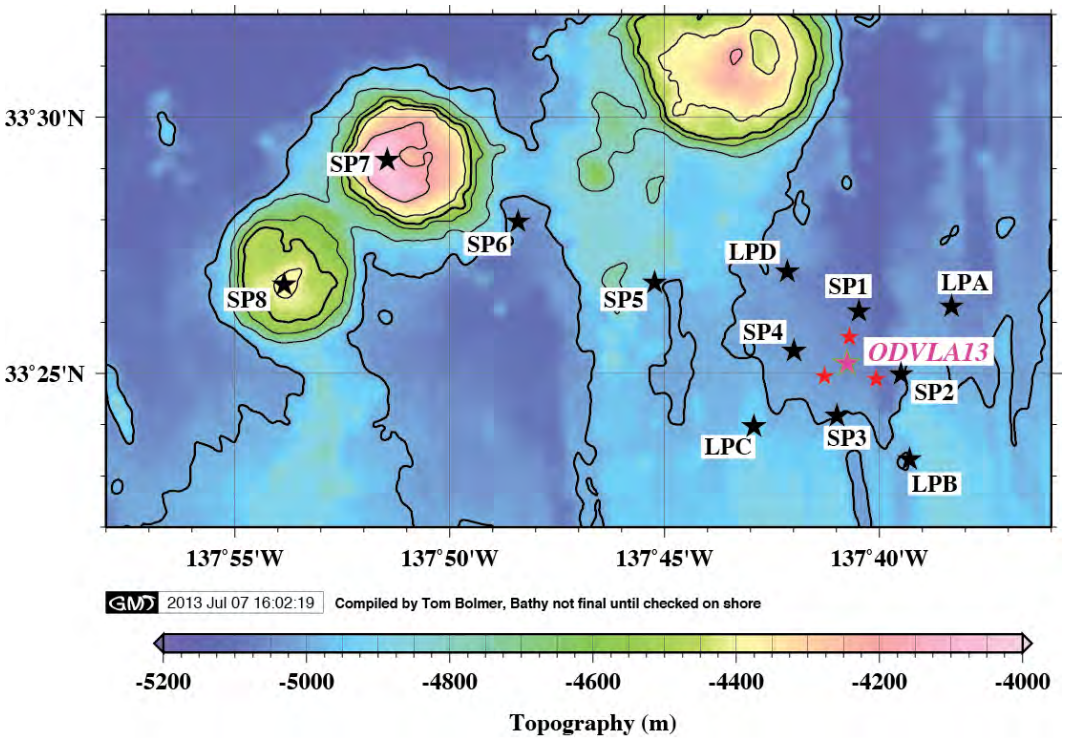

Figure 13.1: Locations of instruments.
Locations of the eight short period OBSs (SP*), the four long period OBSs (LP*), and the OBSANP DVLA (ODVLA13) with respect to the bathymetric relief. The three red stars around ODVLA13 are the acoustic transponders used to measure mooring motion.

13.1 Moored DVLA Receiver

The near-seafloor DVLA, referred to as the OBSANP-DVLA (O-DVLA) consisted of one 1000-m array with a D-STAR controller located at the top of the array and 32 Hydrophone Modules (HM) distributed along it (Figure 13.2). The deepest HM on the O-DVLA was 12 m above the seafloor, which is as close to the seafloor as an HM can conveniently be placed. Preliminary indications are that 27 of the HM worked properly, but for reasons that are not understood, five (5) HM apparently never started recording. Further investigation of the failures cannot be done until after the HM are returned to San Diego.

The O-DVLA was navigated using the long-baseline navigation system in the D-STAR and three Benthos TR-6001-17 recoverable acoustic transponders on the seafloor. The transponders functioned properly throughout the experiment.

A Nortek Aquadopp 6000-m acoustic current meter was located just above the acoustic releases on the O-DVLA. It appears to have functioned properly.

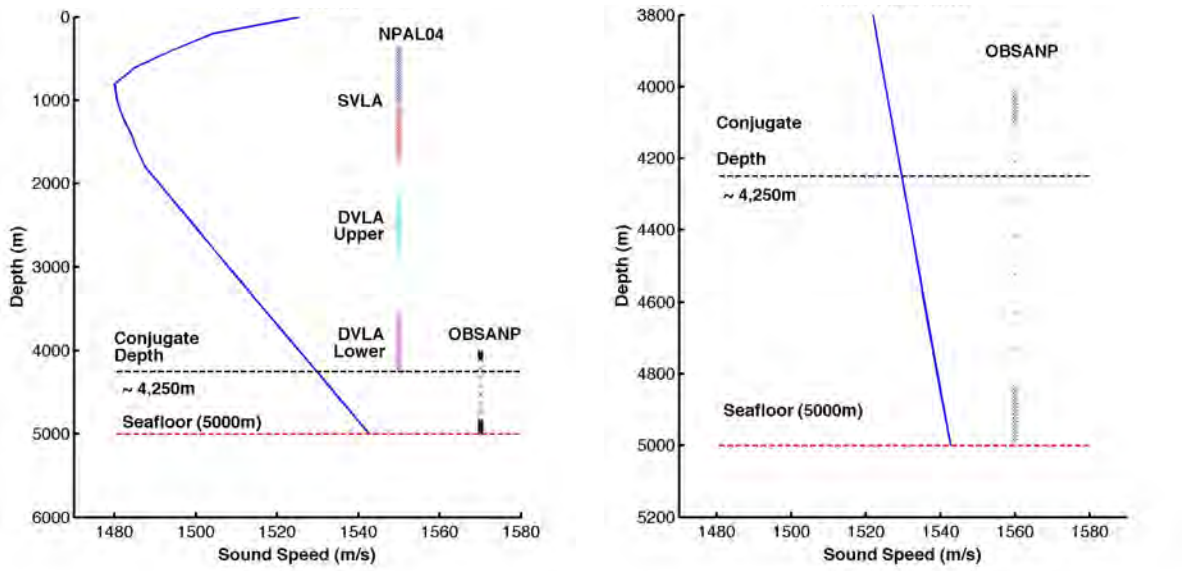

Figure 13.2: NPAL04 and OBSANP DVLA depths
DVLA depths (left) The OBSANP DVLA has 16 elements at 10 m spacing (λ/2 at 75 Hz) at the bottom, and ten elements at 10 m spacing at the top. The two mini-arrays are separated by six elements at 105 m spacing. The Shallow and Deep VLAs deployed for NPAL04 (SVLA and DVLA) are shown for comparison. A nominal sound speed profile from NPAL04 is shown. (right) An expanded view of the OBSANP DVLA.

13.2 Ocean Bottom Seismometers

The SIO OBSIP group provided eight (8) short-period and four (4) long-period OBSs. Four of the short-period OBSs (SP1-SP4) were installed about 2000 m from the O-DVLA. The four long-period OBSs (LPA-LPD) were installed about 4000 m from the O-DVLA. These eight instruments were aligned with respect to the LOAPEX source geodesic. Two short period OBSs (SP7 and SP8) were located as close as possible to the tops of Seamounts B and C, respectively, to measure the incident field at these features. The final two short period OBSs (SP5 and SP6) are on a line between Seamount B and the O-DVLA.

The short-period OBSs have three-component Mark Products L22 28-Hz geophones and an HTI-90-U hydrophone. The long-period OBS have broadband, three-component Trillium 240 seismometers and a Differential Pressure Gauge (DPG). SAIC Ultra-Low-Noise hydrophones (ULN-SAIC) were integrated into two of the long-period OBSs (LPA and LPC). All OBS sampled at 1000 Hz. All OBSs functioned normally.

Hydrophone Modules originally developed for the DVLA were attached to six of the short-period OBSs (SP1-SP4, SP7, and SP8) to supplement the hydrophones included in the short-period instruments. Preliminary indications are that all of these HM functioned correctly, although the data will not be downloaded until after the Secure Digital cards used in the HM are returned to San Diego.

13.3 J15-3 Acoustic Source

J15-3 operations were quite successful with no downtime due to equipment failure and essentially two weeks of scheduled transmissions. We transmitted primarily m-sequences at various frequencies spanning 20 to 310 Hz with the source at depths from 60 m to 100 m. The m-sequences fall into four categories: (1) multi-frequency, short range (< ½ CZ) tows at 77.5, 155, and 310 Hz; (2) single frequency, long range (up to 250 km, ~ 3½ CZ) tows at 77.5 Hz; (3) multi-frequency station stops at ½, 1½, 2½ and 3½ CZ at 77.5, 102.3, 155, 204.6, and 310 Hz; and (4) low frequency transmissions (19.375, 25.575, 38.75, and 51.15 Hz) at short ranges (< ½ CZ) to provide field data for modeling with SPECFEM3D. We also tested Minimum Shift Keying (MSK) format m-sequences, which are an alternative to our usual phase shift keying (PSK) format and could potentially have improved properties for some applications.

In the first phase of the transmission program, we carried out a "pin cushion" pattern of station stops spanning ½ CZ ranges to the O-DVLA and Seamount B (Figure 13.3). This pattern was designed to insonify Seamount B at a variety of sagittal and azimuthal angles and to distinguish bottom-diffracted from bottom-reflected energy.

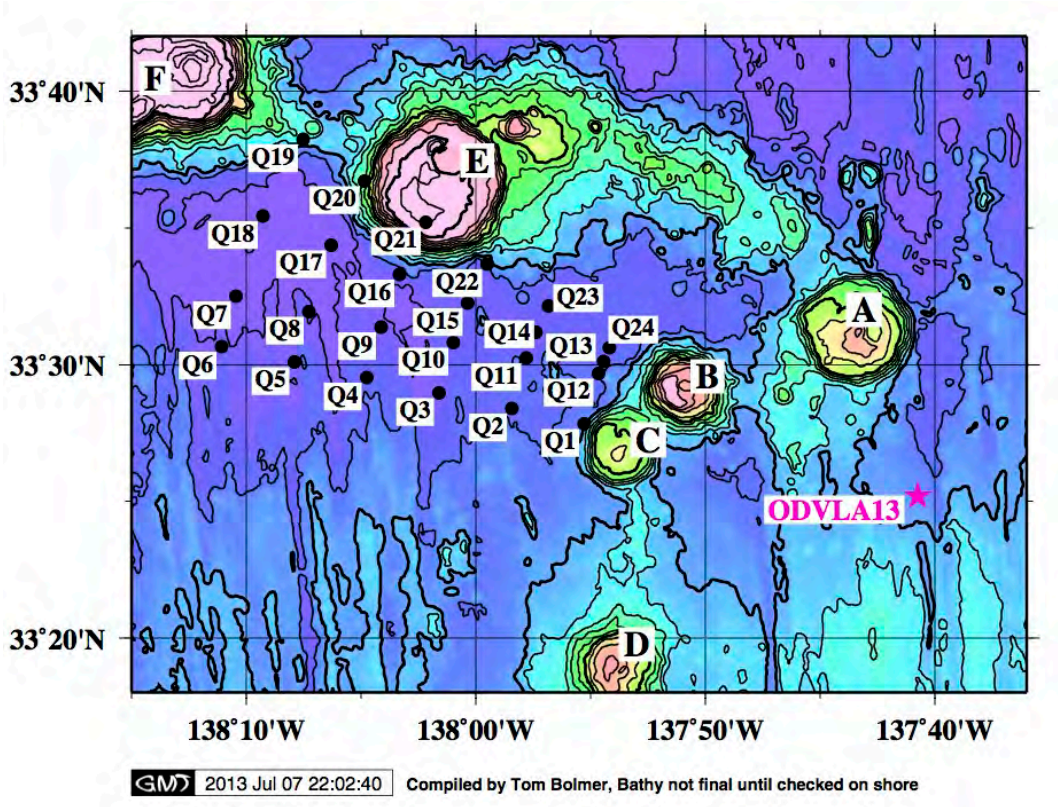

Figure 13.3: "pin cushion" of station stops
A "pin cushion" of station stops was designed to insonify Seamounts B and C at a variety of sagittal and azimuthal angles. The stations span ½ CZ from the O-DVLA and the seamounts. Q1 to Q6 are on the LOAPEX geodesic. Q13 to Q18 are collinear with Seamount B and the O-DVLA.

We attempted to replicate the LOAPEX results as closely as possible by carrying out a series of long- and short-range tows and station stops along the LOAPEX geodesic out to 250 km range (Figure 13.4). During LOAPEX, DSFAs were observed using the HX-554 source at ranges of 500 km and greater, so we could not duplicate the 2004 results directly. These transmissions will, however, fill in the long-range propagation story for short ranges along the same path.

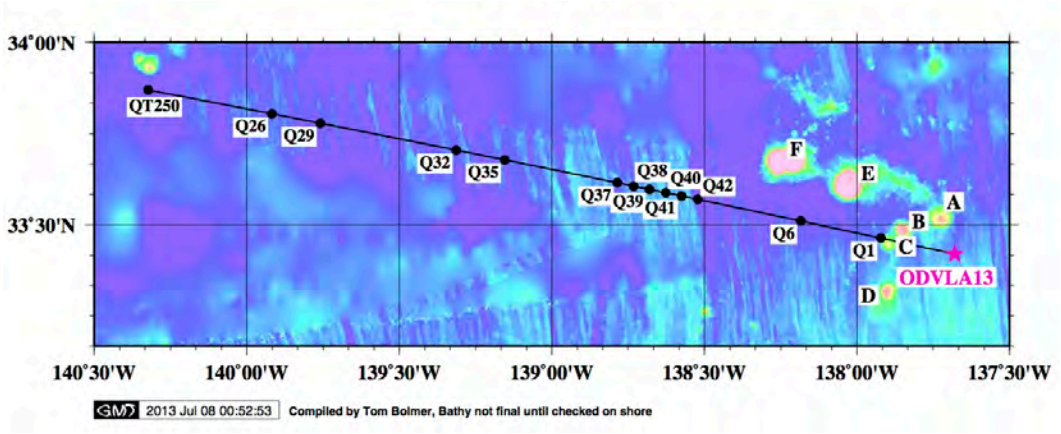

Figure 13.4: OBSANP Long line Station Stops
In an attempt to replicate the 2004 LOAPEX results, we transmitted continuously out to 250 km range on the LOAPEX geodesic and then occupied station stops at ½, 1½, 2½ and 3½ CZ's from the O-DVLA. Stations between Q1 and Q6 are shown in Figure 13.3.

In order to obtain a comprehensive view of propagation and scattering within ½ CZ to receivers on and near the seafloor, we carried out a series of radial line tows out to 50 km range at eight azimuths and half of a "Star of David" pattern over the seamounts across ½ CZ ranges (Figure 13.5). This pattern is similar to the OBSAPS experiment in the Philippine Sea in 2011, so propagation and scattering characteristics at the two sites can be compared.

In the fourth phase, we occupied two station stops within ½ CZ of both the O-DVLA and Seamounts B and C in order to carry out source tests that will be useful in subsequent experiments (Figure 13.6). We transmitted identical m-sequences in both MSK and PSK formats. We had not done MSK format transmissions in the past, but they have smoother phase than the PSK format, which could be an advantage for some types of sources. Also, although the J15-3 is not recommended for use below 100 Hz, we tested the source with CW and m-sequence transmissions down to 20 Hz. Source levels are quite low at these frequencies, but we are at very short ranges from the receivers and are optimistic that we will see useful returns. Full three-dimensional bottom-interaction problems with shear, that can be studied using codes like SPECFEM3D, are more tractable at these low frequencies.

13.4 Other Measurements

Five CTD and 92 XBT casts were made during the cruise. Extensive multibeam (Kongsberg Simrad EM122) and sub-bottom profiler (Knudsen 3260 3.5 kHz) measurements were made in the experimental area. The WaMoS system routinely provided information on the surface waves in the vicinity of the ship. AIS information was logged to provide information on other ships in the vicinity. Finally, routine shipboard data were collected throughout the cruise.

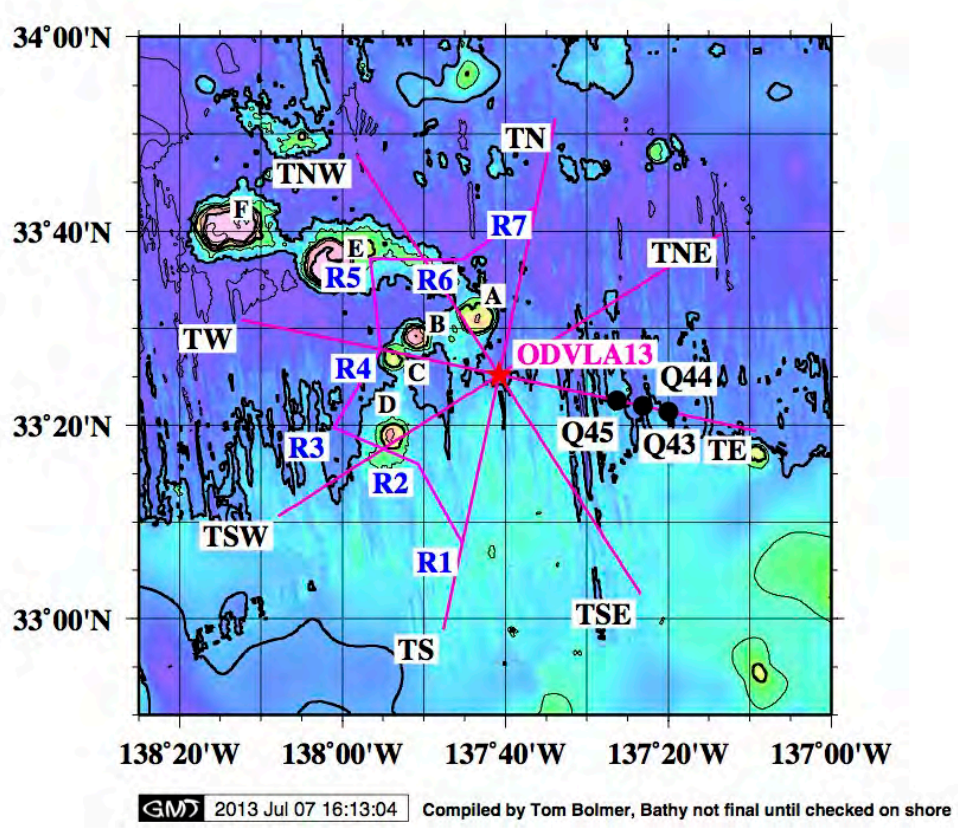

Figure 13.5: Phase 3 of the transmission program
Phase 3 of the transmission program carried out a comprehensive survey (out to 50 km) around the DVLA.

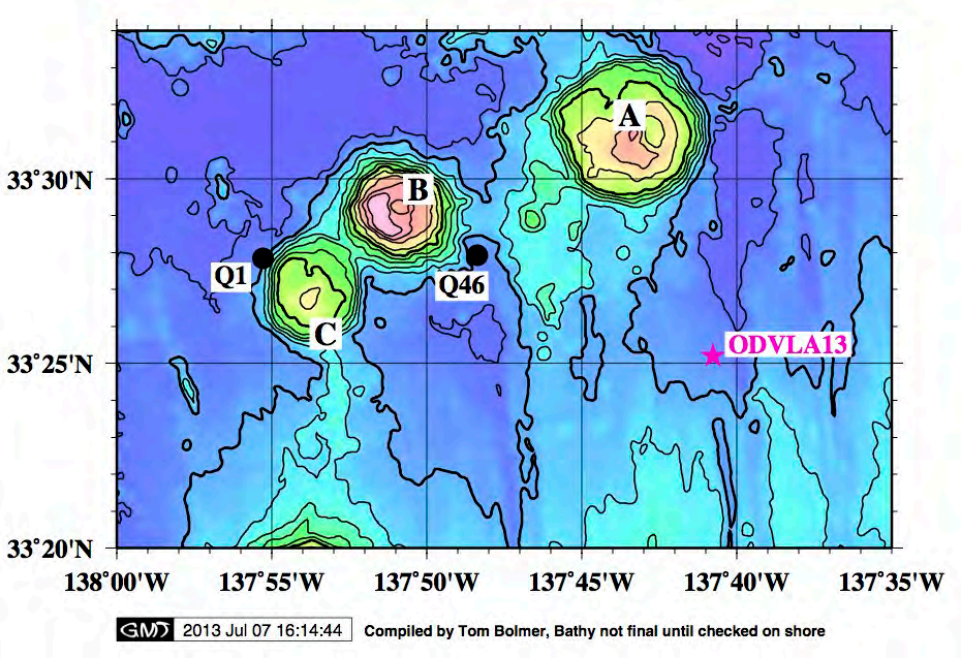

Figure 13.6: Q1 and Q46 were the locations of the MSK and low frequency tests.

13.5 Acknowledgments

The OBSANP experiment was conducted jointly by the Scripps Institution of Oceanography (Worcester) and Woods Hole Oceanographic Institution (Stephen). SIO (Worcester) was responsible for the DVLA. WHOI (Stephen) was responsible for J15-3 operations and was lead PI on the OBSIP effort. The SIO OBSIP group provided the OBS; Aaron (SIO) was responsible for OBS operations. We greatly appreciate the support from Captain Curl, the officers, and crew of the *R/V Melville,* who helped to make the cruise such a success. The experiment was funded by the ONR Ocean Acoustics Program (Code 322 OA).

Scientific Personnel	Institution
1. Ernie Aaron	SIO
2. Tom Bolmer	WHOI
3. Scott Carey	SIO
4. Sean McPeak	APL-UW
5. Matthew Norenberg	SIO
6. Jim Ryder	WHOI
7. Dr. Ralph Stephen	WHOI
8. Dr. Steve Swift	WHOI
9. Dr. Ilya Udovydchenkov	WHOI
10. Dr. Peter Worcester (Chief Scientist)	SIO

14 Appendix C: PE Models - Ilya Udovydchenkov

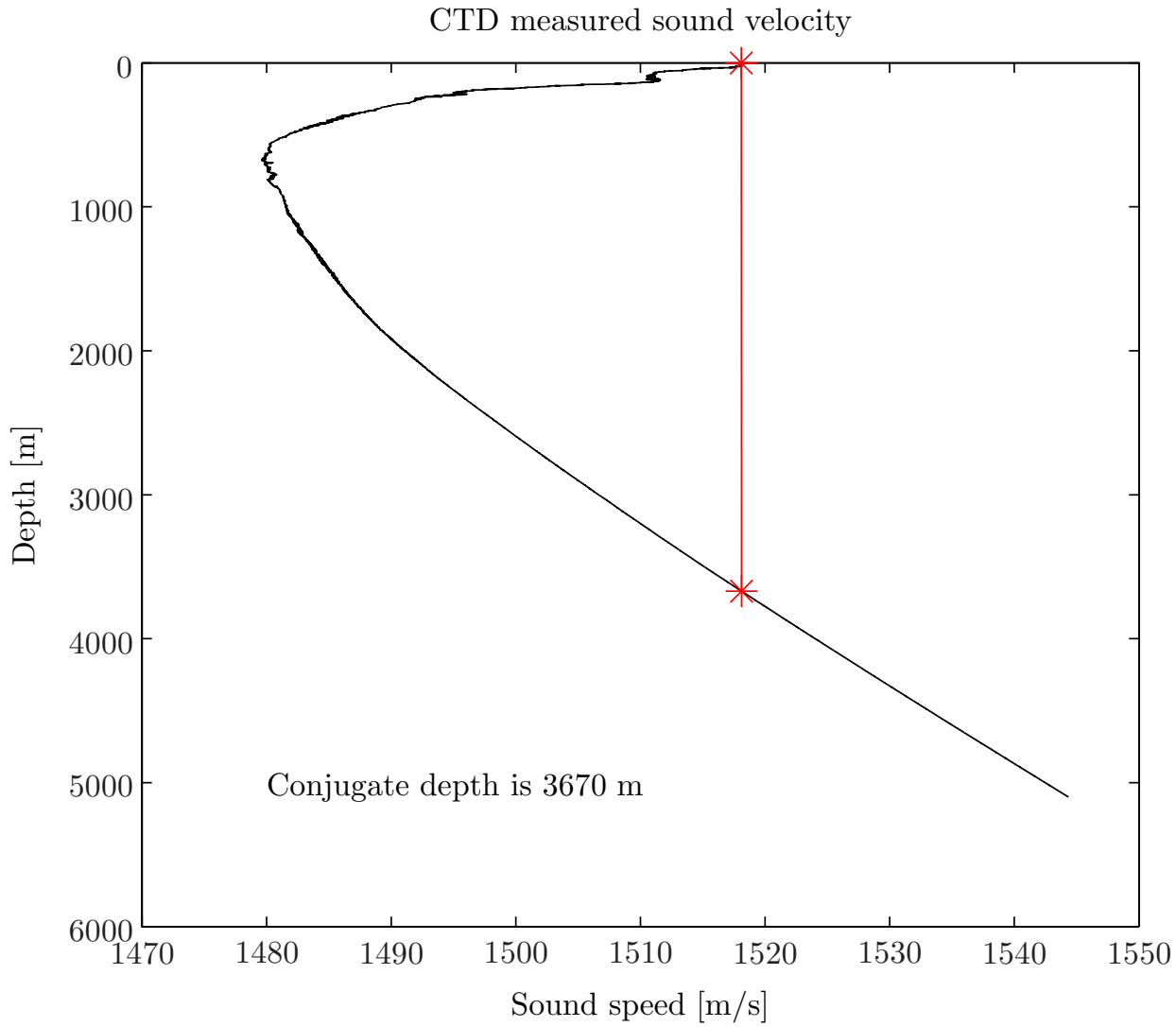

Figure 14.1: Estimate of the conjugate depth using the first CTD cast.

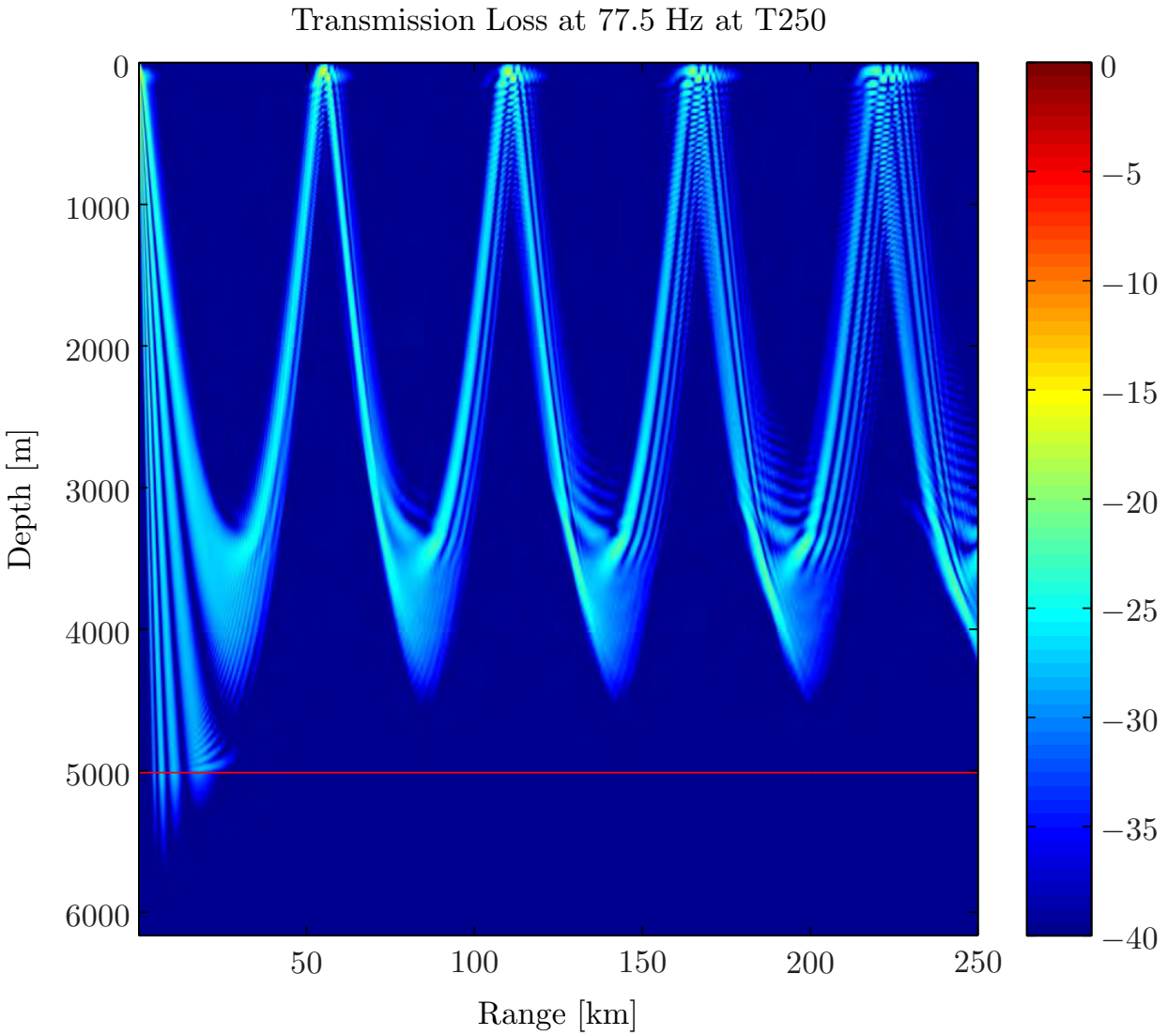

Figure 14.2: Example of transmission loss calculation
An example of the transmission loss calculation (based on the first CTD cast) that was used to estimate ranges for station stops.

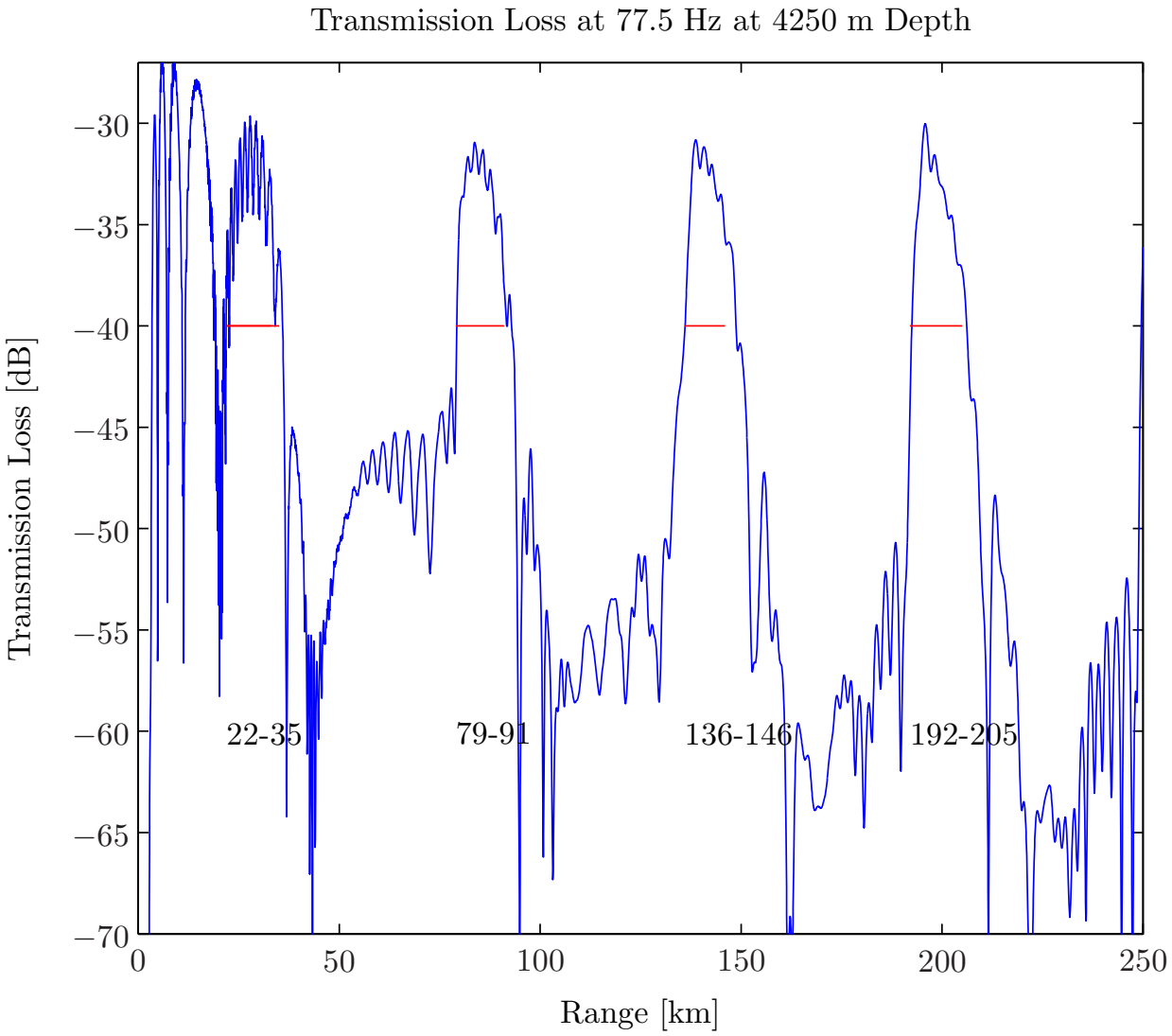

Figure 14.3: transmission loss curve for 4250m
The transmission loss curve for 4259m (depth of seamount B) and ranges for CZ arrivals.

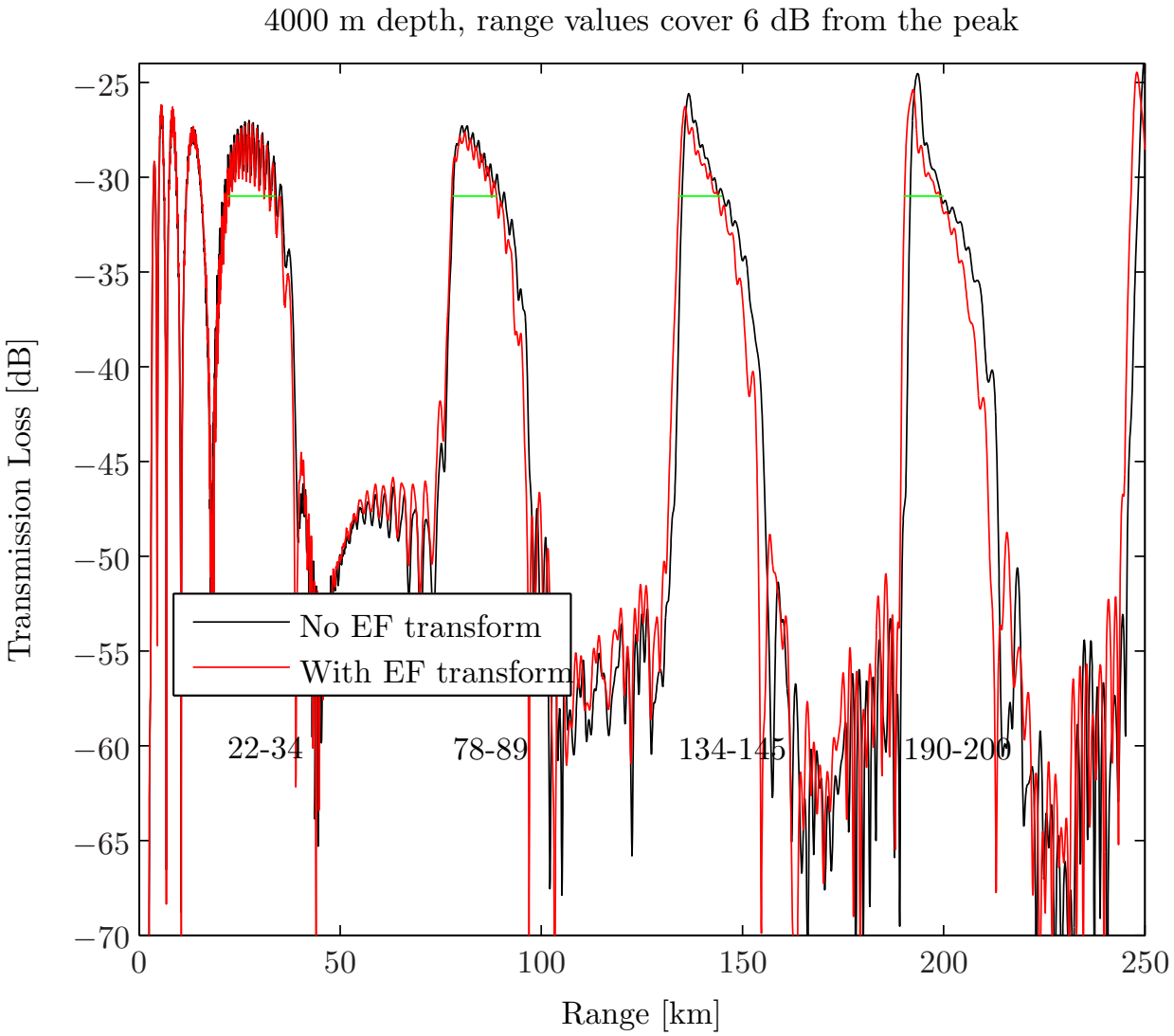

Figure 14.4: Transmission Loss at 4000m Depth

15 Appendix D: MSK tests - Ilya Udovydchenkov

cd('/Users/rstephen/Data/post_01-01-13/Corresp_13/OBSANP_13/M-sequences/Cruise_sequences/At_Sea_Archival/Ilyas_codes')

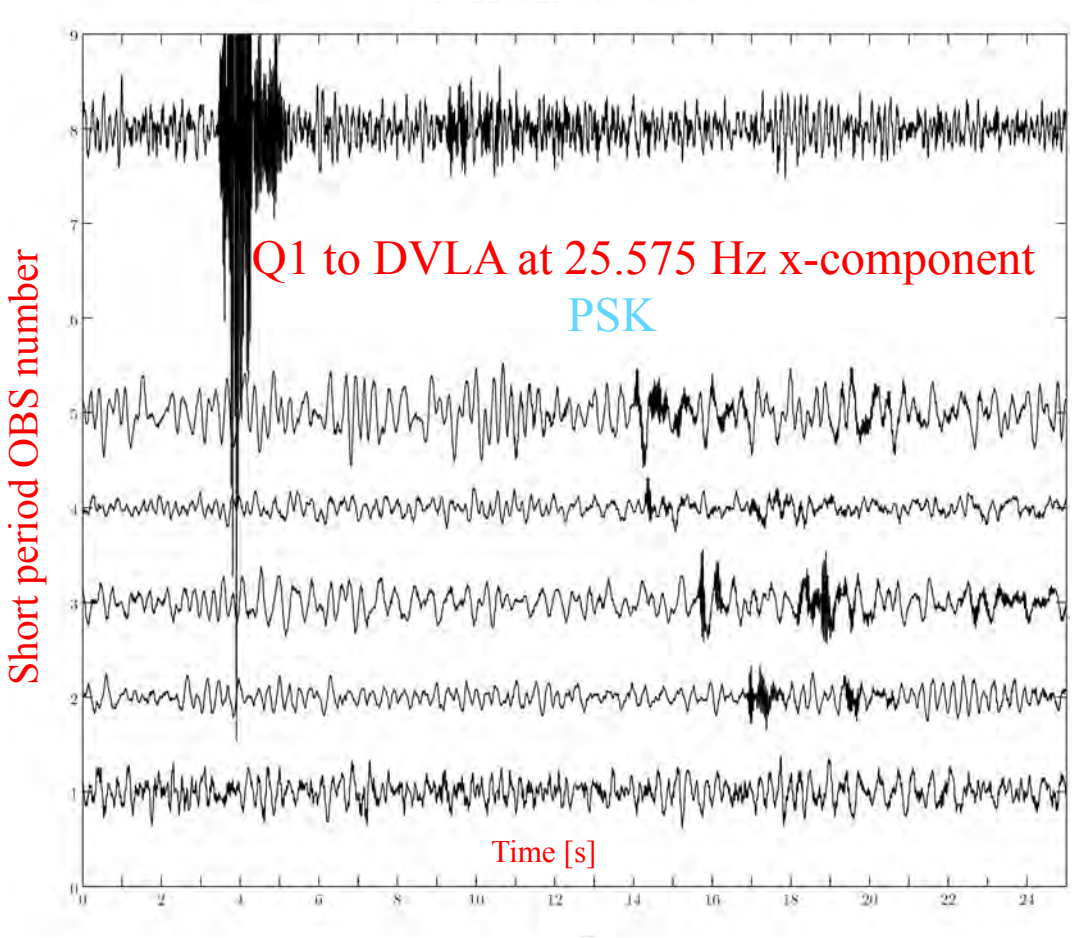

Figure 15.1: 25.575Hz PSK Test from Q1 to Short Period OBSs.

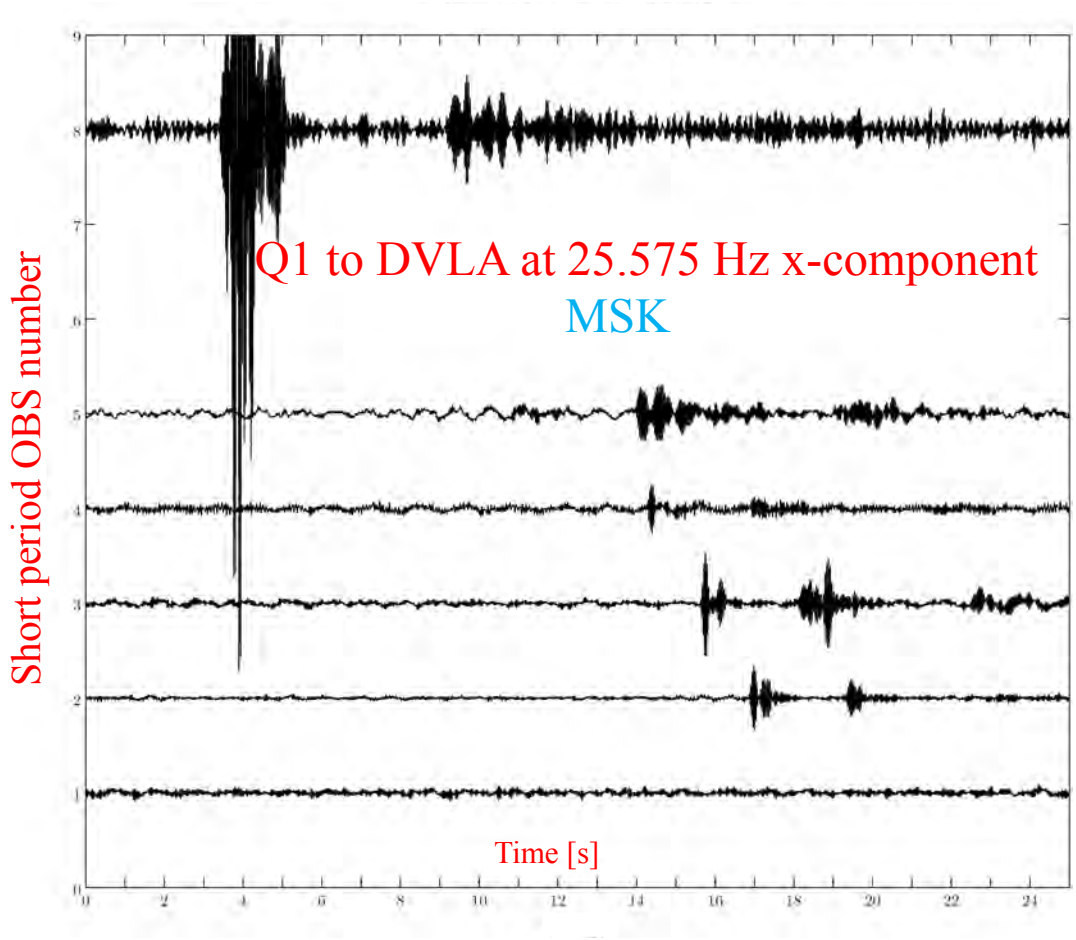

Figure 15.2: 25.575Hz MSK Test from Q1 to Short Period OBSs.

Final stage of the Experiment (Program 7)

Transmissions from Q1:

1. PSK and MSK M-sequences at 77.5, 102.3, 155, 204.6, and 310 Hz
2. PSK and MSK M-sequences and CW at 51.15, 38.75, 25.575, and 19.375 Hz

Transmissions from Q46:

1. PSK M-sequences at 77.5, 102.3, 155, 204.6, and 310 Hz
2. Higher power PSK M-sequence at 19.375 Hz

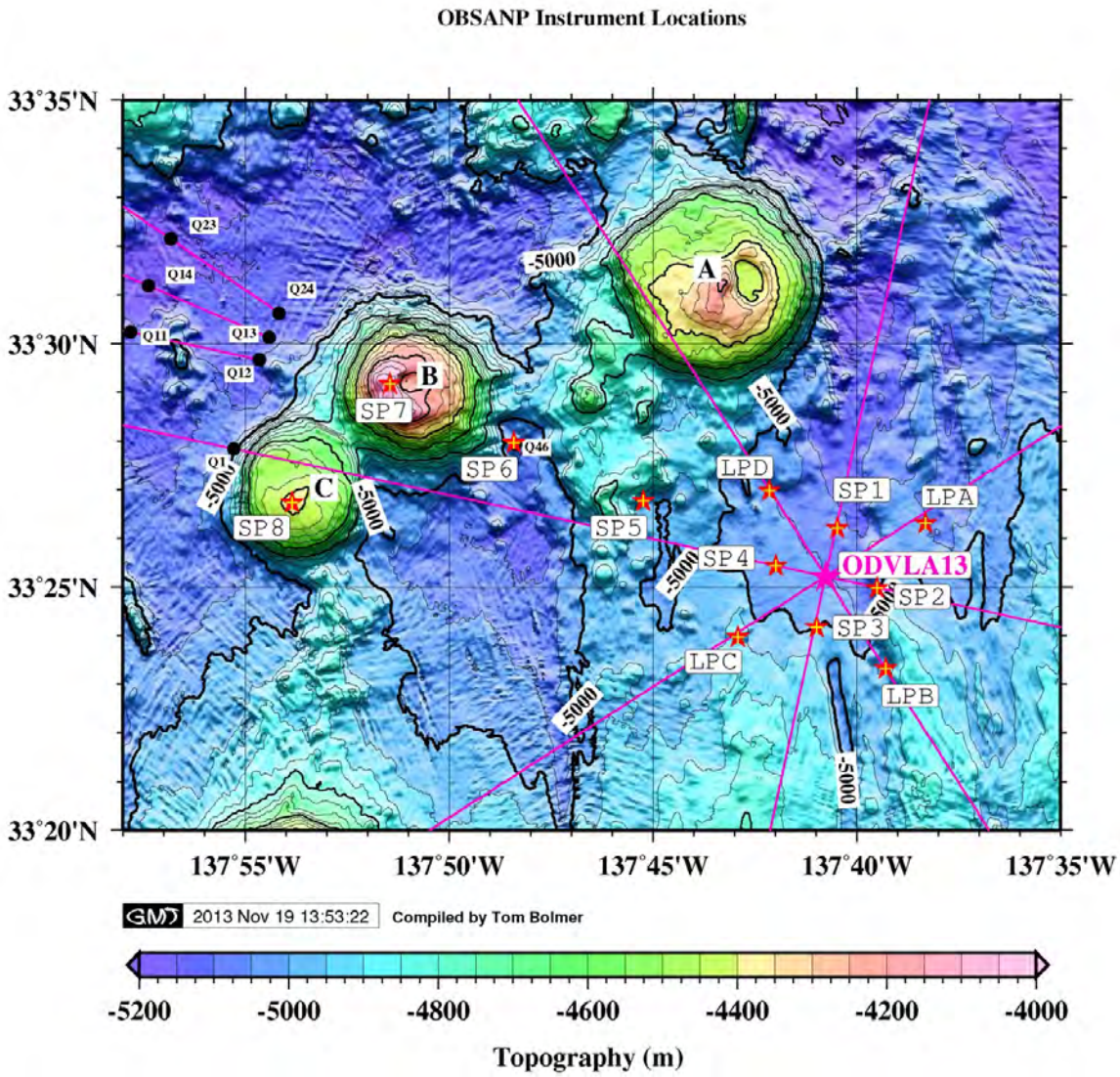

Figure 15.3: Bathymetry with instrument locations and station stops near Seamounts.

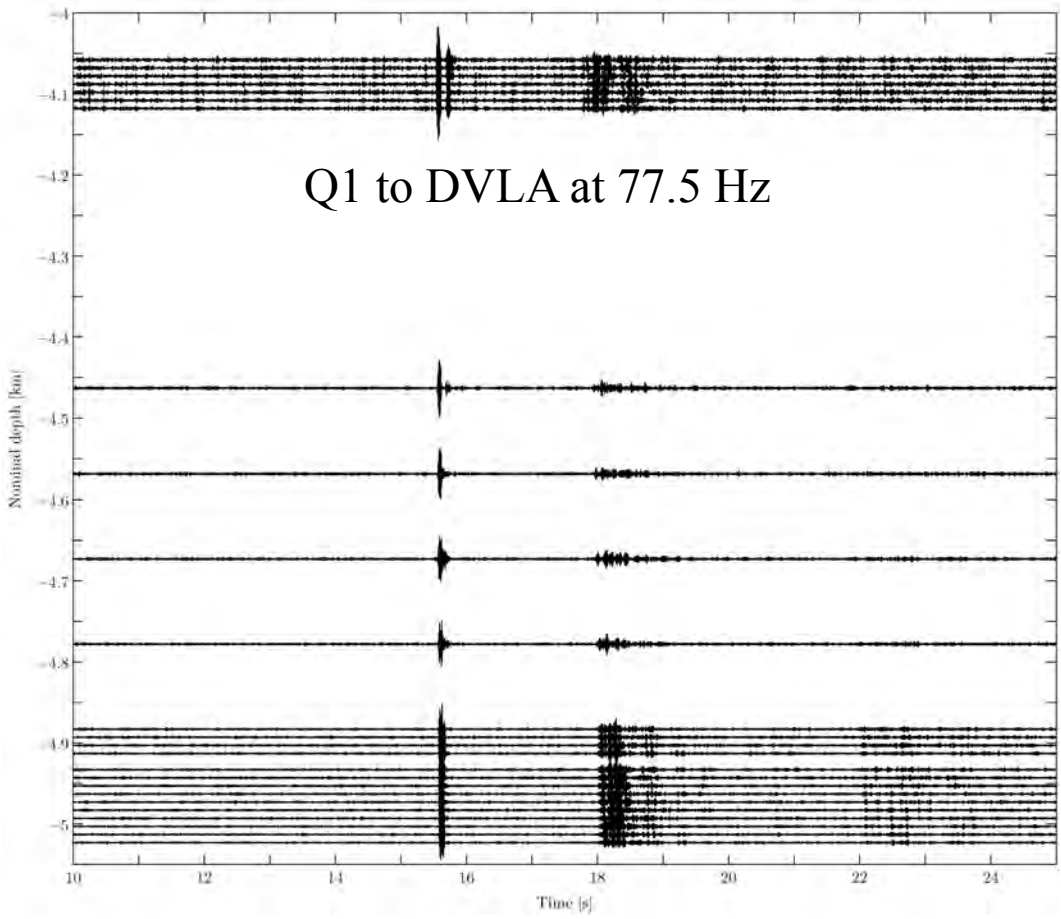

Figure 15.4: 77.5Hz PSK Test from Q1 to ODVLA

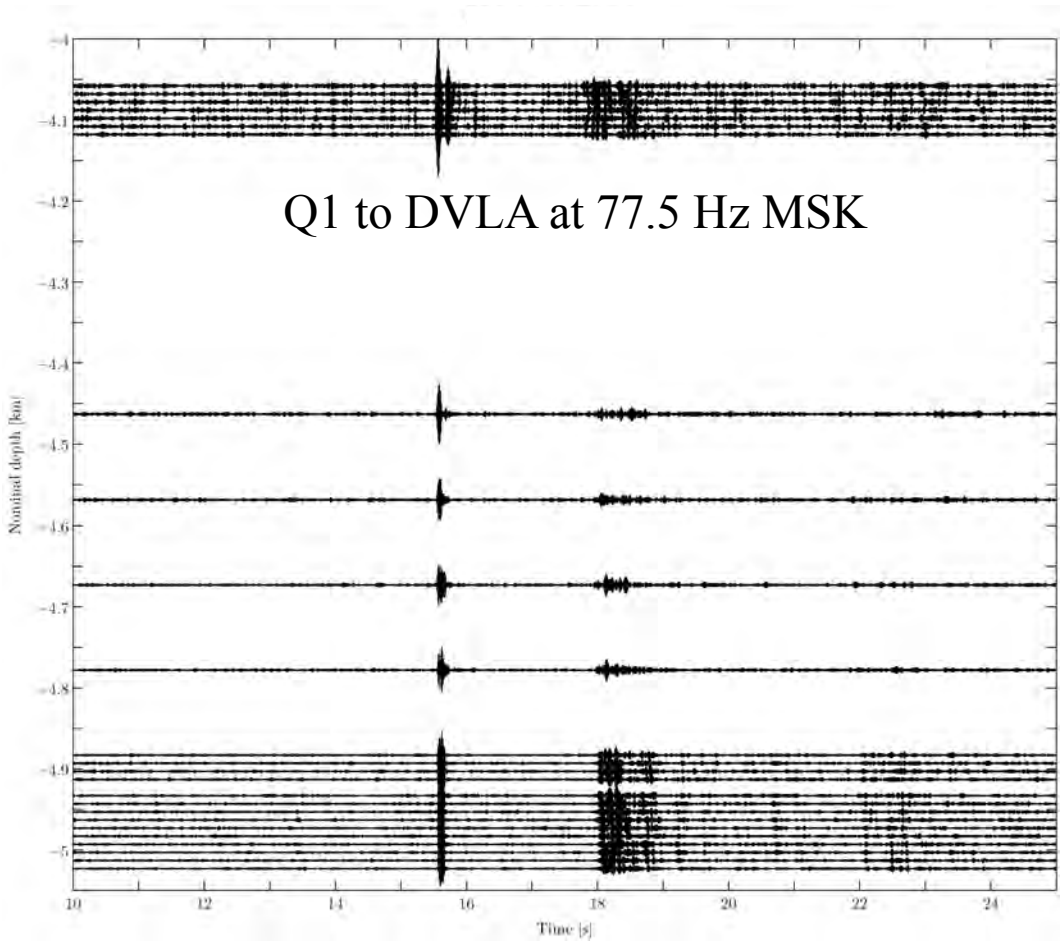

Figure 15.5: 77.5Hz MSK Test from Q1 to ODVLA

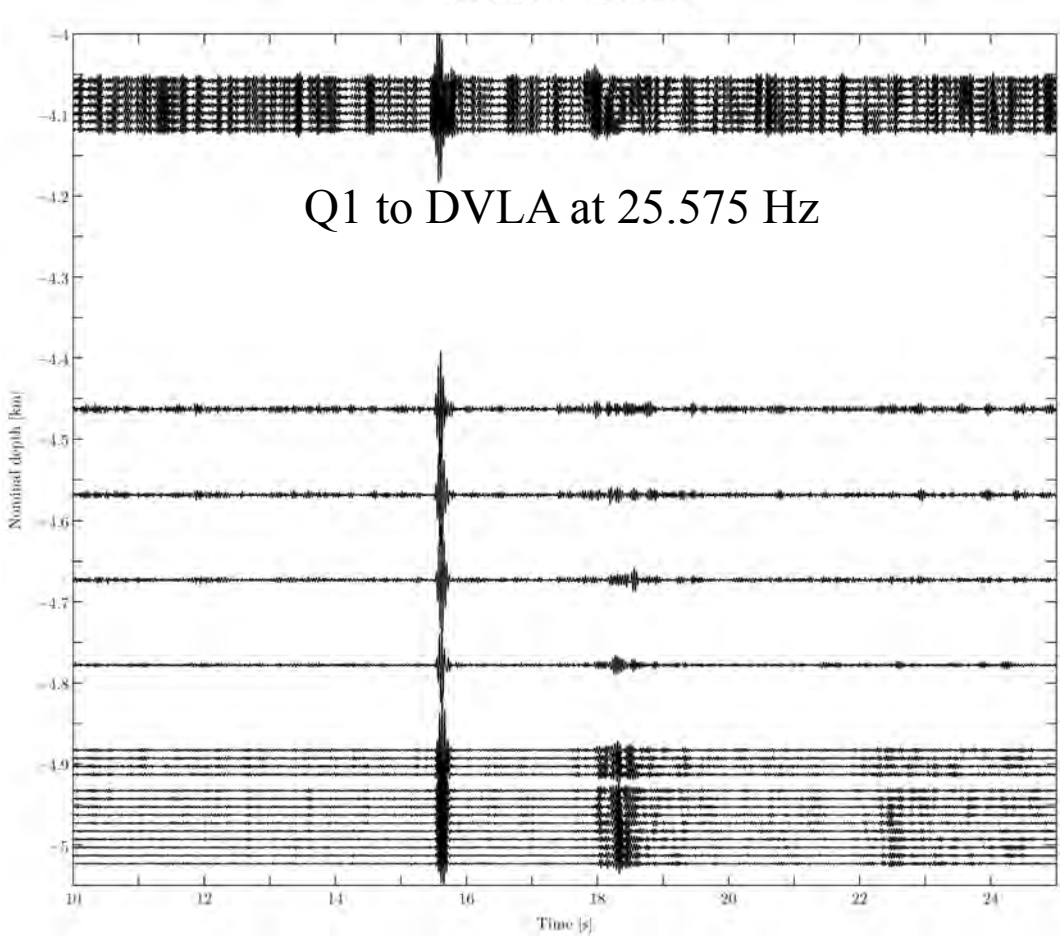

Figure 15.6: 25.575Hz PSK Test from Q1 to ODVLA

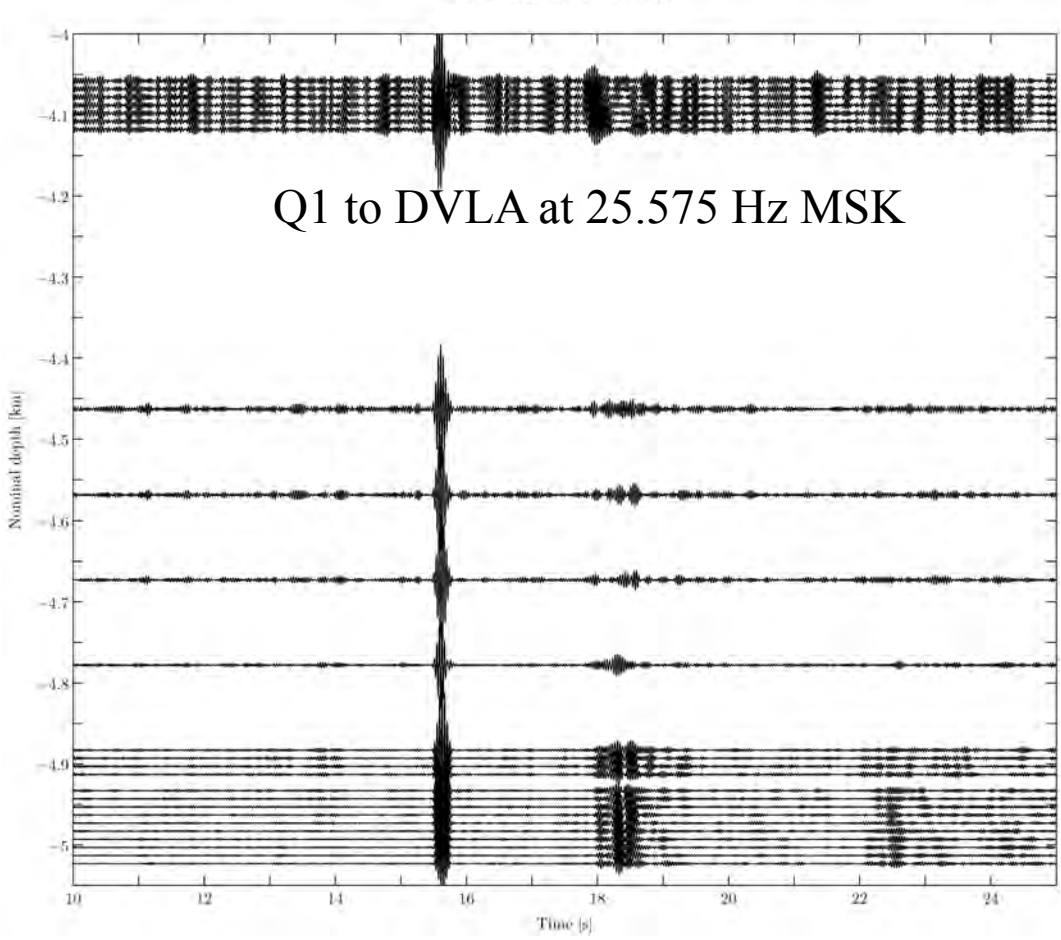

Figure 15.7: 25.575Hz MSK Test from Q1 to ODVLA

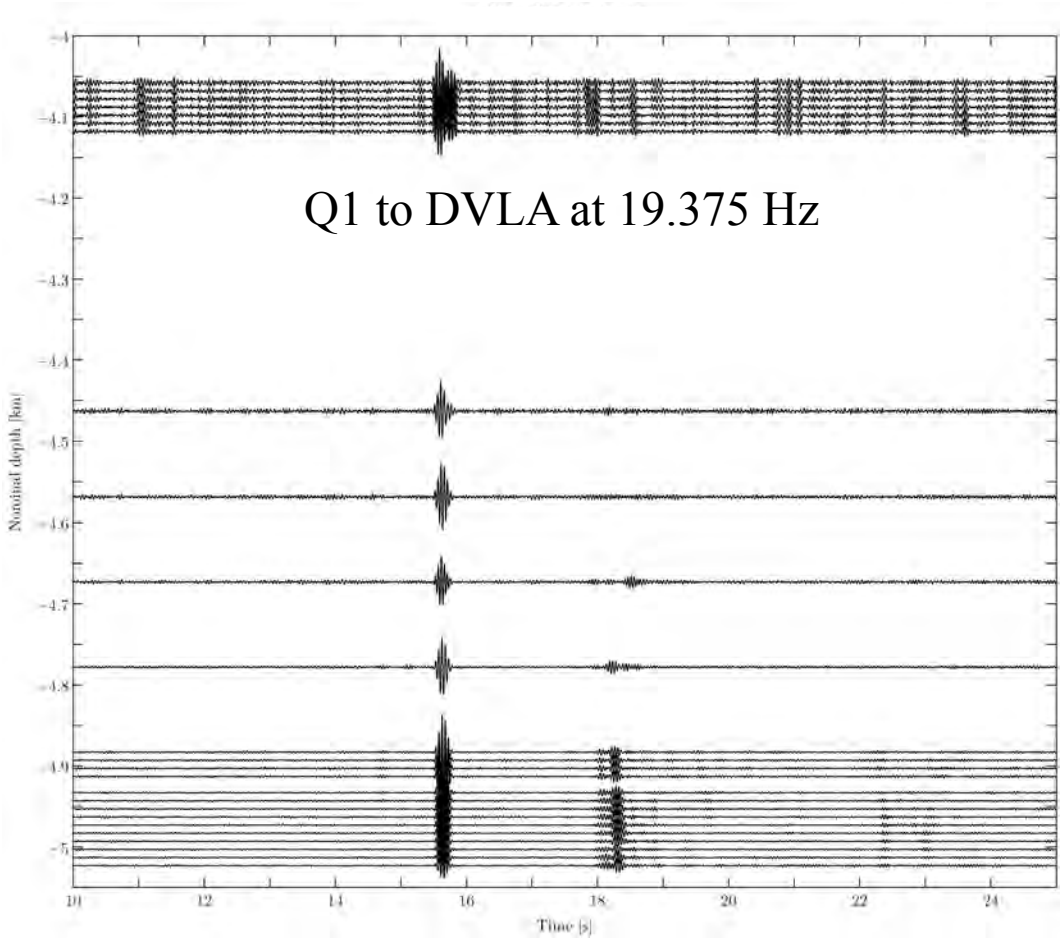

Figure 15.8: 19.375Hz PSK Test from Q1 to ODVLA

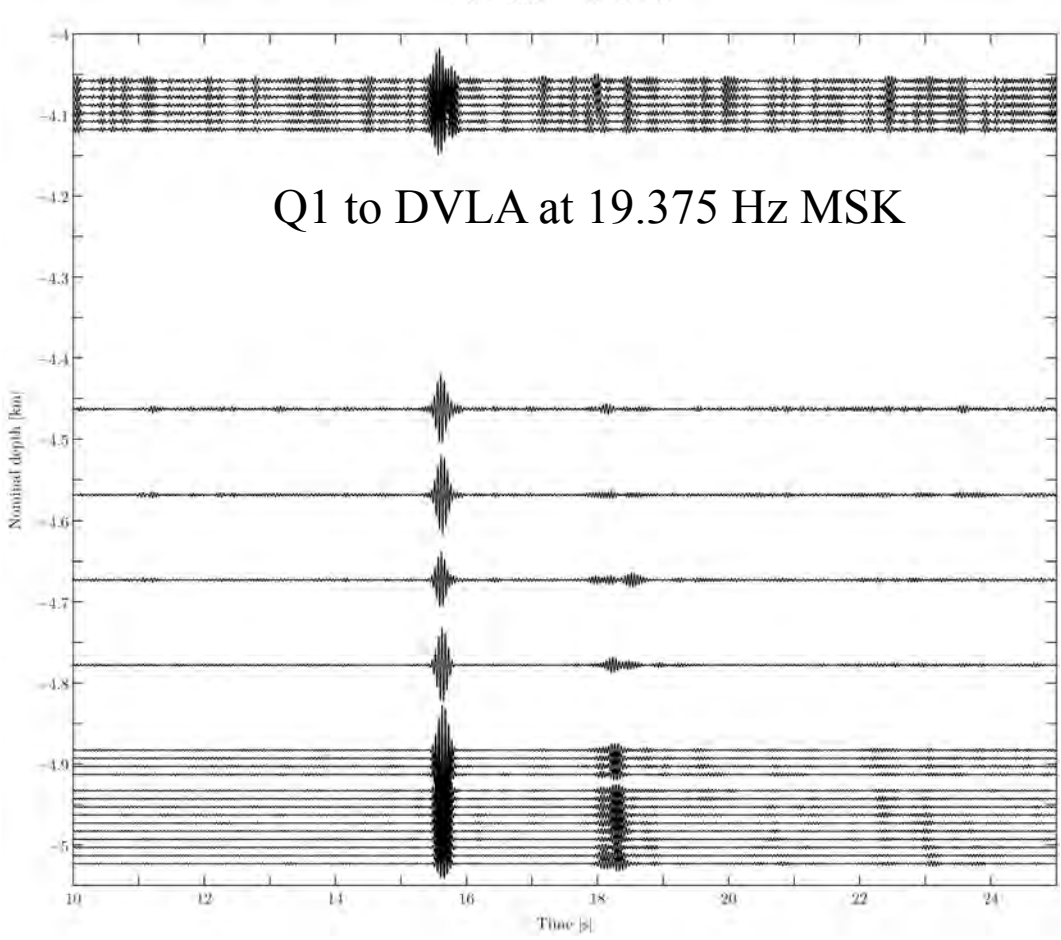

Figure 15.9: 19.375Hz MSK Test from Q1 to ODVLA

16 Appendix E: Low Frequency Feasibility Tests - Ilya Udovydchenkov

Ocean Bottom Seismometer Augmentation in the North Pacific (OBSANP): Program 7. Low Frequency Feasibility Test (LFFT)

16.1 Summary.

Program 7, or Low Frequency Feasibility Test (LFFT), was a phase of the OBSANP experiment conducted during year day 184. This phase lasted for approximately 18 hours. The first goal of this phase was to transmit signals encoded using the minimum shift key (MSK) method and compare receptions with regular m-sequences. Two main advantages of MSKs are that they occupy lower bandwidth (compared to regular m-sequence with similar properties) and that the derivative of the phase of the transmitted signal is continuous (the phase does not have "kinks" at the digit transition times). This behavior is more favorable for the mechanics of the source. The disadvantage of the MSK is a slight loss of time resolution in the compressed pulse, which was not expected to be an issue during this test. The second goal of the program 7 phase was to test the feasibility of very low frequency transmissions with J15-3 acoustic source. The carrier frequencies were chosen to be 51.15, 38.75, 25.575, and 19.375 Hz. Both, regular m-sequences and MSK's were transmitted at these frequencies. These transmissions (especially 19.375 Hz) recorded on the DVLA and OBSs are expected to be useful for 3D numerical propagation modeling studies. The main challenge with low frequency transmissions was that the source response to these signals was not known. It was uncertain at what level the source can be driven at these frequencies and how much power can be sent to the source in order not to cause damage ,while at the same time for signals to be loud enough to be detected on the DVLA and OBSs. The tests were complicated by a non-linear response of the monitoring hydrophone (H91) in this frequency band. It was not clear whether H91 response can be adequately processed to evaluate possible nonlinearities in the source behavior. The situation was complicated even further by constant presence of strong ambient noise (mostly from the ship), which masks the signal. A concern was that the source response might become nonlinear before the sound can be detected and reception can be evaluated for nonlinearities.

During these tests we relied on the data acquired during prior tests made in March 2013 at the CRL facility at WHOI. The number of tests at CRL was limited due to our inability to run a source at high power in a small enclosed basin indoors at those frequencies. However, CRL tests suggested that at 51.15 Hz and 19.375 Hz and 1 AMP current the nonlinearities in the recorded waveforms were either small or not visible. This current was used as a guideline for our tests at sea during LFFT.

There were two stations chosen for this phase: station Q1(33°27.8407N, 137°55.2772W; 33.46401N, 137.9213W) and station Q46(33°27.966N, 137°48.414W; 33.46610N, 137.80690W). Q1 was chosen because it is approximately (slightly less than) ½ convergence zone away from the DVLA and is in the vicinity of interesting topographic features (2 seamounts). Also, OBSs SP7 and SP8 were in the vicinity of Q1. The station Q46 was chosen because it is closer to the DVLA and is in the direct propagation path. Also, Q46 was right on top of the OBS SP6. Should the transmissions from Q1 turn out to be too quiet to be detected on the DVLA, transmissions from Q46 would have much better chance being detected due to shorter range. While transmissions from Q46 are less appealing from the scientific perspective, they provide a valuable benchmark for the signal levels at the DVLA and OBSs.

The outcome of the LFFT experimental phase is that higher frequencies m-sequences and MSK's were transmitted from the station Q1 (the frequencies were 77.5, 155, 310, 102.3, and 204.6 Hz). Also, both m-sequences and MSKs at all four low frequencies were transmitted from Q1. Regular m-sequences at frequencies 77.5 Hz and higher were transmitted from Q46. Due to timing constraints for this phase only one regular m-sequence (at 19.375 Hz) was transmitted from Q46. Low frequency signals at Q1 were transmitted at 1 AMP current (approximately 80 W) and the last low frequency transmission at Q46 was transmitted at 1.2 AMPS (approximately 120 W). No MSKs were transmitted from Q46. The source depth was 100 m for all transmissions.

16.2 Testing procedure.

The goal of the testing procedure during LFFT was to determine the appropriate scaling amplifier gain (and hence, the current) at which the source can be operated without exhibiting nonlinear behavior. It was expected, that the source response at the fixed scaling amplifier gain would be frequency dependent. Thus, all tests were conducted at all four frequencies used in this phase. The following procedure has been adopted:

1) We assumed that the safe starting point at any frequency would be with scaling amplifier gain set to 0.05. This value was used for on-deck testing at higher frequencies to check the source operation. The vibrations of the speakers were barely noticeable (if touched) and could only be heard if an observer was within a few centimeters from them.
2) We gradually increased the scaling amplifier gain (with 0.05 increments) and observed waveforms and spectra on the oscilloscope and in the Labview. This test was repeated at every frequency. At 51.15 Hz the scaling amplifier gain was increased to 0.8, resulting in the current of 1 AMP. At this point secondary harmonics were noted in the Labview spectra, and it was decided to analyze H91 receptions more carefully. At 38.75 Hz the maximum scaling amplifier gain was 0.7 (with the current of 0.93 A). However, at lower frequencies both Labview spectra and H91 waveform, and oscilloscope signal were useless, because it became very difficult to distinguish the signal from the noise. The maximum scaling amplifier gains were 0.45 (0.63 A) at 25.575 Hz, and 0.3 (0.41A) at 19.375 Hz.
3) The test signals (CW, and m-sequences) were created at each frequency and recorded with the maximal gain estimated from the previous test for more thorough analysis. Four 1 minute long CW records were created, and four 2-periods long m-sequence records were created at each frequency. The files were transferred to a laptop and further analyzed with the software developed in Matlab.
4) In Matlab, the H91 monitoring hydrophone record was visually inspected for the signs of nonlinearity ("sharp corners" of the waveform near extremes), a spectrum was analyzed by computing the magnitude of the fast Fourier transform (FFT) and also by estimating power spectral density via the Thomson multitaper method (PMTM). Also, test m-sequences (2-periods long) were pulse compressed (using matched filtering) and a secondary peak (which appears at the digit 531 in this particular m-sequence, *Peter Worcester, priv. comm.*) was analyzed. It was suggested that the nonlinearity is insignificant if a) it is not observed (by visual inspection) on H91 record, and b) the secondary peak in the compressed m-sequence is around 20

dB or more below the main peak, and c) the secondary peak in the spectra (both FFT and PMTM) of the CW signals is around 12 dB or more below the main peak.

5) These tests were repeated for various scaling amplifier gain settings at all four frequencies. The final value for the station Q1 was the gain setting of 0.75 with the current around 1 AMP. At Q46 the last low frequency transmission was done with the scaling factor 0.9, which corresponded to about 1.2 AMPS current.

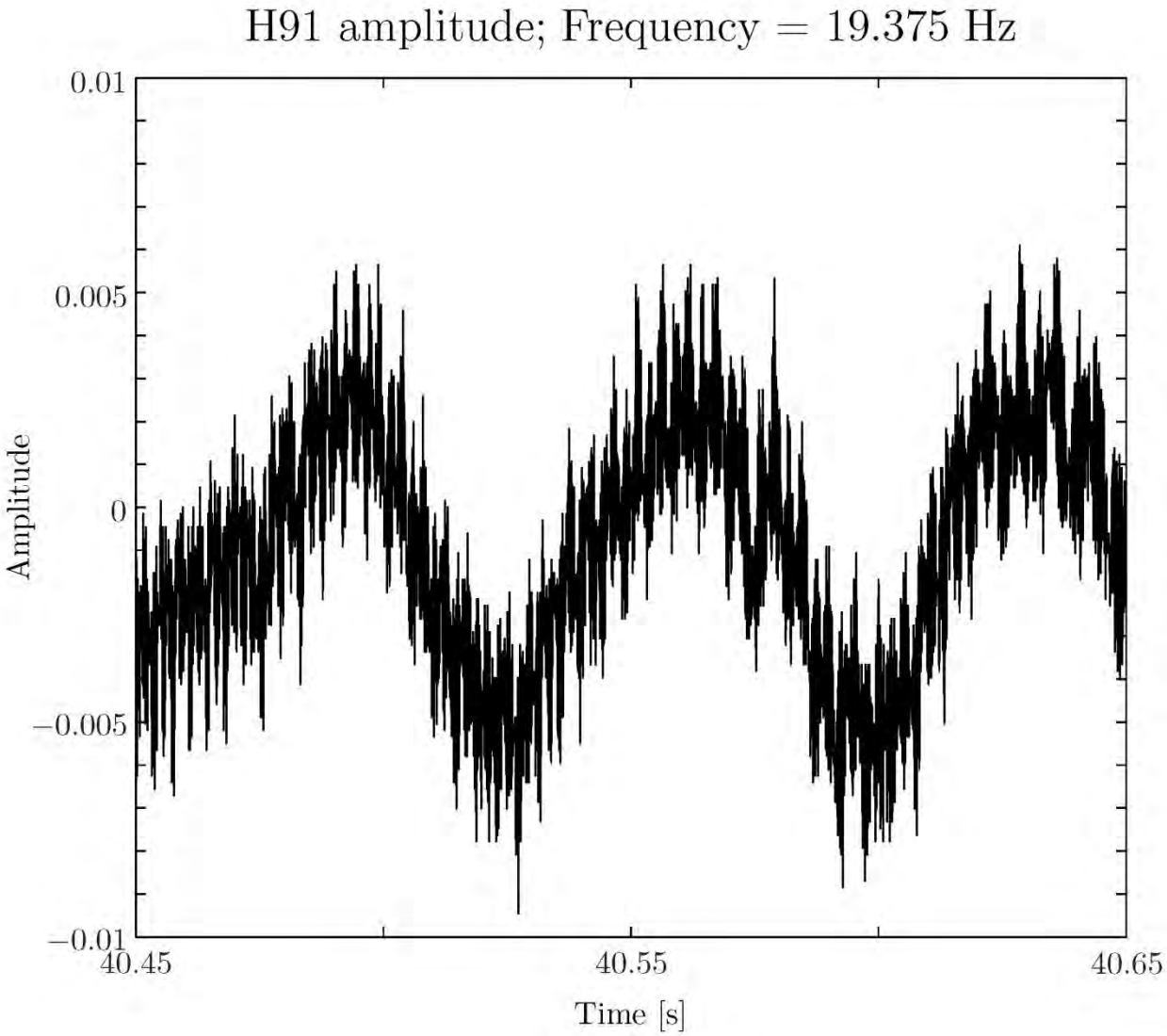

Figure 16.1: Example of the waveform recorded by H91 monitoring hydrophone
An example of the waveform recorded by H91 monitoring hydrophone during a transmission in the LFFT. This example is taken from the 19.375 Hz m-sequence transmission from the Q46 station (last low frequency transmission during LFFT).

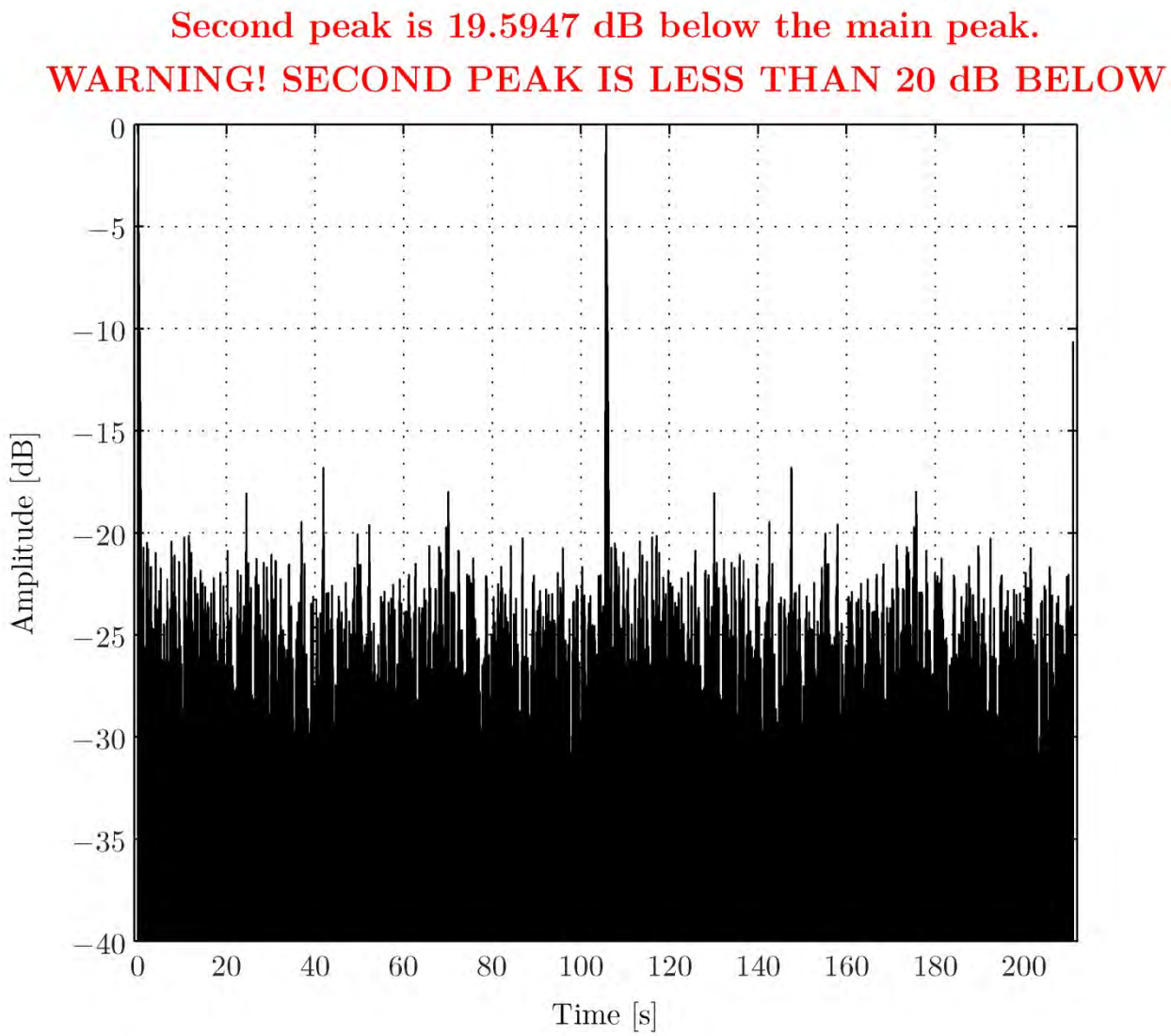

Figure 16.2: Impulse response constructed from the signal recorded on H91
Impulse response constructed from the signal recorded on H91 (Figure 16.1: Example of the waveform recorded by H91 monitoring hydrophone). This example is also taken from the last low frequency transmission at 19.375 Hz. In this example the digit 531 amplitude is below the signal-to-noise ratio, which appears to be around 20 dB. The testing code, however, displays a warning (prompting visual inspection of the signal) that the amplitude within the arrival time of the 531-st digit is less than 20 dB below the main peak.

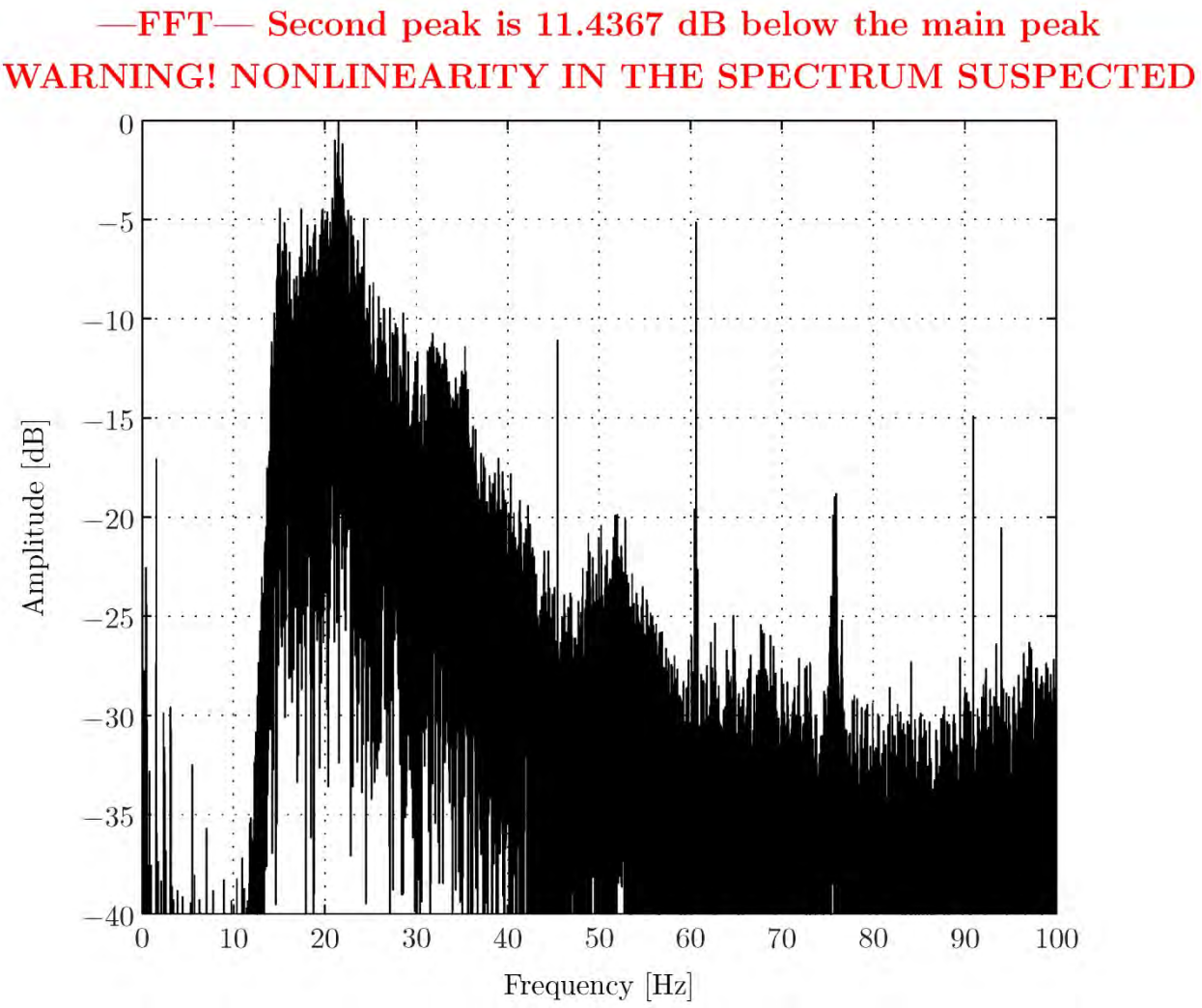

Figure 16.3: Spectrum estimated via the magnitude of the Fourier transform
The spectrum estimated via the magnitude of the Fourier transform of the recorded time series. The spectrum shows that the secondary harmonics are also likely to be below the signal-to-noise ratio. The warning message is displayed. However, PMTM (Figure 16.4: Spectrum estimated via the Thomson multitaper methodFigure 16.4: Spectrum estimated via the Thomson multitaper method) shows that the secondary harmonic is more than 12 dB below the main peak.

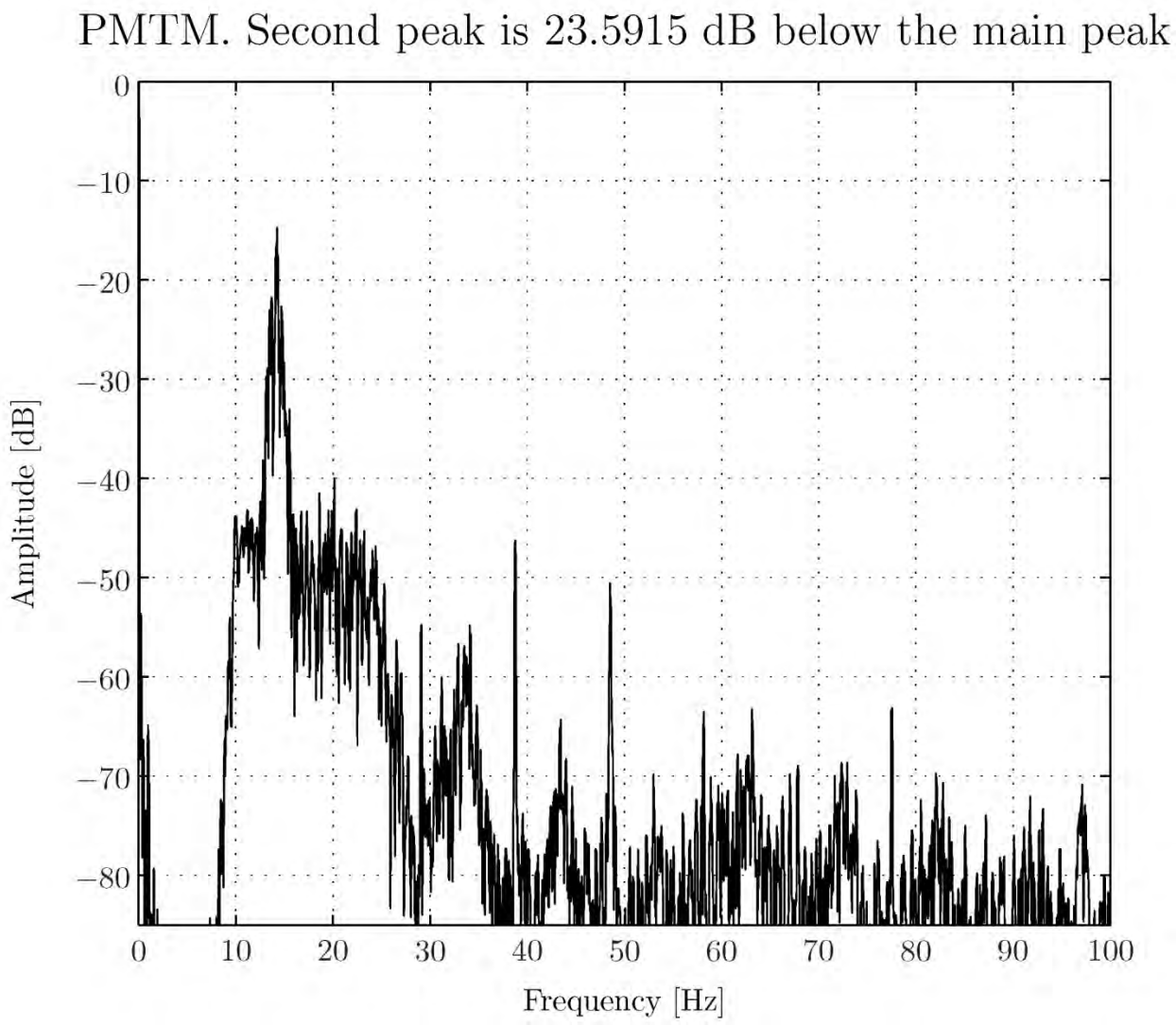

Figure 16.4: Spectrum estimated via the Thomson multitaper method
The spectrum estimated via the Thomson multitaper method (PMTM). The peak below 20 Hz corresponds to the spectrum of the transmitted signal. The secondary harmonic is more than 12 dB below the main peak.

Table 16-1 Low Frequency & MSK Tests

16.2.1 Table of files designed for testing

Name	Type	Filename	Duration [s]
7aCW_1	CW	OBSANP_7a_1_min_Test_CW_IAU.sio	60
7bCW_1	CW	OBSANP_7b_1_min_Test_CW_IAU.sio	60
7cCW_1	CW	OBSANP_7c_1_min_Test_CW_IAU.sio	60
7dCW_1	CW	OBSANP_7d_1_min_Test_CW_IAU.sio	60
7aM_2	M-SEQ	OBSANP_7a_2_per_IAU.sio	80
7bM_2	M-SEQ	OBSANP_7a_2_per_IAU.sio	105.6
7cM_2	M-SEQ	OBSANP_7a_2_per_IAU.sio	160
7dM_2	M-SEQ	OBSANP_7a_2_per_IAU.sio	211.2

16.2.2 Table of files designed for transmissions

Name	Type	Filename	Duration [s]
7a	M-SEQ	OBSANP_7a_IAU.sio	1480 (24’40’’)
7b	M-SEQ	OBSANP_7b_IAU.sio	1953.6(32’33.6’’)
7c	M-SEQ	OBSANP_7c_IAU.sio	2960(49’20’’)
7d	M-SEQ	OBSANP_7d_IAU.sio	3907.2(1h5’7.2’’)
7a_MSK	MSK	OBSANP_7a_MSK_IAU.sio	1440(24’00’’)
7b_MSK	MSK	OBSANP_7b_MSK_IAU.sio	1900.8(31’40.8’’)
7c_MSK	MSK	OBSANP_7c_MSK_IAU.sio	2880(48’00’’)
7d_MSK	MSK	OBSANP_7d_MSK_IAU.sio	3801.6(1h3’21.6’’)
6TX_MSK	MSK	OBSANP_6TX_MSK_IAU.sio	3600 (1 hour)

16.2.3 Formats:

1) 6TX MSK: 36 periods at 77.5 Hz (15 min 50.4 sec) + gap (69.6 sec) = 17 min.
   36 periods at 155 Hz (7 min 55.2 sec) + gap (34.8 sec) = 8.5 min.
   36 periods at 310 Hz (3 min 57.6 sec) + gap (32.4 sec) = 4.5 min.
   36 periods at 102.3 Hz (12 min 00 sec) + gap (30 sec) = 12.5 min.
   36 periods at 204.6 Hz (6 min 00 sec) + gap (30 sec) = 6.5 min.
   + gap (660 sec) = 11 min
   Total: 60 min.

2) 7a, 7b, 7c, and 7d are 37 periods of 51.15 Hz, 38.75 Hz, 25.575 Hz, and 19.375 Hz.

3) 7a_MSK, 7b_MSK, 7c_MSK, and 7d_MSK are 36 periods of 51.15 Hz, 38.75 Hz, 25.575 Hz, and 19.375 Hz.

4) CW files are 1 min each in duration with short ramp-up (4 periods) for testing.

16.2.4 Low frequency transmissions with J15-3

Challenges:

- Unknown impedance curve below 70 Hz.

(*How not to make the source an open circuit?*)

- Undocumented mechanics of the source.

(*How not to break the source mechanically?*)

- Unknown H91 hydrophone unit response.

(*Should we believe the data H91 is sending to us?*)

- High noise level from ship's engines.

(*Even if source and hydrophone are ok, we don't hear anything.*)

Solution:

Use M-sequences to detect nonlinearities.

CW at 51.15Hz:

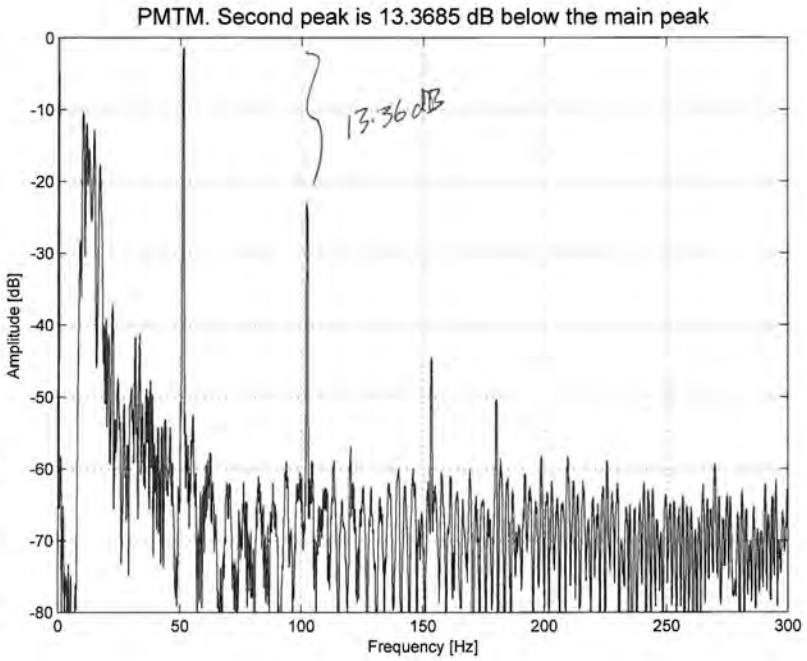

M-sequence at 51.15 Hz

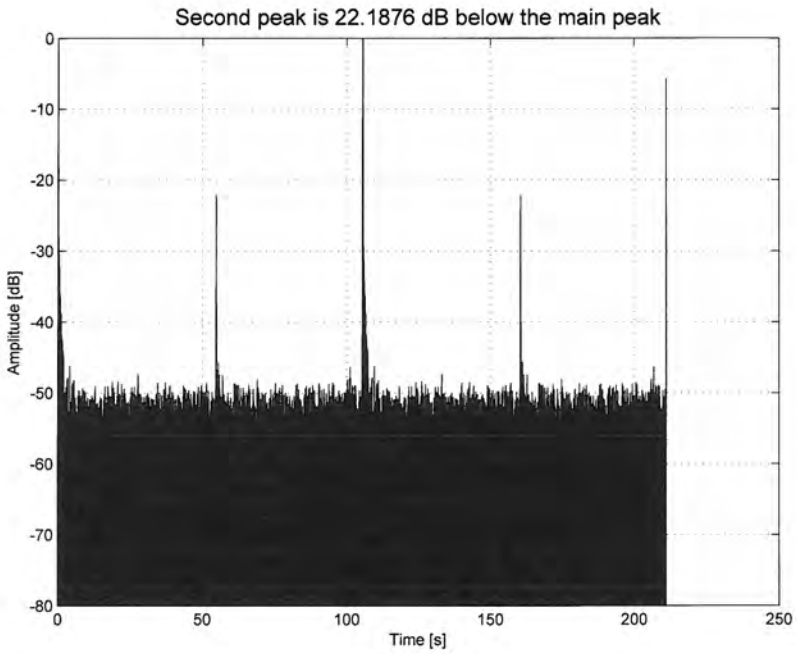

Figure 16.5: Examples of nonlinearities at 51.15Hz

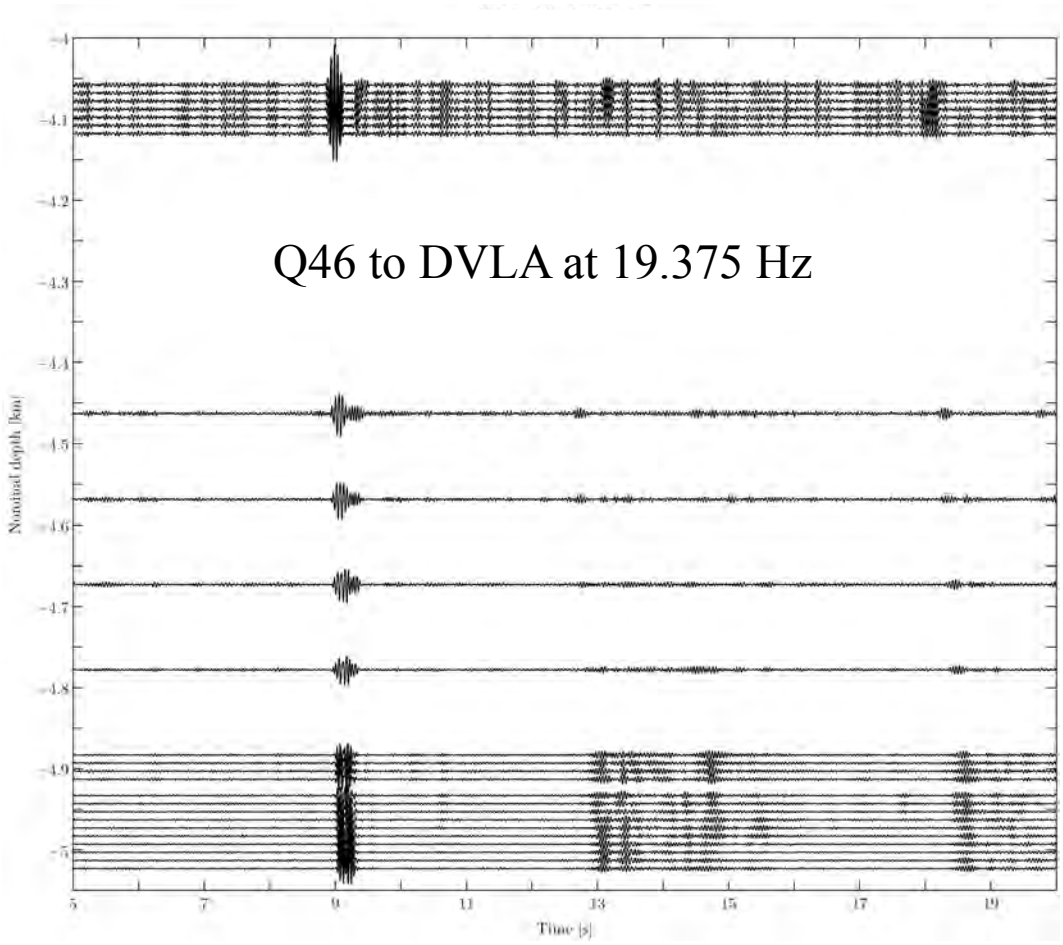

Figure 16.6: 19.375Hz Transmission from Q46 to ODVLA

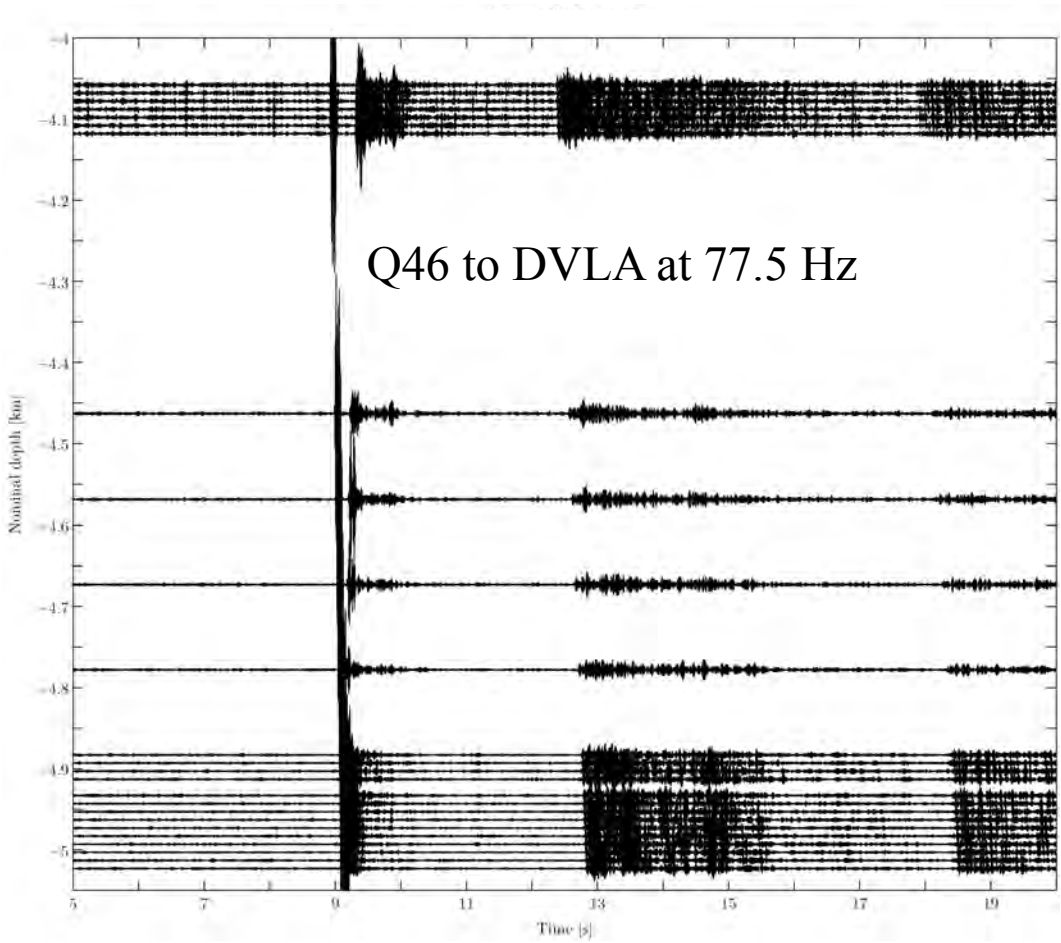

Figure 16.7: 77.5Hz Transmission from Q46 to ODVLA

16.3 Preliminary Conclusions

- Bottom-diffracted surface-reflected arrivals have been observed.
- J15-3 transmissions are successful at ranges as long as 4.5 CZ (250 km).
- MSKs are often better than PSK (regular) M-sequences.
- All low frequency transmissions were successful, providing data at frequencies as low as 19.375 Hz. These transmissions are observed on the DVLA and most OBSs.
- The 20 Hz data is suitable for elastic wave (with shear) modeling with SPECFEM3D.

16.4 Quick Look Analysis

10a: Time-Compressed Data for the ???? Transect

10b: Evidence for Deep Seafloor Arrivals

- i) ???
- ii) ???
- iii) ???

10c: Spectral Analysis

- i) Acoustic Pressure Spectra
- ii) Inertial Sensor Spectra

17 Appendix F: Sub-seafloor Geology in the OBSANP Survey Region – Stephen A. Swift

Sub-seafloor geology in the OBSANP survey region
Stephen A. Swift – WHOI
August 28, 2013

17.1 Introduction

Sound propagating in the ocean interacts with the seafloor and sub-seafloor geology. To better understand the factors affecting sound during OBSANP, I investigated sediment thickness and the nature of acoustic basement at the study site using shipboard echosounder profiles.

17.2 Methods

The primary tool for investigating sub-seafloor structure was the R/V Melville's subbottom profiler system. Ship's specification sheets indicate that the subbottom profiler uses a hull-mounted Massa TR1075 transducer operating at 2.5-10 kHz and producing an 80° conical beam angle. The transducer was powered by a Knudsen chirp 3260 echosounder control and acquisition system capable of outputting up to 10 kW. The Knudsen produces a chirp pulse that sweeps across a band of about 4 kHz centered at 3.5 kHz. For most surveys between stations, the echosounder was operated with a pulse of 16 msec at a power setting of 2, a gain of 0 or 1, and a 'proc shift' of 5. In real time, the Knudsen system software displays the fully processed signal as a continuously scrolling seismic reflection profile. The system also saves images of the reflection profiles in Knudsen's 'keb' proprietary format and records the received signal after deconvolution with the out-going pulse in SEGY-formatted data files.

The deconvolved chirp trace is typically very ringy and requires additional processing to resolve subbottom structure (Quinn et al., 1998). In order to produce detailed images of selected portions of the subbottom profiles, the Knudsen SEGY files were processed using SIOSEIS routine 'mkenv' that is described by Henkart (2006). This routine uses FFT transforms to do a Hilbert transform and then takes the complex modulus to compute the 'instantaneous amplitude' or 'envelope' of the correlated trace. The 'envelope' is a trace of positive numbers with frequency content that is typically less than 500 Hz. Plot routines in SIOSEIS were used to create eight reflection sections. Figure 17.1 shows locations of the profiles. Ashore, routines in SegyMAT (open source Matlab code) were used to extract traces as ascii files for plotting with Generic Mapping Tools.

To obtain the unit thicknesses, we use sound velocity values in Table 17-1 measured in the laboratory by Hamilton and Bachman (1982) on sediment cores of composition similar to those recovered in nearby ocean drilling sites. None of the lithology descriptions from the DSDP sites mentions lithified sediment. Indeed, Moore and Sharman (1970) provide a lithology column for a 9.7 m section of brown clay that was recovered with a 10 m core barrel near DSDP Site 39. This success with a piston core barrel could only be achieved if the sediment were still water saturated and unconsolidated despite millions of years on the seafloor. The apparent uniformity of sediment physical properties with depth in the DSDP site reports (eg., Shipboard Scientific Party, 1970) is likely, at least in part, to be an artifact of sediment disturbance caused by rotary drilling techniques used at that time. It seems more likely that sound velocity would increase moderately with depth as the sediment lost water under increased sediment load. However, Brandes (2011) reports that water content actually increased with depth in a large-

diameter core of brown clay recovered nearby, probably due to changes in clay mineralogy. Thus, the vertical gradients are uncertain, and the measurements of Hamilton and Bachman are the best estimates of sound speed.

17.3 Results

The Knudsen reflection profiles reveal two seismic units beneath the seafloor: (1) an upper transparent layer with relatively low amplitude coherent internal returns overlying (2) a lower layer with prolonged high amplitude returns. Figure 17.2 and Figure 17.3 show typical profiles. The upper transparent layer has the seismic characteristics of pelagic sediments: the layer is draped over topography and appears acoustically transparent with a few laterally coherent, relatively low-amplitude internal reflections. Both the seafloor and the internal reflections are generally smooth with few signs of sedimentary bedforms. The thickness of the upper transparent layer at the survey area ranges from 10 ms of two-way travel time on the slopes of abyssal hills to 15 ms in valleys. Figure 17.4 shows a very clear example of thinning of the upper unit with decreasing water depth (left to right). Figure 17.5 and Figure 17.6 show examples of the transparent unit being much thinner on the crest of hills than on terraces perched on the hill slopes in deeper water.

Along much of the ship's track, acoustic returns from the darker, lower seismic unit are chaotic (Figure 17.2 and Figure 17.3), and the unit only sporadically shows evidence of laterally coherent reflections (green arrow in Figure 17.2). There is no evidence of hyperbola originating in the lower unit except where hyperbola characterize the seafloor reflection. The apparent travel time thickness of the unit varies little being about 10 ms. No lower unit was detected in profiles from the tops of seamounts (Figure 17.7).

Along about 10-20% of the ship's track, the lateral coherence of echoes from the lower unit improves and at least three reflections can be identified. Figure 17.8, Figure 17.9 and Figure 17.10 show examples from hill slopes and from valley floors between abyssal hills. In the trace plots for each figure, it is apparent that there is more variability in the shape and nature of the reflections from the lower unit than in either the seafloor reflection or reflections from within the upper unit. Thus, the source of the variability is inherent to the lower unit. In Figure 17.11 at least one laterally coherent reflection appears in the lower unit in a profile from the top of an abyssal hill illustrating that these features occur across most of the physiographic features in the area.

17.4 Discussion

The geologic nature of the sub-seafloor at the OBSANP survey site can be compared with the results from ocean drilling at nearby sites occupied during Leg 5 of the Deep Sea Drilling Project (DSDP). Figure 17.12 shows a magnetic anomaly map of the region from Atwater (1989). Table 17-2 summarizes the location, water depth, and age of the drill sites, and Table 17-3 provides a summary of the geology. All three sites were continuously cored to basalt with 100% recovery. As part of a site survey for DSDP Site 39, Moore and Sharman (1970) obtained a 9.7 m long core of nearly homogeneous gray-brown mud at about 140°00'W, 33°03'N.

The OBSANP site lies about half way between magnetic isochrons 22 (49-50 Ma) and 23 (51-52 Ma) (Atwater, 1989; Atwater and Severinghaus, 1989) and, thus, has an approximate age of 50.5 Ma (early Eocene - Ypresian) using time scales in Ogg and Smith (2004) and Tsuku and

Clyde (2012). This is the about the same age as basement at DSDP Sites 38 and 39 and considerably older than basement at Site 37 (Table 17-2).

The seismic stratigraphy at the OBSANP survey site comprises two units (Figure 17.2 and Figure 17.3). The upper, low-amplitude unit is interpreted to be a layer of pelagic sediments due to its draping of topography. Thinning of pelagic drape on the crests of abyssal hills and seamounts has been previously observed in the eastern Pacific (Swift et al., 1998; Tominaga et al., 2011) and could be attributed to resuspension of mud by seafloor dwelling invertebrates and local transport by oscillating tidal currents (Johnson and Johnson, 1970; Lonsdale and Southard, 1974). Low-amplitude reflections occurring in the upper unit (Figure 17.2, Figure 17.3, Figure 17.4, Figure 17.5, Figure 17.8, and Figure 17.9) are likely due to small variations in sediment density by either ash beds observed in DSDP cores (Table 17-3) or small local variations in the content of siliceous microfossils.

The nature of the deeper, high-amplitude seismic unit (Figure 17.2 and Figure 17.3) is more problematic. Igneous basement in unmigrated seismic profiles commonly appears as laterally coherent, high amplitude arrivals often with hyperbolic echoes indicating diffractions (eg. Moore and Sharman, 1970). Multiple basement arrivals were commonly due to relatively long airgun source signatures with bubble pulses and to reverberations of low-frequency energy within basement. Neither feature, however, is likely with a 16 ms long chirp echosounding signal centered near 3.5 kHz. The echosounding signal from the ship's transducers are too weak to penetrate – much less reverberate within – igneous basement. Several profiles at OBSANP show a sequence of at least three laterally coherent reflections with an apparent thickness of 10 ms two-way travel time defining the top of the lower seismic unit. These reflection sequences usually extend over lateral distances of 0.5 to 1 km (Figure 17.2, Figure 17.8, Figure 17.9, and Figure 17.10). The occurrence of the reflection sequence on lines oriented perpendicular to the north-south trend in abyssal hills (Figure 17.1) and on slopes as well as valleys with no variation in apparent thickness is inconsistent with these reflections originating as diffractions from igneous volcanic features. Moreover, Figure 17.8 shows that the high-amplitude reflections do not thin across significant changes in dip, which is also inconsistent with a diffraction origin.

An alternative explanation for the lower, high amplitude seismic unit is that the high amplitude arrivals reflected off a laterally coherent sedimentary sequence. Using a seismic system operated at frequencies <160 Hz, Moore et al. (2002) found a high amplitude seismic unit that correlated with early Eocene carbonate sediments lying on basement of early Eocene age in the part of the eastern Pacific between DSDP Site 39 and the equator. This sequence is consistent with a deepening of the carbonate compensation depth (CCD) in the early Paleogene identified by van Andel et al. (1975). Crust created at a spreading center at this time would be shallow enough for carbonate sediments to be preserved. Later, sediment lithology changed to brown clay as seafloor depth deepened due to cooling and sank beneath the CCD. DSDP boreholes Sites 38 and 39, which have basement ages similar to that at OBSANP, recovered carbonate-bearing sediments of early Eocene age just above basalt with thicknesses of 9 m and 2.5 m, respectively (Table 17-2). Using a sound speed of 1534 m/s (Table 17-1), these thicknesses should return a seismic thickness of no more than 12 ms or 3 ms two-way travel time, respectively. These are of the same order of magnitude as the observed interval of 10 ms between the first and third reflections in echosounding profiles noted above. The observed time interval of the deeper seismic unit, thus, could be explained by carbonate sequence thicknesses similar to thicknesses observed in nearby boreholes.

The differences in thickness of the both brown clay and calcareous nannofossil sediment units in DSDP Sites 38 and 39 noted above are consistent with variations in thickness of the transparent upper seismic unit observed during the OBSANP survey. The basal carbonate unit is almost four times thicker at DSDP Site 38 (9 m) than at DSDP Site 39 (2.5 m), and the brown clay unit is more than twice as thick at DSDP Site 38 (39 m) than at DSDP Site 39 (14.5 m) despite a similar crustal age based on both microfossils and magnetic anomalies (Table 17-2 and Table 17-3). The primary difference between the two sites is depth: the seafloor is 208 m deeper at DSDP Site 38 than at DSDP Site 39, and basalt is 239 m deeper. The similarity in the age of sediments overlying basalt at the two DSDP sites indicates that the volcanism that produced the discrepancy in depth occurred very close to the age of formation of the crust. In the OBSANP echosounding profiles in Figures 4-6, we noted above that the transparent layer was thinner on the upper slopes and crests of abyssal hills than on the lower slopes and valleys. This observation is consistent with seismic observations elsewhere in the eastern Pacific (eg. Swift et al., 1998; Laguros and Shipley, 1989; Dubois and Mitchell, 2012). Two inferences can be drawn from these observations. First, it is likely that total sediment thickness at the OBSANP survey site at ~5100 m depth is closer to the 48 m recovered at DSDP Site 38 (5137 m) than to the 17 m recovered at DSDP Site 39 (4929 m) despite the closer proximity of the latter site. Second, both drilling and seismic profiles indicate that both the total sediment column and individual sedimentary units thicken locally within the OBSANP survey from the crests of abyssal hills into the valleys between adjacent hills.

Across much of the OBSANP survey region, the returns comprising the deeper, high amplitude seismic unit lack the degree of lateral coherence seen in the seafloor reflection and the internal reflections in the upper seismic unit (Figure 17.2 and Figure 17.3). If the deeper seismic unit is sedimentary and the coherent arrivals observed in spots are due to reflections from carbonate interbedded with clay, then the lack of seismic coherence must be due to disruptions in the beds on the scale of tens of meters. The radius of the first Fresnel zone for a reflecting surface at a depth of 5100 m in a medium with a velocity of 1500 m/s and a source frequency of 3500 Hz is about 33 m (Yilmaz, 1987, p. 470). Thus, reflecting points within 66 m are theoretically indistinguishable at the sea surface. During the OBSANP survey, echosounding traces were spaced at 10-11 m at ship speeds of about 2.5 knots, 19-20 m at 4.5 knots, and ~25 m at 5.8 knots. At all ship speeds multiple traces should be received from within a Fresnel zone, so the lack of lateral coherence must be due to variations in the reflecting surfaces smaller than ~66 m, the width of the Fresnel zone.

There are three possible sedimentary explanations for variations on lateral scales less than 66 m. In a map of small-scale relief on the fast spreading East Pacific Rise, Fournari et al. (2012, their Figure 3) show both volcanic and tectonic relief of up to 20 m on the scale of 50-100 m. One possible explanation, then, for the disruption of reflections at OBSANP is simply that the carbonate-clay interbeds are ponded in basins with lateral scales of 66 m (the diameter of the Fresnel zone). Alternatively, the layers of sediment that accumulated in thin layers draped over the topography created at the mid-ocean ridge may have been disrupted by slope failures initiated by earthquake shaking. The coherent reflections, then, would represent deposits in basins with widths greater than few hundred meters, which is the scale observed in the echosounding profiles (Figure 17.2, Figure 17.8, Figure 17.9, and Figure 17.10). Thirdly, the carbonate-clay interbeds may have been constructed intact on the ridge crest but been geochemically altered later in a fashion that interrupted the continuity of beds on the scales of 50-100 m. Based on evidence from ocean drilling and detailed seafloor surveys, Beakins (2007) and Moore et al. (2007)

attribute seafloor pits in carbonate sediments across the eastern equatorial Pacific to dissolution of carbonate by hydrothermal fluids. Based on the vertical distribution of chert and siliceous fossils in ocean boreholes, Moore (2008a, b) further suggests that the hydrothermal circulation geochemically alters sediments within 150 m of igneous basement over wide areas of the Pacific. Thus, a model for a geochemical process to alter carbonate layers overlying basalt has been proposed. It is unclear from the existing evidence whether this process is an adequate explanation for disrupting reflections from sediments.

17.5 Summary

Ocean drilling shows that the seafloor in the OBSANP survey region is the top of a relatively homogeneous layer of brown clay with a sound speed of about 1500 m/s. Echosounding profiles indicate that the thickness of the clay layer thins from 10 ms of two-way travel time (7.5 m) on the crests of abyssal hills to 15 ms in valleys (11.2 m). A layer of interbedded carbonate ooze and clay occurs on top of basalt in nearby boreholes. Evidence suggests that this carbonate-bearing sedimentary layer correlates with a seismic unit of high-amplitude returns. A sequence of three reflectors at the top of the deeper seismic unit has a relatively uniform thickness of 10 ms (7.7 m at 1534 m/s). The echosounding profiles show no returns from beneath this layer. Alternatively, the high amplitude layer represents returns from a rough basalt surface.

Table 17-1

Environment/ sediment type	Density (g/cm^3) mean	std err	Porosity (%) mean	std err	Velocity (m/s) mean	std err
A. *Abyssal hill-deep-sea: non-calcareous "red" pelagic clay*						
Clayey silt	1.347	0.020	81.3	0.9	1522	3
Silty clay	1.344	0.011	81.2	0.6	1508	2
Clay	1.414	0.012	77.7	0.6	1493	1
B. *Calcareous silty clay from equatorial Pacific*						
Ontong/ Java Plateau	1.481	0.007	72.7	0.4	1540	2
East Pacific	1.376	0.007	78.6	0.4	1534	1

Table 17-2

DSDP Site	Lat	Long	Water depth (m)	Sediment thickness drilling (m)	seismic (s)	Magnetic anomaly	Age Ma	Epoch
37	40°58.74'	140°43.11'	4682	30	0.04	10	28.4	E/L Oligocene
38	38°42.12'	140°21.27'	5137	48	0.07	24-25	53.0	Early Eocene
39	32°48.28'	139°34.29'	4929	17	0.03	24	52.8	Early Eocene

Table 17-3

Site 37			
Unit 1	0-5 m	Light brown pelagic clay with thin streaks of nannofossil ooze	Pleistocene
Unit 2	5-20 m	Interbedded dark brown clay and yellow zeolitic clay	No fossils
Unit 3	20-30 m	Very dark brown iron oxide and 2 ash beds (zeolites)	No fossils
Site 38			
Unit 1	0-39 m	Yellow brown zeolitic clay with one ash layer	No fossils
Unit 2	39-48 m	Yellow brown foraminifera nannofossil ooze	Lower Eocene
Site 39			
Unit 1	0-14.5 m	Yellow brown zeolitic clay with one ash layer	No fossils
Unit 2	14.5-17m	Iron-oxide rich clay with thin beds of nannofossil ooze	Early Eocene

17.6 References

Atwater, T., 1989, Plate tectonic history of the northeast Pacific and western North America. In: Winterer, E.L., Hussong, D.M., Decker, R.W. (Eds.), The Eastern Pacific Ocean and Hawaii, Volume N: The Geology of North America. Geological Society of America, Boulder, Colorado, pp. 21–72.

Atwater, T., Severinghaus, J., 1989, Tectonic maps of the northeast Pacific. In: Winterer, E.L., Hussong, D.M., Decker, R.W. (Eds.), The Eastern Pacific Ocean and Hawaii, Volume N: The Geology of North America. Geological Society of America, Boulder, Colorado, pp. 15–20.

Bekins, B.A., A.J. Spivack, E.E. Davis, and L.A. Mayer, 2007, Enhanced ventilation of ocean crust due to dissolution of biogenic ooze over oceanic basement edifices, Geology, 35, 679–682, doi:10.1130/G23797A.1.

Brandes, H.G., 2011, Geotechnical characteristics of deep-sea sediments from the North Atlantic and North Pacific oceans, Ocean Engineering, 38, 835–848.

Dubois, N., and N.C. Mitchell, 2012, Large-scale sediment redistribution on the equatorial Pacific seafloor, Deep-Sea Research I, 69, 51–61.

Fornari, D.J., K.L. Von Damm, J.G. Bryce, J.P. Cowen, V. Ferrini, A. Fundis, M.D. Lilley, G.W. Luther III, L.S. Mullineaux, M.R. Perfit, M.F. Meana-Prado, K.H. Rubin, W.E. Seyfried Jr., T.M. Shank, S.A. Soule, M. Tolstoy, and S.M. White, 2012, The East Pacific Rise between 9°N and 10°N: Twenty-five years of integrated, multidisciplinary oceanic spreading center studies. Oceanography 25, 18–43, http://dx.doi.org/10.5670/oceanog.2012.02.

Hamilton, E.L., and R.T. Bachman, 1982, Sound velocity and related properties of marine sediments, Journal of the Acoustical Society of America, 72, 1891-1904.

Henkart, P., 2006, Chirp sub-bottom profiler processing – a review, Sea Technology, 40, 35-38.

Johnson, D.A., and T.C. Johnson, 1970, Sediment redistribution by bottom currents in the central Pacific, Deep-Sea Research, 17, 157–169.

Laguros, G.A., and T.H. Shipley, 1989. Quantitative estimate of resedimentation in the pelagic sequence of the equatorial Pacific. Marine Geology, 89, 269–277.

Lonsdale, P., and J.B. Southard, 1974, Experimental erosion of North Pacific red clay, Marine Geology, 17, M51-M60.

Moore, G.W., and G.F. Sharman, 1970, Summary of Scan Site 7, in McManus, D.A., et al., Initial Reports of the Deep Sea Drilling Project, 5, 801-811.

Moore, T.C., Jr., 2008a, Biogenic silica and chert in the Pacific Ocean, Geology, 36, 975–978, doi:10.1130/G25057A.1.

Moore, T. C., Jr., 2008b, Chert in the Pacific: Biogenic silica and hydrothermal circulation, Palaeogeogr. Palaeoclimatol.Palaeoecol., 261, 87–99, doi:10.1016/j.palaeo.2008.01.009.

Moore, T.C., D.K. Rea, M. Lyle, and L.M. Liberty, 2002, Equatorial ocean circulation in an extremely warm climate, Paleoceanography, 17, 1005, 10.1029/2000PA000566, 6 pp.

Moore, T.C., Jr., N.C. Mitchell, M. Lyle, J. Backman, and H. Pälike, 2007, Hydrothermal pits in the biogenic sediments of the equatorial Pacific Ocean, Geochem. Geophys. Geosyst., 8, Q03015, doi:10.1029/2006GC001501.

Ogg, J.G., and A.G. Smith, 2004, The geomagnetic polarity time scale, *in* Gradstein, F.M., Ogg, J.G., and Smith, A.G., eds., A Geologic Time Scale 2004: Cambridge, UK, Cambridge University Press, p. 63–86.

Quinn, R., J.M. Bull, and J.K. Dix, 1998, Optimal processing of marine high-resolution reflection (chirp) data, Marine Geophysical Researches, 20, 13-20.

Shipboard Scientific Party, 1970, Site 39, in McManus, D.A., et al., Initial Reports of the Deep Sea Drilling Project, 5, 297-307.

Swift, S.A., G.M. Kent, R.S. Detrick, J.A. Collins, and R.A. Stephen, 1998, Oceanic basement structure, sediment thickness, and heat flow near Hole 504B, Journal of Geophysical Research, 103, B7, 15,377-15,391.

Tominaga, M., Lyle, M., and N.C. Mitchell, 2011, Seismic interpretation of pelagic sedimentation regimes in the 18–53 Ma eastern equatorial Pacific: basin-scale sedimentation and infilling of abyssal valleys. Geochem. Geophys. Geosyst. 12, Q03004, http://dx.doi.org/10.1029/2010GC003347.

Tsuku, K., and W.C. Clyde, 2012, Fine-tuning the calibration of the early to middle Eocene geomagnetic polarity time scale: Paleomagnetism of radioisotopically dated tuffs from Laramide foreland basins, Geological Society of America Bulletin; 124, 870–885, doi: 10.1130/B30545.1

van Andel, T.H., G.R. Heath, and T.C. Moore Jr., Cenozoic history and paleoceanography of the central equatorial Pacific Ocean, Memoirs Geological Society America, 143, 1975.

Yilmaz, O., 1987, Seismic data processing. Tulsa, Society of Exploration Geophysicists.

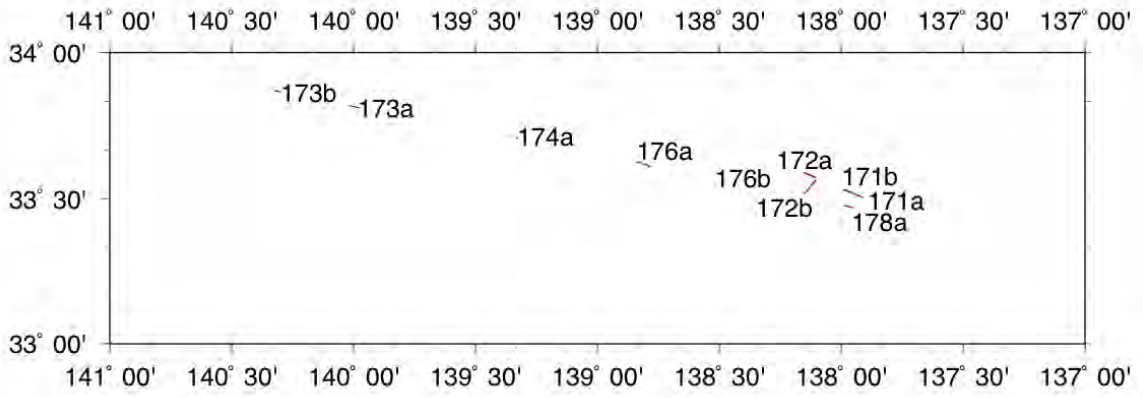

Figure 17.1: Map shows location of Knudsen seismic profiles shown in Figures 17.2-17.11.

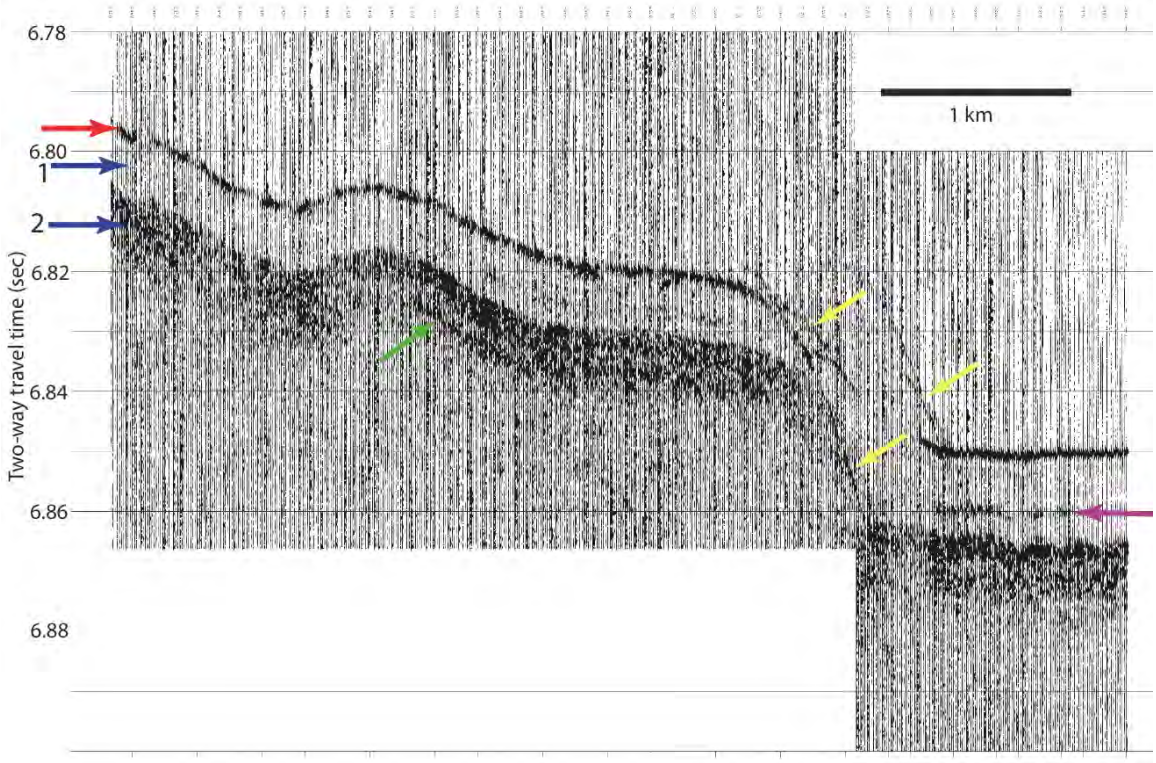

Figure 17.2: Subbottom profile 171a
Subbottom profile 171a shows a typical profile for survey area. Red arrow marks the seafloor and the blue arrows point to the (1) upper transparent seismic unit and the (2) lower, high amplitude seismic unit. Yellow arrows indicate hyperbola originating at the seafloor. Magenta arrow points to a weak, sedimentary subbottom reflection in the upper unit. Green arrow points to an 800-900 m long, laterally coherent reflection within the high-amplitude unit. Figure 17.1 shows location of profile.

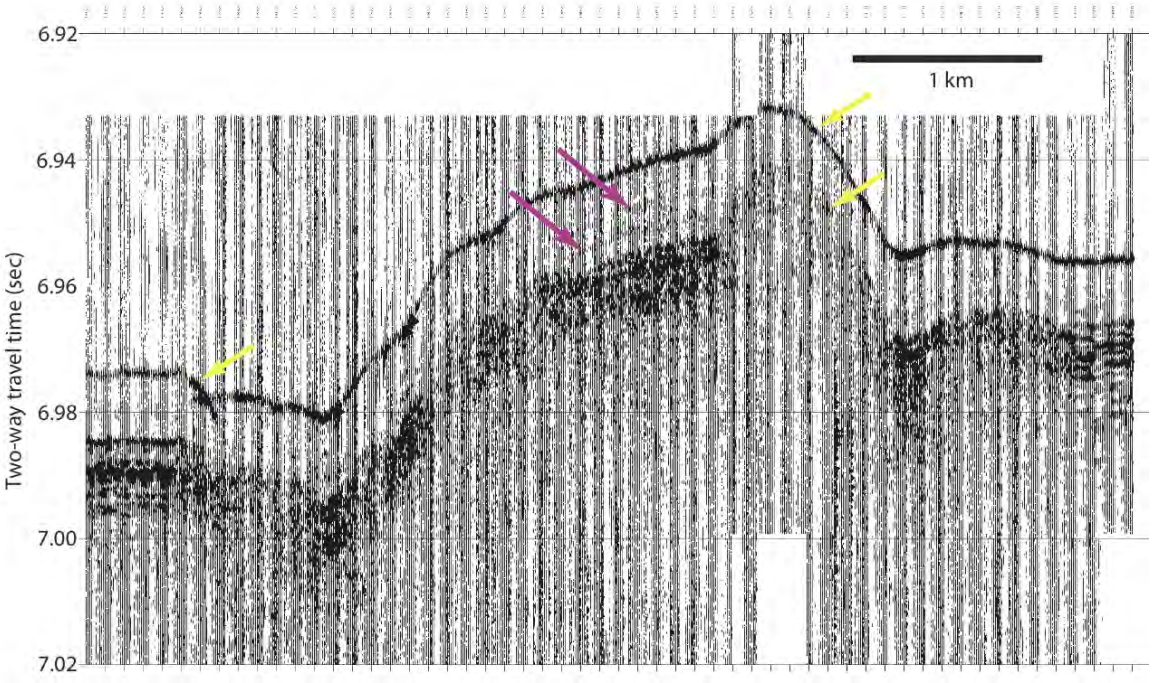

Figure 17.3:Subbottom profile 172a
Subbottom profile 172a shows weak sedimentary reflections (magenta arrows) in the upper transparent unit and possible hyperbola from both the seafloor and the top of the lower, high-amplitude seismic unit. The lateral coherence of echoes from the lower, darker unit is low. Profile shows a complete transit between two stations. Flat-lying returns at the right and left edges of the profile occur when the ship was stopped for stations. Figure 17.1 shows location of profile.

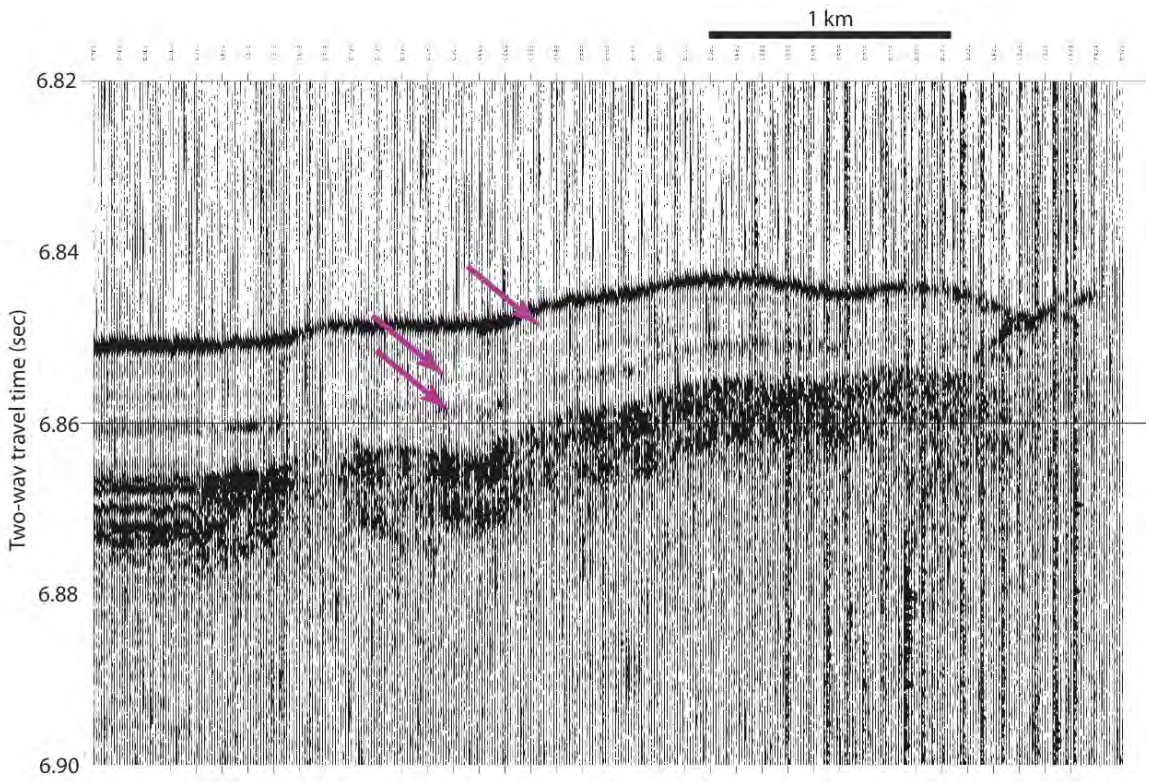

Figure 17.4: Subbottom profile 171b
Subbottom profile 171b shows the upper transparent unit thinning upslope on a small abyssal hill. Magenta arrows point to weak reflections within the transparent unit. These features are consistent with the upper unit being composed of draped pelagic clay. Left end of profile begins while the ship was on station. Figure 17.1 shows location of profile.

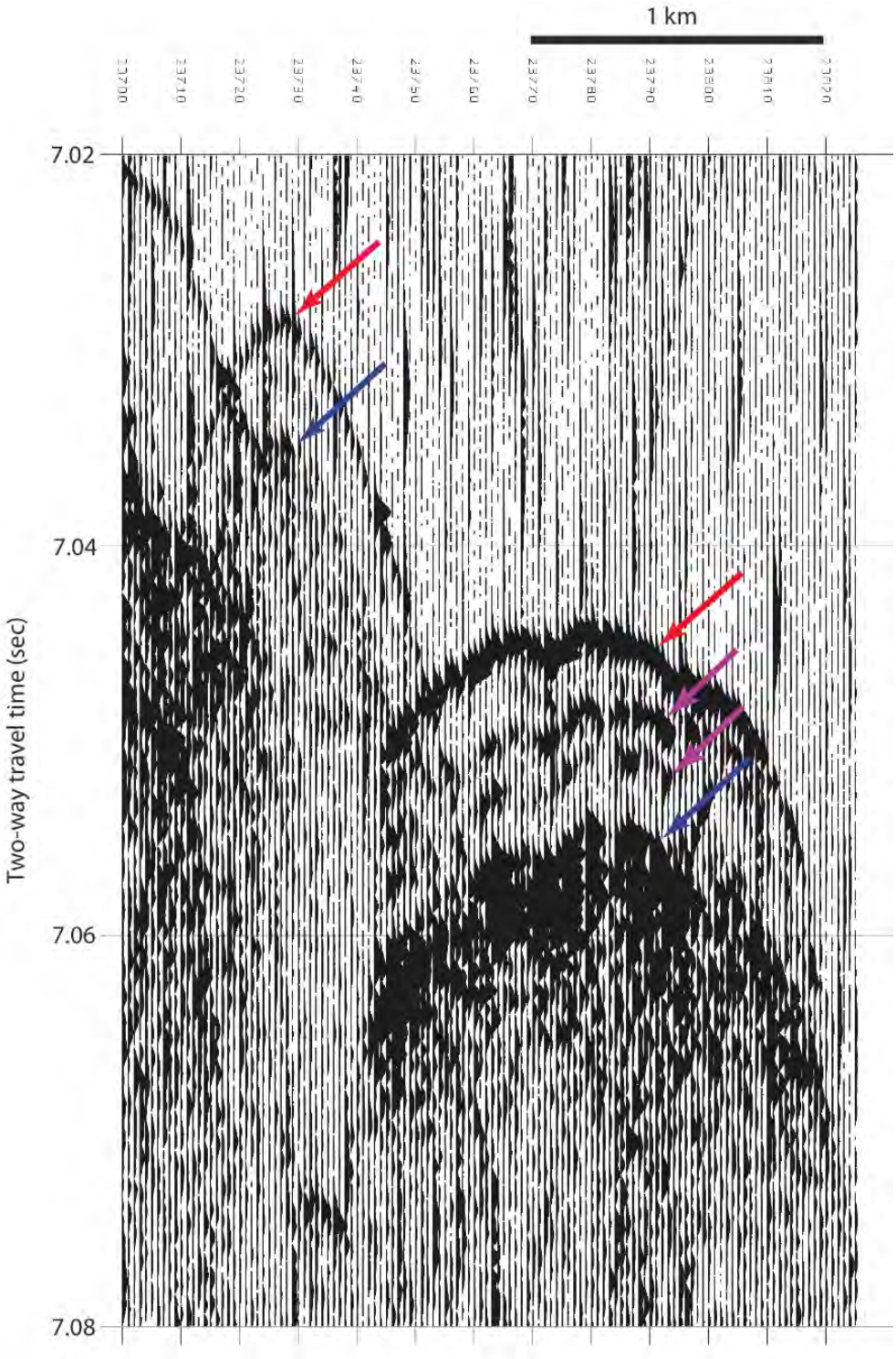

Figure 17.5: Profile 173b
Profile 173b shows a thinning of almost a factor of two in the thickness of the upper transparent unit between small terraces perched on the flanks of an abyssal hill. The upper unit is defined by the seafloor (red arrows) and the top of the high-amplitude lower unit (blue arrows). Internal reflections (magenta arrows) have higher amplitudes on the deeper terrace (right). Figure 17.1 shows location of profile.

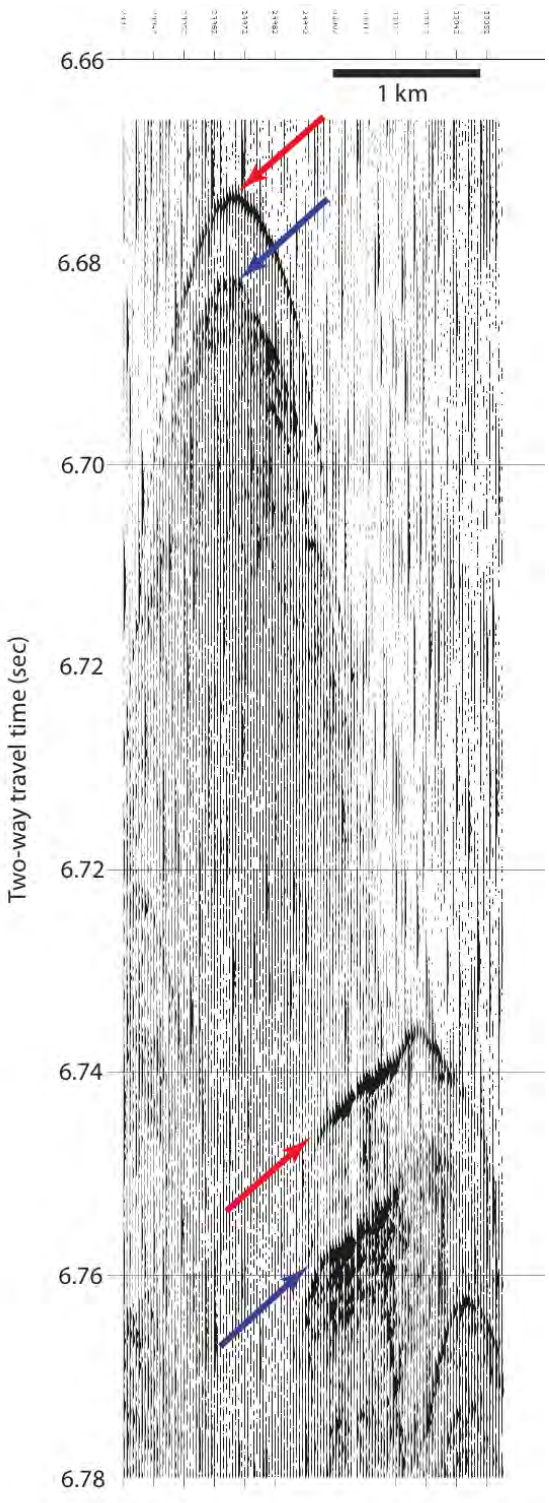

Figure 17.6: Thickness of the upper seismic unit thins
As in Figure 17.5, the thickness of the upper seismic unit, which is defined by the seafloor (red arrows) and the top of the lower high-amplitude unit (blue arrows), thins from the crest of an abyssal hill (left) to a terrace on the flank of the hill (right). Figure 17.1 shows location of profile.

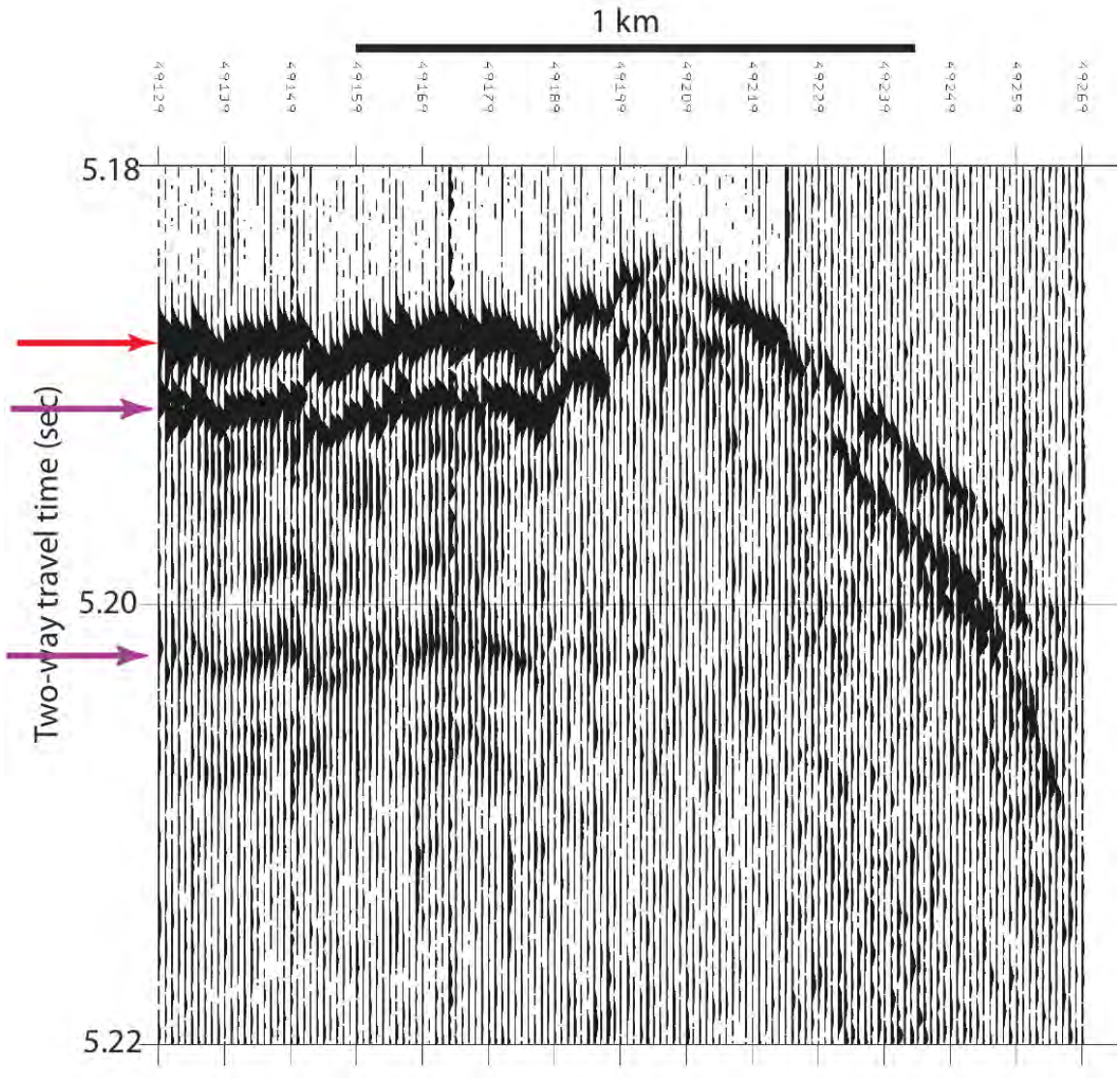

Figure 17.7: subbottom profile from the top edge of a seamoun
A subbottom profile from the top edge of a seamount shows a wavy seafloor (red arrow) suggestive of possible sedimentary bedforms and at least two unambiguous subbottom reflections (magenta arrows). The high amplitude lower unit is not present here. Figure 17.1 shows location of profile.

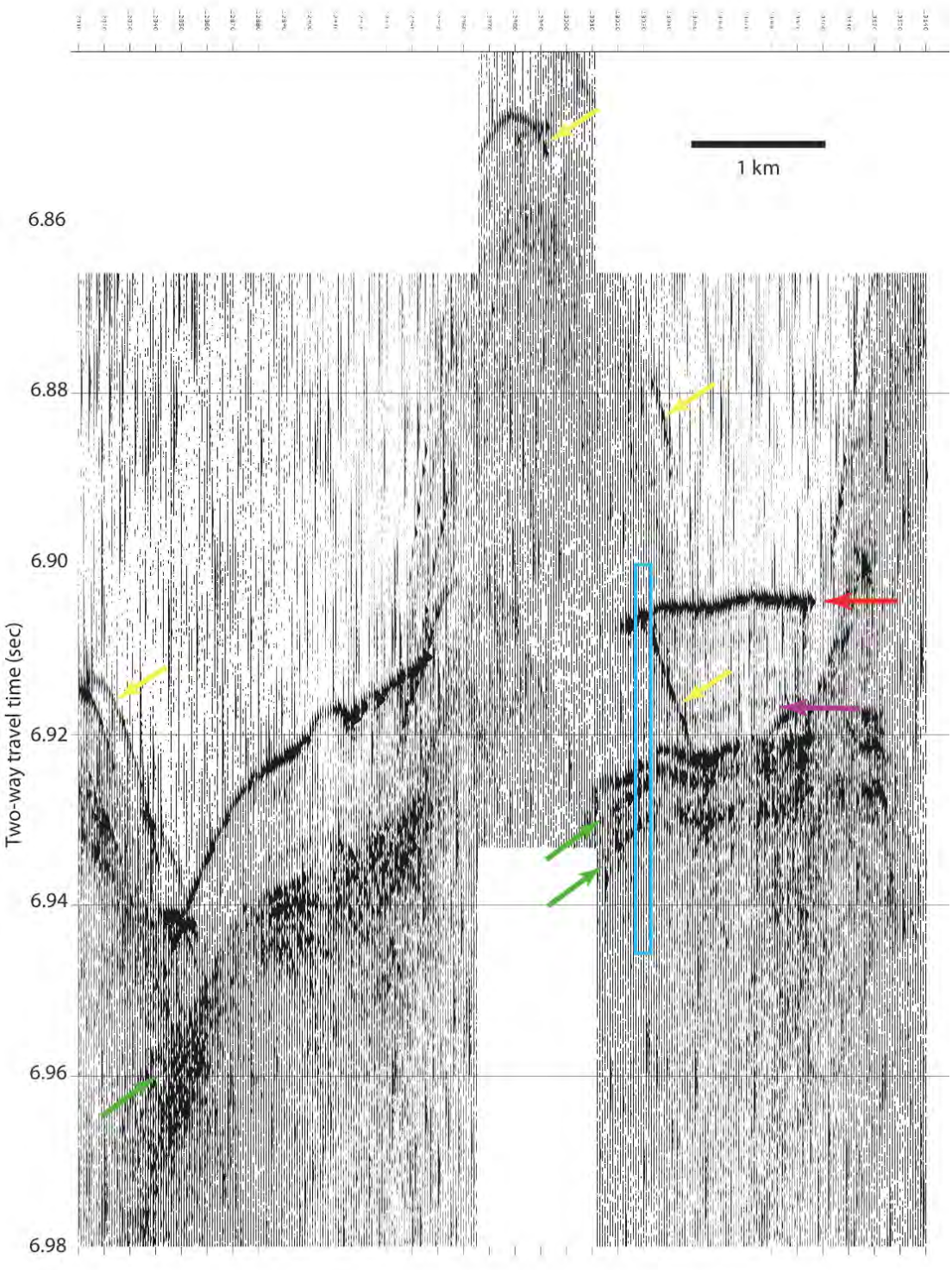

Figure 17.8: Profile 172b
Profile 172b shows a clear example of internal reflections within the upper transparent unit (magenta arrow) and within the deeper, high-amplitude seismic unit on the flank of an abyssal hill (green arrows). The seafloor (red arrow) is offset by isolated highs that produce seafloor hyperbola (yellow arrows). The light blue box marks the location of traces plotted in Figure 8b. Figure 17.1 shows location of profile.

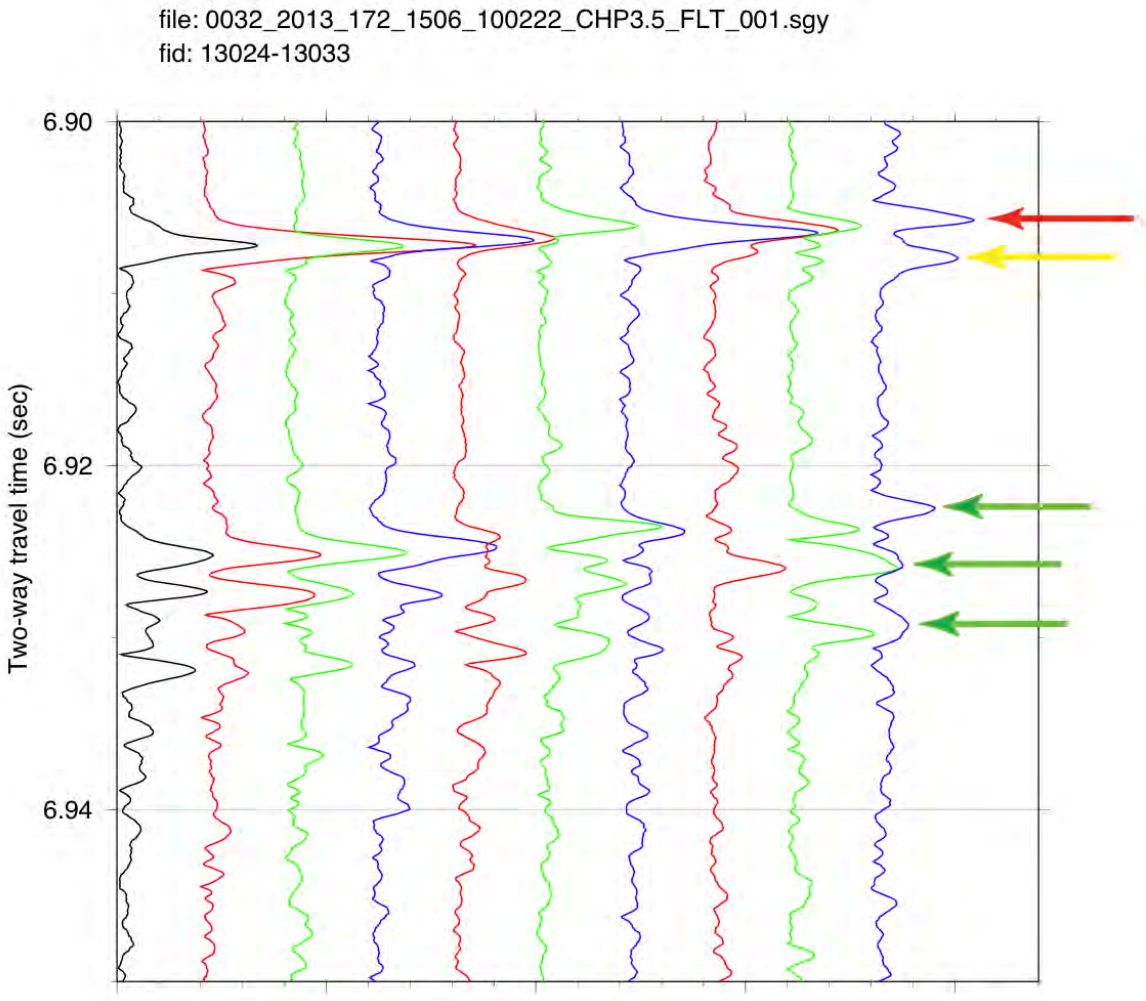

Figure 17.9: Processed traces from the light blue box in Figure 17.8
Processed traces from the light blue box in Figure 17.8 show clear evidence of the lateral coherence of the seafloor (red arrow) and the three high-amplitude reflections (green arrows) comprising the top of the lower, high-amplitude unit.

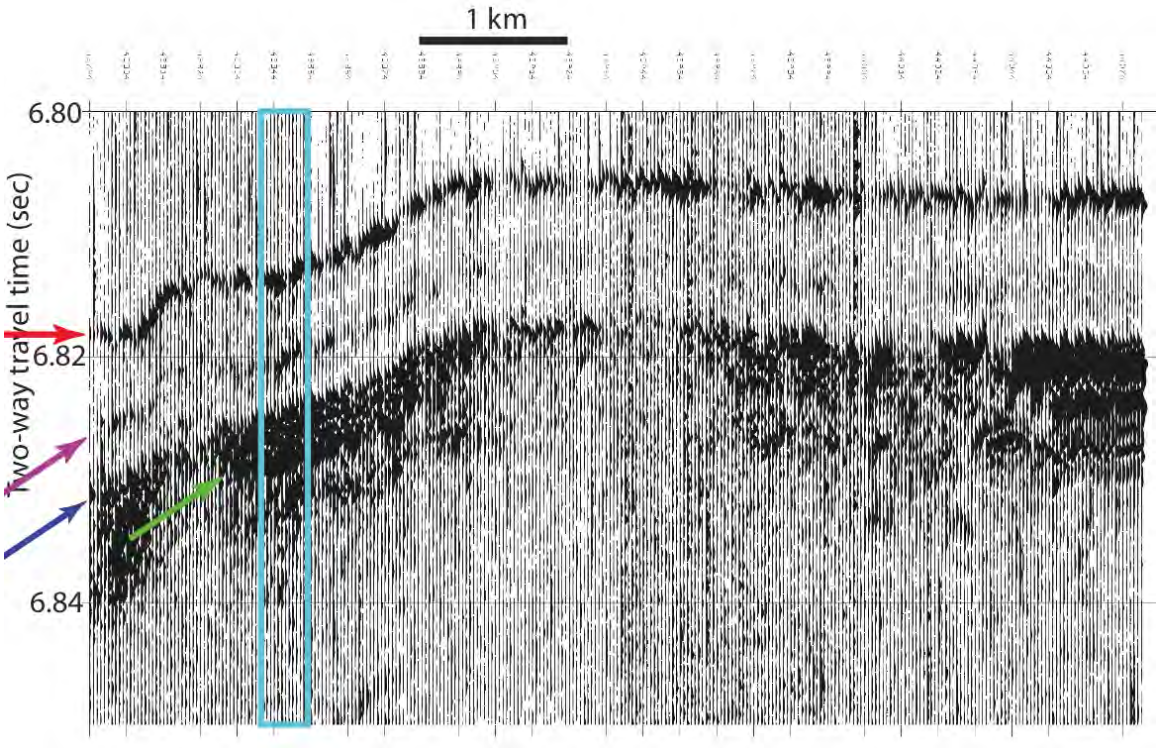

Figure 17.10: Profile 176b
Profile 176b shows an example of a well-defined internal reflection within the upper transparent unit (magenta arrow) and less-well defined reflections (green arrows) within the deeper, high-amplitude seismic unit on the flank of an abyssal hill. Blue arrow marks the top of the lower unit. The light blue box marks the location of traces plotted in Figure 17.11. A small bump is present in the seafloor (red arrow) between the left edge of the profile and the light blue box. Note that the absence of returns from the deeper unit just below the bump indicative of scattering. Figure 17.1 shows location of profile.

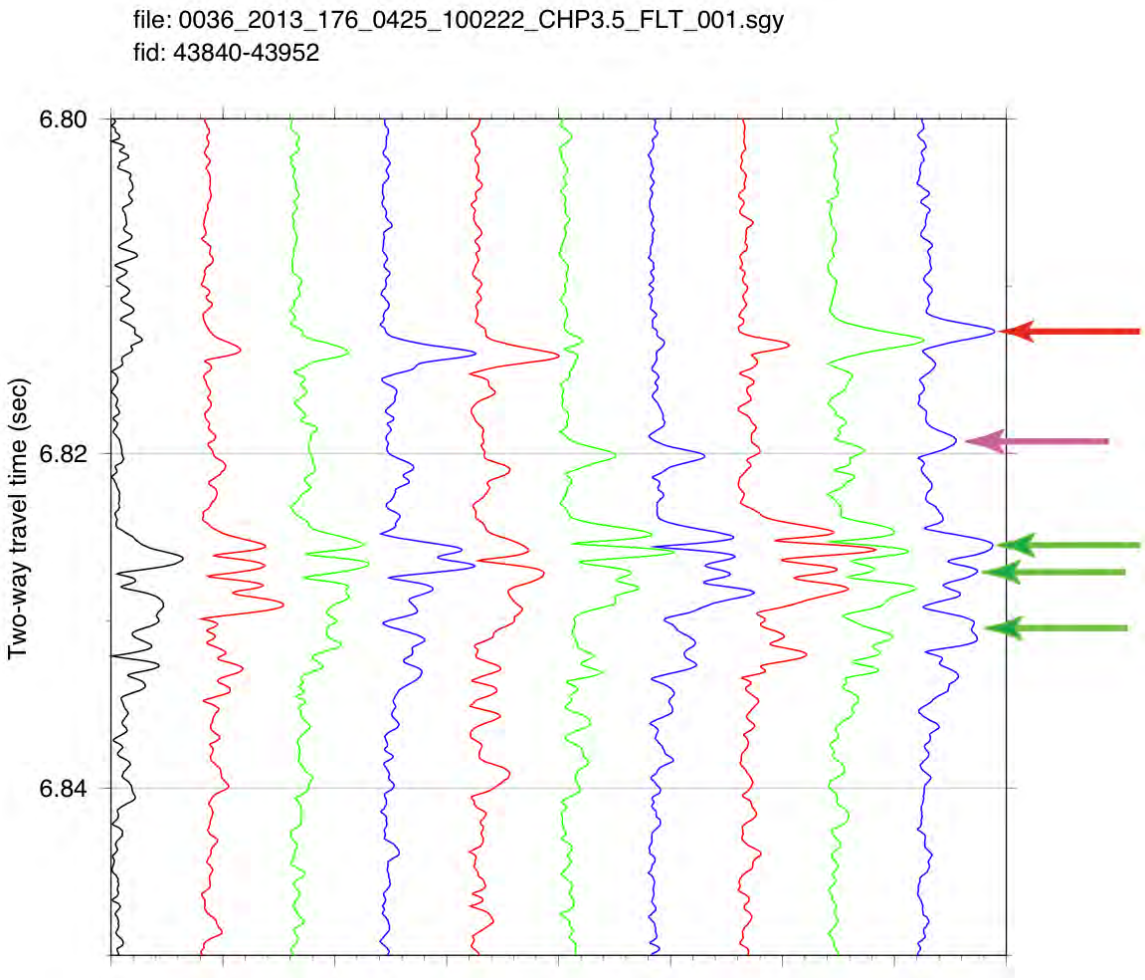

Figure 17.11: Processed traces from the light blue box in Figure 17.10
Processed traces from the light blue box in Figure 17.10 show a laterally coherent seafloor (red arrow) and a weak reflection within the upper transparent unit (magenta arrow). Within the deeper unit, the green arrows mark the depth of high amplitude reflections. Note the much lower coherence than in Figure 17.9.

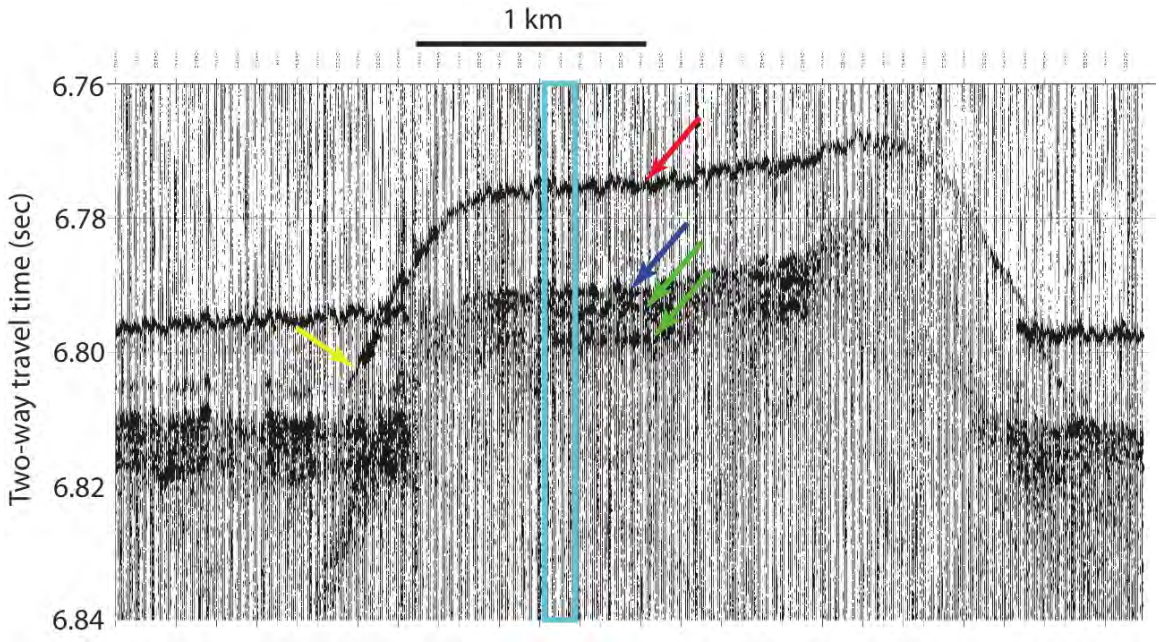

Figure 17.12: Profile 178a
Profile 178a shows a clear example of internal reflections within the deeper, high-amplitude seismic unit on the flank of an abyssal hill (green arrows). The seafloor (red arrow) is offset by a narrow high that produces hyperbola (yellow arrow) where the seafloor drops down to the floor of the valley. The light blue box marks the location of traces plotted in Figure 17.11. Since the low-amplitude waviness to the seafloor does not occur in the hyperbola, it is unlikely that the cause is ship motion. Figure 17.1 shows location of profile.

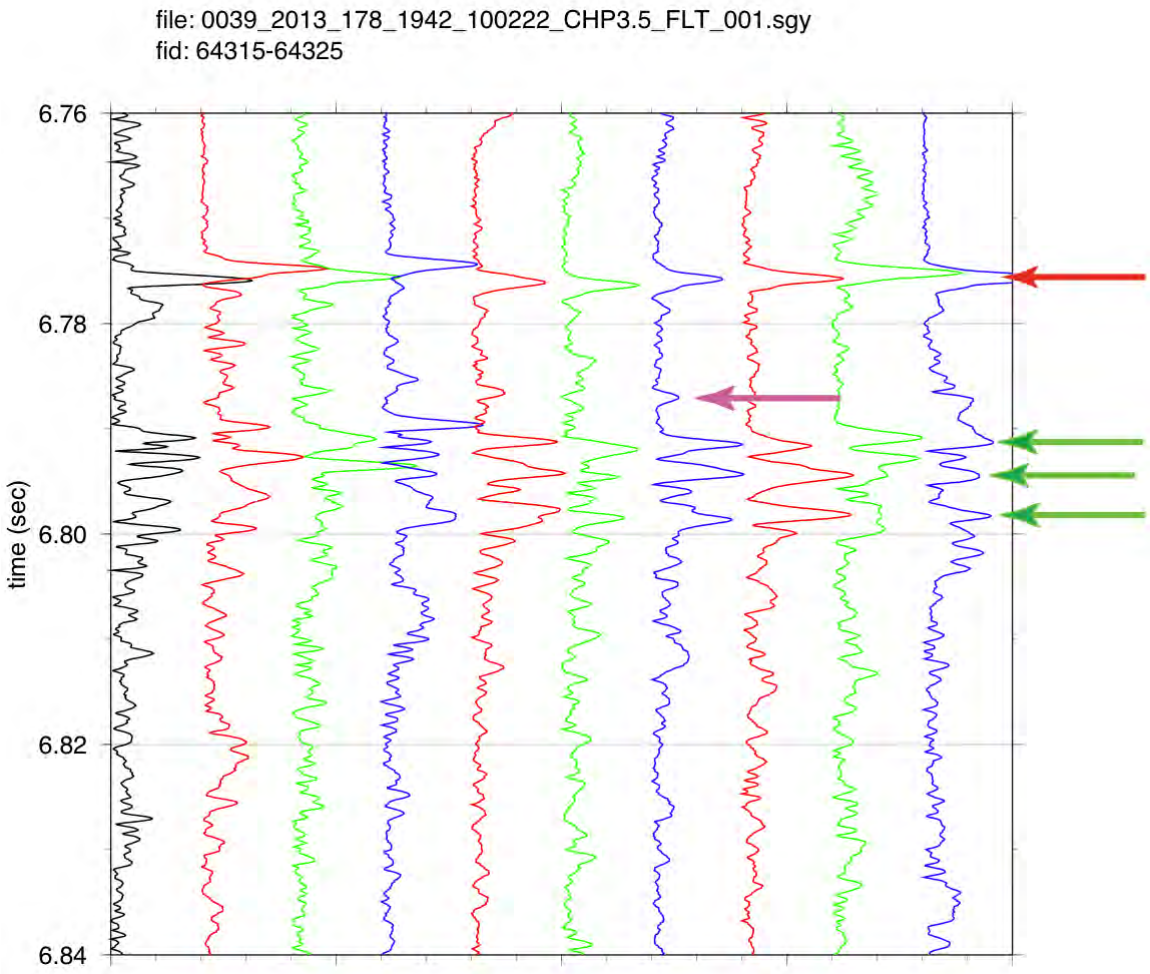

Figure 17.13: Processed traces from the light blue box in Figure 17.12
Processed traces from the light blue box in Figure 17.12 show clear evidence of the lateral coherence of the seafloor (red arrow), a low-amplitude reflection within the upper unit, and the three high-amplitude reflections (green arrows) comprising the lower, high-amplitude unit.

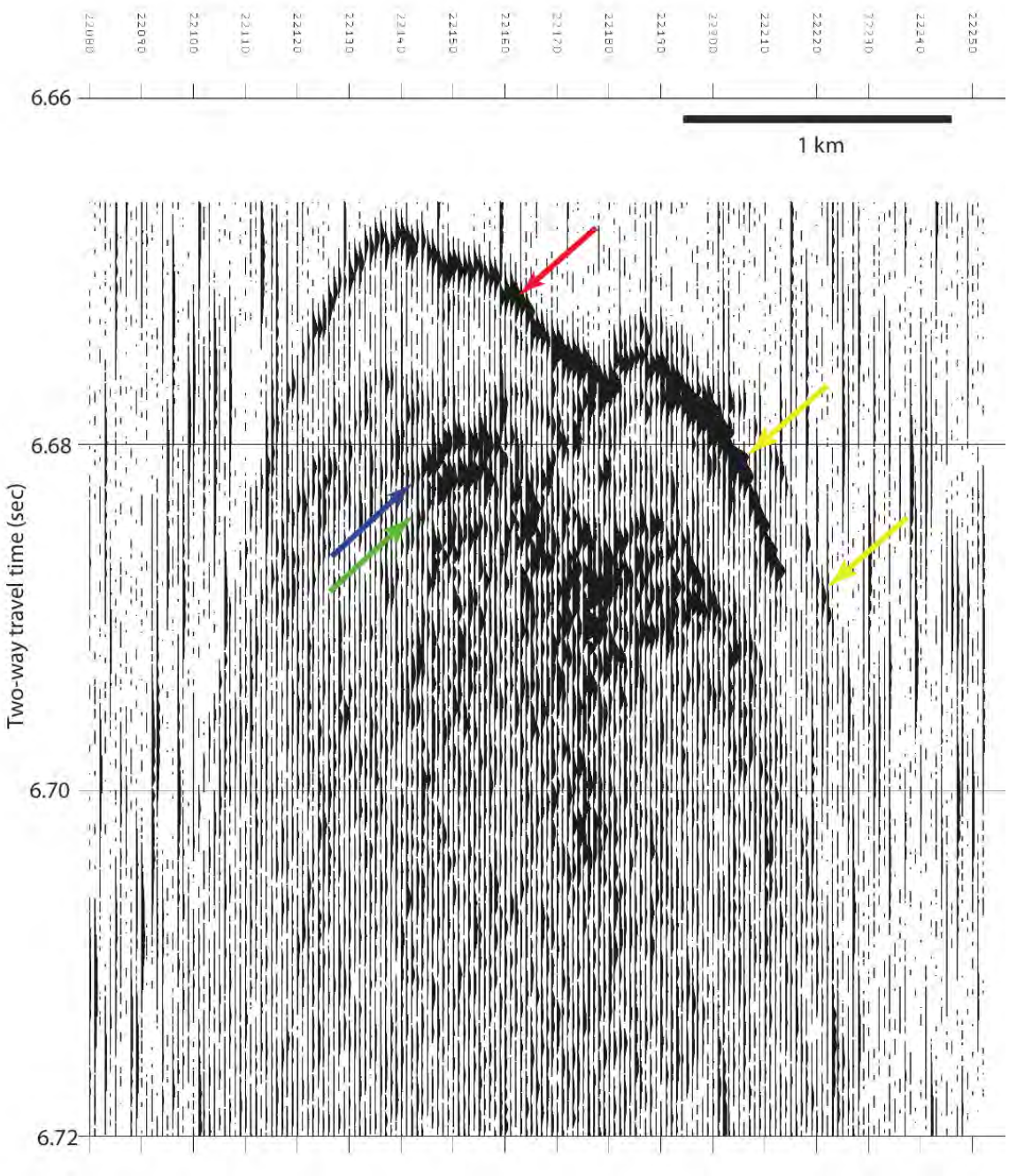

Figure 17.14: Profile 173a
Profile 173a shows reflections from the deep, high amplitude unit (blue and green arrows) are laterally coherent even on the crests of abyssal hills. Red arrow marks the seafloor, and the yellow arrows indicate hyperbole originating from the seafloor at the edges of the hillcrest. Figure 17.1 shows location of profile.

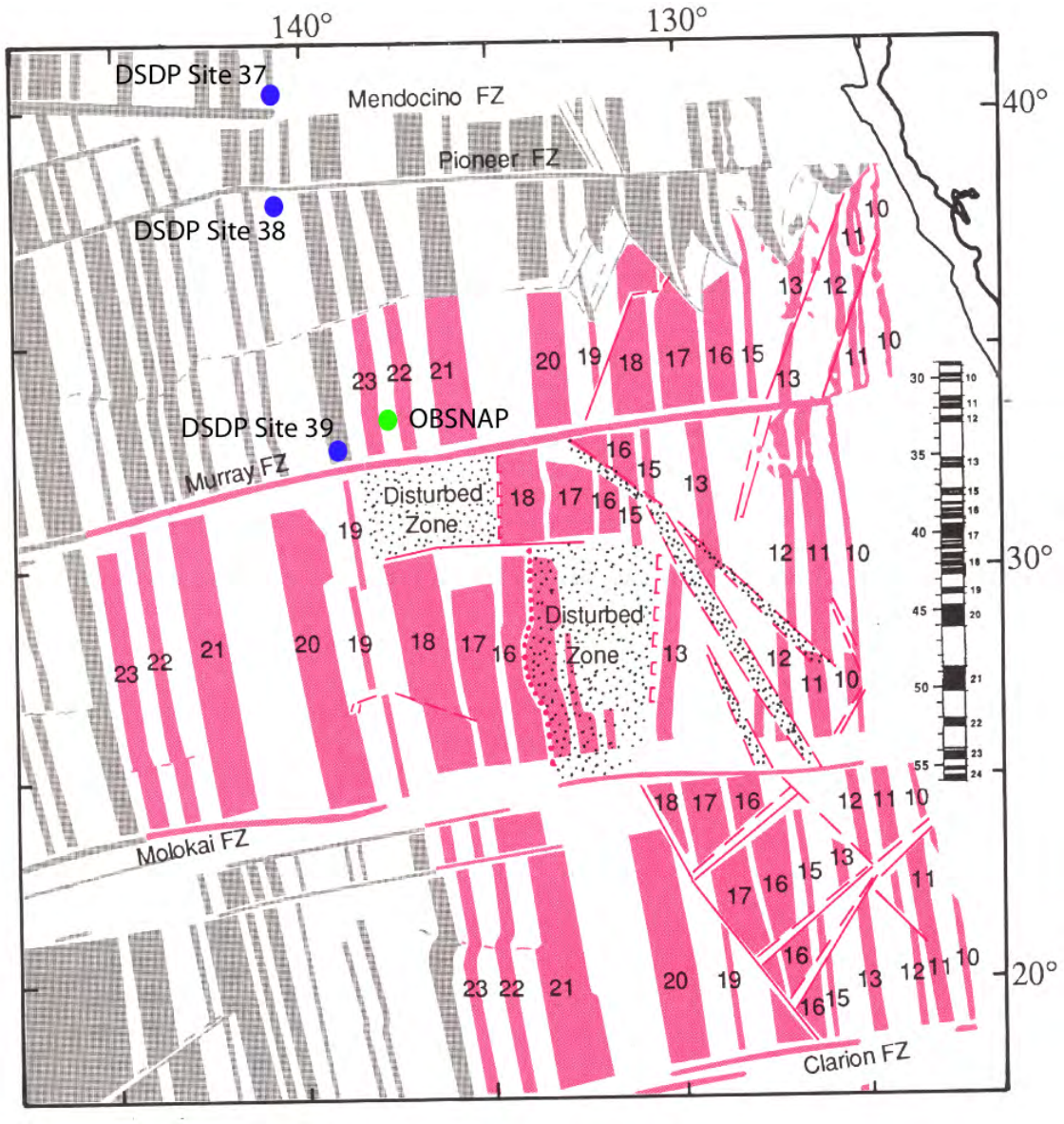

Figure 17.15: Magnetic anomaly map of the eastern north Pacific
Magnetic anomaly map of the eastern north Pacific from Atwater (1989) shows that the OBSANP survey (green dot) is on oceanic crust of age similar to that of crust drilled at DSDP Sites 38 and 39 (blue dots). DSDP Site 37 is much younger (chron 10). Magnetic anomalies colored red were the subject of a particular discussion in Atwater's paper.

18 Appendix G: Discussion of the XBT and CTD Results on Melville Cruise 1308 – Stephen A. Swift

Discussion of the XBT and CTD Results on Melville Cruise 1308

Stephen Swift (WHOI)

August 19, 2013

18.1 Introduction

Watchstanders on Melville Cruise 1308 deployed XBTs throughout the leg to characterize the temperature and – by inference – the speed of sound in the upper 2000 m. SIO technicians lowered the ship's CTD to the seafloor five times to measure temperature and salinity through the entire water column. Details are available in the cruise report. Shipboard analysis revealed patterns in the temperature structure of the upper 200 m. This report includes figures documenting these patterns and suggests that the water masses are features of the northern subtropical front of Lynn (1986).

18.2 Results

Temperature profiles from both XBTs and CTDs diverge in the 80-210 m depth interval with maximum separation at about 130 m water depth. Figure 18.1 shows traces of all reasonable XBT profiles in black over-printed with temperature profiles from the five CTDs in color. In the majority of profiles, temperature at 130 m ranges from 15.5° to 17.2°C. The temperature in a separate, smaller group of profiles is lower, ranging from 12° to 15°C. Close examination of Figure 18.1 reveals that a gap at about 16.2°C separates two clusters within the higher temperature group. The numbers of XBTs within each of the two higher temperature clusters appears to be about the same. Figure 18.2 shows that salinity from CTD profiles also separates in three groups consistent with the temperature values, so the cluster distinction identifies true water masses and is not an artifact of XBT operations. Thus, both XBT and CTD profiles can be separated into three clusters based on the temperature at 130 m water depth. Salinity values in the upper 100 m range from 34.0 to 34.3 psu. Figure 18.3 shows depth profiles of the three clusters identified by color, and Table 18-1 sorts the casts by the temperature at 130 m water depth.

The geographic distribution of clusters indicates that the groups are not simply related by mixing, and that they probably represent the results of more complex dynamics. Figure 18.4 shows location maps for each cluster. XBTs with low temperature at 130 m depth (yellow) fall to the east, north, and west of the two higher temperature clusters (orange and purple). The separation between low temperature profiles and the higher temperature profiles is distinct, whereas the locations of the two higher temperature clusters intermingle somewhat. Most intermediate temperature profiles (orange in Figure 18.3 and Figure 18.4) occur in a group around the DVLA site with a diameter of about 100 km (55 nmi), although two profiles fall further to the west. Most XBT profiles in the highest temperature group (purple in Figure 18.3 and Figure 18.4) occur along the outer edge of the intermediate cluster. However, overlap occurs between the two clusters (Figure 18.4). These mapping results indicate geographic separation of the three temperature clusters, although the separation of the two higher temperature clusters is incomplete. More importantly, these results also demonstrate that the profiles with the highest temperature occur between profiles with low and intermediate temperature. Although mixing occurs along density surfaces rather than depth surfaces, it seems unlikely that mixing can explain the distribution of water mass types observed.

The XBT and CTD profiles are spot geeographic measurements, so we examined data from two instruments that continuously recorded water properties during the experiment to investigate the boundaries between the three water types defined in Figure 18.4. Data was continuously recorded by the ship's thermosalinograph (TSG) and by a SeaBird temperature-pressure probe lashed to the J-15. First, we mapped temperature and salinity measured by the TSG salinometer in the forward wet lab, to which seawater was pumped from the ship's bow intake, and temperature from a probe mounted in the bow intake. Figure 18.5 shows maps of sea surface temperature (SST) and sea surface salinity (SSS) along with the distribution of the three water types defined by the XBT profiles. Close examination reveals several problems. First, cooler temperatures associated with Group 1 XBTs (yellow dots) nicely correlate with cooler temperatures recorded by the TVG to the east of the DVLA site during the inbound transit from San Diego. But cooler XBT temperatures at 130 m depth (Group 1 yellow dots) correlate with warmer TSG temperatures to the north and west of the DVLA site. Second, the TSG data at any one location appear to change with time. Figure 18.6 shows maps of SST and SSS data separated arbitrarily by midnight between June 20 and 21. Surface water near the DVLA site appears to get warmer and less saline after June 20. Third, Figure 18.7 shows a temperature-salinity plot of the TSG data. Whereas the results for the two transits at the beginning and end of the experiment appear roughly linear, indicating mixing between water masses, the intervening data (red dots) show extreme variations that cross isopycnals suggesting the influence of air-sea interaction such as rain and changes in solar irradiation due to the presence and absence of clouds and, perhaps, instrument malfunction. The difference between the results of the TSG while transiting and surveying may indicate that ship speed affects the performance of the TSG system. Thus, the TSG data are unreliable for investigating the boundaries between the water masses defined at 130 m depth.

Data from the SeaBird temperature-pressure probe lashed to the J-15 are more useful. The depth of the J-15 varied during the experiment due to changes in length of the tow cable and to changes in tow speed. Figure 18.8 shows that the J-15 hung at about 60 m during most of the cruise, but sailed aft to 35-50 m depth during transits. This is particularly true between stations on the long WNW-ESE line. Although the time required for these transits was relatively short compared to station time, they covered nearly all of the long line (see coverage in Figure 18.9 top panel). The map of temperature at 35-50 m in the top panel of Figure 18.9 shows warmer water along the middle portion of the line and a transition to colder water near 140° 45'W (red arrow). The inset in the top panel of Figure 18.9 shows that the apparently colder water at the east end of the long line is likely an artifact of the sequence in which points were plotted. The transition from cold to warm marked by the red arrow occurs about 75 km further to the east at 60 m depth (middle panel in Figure 18.9) than at 35-50 m depth (top panel in Figure 18.9). The transition at 60 m depth is close to the depth below which the three water masses defined by the XBT profiles become apparent (Figure 18.1). The map of temperature at 35-50 m indicates that the transitions in water masses occur over distances as short as 9-10 km. The overlap between water mass types seen in temperature at 130 m (Figure 18.4) also occurs in temperature mapped at 60 m (Figure 18.9). To investigate why the transition in temperature occurs so far west at 35-50 m depth, we plotted temperature in a depth section as a function of longitude along the WNW-ESE line. In Figure 18.10, the longitude of the transition in water deeper than 45 m (red arrow) is consistent with the XBT data. The warm anomaly in upper water temperature is confined to depths above 42 m. This surface water is separated from the three water mass types

by a thermocline and halocline (Figure 18.1 and Figure 18.2) and, thus, is more likely to be more affected by recent air-sea interaction, winds and solar insolation, in particular.

The XBT and CTD profiles indicate that the intermediate and high temperature/salinity water groups at 130 m depth intermix west of the DVLA mooring (Figure 18.4). Examination of Table 1 shows that the temperature overlaps occur at different times during the cruise and, thus, are likely due to lateral movement of the boundaries between water masses. From Table 18-1, the sense of offset between the high and intermediate temperature water mass observations produces conflicting results if interpreted as simple east-west motion along the long line. It is likely, then, that motion in this region includes a north-south component. This is consistent with current vector maps produced by the ADCP acquisition system (Figure 18.11).

In summary, the J-15 temperature data confirm the existence of water mass boundaries below ~42 m depth and indicate that the boundaries are abrupt and laterally mobile. Surface water is isolated from deeper water by vertical gradients in water properties at 40-50 m.

18.3 Discussion

The distribution of water masses at 130 m mapped with the XBT temperature profiles (Figure 18.4) and confirmed by the CTD profiles (Figure 18.2) and the temperature recorded on the J15 (Figure 18.9) can not reasonably be explained by simple mixing along isopycnals, if only because the water masses are spatially out of order. The higher temperature, higher-salinity end-member (purple in Figure 3) occurs between the low-temperature, low salinity and intermediate end members (Figure 4). The data require an alternative – more dynamic – explanation.

The study site is located in the transition zone between subarctic and subtropical water masses, and a front between surface water masses would seem sufficiently dynamic to explain the structure we observed during the DVLA experiment. Roden (1975) ascribed surface water fronts in the North Pacific to narrowing of north-south gradients in water properties at the surface by wind systems with opposing Ekman wind stress. Figure 18.12 from Roden (1975) shows the subtropical frontal zone separating westward-flowing ocean surface currents to the south from easterly currents to the north. This pattern is consistent with convergence in the long-term mean Ekman flow forced by atmospheric winds shown in Figure 18.13.

Roden (1980) showed that the subtropical frontal zone actually comprised three separate fronts (Figure 18.14). Looking at just sea surface salinity analyses, Saur (1980) also distinguished three fronts. Both the number of fronts and their position varied with time - both seasonally and from year-to-year. Lynn (1986) examined CTD sections and confirmed the presence of three fronts. The occurrence and latitudinal position of these fronts varies on weekly time scales as well as by season due to changing locations in atmospheric pressure systems (Roden, 1975; Saur, 1980).

In Figure 18.14, a vertical section obtained in winter by Roden (1980) shows that the fronts separate warm, salty surface water (south) from cooler, fresher water (north) and that lateral gradients in both temperature and salinity extend up to the sea surface. This might not be the case in summer when solar heating warms the seasurface on both sides the front. Shcherbina et al. (2009) show that a front they mapped in July could be detected in MODIS imagery of SST (Figure 18.15). The SST image, however, poorly defines the extent of the front. On the other hand, their vertical sections (Figure 18.16) show that the front they label as F1 at ~31°N is well defined by salinity at the sea surface but poorly defined by temperature. In Figure 18.17 from Wilson et al. (2013), vertical profiles near a front indicate that salinity varies widely at the sea surface whereas temperature profiles vary little, showing a seasonal thermocline and thin well-

mixed layer in the upper 60 m. These temperature profiles resemble our profiles (Figure 18.1) in (1) the presence of a surficial seasonal layer and (2) they separate into high, intermediate, and low temperature/salinity groups at 120-130 m depth. Although an eddy may be present (Figure 18.17), Wilson et al. argue that a front controls the distribution of profile types. These data were collected >100 km to the southwest of the DVLA survey.

Lynn (1986) presents hydrographic data from surveys of the subtropical front zone in the region of our experiment (Figure 18.18). Lynn refers to the particular front closest to the DVLA experiment site as the "northern subtropical front." Salinities present in this front are commonly around 34.0-34.2 psu, which agrees well with those measured by our CTD casts (Figure 18.2). Figure 18.19, Figure 18.20, Figure 18.21, and Figure 18.22 show Lynn's north-south vertical sections through the "northern subtropical front" during June of four separate years in the 1970s. The section in Figure 18.22 reveals more detail because the separation between CTD casts is much smaller. These sections reveal three useful observations. (1) None of the sections shows an unambiguous feature in temperature at the sea surface that signals the location of the front. (2) Sea surface salinity, however, clearly marks the position of the front. Maps of SS in Figure 18.23 and Figure 18.24 show that the sea surface expression of the front appears to be linear but is not always oriented east-west. (3) The offset in salinity associated with the front extends down to 150-200 m water depth. (4) The strongest computed geostrophic currents flow towards the east along the front (eg, Figure 18.19). ADCP observations by Shcherbina et al. (2010) also reveal eastward flow. (4) Water with locally higher salinity and higher temperature occurs just to the south of the front at water depths of 50-180 m (arrows in Figure 18.19, Figure 18.20, Figure 18.21, and Figure 18.22). Lynn (1986) describes this feature and points out that the anomalous water is offset by about 100 km to the south of the front in June 1974 (Figure 18.21).

The high temperature/high salinity water anomaly is not mentioned in other published descriptions of the "northern subtropical front", although no other surveys at this longitude were done with sufficiently close spacing of CTDs to image the feature. Shcherbina et al. (2009, 2010) provide very detailed analysis of a subtropical front, but their surveys were done at 156°-158°W, the sea surface expression of the front is non-linear and oriented NW-SE (Figure 18.15), and the salinities are generally higher (>34.2 psu; Figure 18.16). They also describe an anomalous water mass on the south side of the front, but these features differ from those described by Lynn (1986) by being both narrower (5-10 km north-to-south) and cooler and less saline than the water they intrude.

The "northern subtropical front" described by Lynn (1986) provides a good model for our observations in June-July 2013. In particular, Lynn's observations along north-south transects provides an explanation for the spatial pattern of water mass types that we observed at ~130 m depth. Our survey found water with low temperature and low salinity at ranges greater than 120 km to the east, north, and west of the DVLA mooring (yellow dots in Figure 18.4). Water with the highest salinity and temperature separates this water mass from water with intermediate properties that clusters around the DVLA site (Figure 18.4 and Figure 18.9). This transition in water types is analogous to the transition that Lynn found across the "northern subtropical front." To illustrate the agreement, Figure 18.25 shows one of Lynn's vertical sections modified with a horizontal bar at 130 m depth. The transitions in the color of the bar are placed to distinguish the water masses recognized by Lynn, but the relative change in temperature and salinity are coded using the color pattern used in displaying our results in Figure 18.3, Figure 18.4, and Figure 18.9. Using this match to Lynn's results, a vertical front in salinity and temperature between the surface and ~200 m depth probably occurs at the inner boundary of the low-temperature, low-

salinity water (yellow dots in Figure 18.4). Our results document the position of the front only along the long survey line run out to the WNW of the DVLA site. The position of this boundary is marked with the red arrows in Figure 18.9. In Figure 18.26 the position of the front is extrapolated around the north side of the DVLA site using the approximate distance found along the WNW survey line. The vertical distribution of water properties to the south of the DVLA site is likely to be similar to the intermediate water profiles (brown in Figure 18.3). This application of Lynn's observations of the "northern subtropical front" to our survey results provides a rational basis for generating models of sound speed for numerical simulations.

18.4 References

Lynn, R. J., 1986, The subarctic and northern subtropical fronts in the eastern North Pacific Ocean in spring,J. Physical Oceanography, 16, 209–222.

Roden, G.I., 1975, On North pacific temperature, salinity, sound velocity and density fronts and their relation to the wind and energy flux fields, J. Physical Oceanography, 5, 557-571.

Roden, G. I., 1980, On the subtropical frontal zone north of Hawaii during winter, J. Physical Oceanography, 10, 342–362.

Saur, J. F. T., 1980, Surface salinity and temperature on the San Francisco-Honolulu route June 1966-December 1970 and January 1972-December 1975, J. Physical Oceanography, 10, 1669–1680.

Shcherbina, A. Y., M. C. Gregg, M. H. Alford, and R. R. Harcourt (2009), Characterizing thermohaline intrusions in the North Pacific subtropical frontal zone, J. Physical Oceanography, 39, 2735–2756.

Shcherbina, A. Y., M. C. Gregg, M. H. Alford, and R. R. Harcourt (2010), Three-dimensional structure and temporal evolution of submesoscale thermohaline intrusions in the North Pacific subtropical frontal zone, J. Physical Oceanography, 40, 1669–1689.

Wilson, C., T.A. Villareal, M.A. Brzezinski, J.W. Krause, and A.Y. Shcherbina, 2013, Chlorophyll bloom development and the subtropical front in the North Pacific, J. Geophysical Research, 118, 1473-1488, doi:10.1002/jgrc.20143.

Table 18-1 CTD and XBT Profile Temperature Groupings

18.4.1 Low temperature cluster (12°-15°C at 130 m water depth)
CTD: 2
XBT: 3, 24, 26, 27, 28, 29, 30, 31, 32, 90

18.4.2 Intermediate temperature cluster (15°-16.2°C at 130 m depth)
CTD: 1, 3, 5
XBT: 4, 34, 37, 41, 42, 44, 45, 46, 47, 48, 50, 51, 52, 53, 54, 55, 56, 57, 58, 59, 60, 61, 62, 65, 67, 68, 69, 75, 77, 78, 82, 87, 88

18.4.3 High temperature cluster (16.2°-17.2°C at 130 m depth)
CTD: 4
XBT: 5, 6, 7, 9, 11, 12, 13, 14, 15, 16, 18, 19, 20, 21, 22, 33, 36, 38, 39, 40, 70, 71, 73, 81, 89

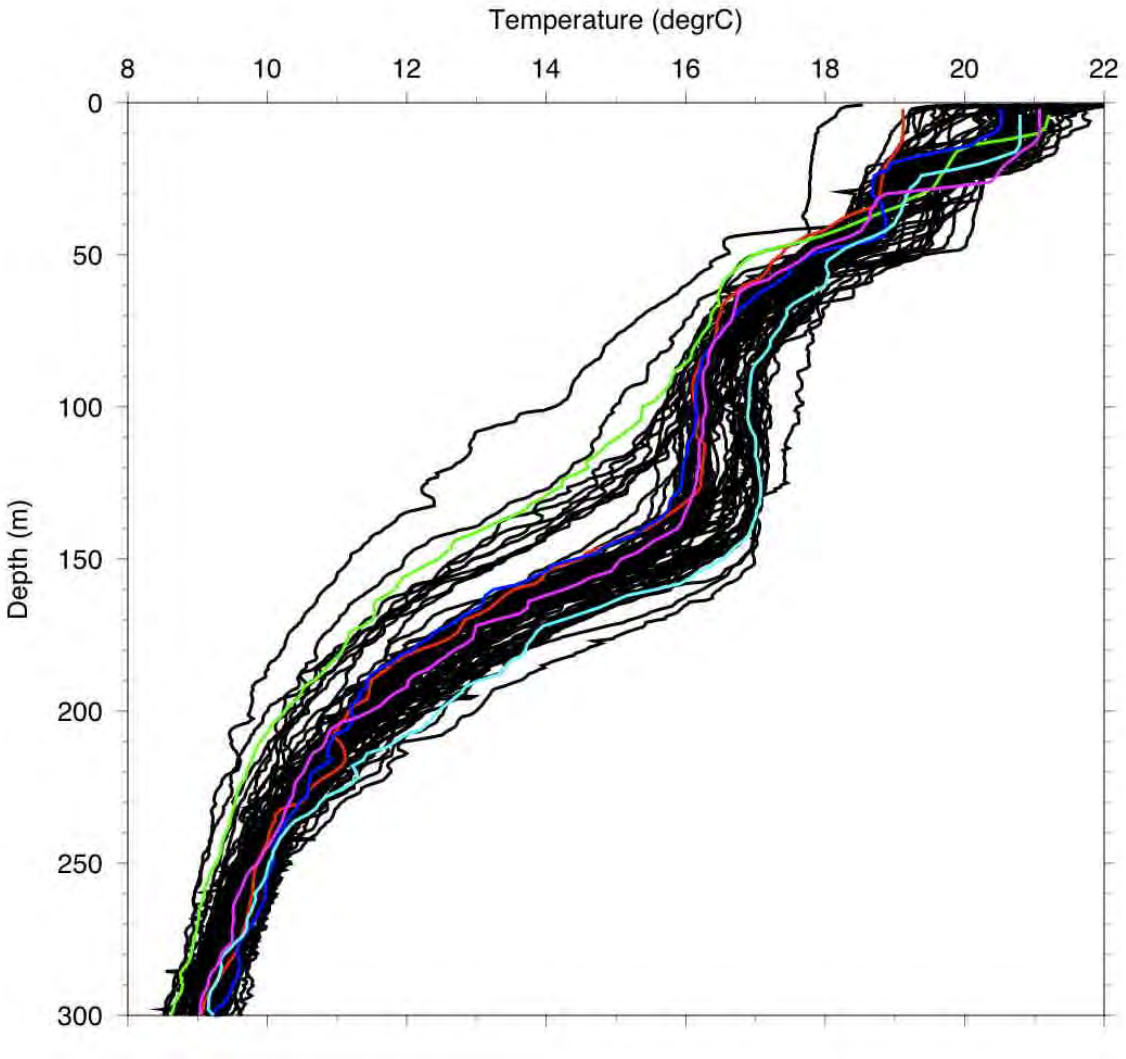

Figure 18.1: Vertical temperature profiles
Vertical temperature profiles separate into three different groups between 80 m and 210 m water depth. The separation is most clear at 130 m depth. Above 80 m depth, temperature decreases downward in the seasonal thermocline. Black lines: all XBTs on Melville 1308 with reasonable results. Colored lines: five CTDS on Melville 1308. See Figure 18.4 for locations of profiles.

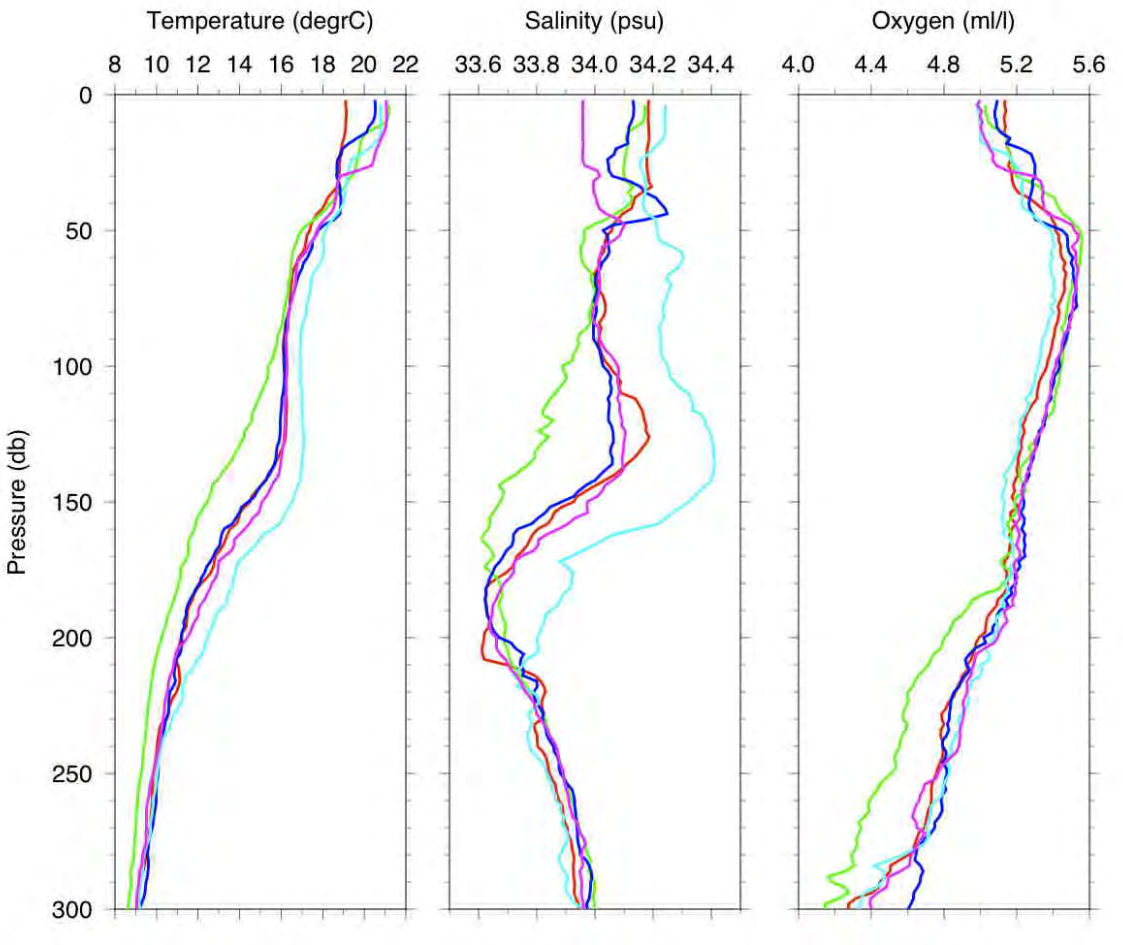

Figure 18.2: Vertical profiles from the five CTDs
Vertical profiles from the five CTDs indicate that the separation into groups at 80-210 m depth is apparent in temperature and salinity but not in oxygen. Figure 18.4 shows the locations of CTDs.

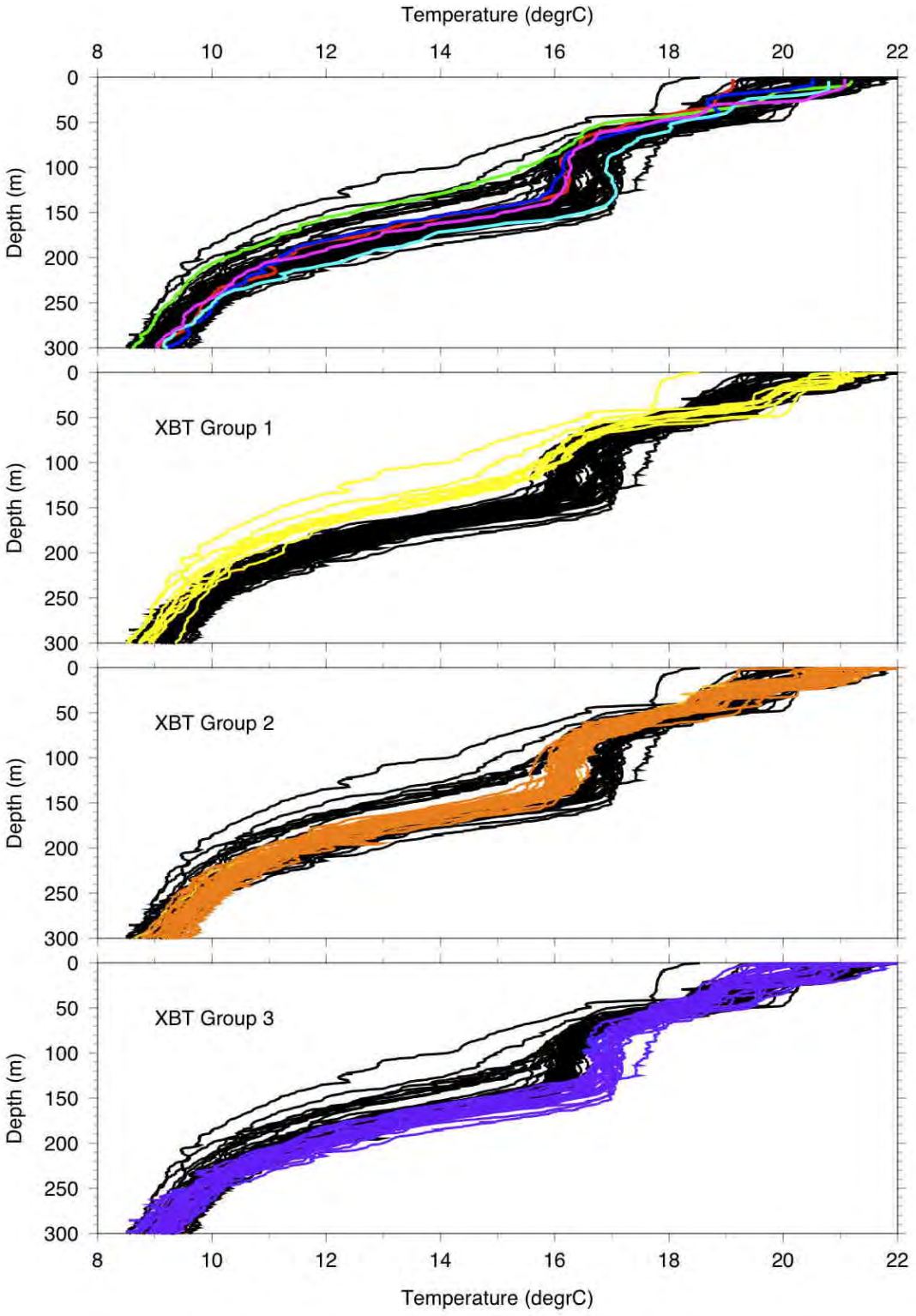

Figure 18.3: Grouped XBT profiles
The top panel shows all temperature profiles plotted as in Figure 18.1: all XBTs are black and the five CTDs are coded by color. In the lower three panels the XBTs in each temperature group are plotted in a single color. Groups were separated using the temperature at about 130 m depth. Figure 18.4 shows the location of XBT profiles by group and the locations of CTDs.

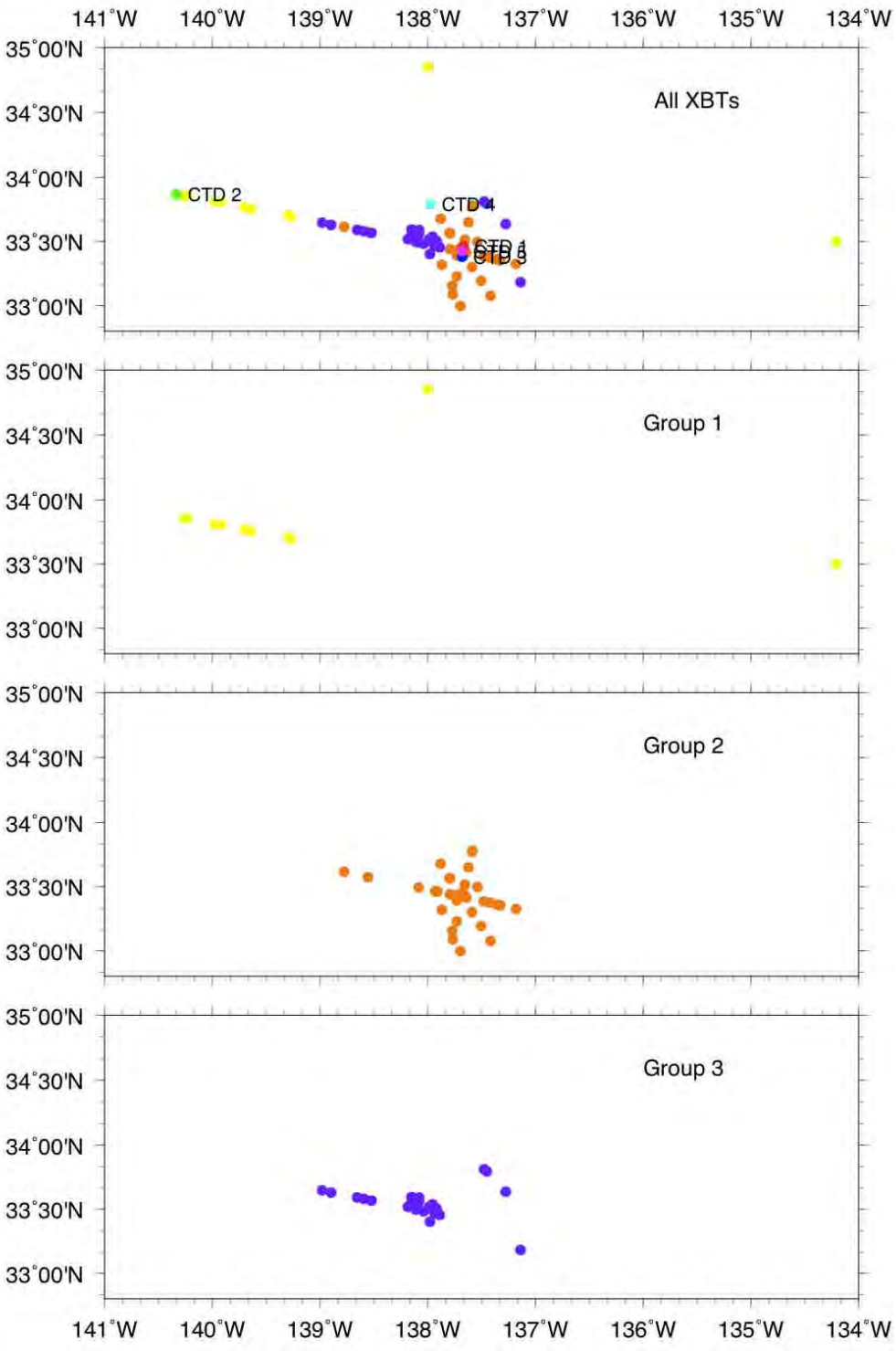

Figure 18.4: XBT and CTD group locations
Top panel shows the locations of the five CTDs and the locations of XBT groups by color: yellow-low temperature, brown-intermediate temperature, and purple-high temperature. Lower three panels show the locations of XBTs by group. Figure 18.3 shows the temperature profiles.

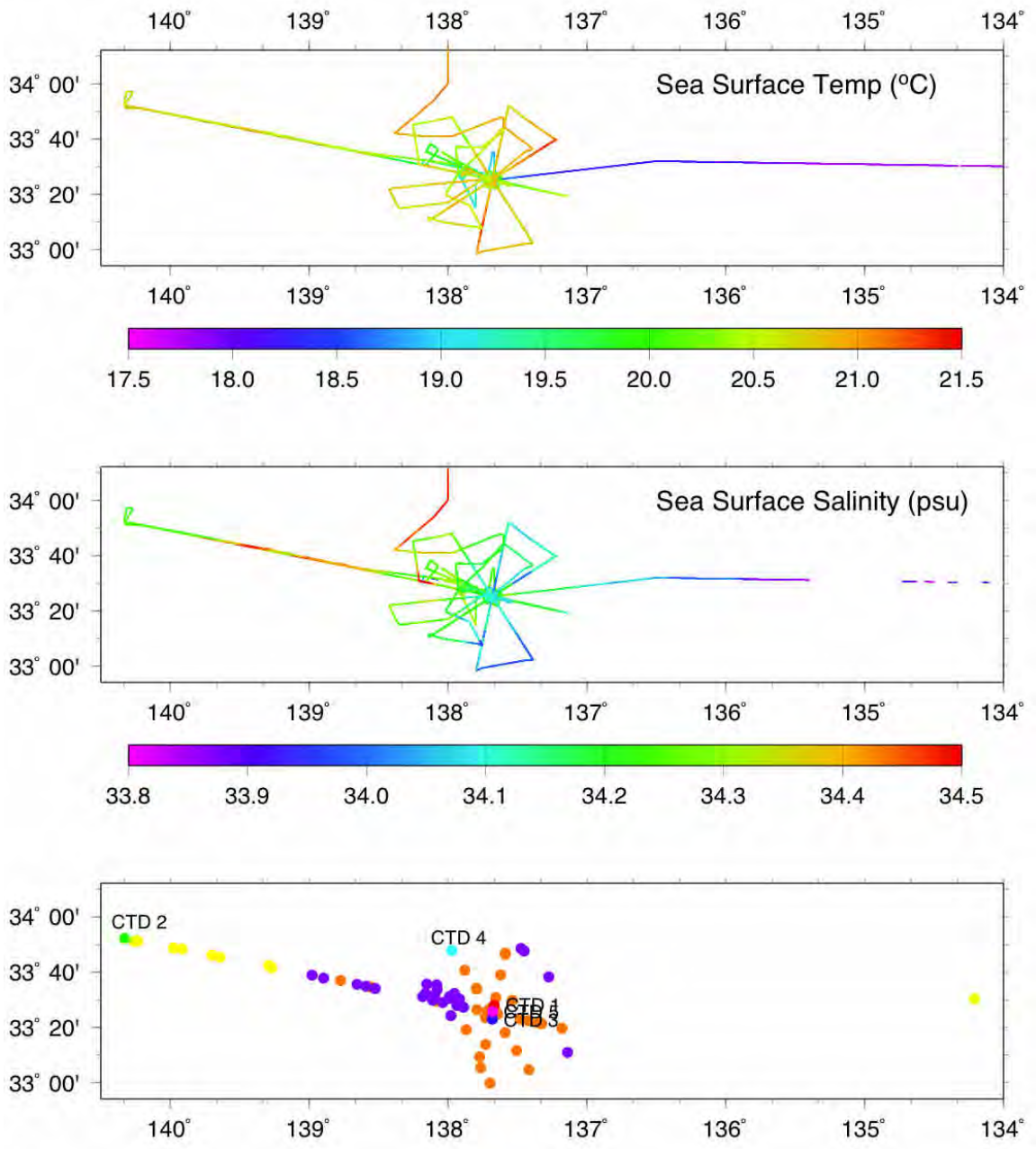

Figure 18.5: Sea Surface temperature and Slinity
The top two panels show sea surface temperature measured by a probe in the salt water intake port in the bow of the ship and sea surface salinity measured by the thermosalinograph in the forward wet lab on flow of sea water from the bow intake port. For reference, the lower panel shows at the same scale the locations of CTDs and the locations of XBT by temperature group (copy of the top plot in Figure 18.4).

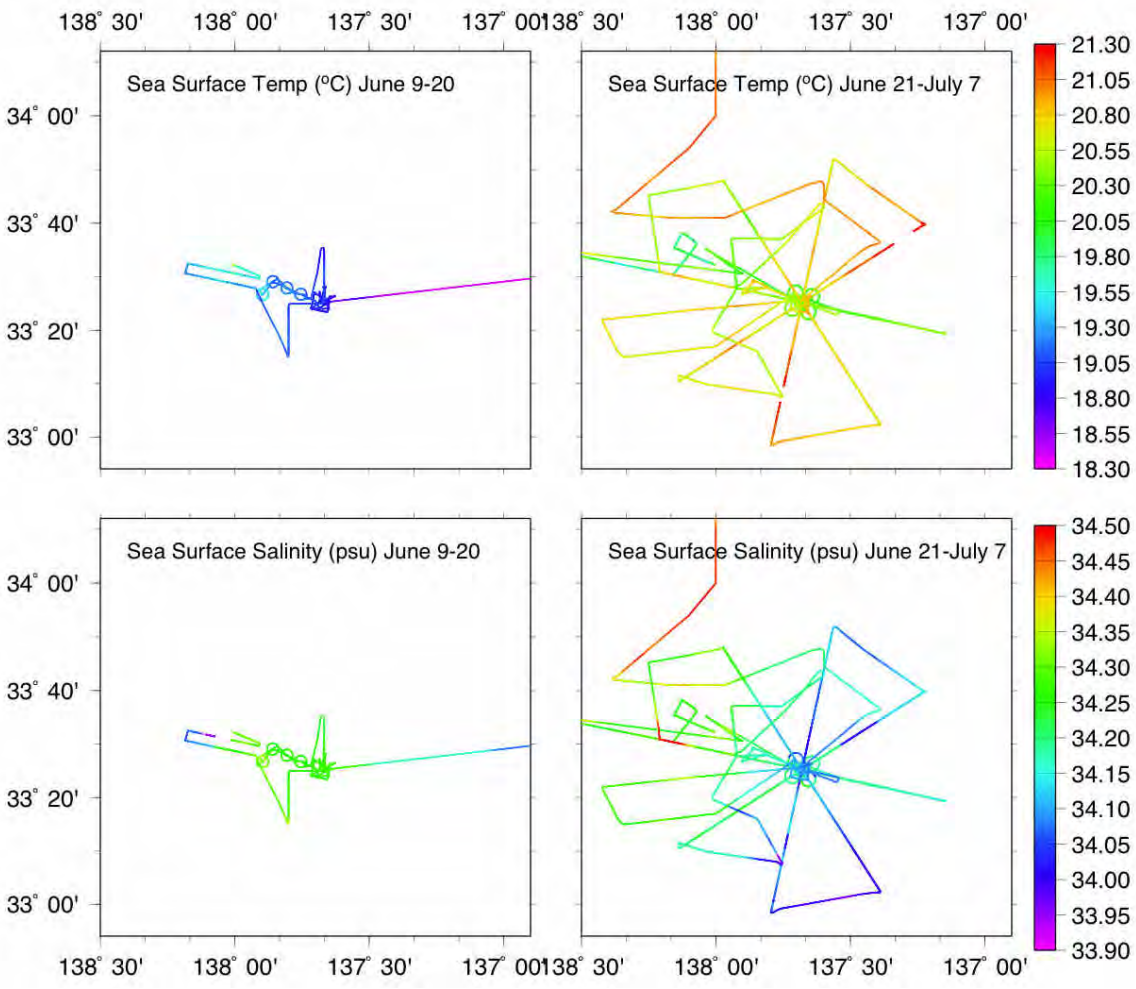

Figure 18.6: sea surface temperature and salinity near DVLA change with time
Both sea surface temperature and salinity near the DVLA mooring change with time during the survey. Top two panels show sea surface temperature for the region close to the DVLA mooring separated into two time periods: (left) all measurements before 2400 on June 20, and (right) all measurements after 0000 on June 21. The lower two panels show sea surface salinity broken into the same two time periods. However, the data are likely to be unreliable (see Figure 18.6).

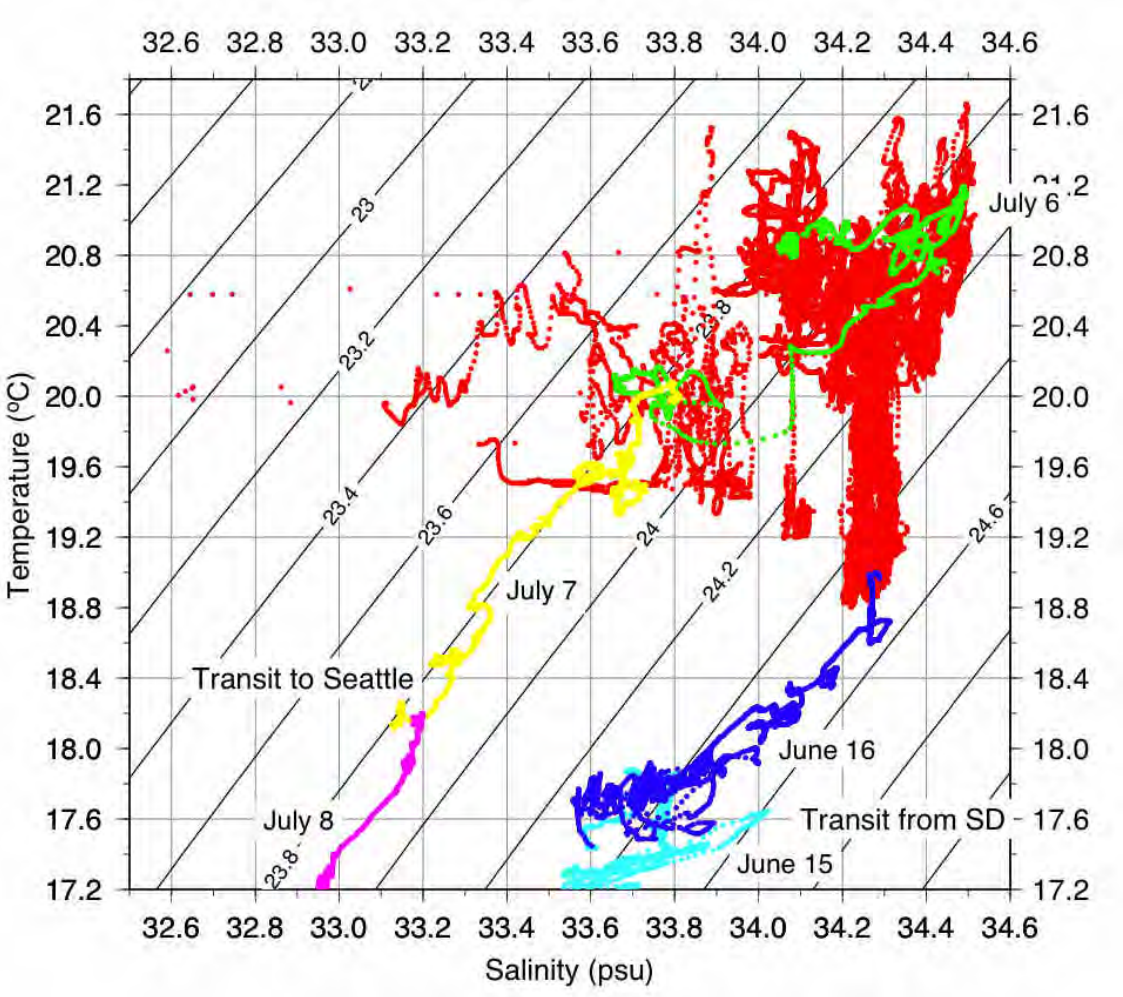

Figure 18.7: temperature -salinity plot of the thermosalinograph
A temperature (Y)-salinity (X) plot of the thermosalinograph records shows large changes in both temperature and salinity that are likely due to air-sea interaction (rain, heat exchange) or inaccurate measurements making the data unreliable for tracking the locations of the temperature groups identified by water properties at 80-210 m depth. Data measured during both the transit from San Diego (blue and light blue) and the transit to Seattle (yellow and magenta) are relatively linear along isopycnals lines, so these data appear reliable. The data in red and green, however, cross isopycnals suggesting poor quality data during the survey. Since the data collected during transits show reasonable trends, low or zero ship speeds during J-15 survey may have affected flow of seawater through the intake port to the wet lab.

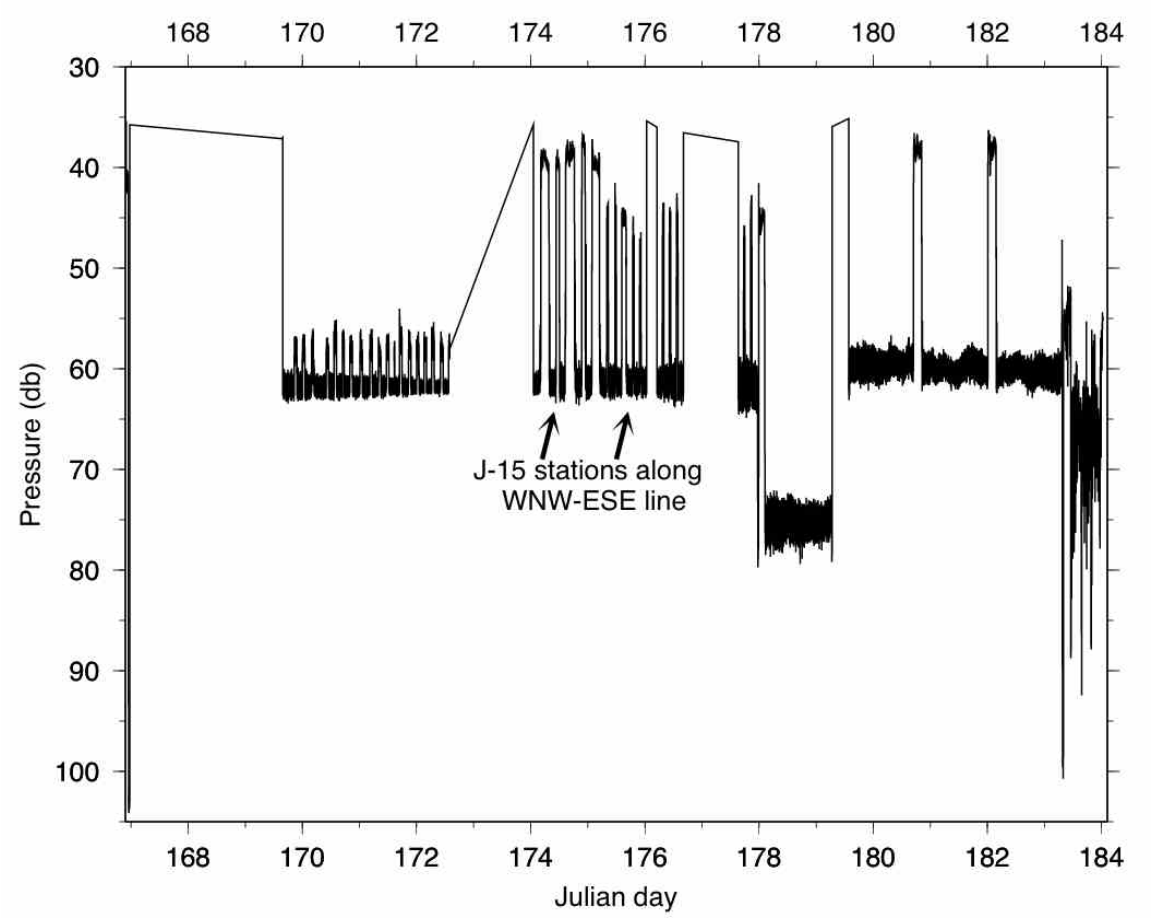

Figure 18.8: Pressure records from Seabird temperature-pressure probes lashed on J-15
The pressure records from Seabird temperature-pressure probes lashed to the J-15 can be used to identify depth horizons useful for mapping the horizontal distribution of temperature with which the XBT profiles can be compared. Linear line segments indicate time intervals when the battery in a probe failed. During most of the cruise, the temperature probe hung at 59-64 m depth. However, more area was covered during brief transits when the probe sailed up to 35-50 m.

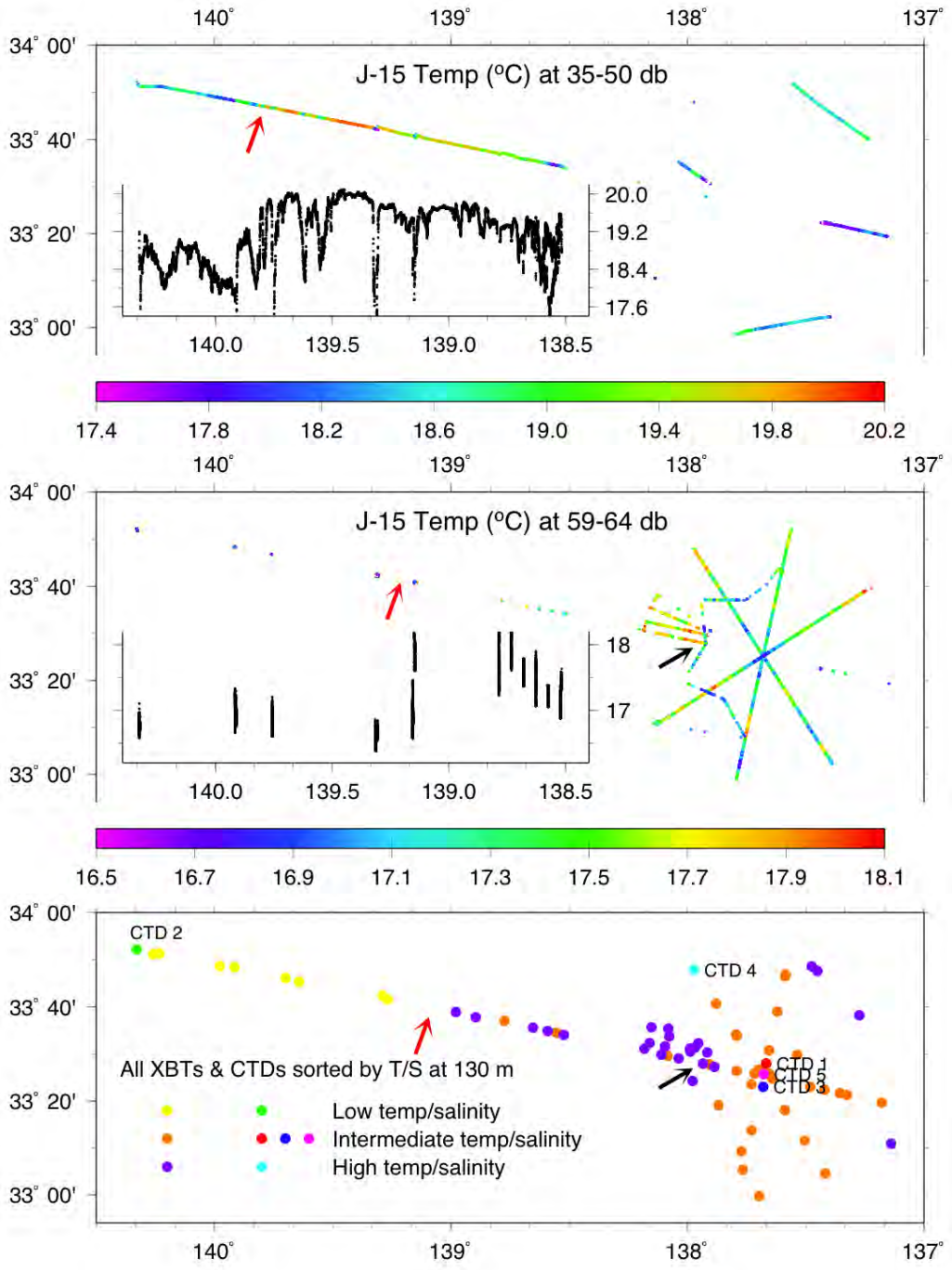

Figure 18.9: J-15 temperature probe tow depths and locations
Maps show temperature at the two most common tow depths for the probe attached to the J-15: (top) 35-50 m depth and (middle) 59-64 m depth. Bottom panel shows distribution of temperature groups based on XBT and CTD profiles (see Figure 18.3-Figure 18.4). Temperature at 59-64 m depth changes at two locations along the long survey line to the west (middle panel: red and black arrows). These locations are very similar to locations where the XBT temperature groups change (bottom panel: red and black arrows). Temperature at 35-50 m depth (top panel) changes mid-way along the WNW survey line (red arrow). Another temperature change (black arrow) suggests lateral changes in near surface water that was not detectable in the XBT profiles.

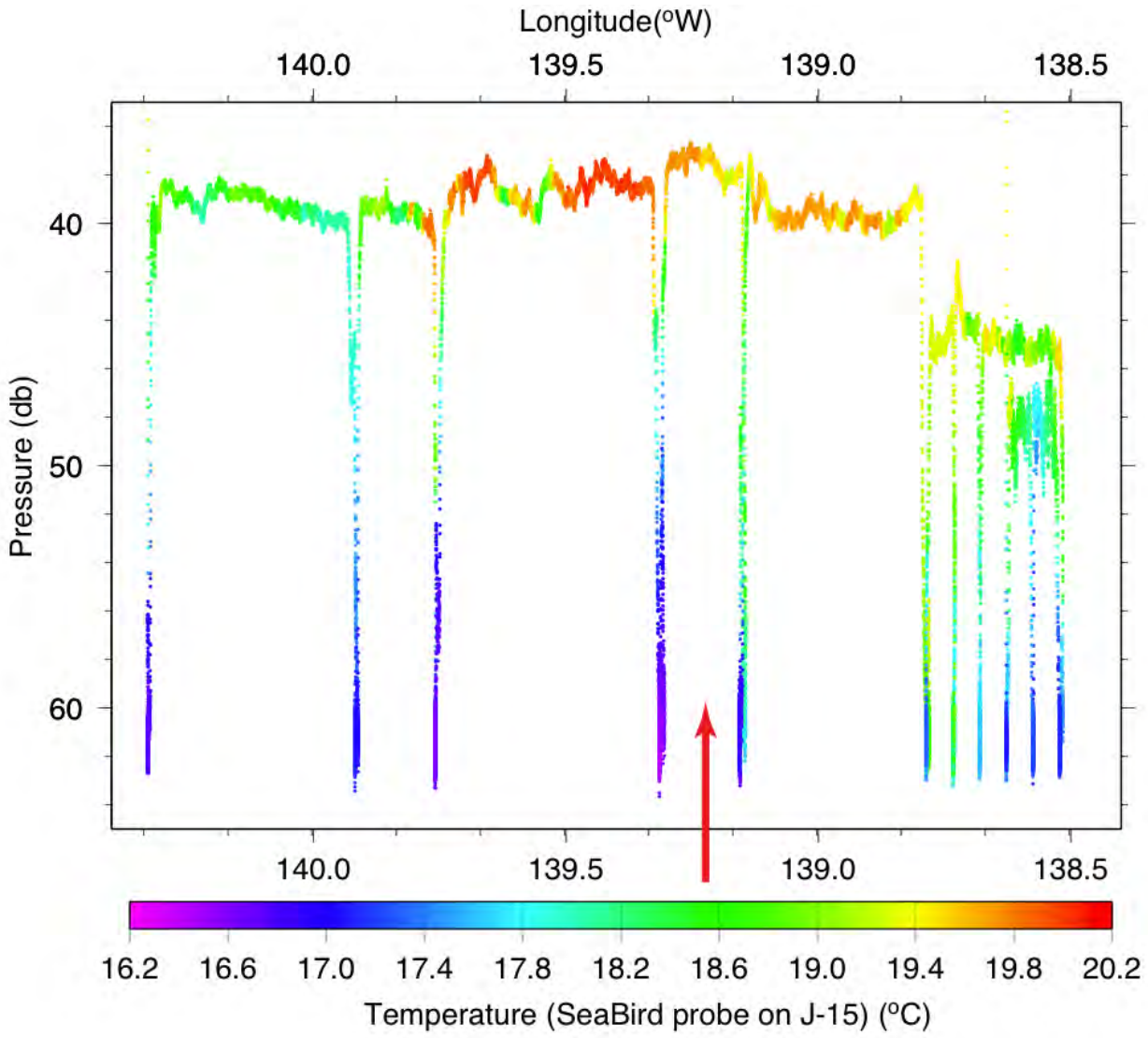

Figure 18.10: Temperature on a vertical section along the WNW-ESE survey line
Plot of temperature on a vertical section along the long WNW-ESE survey line confirms that a boundary between deep water masses is located near 139°15'W (red arrow). The lateral transition in surface water temperature occurs farther to the west and is likely controlled by separate processes. Temperature was measured by the SeaBird probe attached to the J-15. Excursions of the probe to deeper water occur at acoustic survey stations. Survey progressed from west (left) to east (right). Note that as the J-15 sank when the ship slowed to approach a survey station, warmer shallow water was pulled down. Conversely, colder, deep water was pulled up as the J-15 rose when the ship began to head to the east. This artifact accounts for the temperature contrasts at each station.

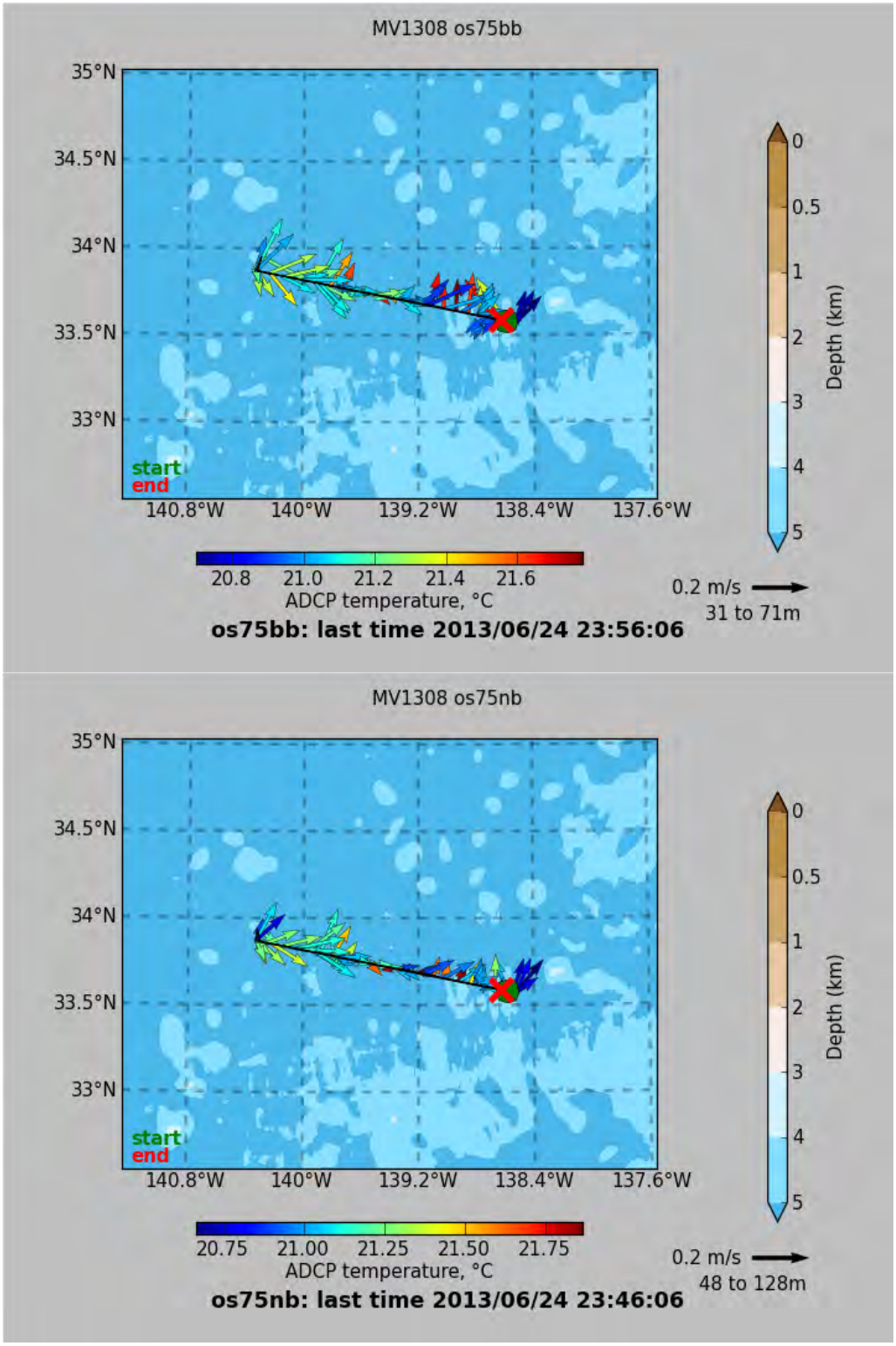

Figure 18.11: Average current vectors for the 31-71
(a) Average current vectors for the 31-71 m depth interval indicate eastward flow on the outer segment of the long WNW survey line (west of about 139° 36'W) and northward flow on the inner segment (east of 139° 12'W). (b) There is little change in average current vectors when the flow is averaged over a broader depth interval (41-128 m). Plots were generated automatically by the ADCP acquisition system.

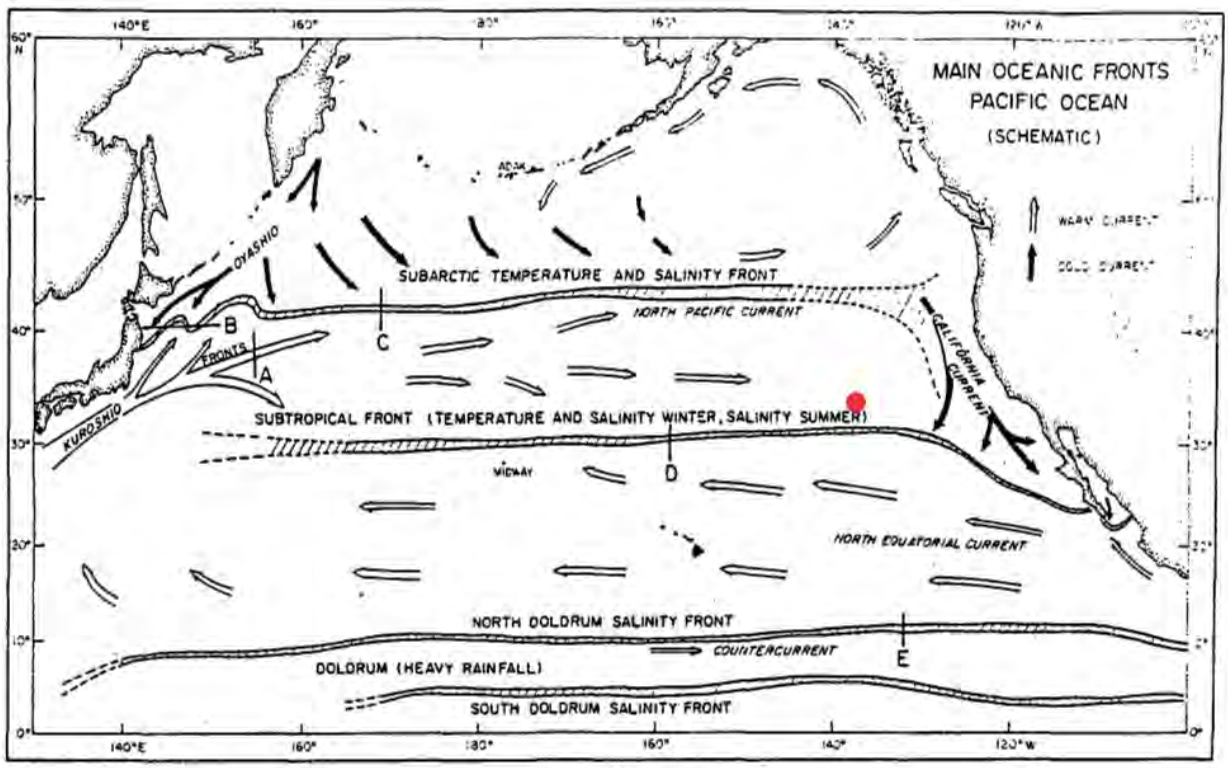

Figure 18.12: Map of Surface Currents
Map from Roden (1975) indicates that the Melville 1308 survey was done near a front between surface water currents. Arrows indicate prevailing current directions. Letters refer to fronts: A, Kuroshio front; B, Oyashio front; C, subarctic front;, D, subtropical front; and E, doldrums front.

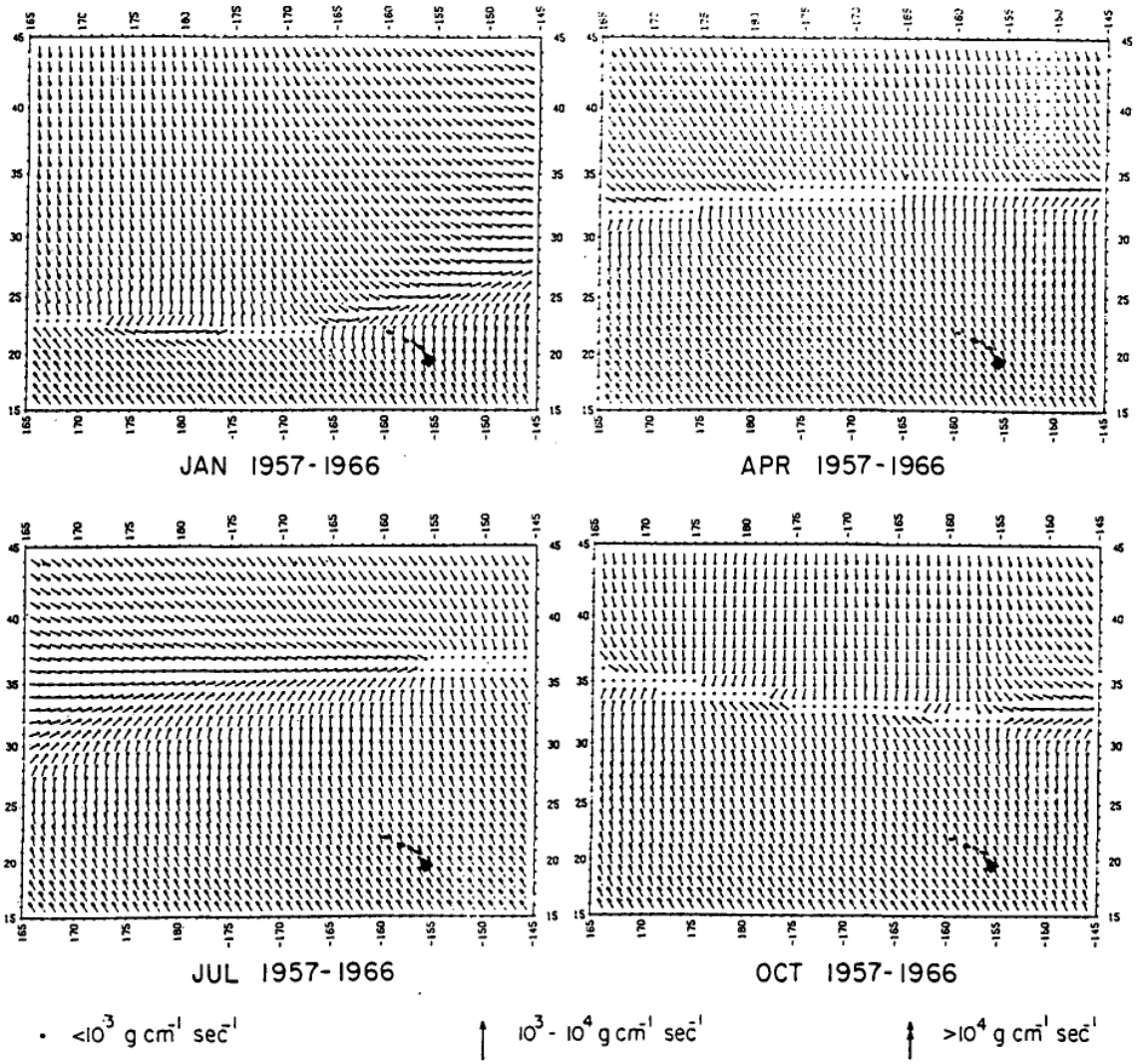

Figure 18.13: Map showing wind convergences
Map from Roden (1975) shows a convergence of west winds (north) and trade winds (south) matches the position of the subtropical front supporting Roden's inference that atmospheric forcing is responsible for fronts in the upper 200 m of the ocean. Seasonal variation of the spatial distribution of the surface Ekman transport on a 1° latitude-longitude grid is based on the stress of the geostrophic wind. Arrows indicate the direction of transport.

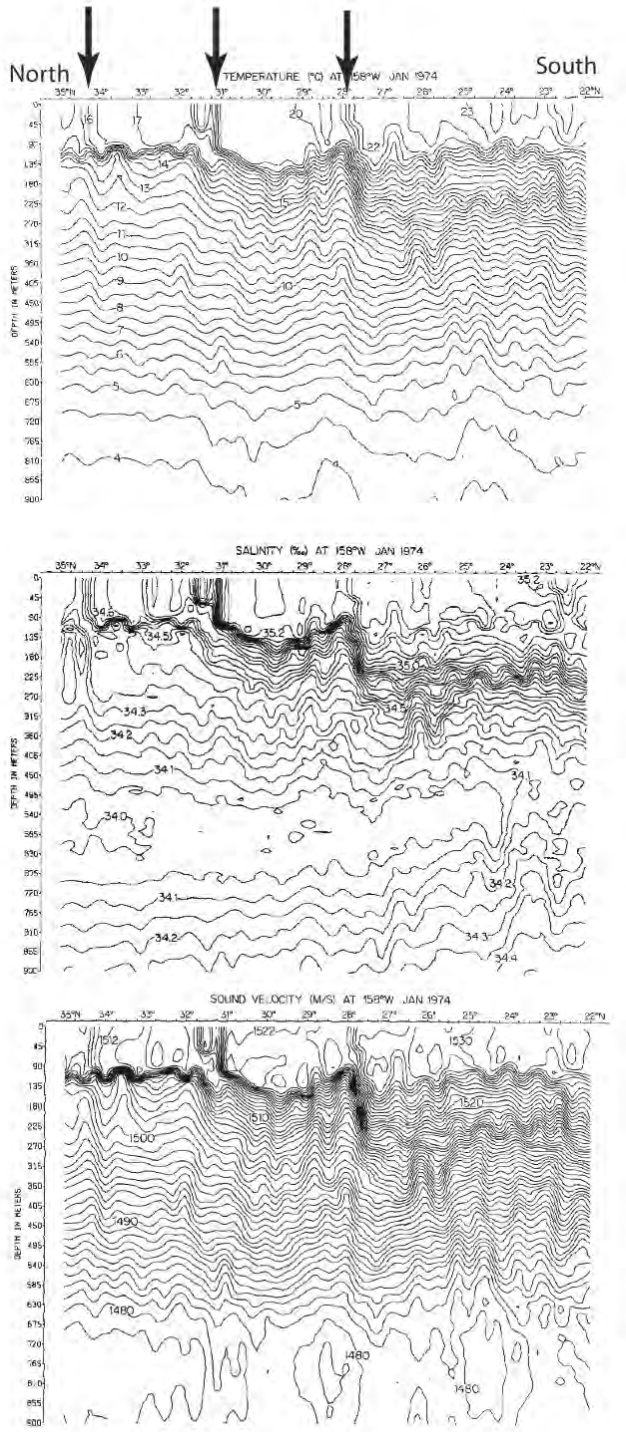

Figure 18.14: Section of temp, salinity and sound speed along 158°W
North (left) to south (right) section of temperature (top), salinity (middle), and sound speed (bottom) along 158°W during January of 1974 from Roden (1980) shows the locations of individual fronts (arrows) making up the subtropical frontal zone. Salinity values suggest that the northern most front is analogous to the front surveyed on Melville 1308. Note that variations of 10-20 m in the depth of the thermocline at 100-110 m produce variations in the depth of sound speed isopleths that extend down to at least 500 m.

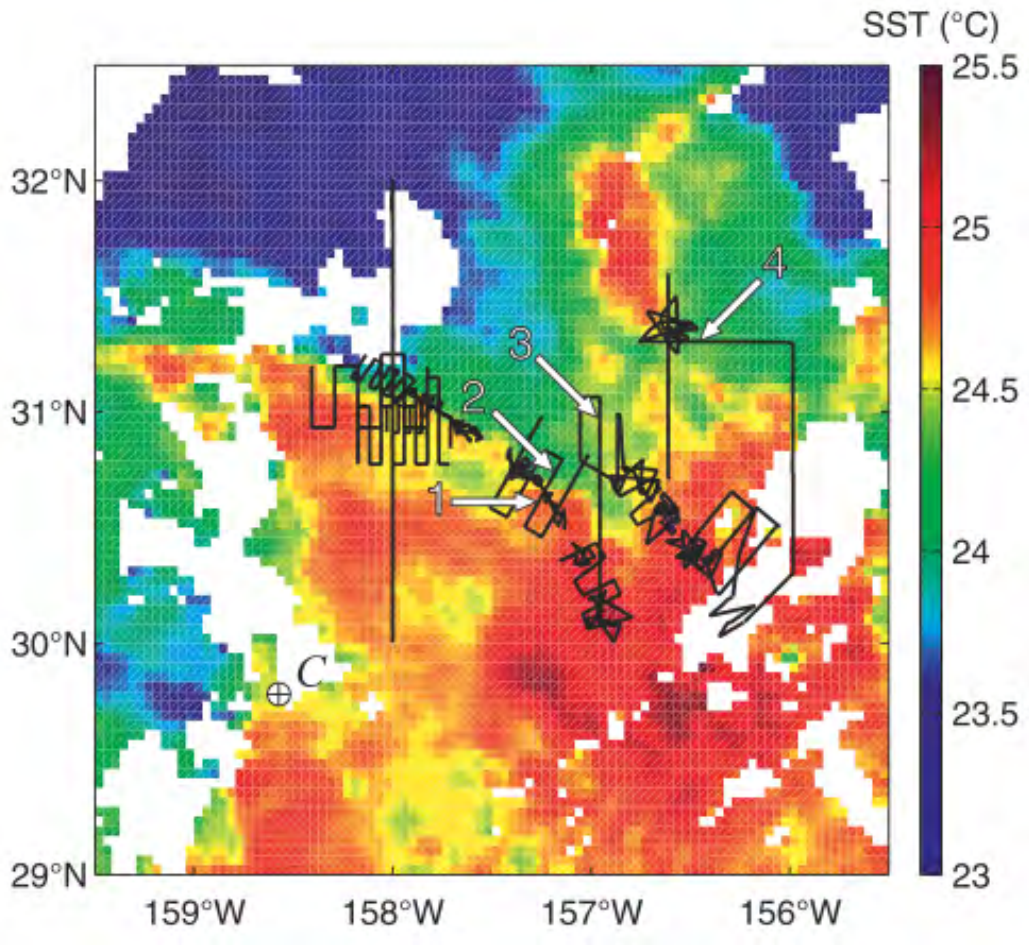

Figure 18.15: Map of SST from Shcherbina et al. (2009)
Map from Shcherbina et al. (2009) shows that SST can detect portions of subtropical fronts in summer, and that the fronts are curvilinear and oblique to lines of latitude. Black lines indicate survey lines of individual fronts by a towed vehicle from 5 to 29 July 2009. Colors indicate SST on July 7, 2007, based on Moderate Resolution Imaging Spectroradiometer (MODIS) Aqua imagery (courtesy of NASA JPL).

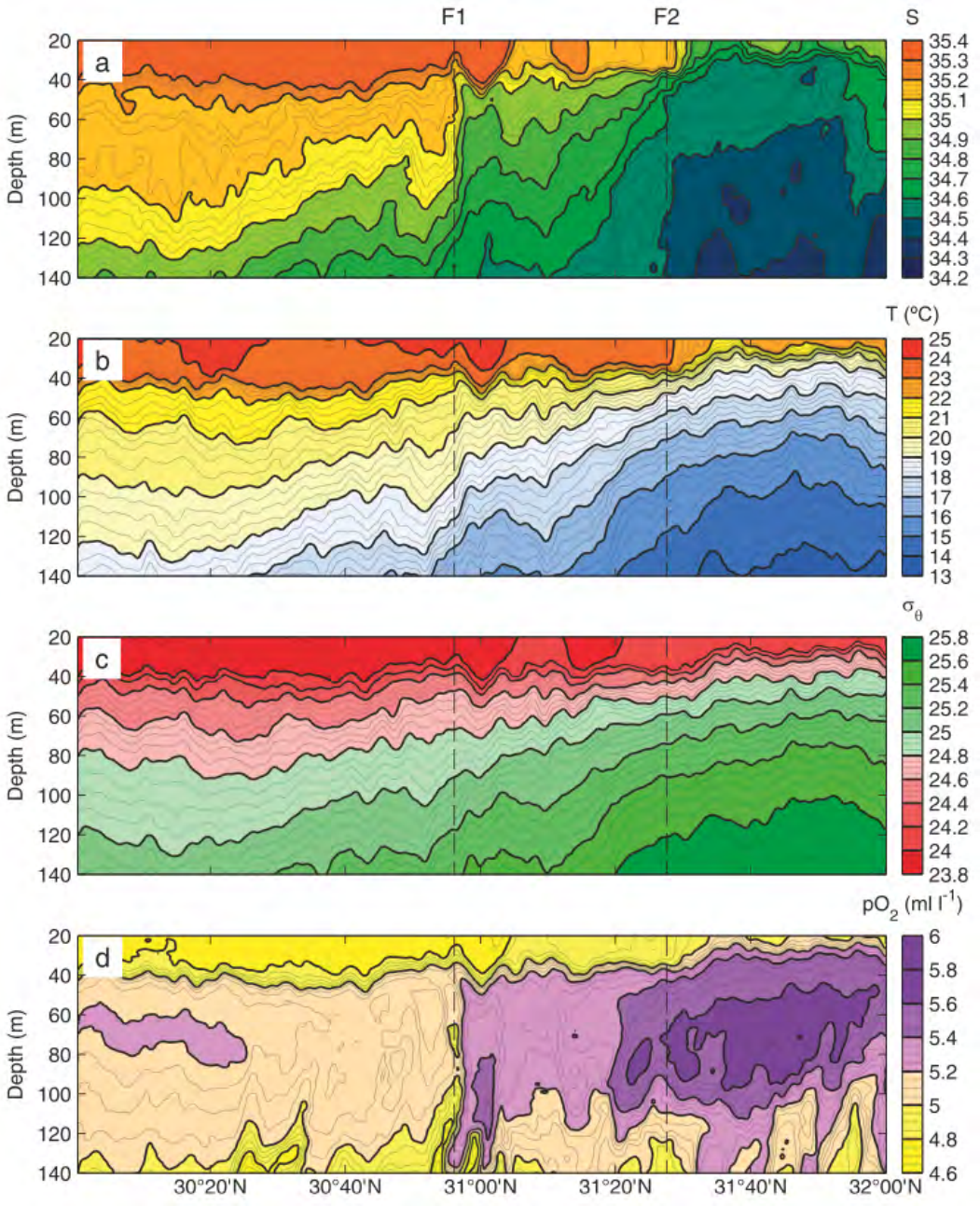

Figure 18.16: Section along 158°W during July 6, 2007
South (left) to north (right) vertical section shows (a) salinity, (b) temperature, (c) density, and (d) dissolved oxygen concentration along 158°W during July 6, 2007 (Figure 18.2 in Shchebina et al., 2009; location in Figure 18.15). Vertical dashed lines mark the locations of two fronts with significant differences. Whereas at front F1, water properties change across a near-vertical plane, the change in depth of water properties associated with front F2 extend over 30 minutes of latitude (~55 km). Note that salinity increases upward across the entire section.

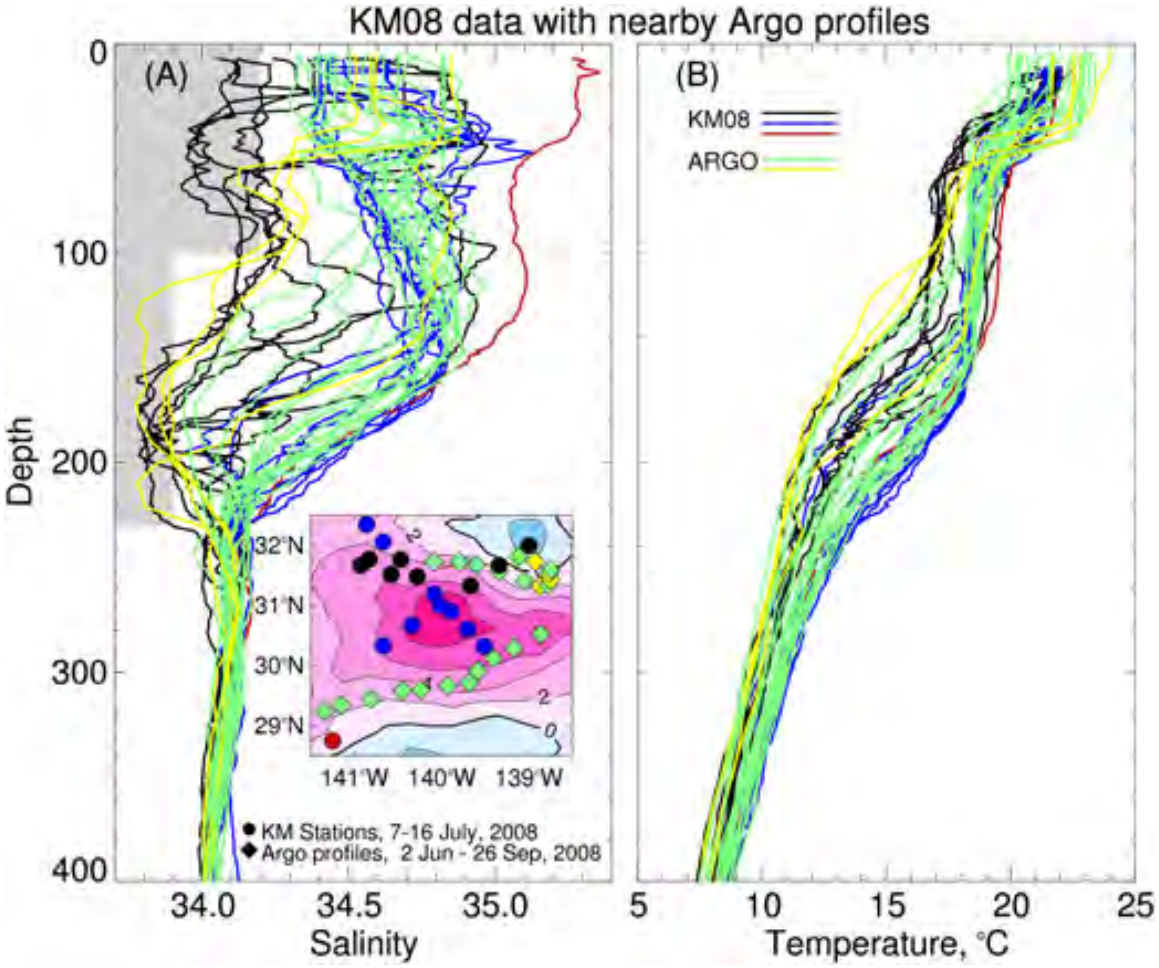

Figure 18.17: Profiles of salinity and temperature in 2008 near MV1308
Vertical profiles of salinity and temperature from a biology survey in the summer of 2008 near the Melville 1308 survey are very similar to those collected in 2013 with one significant difference: the lateral gradient at 130 m depth is consistent with lateral mixing. That is, the cast with highest salinity and temperature at 130 m (red, ~28.8°N) lies south of the casts with intermediate properties (blue and green) that, in turn, lie south and intermingle with casts with the lowest salinity and temperature (black and yellow). In general, though, the results indicate that the Melville results are consistent with other recent observations in this area. The figure is from Wilson et al. (2013).

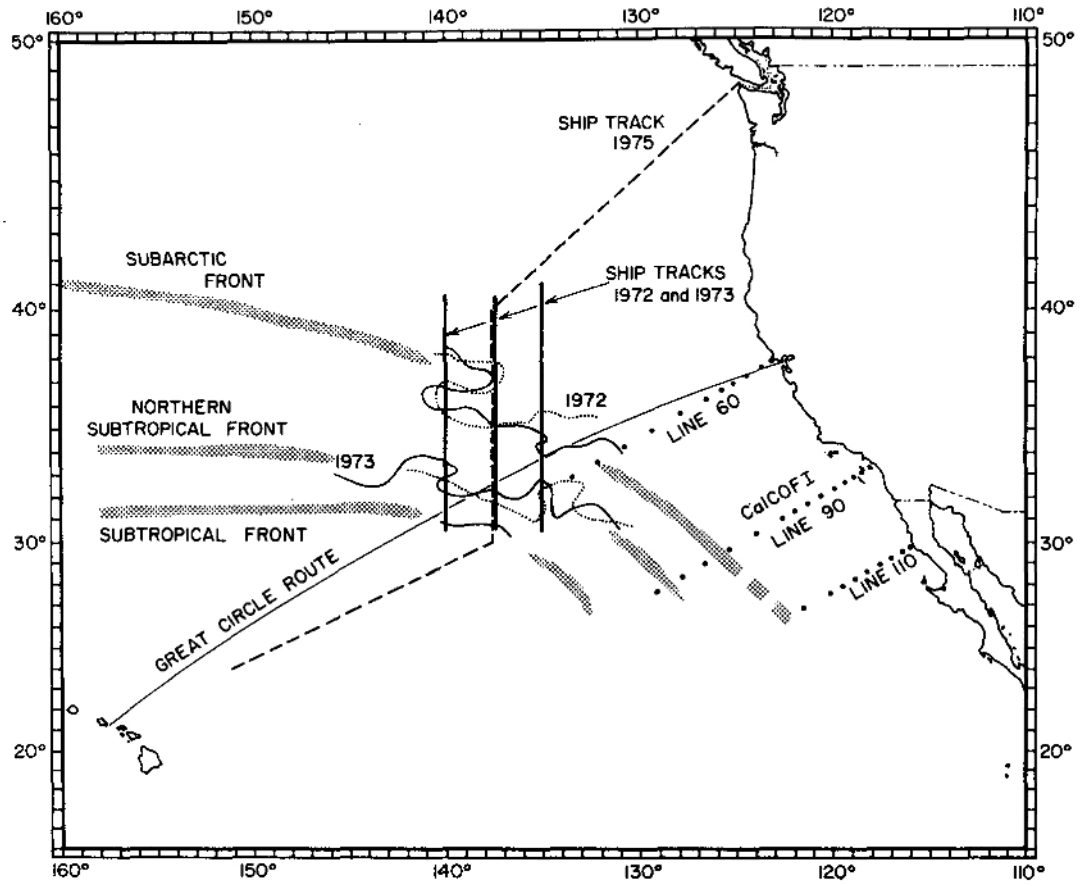

Figure 18.18: map of CTD transects used used to study fronts
Figure from Lynn (1986) shows the location of north-south CTD transects made in June 1972-1976 that were used to study fronts comprising the subtropical frontal zone. The center section crosses the fronts at the same longitude as the DVLA mooring in June 2013. Great circle line indicates the location of surface temperature and salinity data reported by Saur (1980).

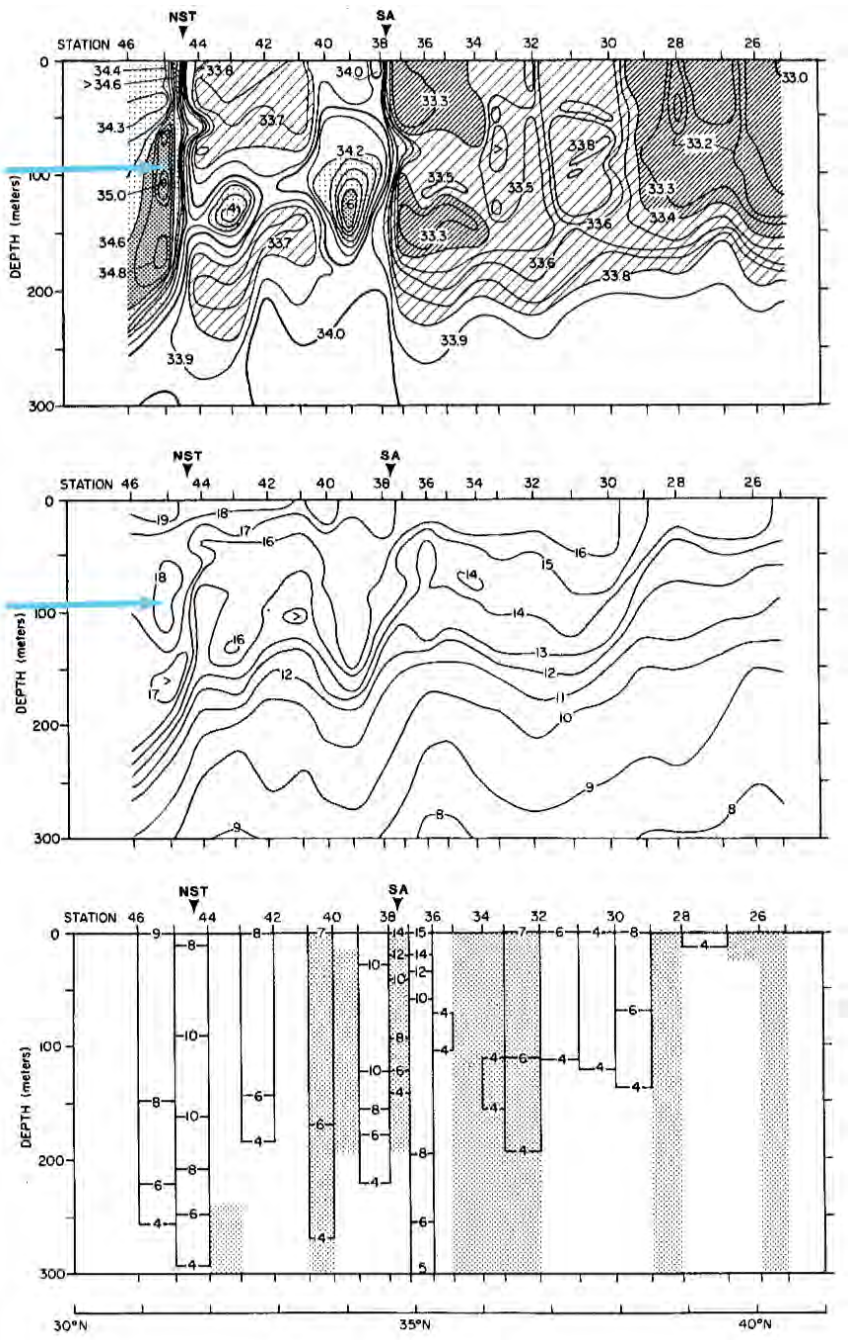

Figure 18.19: section along 137°30'W in June 1972
South (left) to north (right) vertical section along 137°30'W in June 1972 from Lynn (1986; his Figure 2) shows salinity (psu; top), temperature (°C, middle), and geostrophic velocity relative to 500 db (cm/s, bottom panel, shaded flow is towards the west). Figure 18.18 shows location. Based on salinity values, the front at 31.5°N (left, labeled NST=northern subtropical front) is most analogous to the conditions observed in June 2013. Note that to the north of this front salinity increases downward – the opposite of what Shcherbina et al. (2009) observed at 158° in 2007. Note high flow to the east along the front. Arrow points to parcel of high salinity, high temperature water attached to the south side of the front at 60-210 m depth. ST: subtropical front, NST: northern subtropical front, and SA: subarctic front.

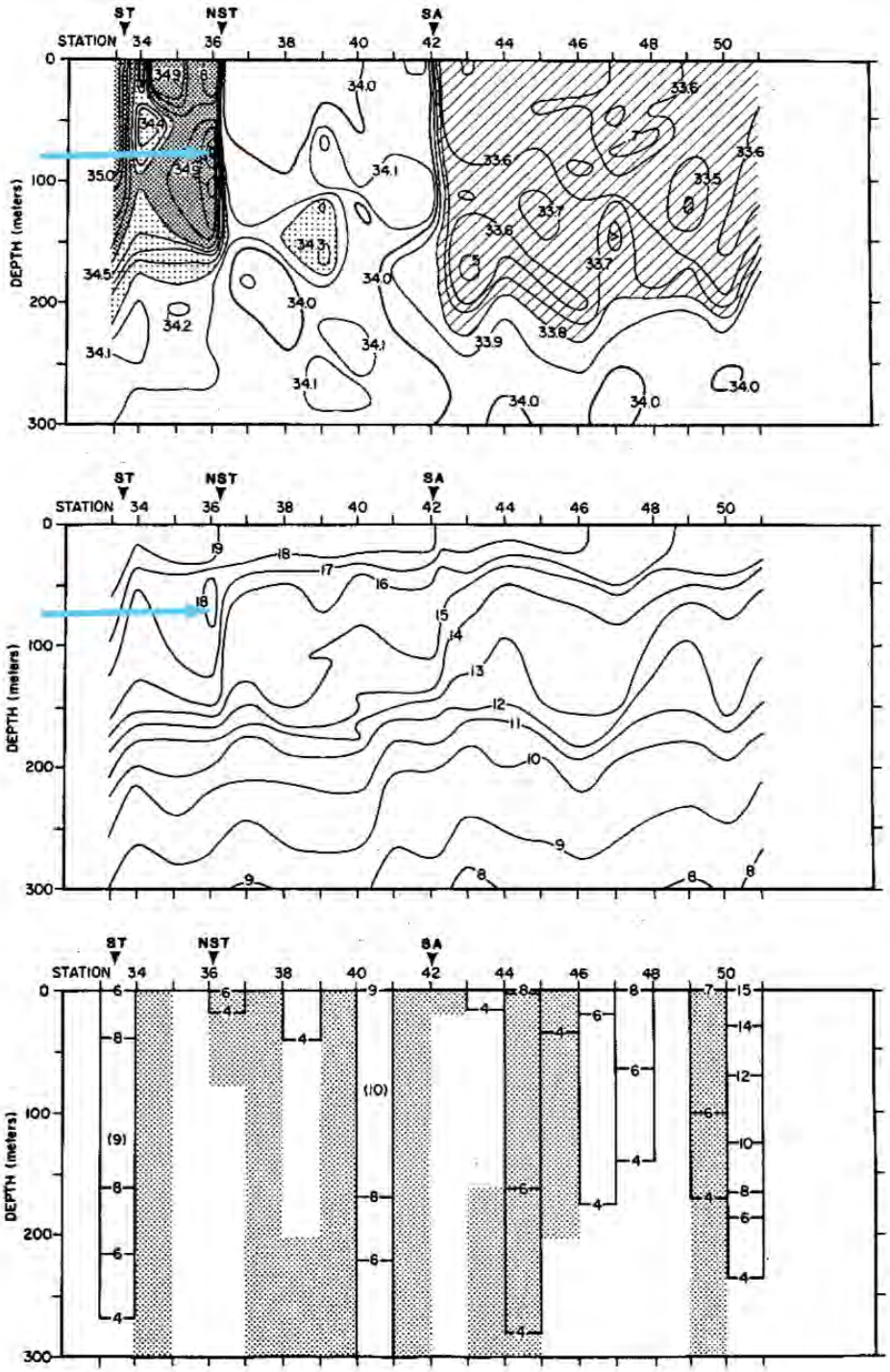

Figure 18.20: section along 137°30'W in June 1973

South (left) to north (right) vertical section along 137°30'W in June 1973 from Lynn (1986; his Figure 3) shows salinity (psu; top), temperature (°C, middle), and geostrophic velocity relative to 500 db (cm/s, bottom panel, shaded flow is towards the west). Figure 18.18 shows location. Eastward flow associated with the front is much weaker than in 1972 (Figure 18.19). Arrow points to parcel of high salinity, high temperature water attached to the south side of the front at 50-160 m depth. ST: subtropical front, NST: northern subtropical front, and SA: subarctic front.

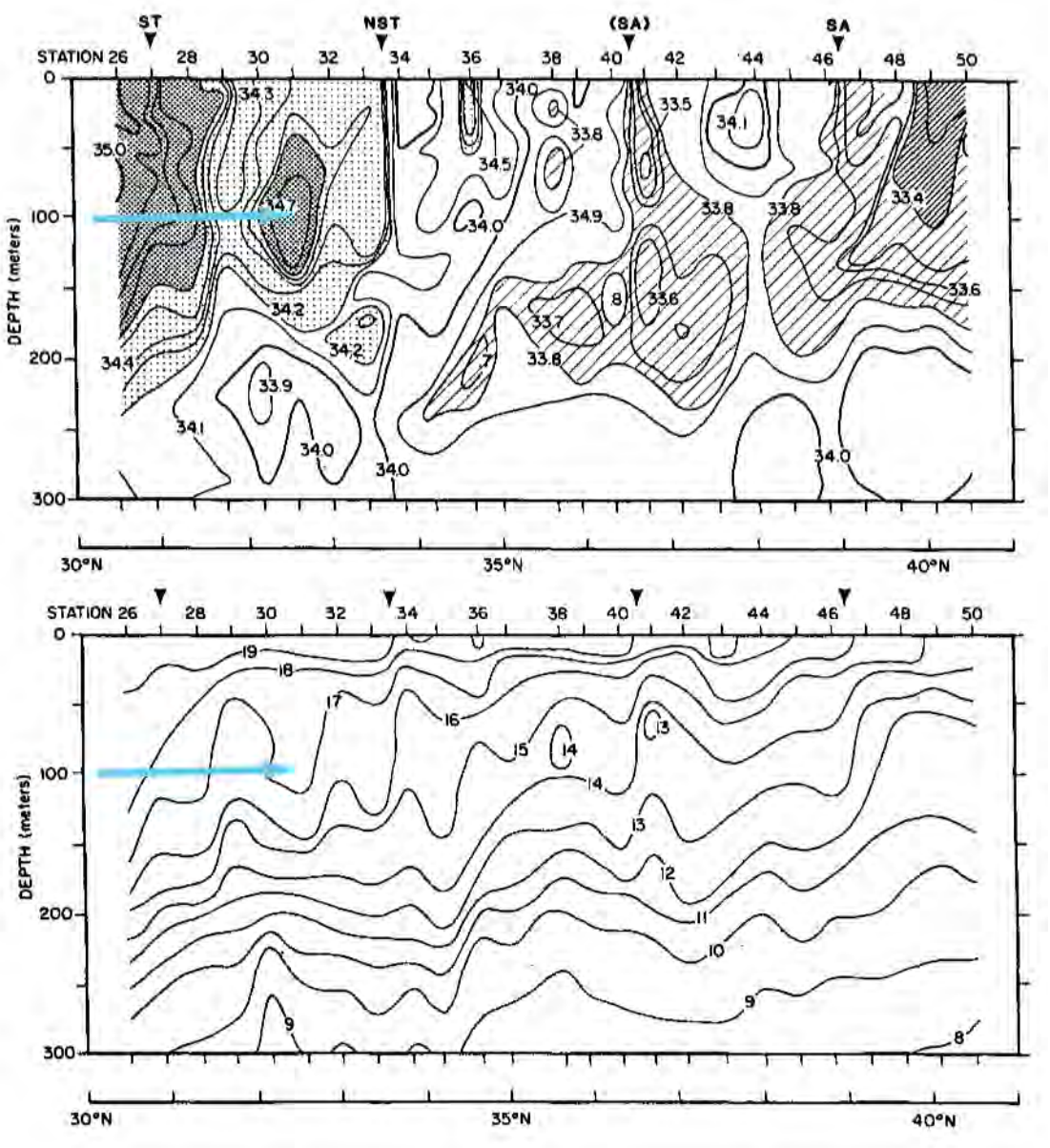

Figure 18.21: section along 137°30'W in June 1974
South (left) to north (right) vertical section along 137°30'W in June 1974 from Lynn (1986; his Figure 6) shows salinity (psu; top) and temperature (°C, bottom). Figure 18.18 shows location. Note that salinity decreases with depth between the subtropical front (ST) and the northern subtropical front (NST), which is the opposite of what is observed to the north of NST (Figure 18.19 shows this more clearly). Arrow points to parcel of high salinity, high temperature water at 40-150 m depth that is detached from the NST this year. SA: subarctic front.

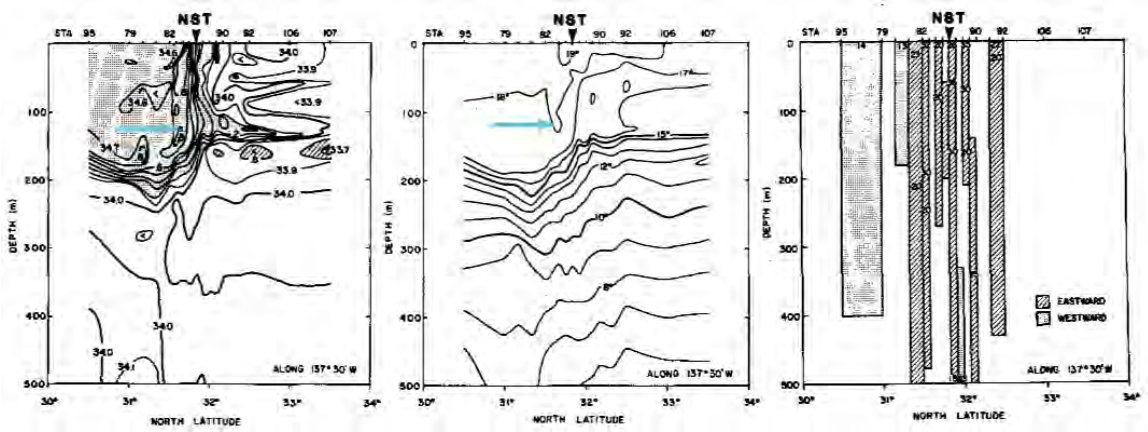

Figure 18.22: More detailed vertical section along 137°30'W in June 1976
More detailed vertical section (closer spaced stations: ~9 km) along 137°30'W in June 1976 from Lynn (1986; his Figure 7; south (left) to north (right)) shows salinity (psu; left), temperature (°C, middle), and geostrophic flow relative to 500 db (cm/s, right). Figure 18.18 shows location. Arrow points to parcel of high salinity, high temperature water attached to the south side of the front at 20-180 m depth. NST: northern subtropical front. Note that water flows eastward along the front, consistent with ADCP records in June 2013 (Figure 18.11).

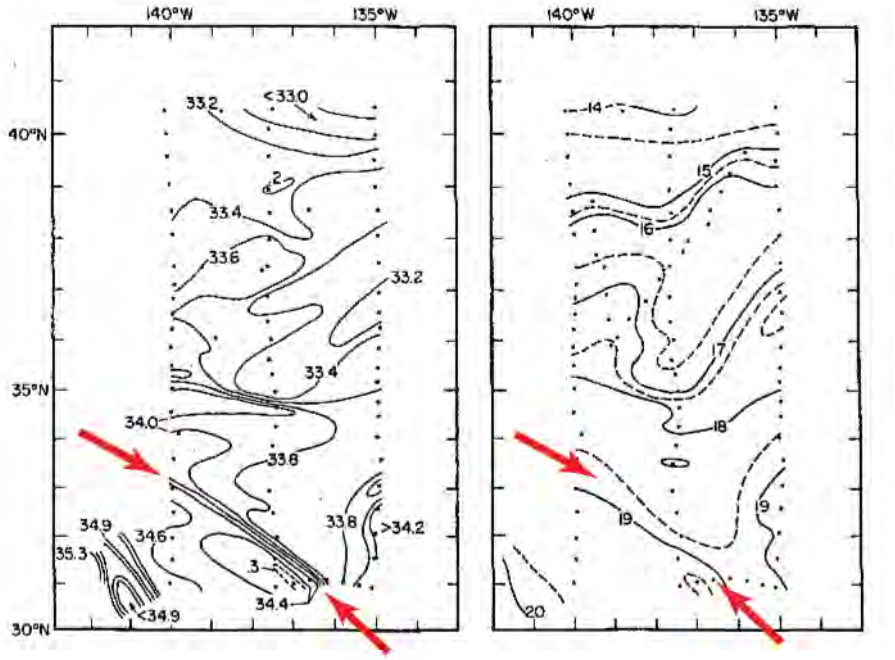

Figure 18.23: map of sea surface in June 1972
Map from Lynn (1986) of sea surface in June 1972 shows salinity (psu, left) and temperature (°C, right). Red arrows indicate the surface trace of the northern subtropical front (NST). Figure 18.19 shows vertical cross-sections of water properties along 137°30'W. Note that the front is much better defined in salinity than in temperature, and that the front is oriented NW-SE. It is unclear whether the orientation is due to a local eddy or a meander in the front or whether the orientation is due to the bending of the front by the California Current as shown in Figure 18.12.

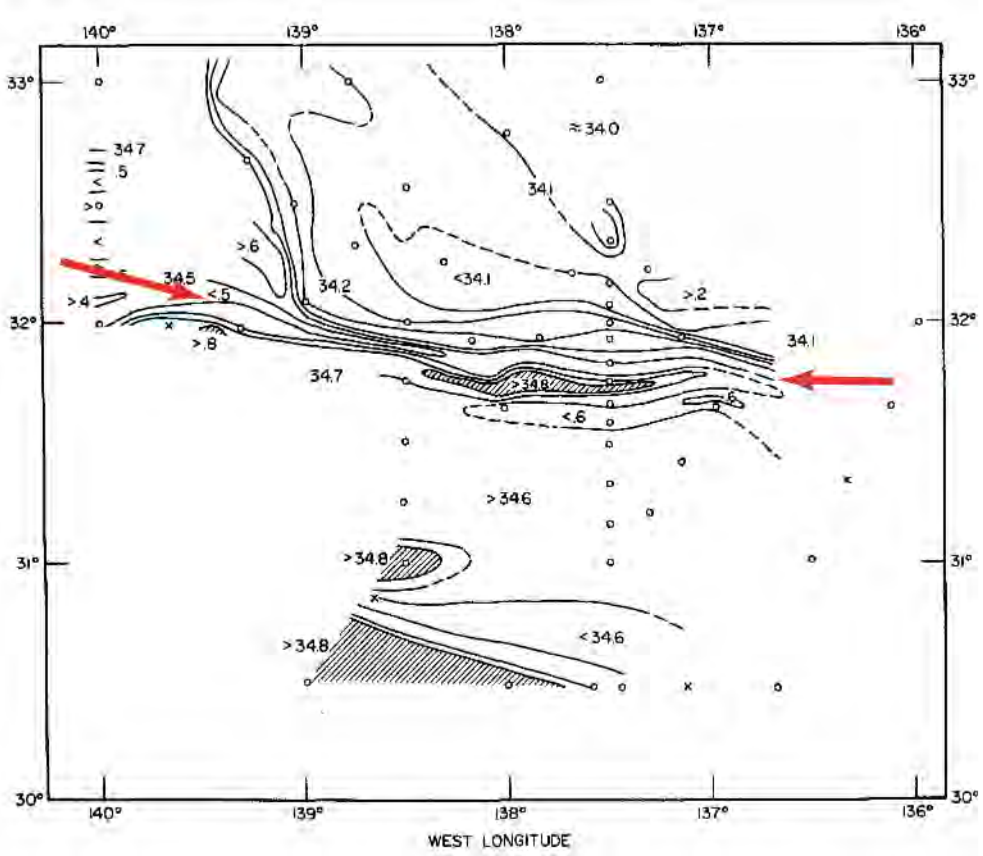

Figure 18.24: Map of sea surface salinity (psu) in June 1976
Map from Lynn (1986) of sea surface salinity (psu) in June 1976 shows multiple filaments marking the surface expression of the northern subtropical front (NST in Figure 18.22). Arrow mark the trace of a salinity low. Just to the south of the low is a salinity high (shaded) connected vertically to the high salinity, high temperature water that lies just to the south of the front that is marked by arrows in Figure 18.22. Lynn indicates that the filament extends at least 250 km and that the presence of the filament at the sea surface is intermittent.

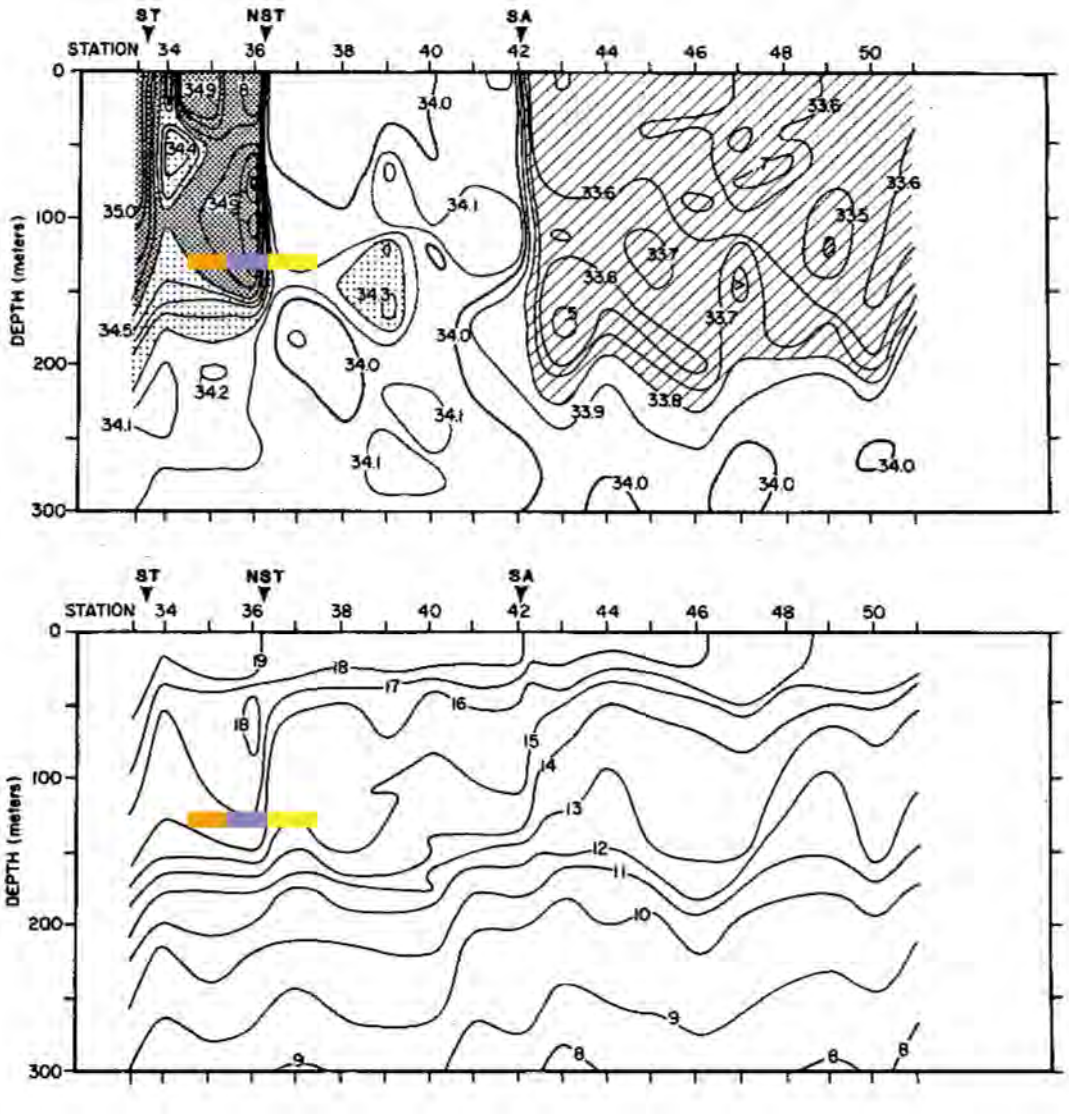

Figure 18.25: section of salinity and temperature along 137°30'W in June 1973
The vertical section of salinity (psu, left) and temperature (°C, right) along 137°30'W in June 1973 (from Lynn, 1986; see Figure 18.20) is modified with a horizontal colored bar to indicate how the three water masses observed at 130 m depth in 2013 can be mapped onto the historical interpretation of the structure of the northern subtropical front. Here, the high salinity water (purple) is assigned to the high-salinity filament mapped by Lynn between low salinity water (yellow) to the north and the intermediate salinity water (orange) to the south.

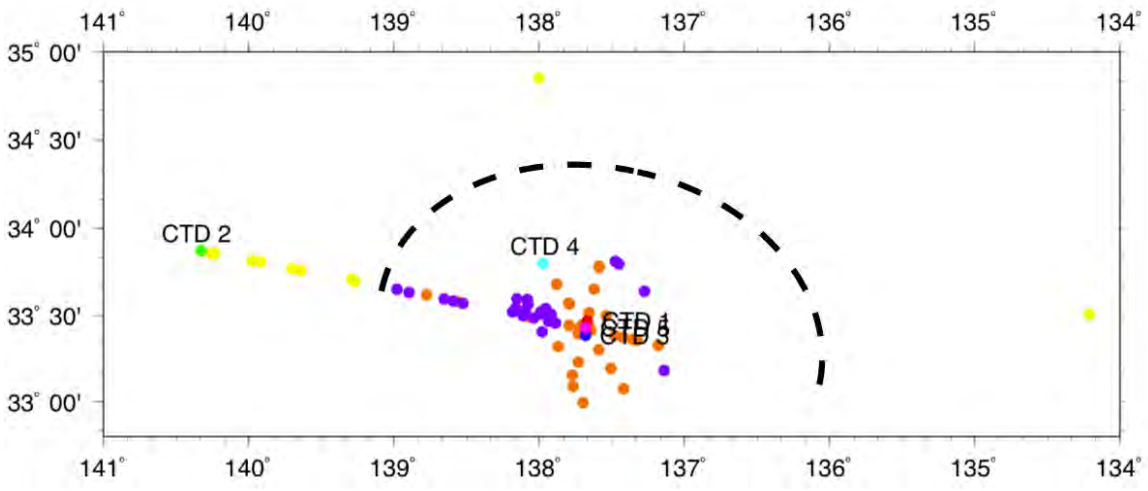

Figure 18.26: Map showing the distribution of water mass types at 130 m depth
Map shows the distribution of water mass types at 130 m depth (from Figure 18.4) modified with a dashed line to indicate a possible position of the northern subtropical front of Lynn (1986) based on the interpretation in Figure 18.25. Clearly, the frontal position is poorly constrained and there is ample room for alternative placements. The meander shape is consistent with mapping by Shcherbina et al. (2009) and Wilson et al. (2013) who found similarly shaped frontal boundaries.

19 Appendix H: OBSANP J15 Lat/Long Locations - Tom Bolmer

Tuesday, August 27, 2013

On the OBSANP cruise on the R/V Melville in June/July 2013 we towed a J15-3. We need to get the Latitude and Longitude of this Instrument. The ship's fs185 Gyro had a GPS it used and recorded. These data were recorded at 5 samples/second. This document is an attempt to describe how this Latitude and Longitude recoded with the fs185 GPS was used to get the Latitude and Longitude of the J15-3.

The fs185 GPS was between the 4 Ashtech GPS receivers (antennas) on the 02 deck above the aft High Bay. The locations of the Ashtech antennas are listed in Table 19-1. The fs185 is calculated to be in the middle of the two antennas number 2 and 4. The fs185 had two antennas, the center of these was the center point between the Ashtech Antennas. This was confirmed by visual inspection. This is shown in the below Figure 19.1.

Table 19-1 Ashtech Antennas.

These locations were relative to the Hippe in the lower computer lab.

	Ant. 1	Ant. 2	Ant. 3	Ant. 4
Meters Aft from Hippe	11.2727	-10.809	-9.993	-10.772
Meters Port from Hippe	8.025	-8.052	-8.074	-5.547

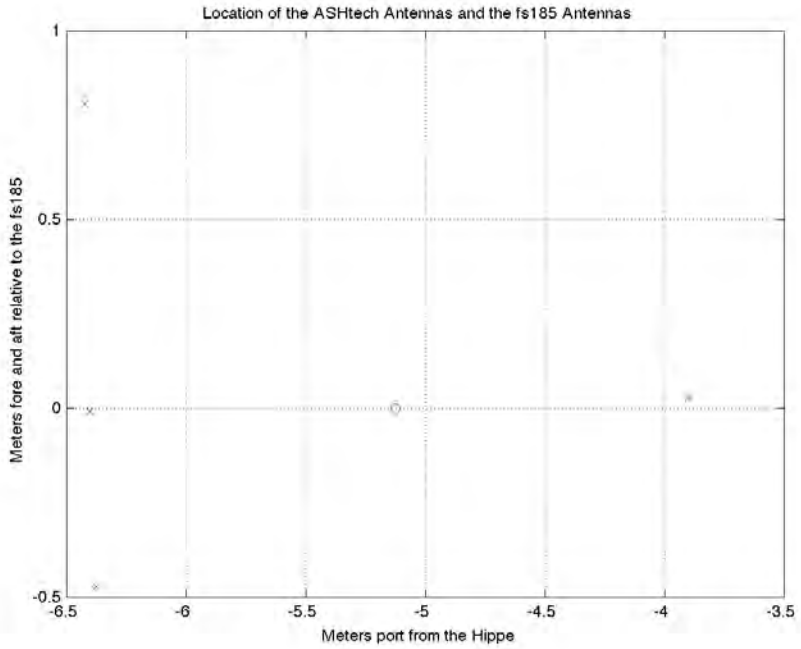

Figure 19.1: Ashtech and fs185 GPS Antenna locations

Figure showing the location of the Ashtech Antennas (blue Xs) relative to the center of the fs185 antennas (red circle).

The locations of these antennas were placed onto the ship's deck diagram. This diagram showed the frame spacing and numbers. These frame numbers were used to get the distances of the center of the fs185 antennas from the ship's center line and the forward offset from the stern of the ship. Figure 19.2 used the ship's diagram and has the antenna locations and distances shown.

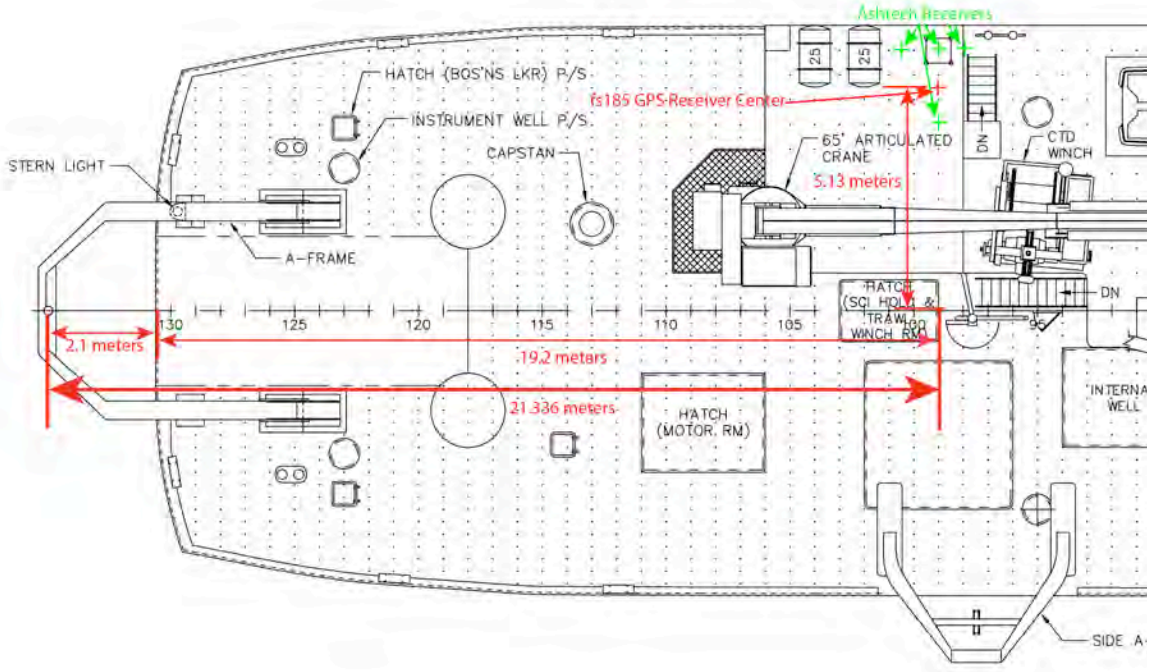

Figure 19.2: Melville Fantail Framing diagram
Figure showing the Ashtech antennas, the fs185 antenna's center, and the distances to the Sheave on the A-Frame in it's deployed location. These locations are on top of the ship's deck diagram. The center line show the frame numbers on the ship. Each frame is 2 feet long.

The A-Frame in it's extended position extends beyond the stern of the ship. Figure 19.3 is the one the ship provides for use in locating instruments. By visual inspection the Sheave is decided to be 7 feet aft of the ship's stern. Also by visual inspection the Sheave is decided to be 2 feet below the "Outboard" height of the underside of the A-Frame's cross bar. This results in a 15 foot height above the ship's deck.

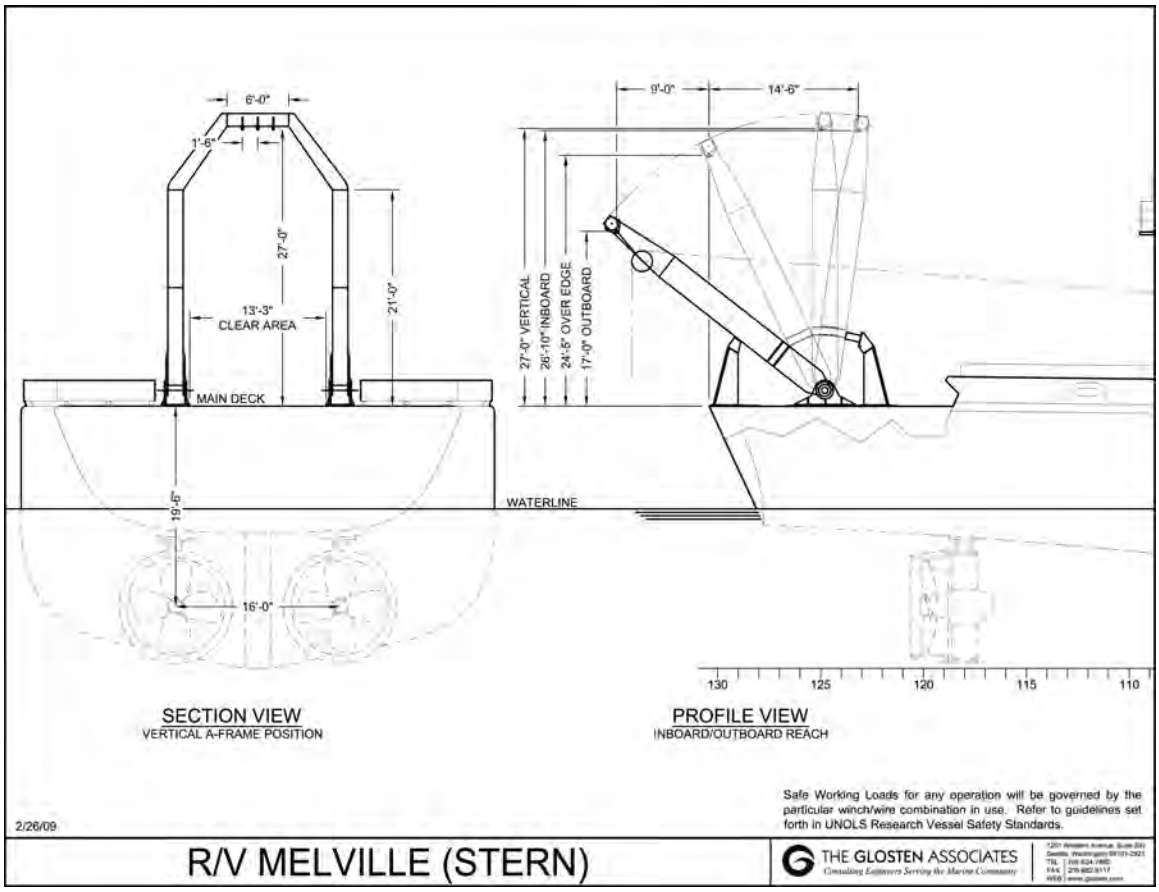

Figure 19.3: A-frame measurements
This figure shows the measurements of the Melville A-frame. This document is from the ship's online documents.

19.1 Matlab code used to plot and get distance from the fs185 to the Sheave in the A-Frame

```
gpsx = [-11.2727 -10.809 -9.993 -10.772];  %  Meters from Hippe
gpsy = [-8.025   -8.052  -8.074  -5.547];  %  Meters from Hippe

plot(gpsy,gpsx,'x');
grid on;
hold on;
xlabel ('Meters to port from Hippe');
ylabel ('Meters to aft from Hippe');
title ('FS185 location between Ashtech Antennas');
hold off;

fs185Port    = 10.5;        % frames for outer Ashtech
fs185Aftfr   = 130.5 - 99.0; % frames
sheaveAftft  = 7.0;         % feet
sheaveHeight = 17.0 - 2.0;   % feet
DeckHeight   = 11.0;        % feet
feet         = 0.3048;      % 1 foot in meters

%  convert to meters on the ship relative to fs185 Antenna

fs185side    = (fs185Port * 2) * feet;       % meters to Port to Ashtech
fs185side    = fs185side - ((8.05 - 5.5) /2); % difference Ashtech to fs185
stern        = (fs185Aftfr * 2) * feet;      % meters aft of the Antenna to Stern
sheaveAft    = ((fs185Aftfr * 2) + sheaveAftft) * feet;  % meters aft of the Antenna
plot(-fs185side,0,'ro');
hold on;
shiftcenter = 8.05-((fs185Port * 2) * feet);
plot(gpsy+shiftcenter,gpsx+10.8,'x');
grid on;
hold on;
plot ((-8.052+((8.05 - 5.5) /2))+shiftcenter,0,'ro');
xlabel ('Meters to port from center line');
ylabel ('Meters to aft from fs185');
title ('FS185 location between Ashtech Antennas');

plot(0,-stern,'kx');     % Location of the Stern
plot(0,-sheaveAft,'gx'); % Location of the Sheave
axis ([-10 5 -25 5]);

hold off;
```

20 Appendix I: OBSIP MV1308 OBS Report - Ernest Aaron

Cruise:	OBSANP (MV1308)
IRIS Network Code:	NA
SIO Purpose:	Deploy 4 LPOBS and 8 SPOBS, then recover everything
Vessel:	R/V Melville
Ports:	San Diego, CA – Seattle, WA
Master/Captain:	Chris Curl
Chief Scientist:	Peter Worcester
SIO OBS Personnel (OBSIP):	Ernest Aaron
WHOI Personnel:	Ralph Stephen, Tom Bolmer, Steve Swift, Jim Ryder
APLUW:	Sean McPeak
Marine Technician (STS):	Keith Shadle
SIO Worcester Lab:	Matt Norenberg, Scott Carey
Cruise Dates:	06/12/13 – 07/11/13

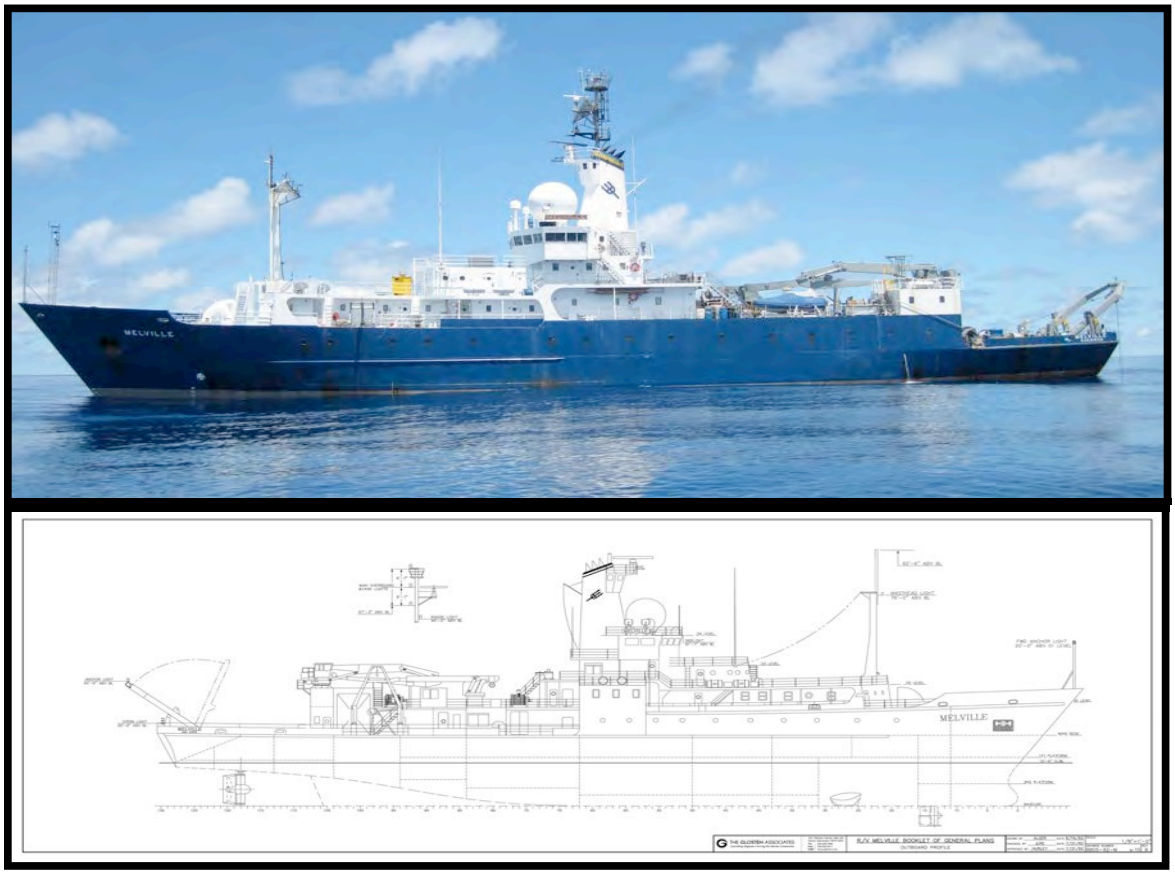

R/V MELVILLE

Table of contents

20.1 I. Summary of SIO OBS Activities

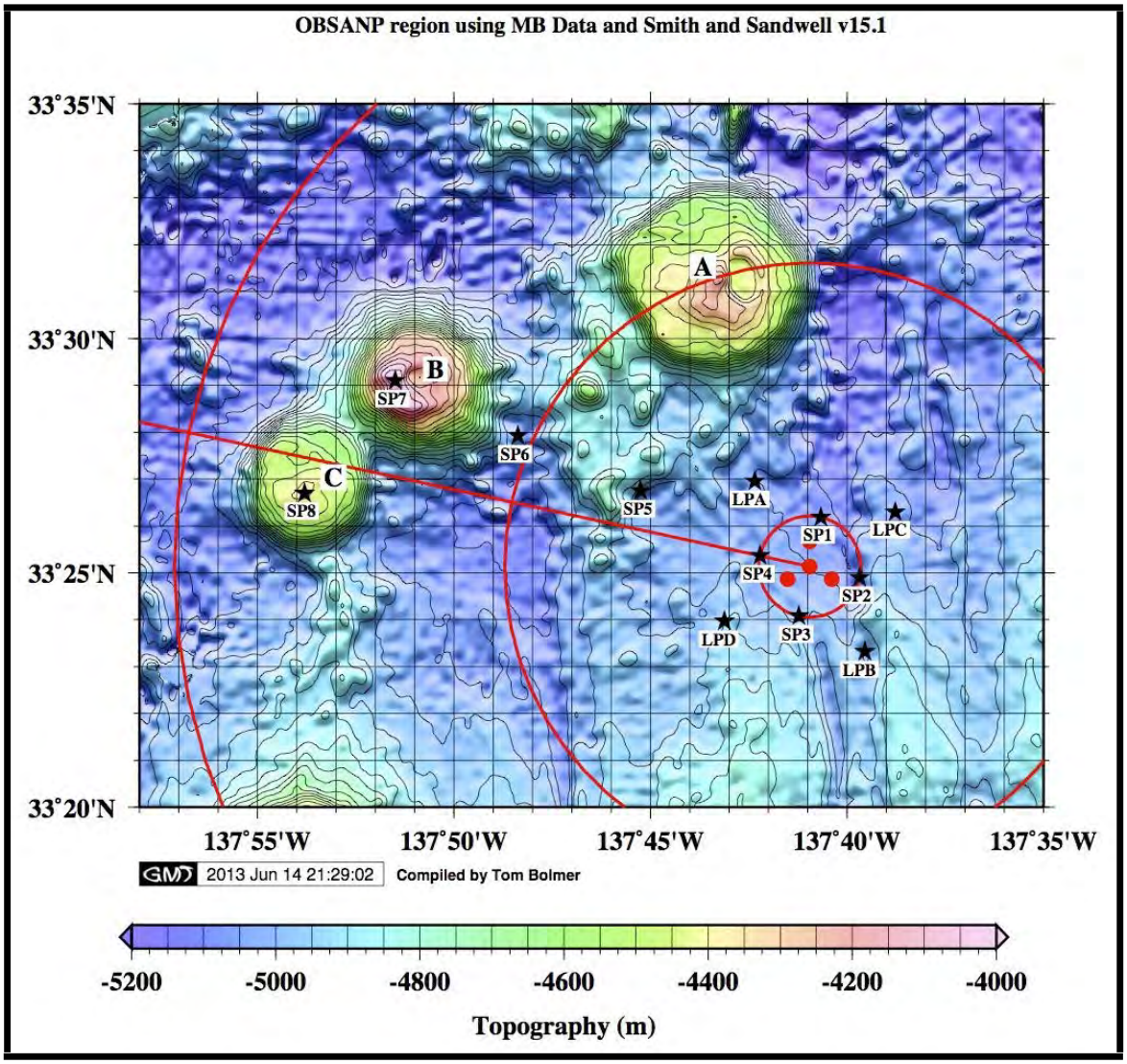

Figure 20.1: OBS locations map provided by Ralph Stephen

20.2 II. Instrumentation

SIO LC4X4, LPOBS

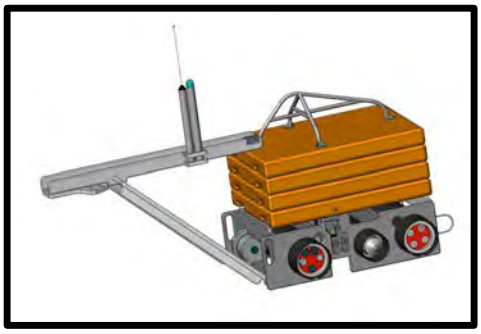

Scripps provided 4 syntactic long period OBS for this experiment. The sensors associated with these instruments are Trillium 240 seismometers and a differential pressure gauge (DPG). Two of these syntactic LP's will have an SAIC hydrophone mounted to the frame opposite the sensor ball. Each instrument consists of a 160# anchor, four-slab syntactic float assembly. Additionally, two syntactic foam blocks are added for supplemental floatation to compensate the full payload of lithium batteries. The polyethylene frame holds the acoustic release transponder the data logger, the battery bottle, and a dual mechanical release system.

After the anchor is released for recovery, the instrument ascends at approximately 45 m/min. To increase visibility once at the surface, an orange flag on a 48" fiberglass staff is attached to the lift bale. Also, a Novatech low- pressure activated strobe-beacon and radio are mounted near the base of the flag on the lift bale. The radio operates at 160.725 MHz.

The acoustic release transponder developed in conjunction with ORE/EdgeTech is interrogated at 11kHz and responds at 13kHz. Alkaline batteries provide 18 volts power for the burn, 12 volts power for the transponder, and 9 volts power for the circuit board logic. The release mechanism includes two double wire burn elements. When fresh, two battery strings are combined to provide the 18 volts to burn one of two release wires in an average of 7-minutes for water depths encountered during this experiment.

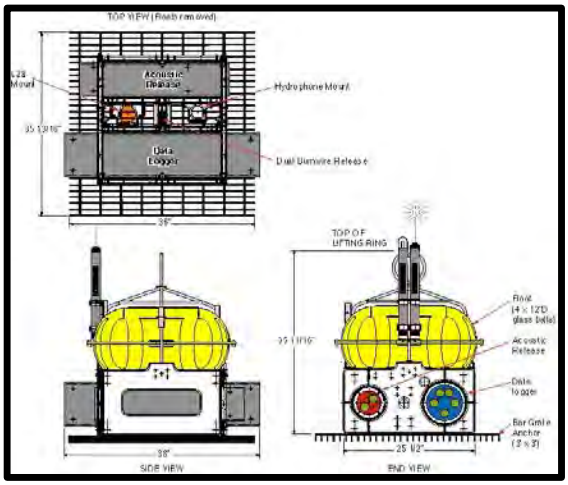

The SP-OBS float and frame components are typically stored separately in a custom rack system, and are assembled and tested prior to deployment. The complete instrument weighs approximately 400 pounds in air. This is inclusive of the 100-pound iron anchor grate held to the base of the poly frame, by a single 2" oval quick-link. When the anchor is released for recovery, the four 12" glass spherical floats, as well as the syntactic foam blocks provide sufficient buoyancy to lift the instrument at about 42 m/min to the sea surface.

20.3 III. Areas of Concern

There are 12 OBS to be deployed in fairly rapid succession, which will require a good deal of focus and attention to detail. Hopefully we can split these into two separate deployment efforts to allow Steve Swift and myself a little rest during this process, although it is possible that things will go smoothly enough that we are able to run through all the deployments in a reasonable amount of time. The recoveries are going to be more time consuming and an intermission during this process will likely be required.

20.4 IV. Ships Equipment and Condition

Excellent. There is plenty of space on the main deck to accommodate our 12 OBS and additional equipment. All OBS operations will be carried out from the starboard amidships forward utilizing the small Alaska Crane, or the hydro-boom.

20.5 V. Journal of Events in Chronological Order

All times and dates in this report are UTC/GMT unless otherwise noted.

20.5.1 1. Loading & Setup

06/10/13 10:00

Mark and I arrived at MarFac with a truckload of recovery gear. Everything was loaded that day and the lab was mostly setup, but we were unable to secure some of our gear on the main deck because of a painting project.

06/11/13 10:00

We returned to MarFac and were able to finish securing gear and run tests on the electronics. Paul and Phil arrived with the last two LP loggers (SAIC around 11:00 and we were able to finish all electronics troubleshooting by 15:00.

20.5.2 2. Transit

06/12/13 08:00 Local

We just pulled away from the MarFac pier and are on our way to the study site.

We have approximately 4-day transit to the study site and we will stop along the way to perform the acoustic rosette test and to test the J-15 once we are in waters deeper than 4500 meters.

20.5.3 3. Acoustic Rosette Test
06/15/13 09:00, Local
We have just deployed the 12 acoustic rosette and will make two stops; first at 100 meters to verify one acoustic enable, and then again at 4500 meters to test all 12 acoustics.

At ~2000 meters the hydro-boom winch was experiencing issues that required us to stop payout. I ran the acoustic tests at this depth and during the retrieval just to get some feedback. Once the rosette is onboard we will move it to the starboard A-frame and redeployed for a full 4500- meter test.

11:00, Local
The rosette is in the water and descending to test depth.

12:30, Local
All of the acoustics checked out fine at 4500 meters. The communications are very clear. The rosette is currently being retrieved at 60 meters/min.

14:00, Local
Rosette recovered and secured.

20.5.4 4. OBS Deployments
2013:168:02:34:00
We started OBS deployments with the four LP's going in first.

This will give some continuity to

The LP's consist of the following: LPA - Standard T240/DPG LP OBS LPB - T240/DPG/SAIC AOG1 LPC - Standard T240/DPG LP OBS LPD - T240/DPG/SAIC AOG2

All of these LP loggers went through the checkout procedure without serious issue. For OBS LPA, channel 4 (M5-SAIC Hydrophone) was latched and showing all zeros when tested, so I powered off the A2D, and then repowered the A2D, cleared the analog card, and then reconfigured the sampling rates. The second time around all of the channels tested fine.

2013:168:07:50:00
I am setting up the first of the SP OBS and the first logger (13040) says "not in shipping mode" when I try to power on the main. It also says to type "yes" to continue, or it will abort. After typing yes it appears to power up.

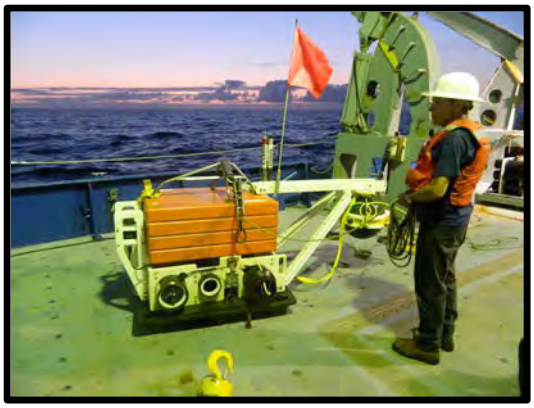

The next issue I ran into with this logger (13040) is that the system TAG (PS) is not as accurate as I believe it should be (00.0008927). All of the LP's were nearly perfect. I synchronized the clocks twice before I checked the system TAG. The computer TAG (PC) is a strange off number as I was told would be the case for the LP's. Because of the drift, I powered this logger down and started the setup procedure from the beginning, but I received a similar system TAG as before (00.0009095), so I just went with it.

2013:168:17:53:00
I just setup the logger (13041) for site SP2. This logger had a better PS TAG by one decimal place. It also had a very good PC TAG unlike the previous SP logger (SP1).

All deployments went fairly smoothly. The deck operations were perfect and the electronics setups had a few minor issues that required resetting the analog card and a couple of the clocks had a less than perfect PC TAG, which would not improve by cycling power and restarting the setup. One logger was powered up from the lab, which I discovered when I checked voltage and temperature after configuring the USB port. Its voltage was slightly lower than those loggers that were off from the beginning on the cruise.

20.5.5 5. OBS Surveys
2013:169:01:43:00
I have started the survey of site SP8, which was the last OBS to be deployed. We will work our way through the surveys in reverse order, more or less, until I am too tired to continue. At that point we will begin J15 operations, returning to the surveys at a later time in the cruise.

Halfway through the survey of site SP7 the 8011M froze, screeched continuously and the keypad went ape-shit (button selections mixed up). Power cycling The 8011M would not correct its issues, so I switched to the Saber, which would not cooperate with the new relocation program. At least it wouldn't work with the version I have. It is also possible that the latest Saber updates changed something. Either way, it was not working, so I dismantled the 8011M and discovered that two of its capacitors had fallen off the main board. This may be why I have noticed a decline in its power output over the years. To halt the screeching I disconnected the speaker/beeper and then I pressed on all of the connections and chips I could reach to be sure they were seated properly. Some of them moved a little. Upon reassembly and power up all seems to be functioning as one might expect, less the beeper. I have resumed the surveys with this unit, but I am not confident that it will last too much longer.

06/19/13
The instruments at site OBS7 and OBS8 are located on seamounts and the accuracy of the drop was a fairly critical component of the science. After I relocated these two OBS we discovered that they drifted little more than 20-40 meters in latitude and longitude. There are virtually no currents out here and the OBS dropped like lawn darts onto their respective targets.

2013:176:18:15:00
The OBS surveys continue for the remaining eight stations. For these water depths we are at a radius equal to 2.5Km from the central point (DVLA) while surveying the four closest OBS to this position. We are receiving consistent returns at 8kts.

After surveying the four remaining SP OBS Steve and I took a break and will continue the surveys after a CTD cast is performed.

2013:177:06:50:00
We have just begun with site LPB survey. The seas are a bit rougher, so we are steaming at 6kts.

2013:177:12:30:00
We have finished with the OBS relocation surveys. Although we did see some temporary shadowing (Event Skipped) whenever the ship rode parallel to the seas (in the trough) all of the OBS acoustics talked very clearly.

20.5.6 6. J15-3 Deployment

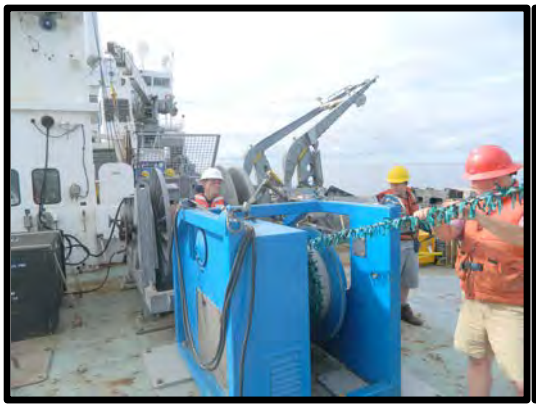

20.5.7 7. OBS Recoveries

2013:185:00:00:00
The J15-3 has been recovered and secured and we are moving towards site OBS7 for the first recovery.

2013:185:00:24:00
Site SP7- acoustic 28 is in the burn cycle and talking loud and clear. The OBS released on the first burn #1 attempt.

SP8 is good to go. It surfaced with a disabled strobe (night recovery with dense fog). The switch was just a few degrees off of full on, which prevented it from enabling. Thank goodness for the functional radio and our ability to acoustically range to the OBS, which made blind navigation to the instrument without collision possible.

2013:185:22:07:00 Happy 4th of July!
We are at site SP1 and it is on it is way to the surface.

SP1 had an unattractive PS TAG. This was the logger that started up at setup with the message "not in shipping mode" and the PS tag was not very accurate from the beginning, so I powered it down and started over with setup, but it still had a less than desirable PS tag.

2013:186:16:30:00
LPD recovery went smooth. The NovaTech radio was not functioning and upon inspection we discovered that it had flooded. I salvaged the switch and tossed the rest. These LP's have a 50-meters/minute rise rate.

LPC, LPB, and LPA all released from their anchors on the first burn and were recovered without issue.

20.5.8 8. Data Processing & Instrument assessment

site	acoustic	logger	sensor	PS TAG (deployment)	PS TAG (recovery)	corrected LAT	corrected LON	depth (m)	sound velocity	survey	comment
LPA	24	LP98	10-T240	2013:168:02:38:00.0000016	2013:187:02:23:59.9634769	33.43840	-137.63870	5033	1504	Y	
LPB	14	LP82	44-T240	2013:168:03:30:00.0000011	2013:186:23:51:59.9746527	33.38870	-137.65500	5002	1504	Y	SAIC-AOG1
LPC	25	LP101	57-T240	2013:168:05:13:59.9999999	2013:186:21:33:59.9748889	33.39950	-137.71530	4922	1503	Y	
LPD	23	LP110	36-T240	2013:168:06:00:00.0000012	2013:186:19:03:00.0188746	33.44970	-137.70250	5048	1504	Y	SAIC-AOG2
SP1	108	13040	GP42	2013:168:07:55:00.0009095	2013:186:00:30:19.1265525	33.43680	-137.67460	5084	1504	Y	HM150
SP2	95	13041	GP47	2013:168:17:54:59.9999050	2013:186:02:51:59.9663408	33.41630	-137.65840	5036	1504	Y	HM151
SP3	87	13037	GP36	2013:168:19:20:00.0000538	2013:186:04:59:59.9895419	33.40290	-137.68320	5017	1504	Y	HM152
SP4	40	13039	GP01	2013:168:20:45:59.9999770	2013:186:07:12:59.9845756	33.42400	-137.69980	5023	1504	Y	HM153
SP5	11	13038	GP24	2013:168:21:35:59.9999714	2013:185:11:31:00.0205424	33.44620	-137.75390	4896	1503	Y	
SP6	85	13042	GP40	2013:168:21:59:59.9999787	2013:185:08:55:59.9922751	33.46610	-137.80690	5003	1504	Y	
SP7	28	13043	GP57	2013:168:22:39:00.0000022	2013:185:02:29:59.9868595	33.48610	-137.85760	4003	1497	Y	HM154
SP8	33	13044	GP51	2013:168:23:19:59.9999241	2013:185:05:45:59.8536405	33.44550	-137.89750	4385	1499	Y	HM155

Due to the complexities associated with the specialized 5-channel LP's and the higher sampling rates of all I was not able to process the raw OBS data to miniseed. Paul and Phil will handle this back at the OBS Lab.

The only logger that exhibited any strange behavior was #13040 from site SP1. It gave a message at setup that said "not in shipping mode" and it had an poor time tag that I couldn't improve with power cycling during the setup procedure. Also, this logger had a very poor recovery tag.

I saved all of the screen text from the console window for the logger setups and recovery time checking operations for future reference. It is saved to the desktop of the OBSLAB_1, IBM laptop and on the data drive.

Trillium tilt data: All four LP sensor balls recorded 13 records, which were downloaded prior to packing them for shipment.

20.5.9 9. Zyfer antenna to hull transducer offsets for Melville:

Starboard=(+), Port=(-), Vert Down=(+), Fwd=(+)	X	Y	Z
Hippy Base	0	0	0
Fore point instrument well, port -offset to Hippy Base	-6.455 meters	-6.069 meters	3.114 meters
OBS Lab Zyfer antenna -offset to Fore point instrument well, port	13.106 meters	5.54 meters	4.36 meters
OBS Lab Zyfer antenna -offset to Hippy Base	7.037 meters	2.915 meters	7.474 meters
Fwd hull mounted transducer- offset to Hippy Base	23.000 meters	-3.100 meters	5.300 meters
Aft hull mounted transducer- offset to Hippy Base	-14.000 meters	-1.200 meters	5.300 meters

Left picture: Fore point instrument well-port looking AFT (red arrow)
Right picture: Zyfer GPS antenna position looking FWD (blue arrow)

20.5.1010. Cruise Summary
The OBS operations for this cruise went very well. With the exception to one logger (SP1) having some sort of timing issue, everything else seemed to function properly. All deck operations were routine with exception to two of the SP OBS that had modular hydrophones and brackets mounted to the float frame. For these instruments it was very east for the lifting line to become entangle and wedge underneath the bracket- forcing a cockeyed recovery.

Thanks to the hard work and dedication of the ships crew and science personnel, MV1308 was a safe, productive, and very enjoyable working experience.

20.5.1111. Room for improvement:
- New electronics processing software availability
- Saber acoustic box and relocation software functionality improvement

We lost, or damaged:
- One NovaTech radio, which flooded at the top o-ring
- The 8011M is issue prone, but still useable

21 Appendix J. OBSANP Navigation Notes

Maps of station stops and way-points were prepared on the cruise to give the watchstanders and the bridge the information they needed to carry out the J15-3 transmisison program. Annotated summaries of these maps provide interesting and useful information.

Figure 21.1 shows the actual location of the OBSANP Distributed Vertical Line Array (O-DVLA or DVLA13), that was determined onboard and that was used for planning the transmission program, and the NPAL04 DVLA (DVLA04) along with the drop locations of the short and long-period OBSs. The DVLA13 location was revised ashore and sent to us later in the cruise (ODVLA13rev)(Figure 21.2). The new location is about 46m south of the old one.

Figure 21.3 summarizes the station stop locations for the "pin cushion". Station stops Q1-Q6 fill-in the NPAL04 geodesic. These transmissions could excite out of plane diffractions from Seamount B and almost in-plane diffractions from Seamount C. Q13 to Q18 (ranges to DVLA13 of 23, 28, 33, 38, 43, and 48km) were intended to be in-line with Seamount B and DVLA13. Q13 to Q15 spanned 1/2CZ from DVLA13 and Q16 to Q18 spanned 1/2CZ to Seamount B. With this line of sources it should be possible to distinguish bottom-reflected surface-reflected (BRSR) paths and bottom-diffracted surface-reflected (BDSR) paths in an in-line geometry. Q7 to Q12 and Q19 to Q24 were intended to ensonify Seamount B obliquely to DVLA13.

For the long-line we did a continuous tow out and station stops on the way back. The bridge used a rhumb line from Q6 to TW250 to navigate out but the Q-stations were computed on the DVLA13 to TW250 geodesic. The difference at a station near the middle, for example Q35, is 530m (Figure 21.4).

We planned station stops at 3-1/2CZs from the DVLA and Seamount B (Q29 and Q26 respectively) as well as at TW250 to reoccupy the NPAL14 station (Figure 21.5). We received receptions on the continuous tow at 250km range which was actually at 4-1/2CZ.

The 2014 and 2013 geodesics are compared in Figure 21.6. They are a couple of hundred meters apart.

Due to some discrepancies in the matlab code TW250 (2013) is about 500m further from the DVLA locations than T250 (2004) (Figure 21.7 and Figure 21.8).

The bridge likes to use rhumb lines between way-points. For the radial lines from TE to TW the rhumb line would have been about 130m off the geodesic. (Figure 21.9). Additional way points were added to reduce this discrepancy to less than 5m.

The actual (surveyed) OBS locations are compared with their drop locations in Figure 21.10 and Figure 21.11.

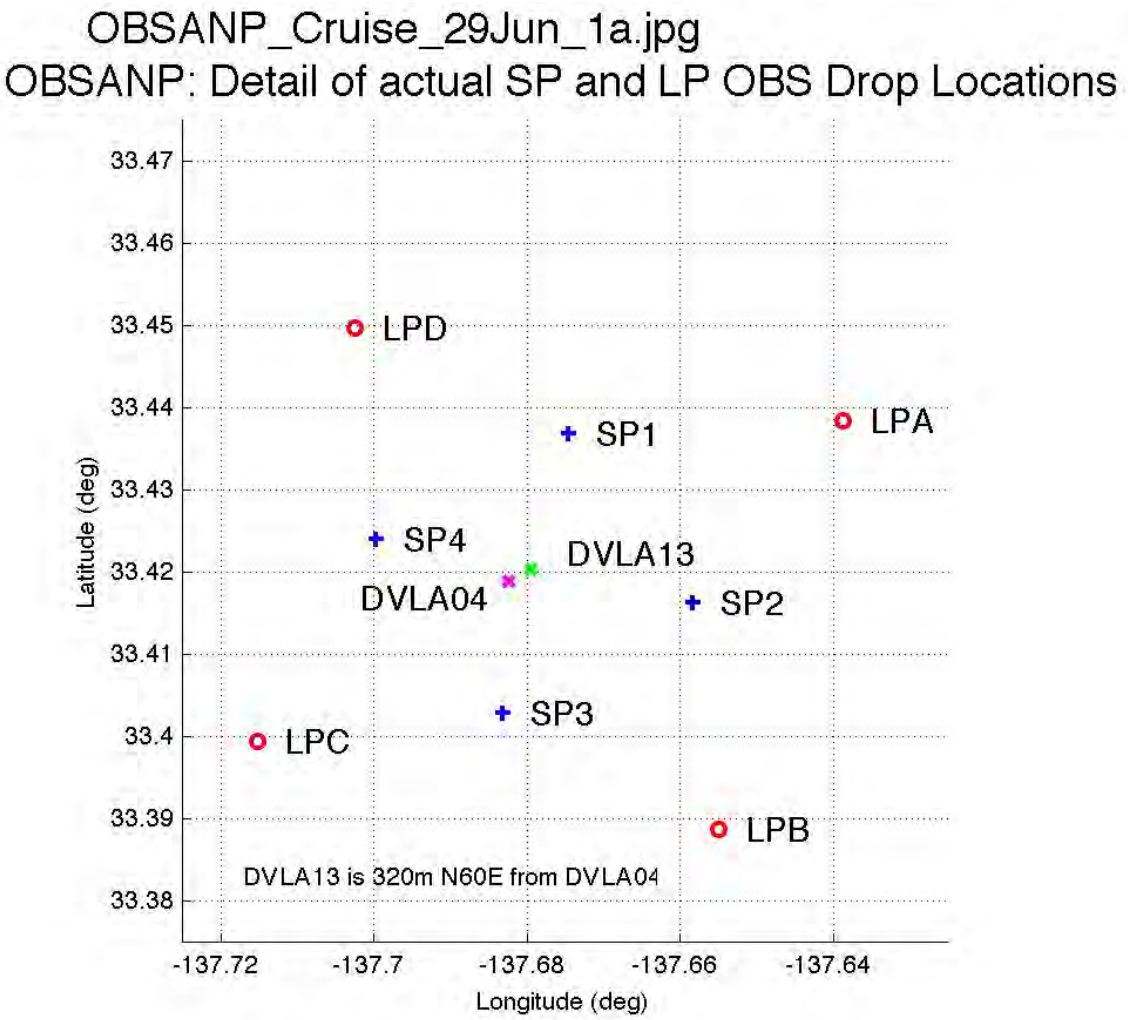

Figure 21.1: OBS Drop Locations
DVLA13, which was intended to be at the same location as DVLA04, was actually 320m N60degE from DVLA04.

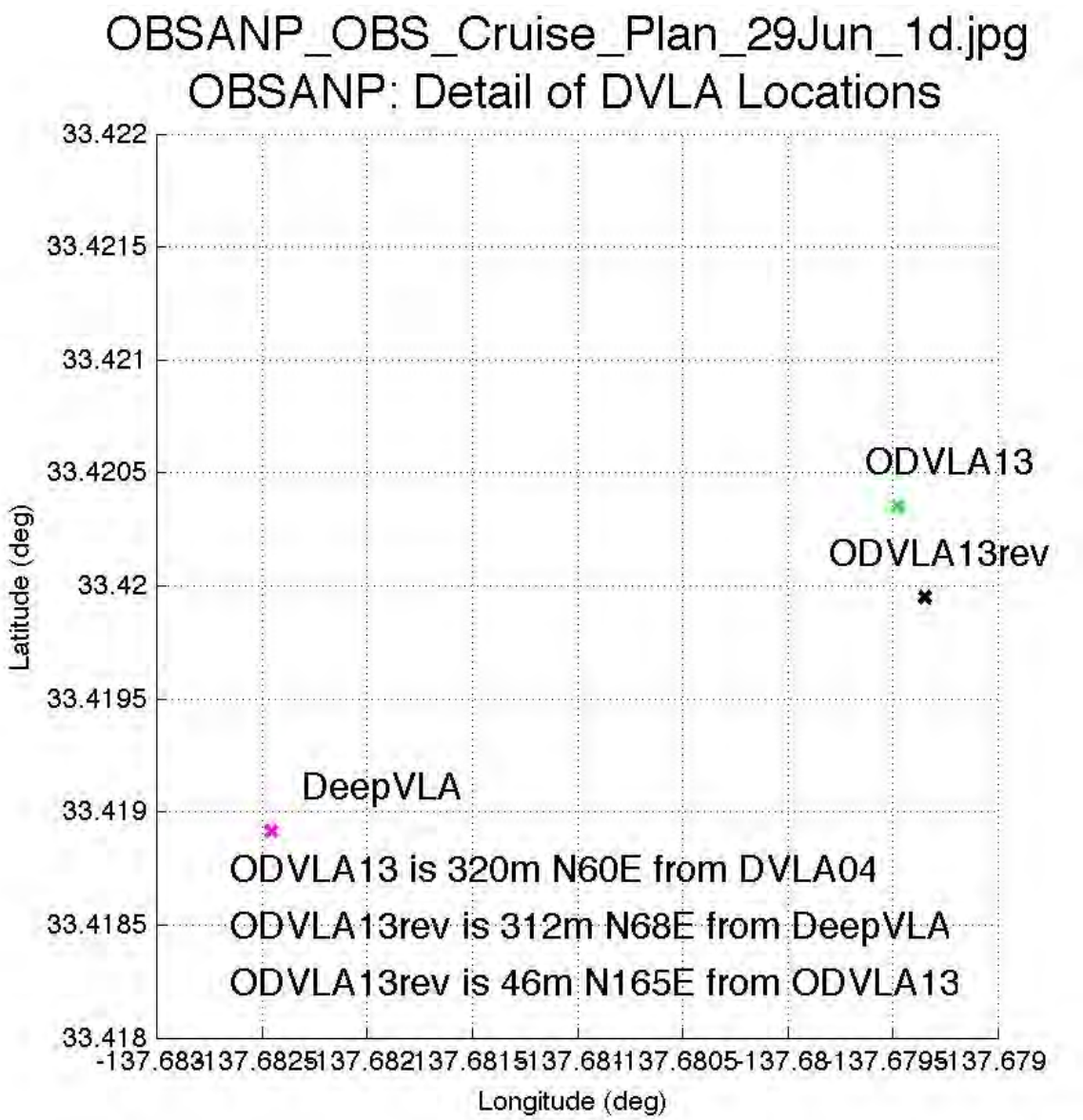

Figure 21.2: ODVLA (Original and Revised) and DVLA04 Locations

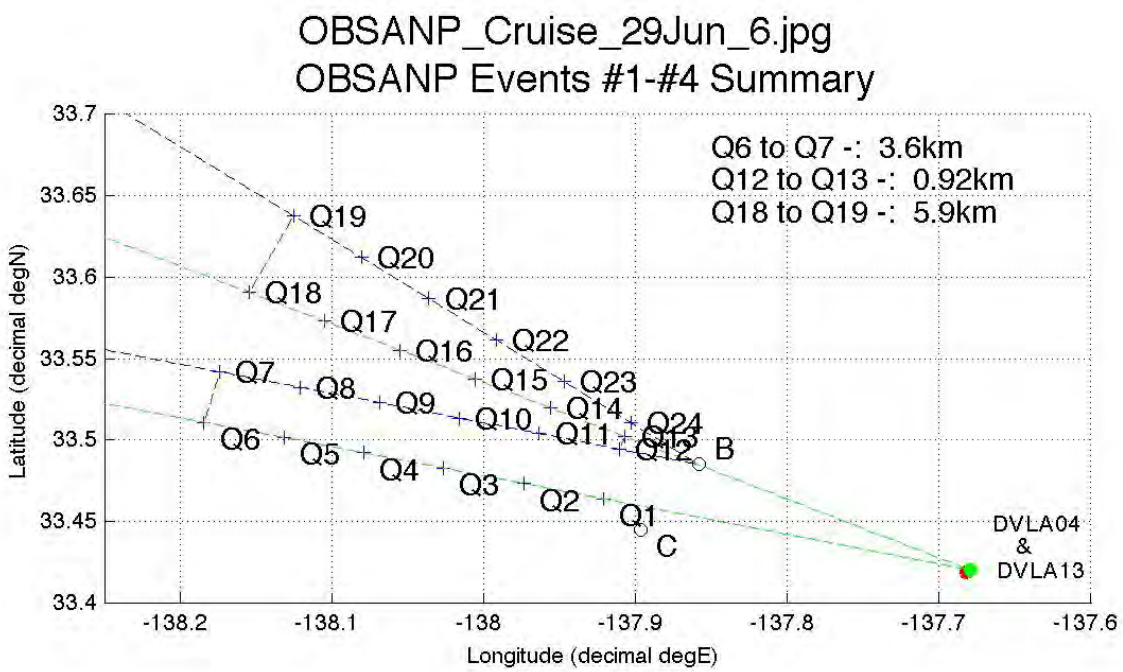

Figure 21.3: Pin Cushion Summary

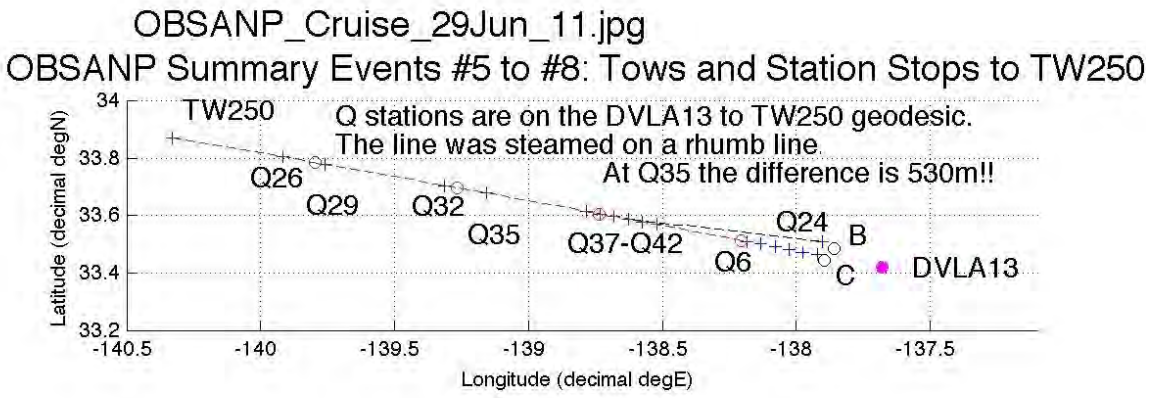

Figure 21.4: The 250km Long-Line

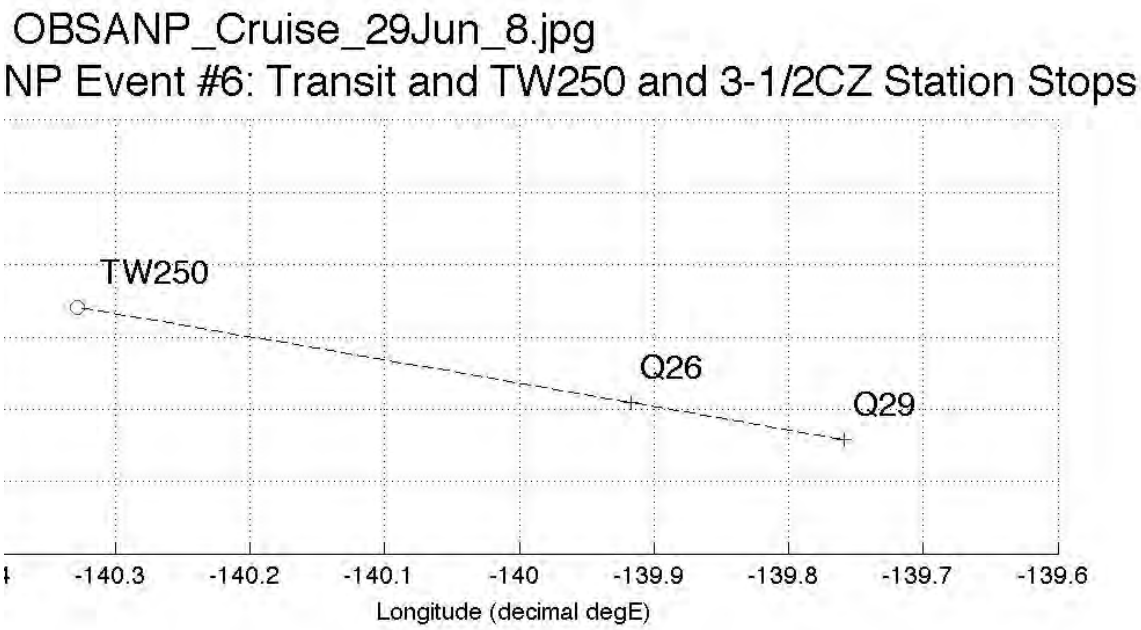

Figure 21.5: Detail at TW250
Q26 and Q29, 212 and 197km respectively from ODVLA13, were planned to be at 3-1/2CZ from ODVLA13 and Seamount B, respectively. TW250 was at 4-1/2CZ.

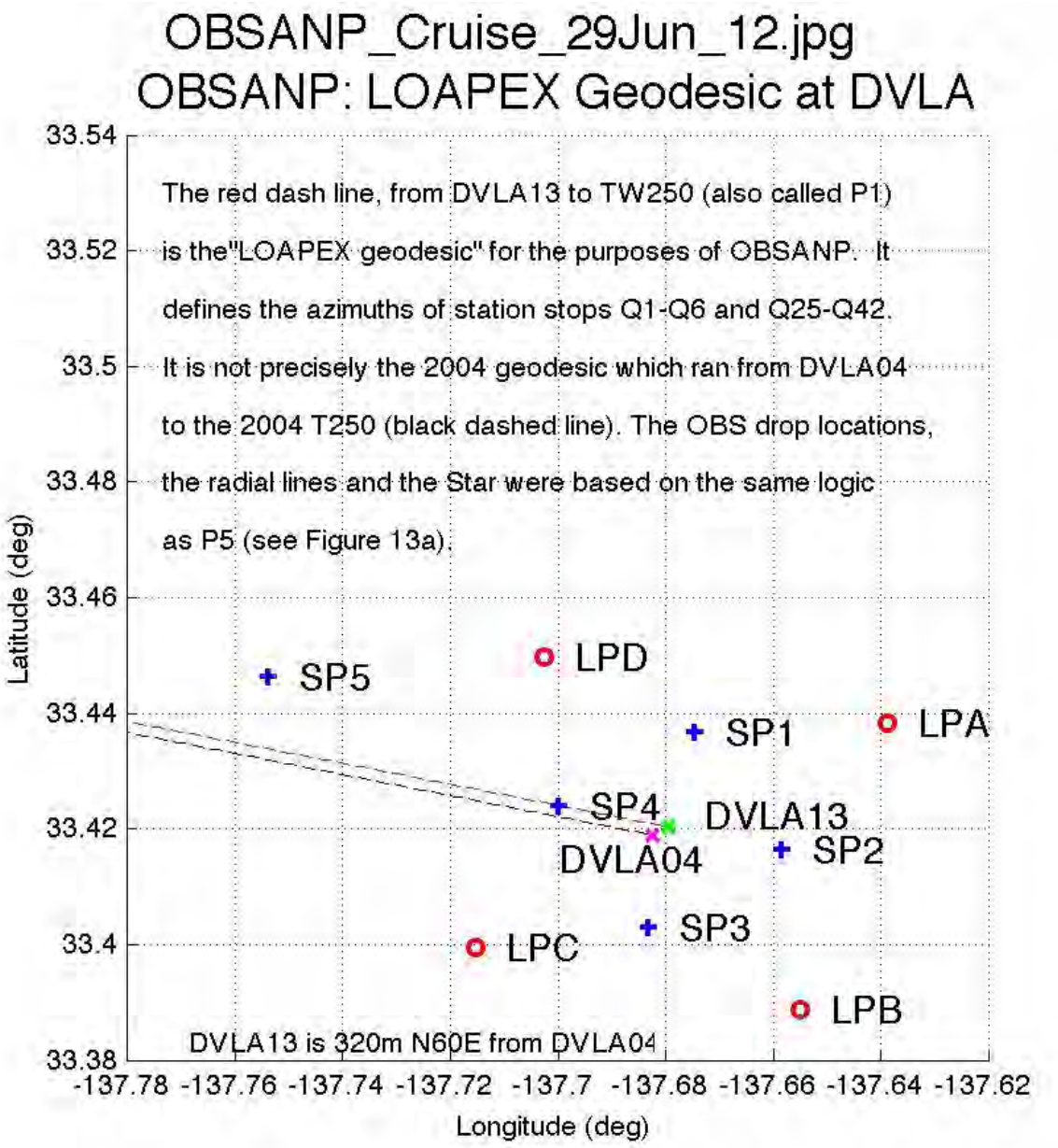

Figure 21.6: 2004 and 2013 Geodesics Compared

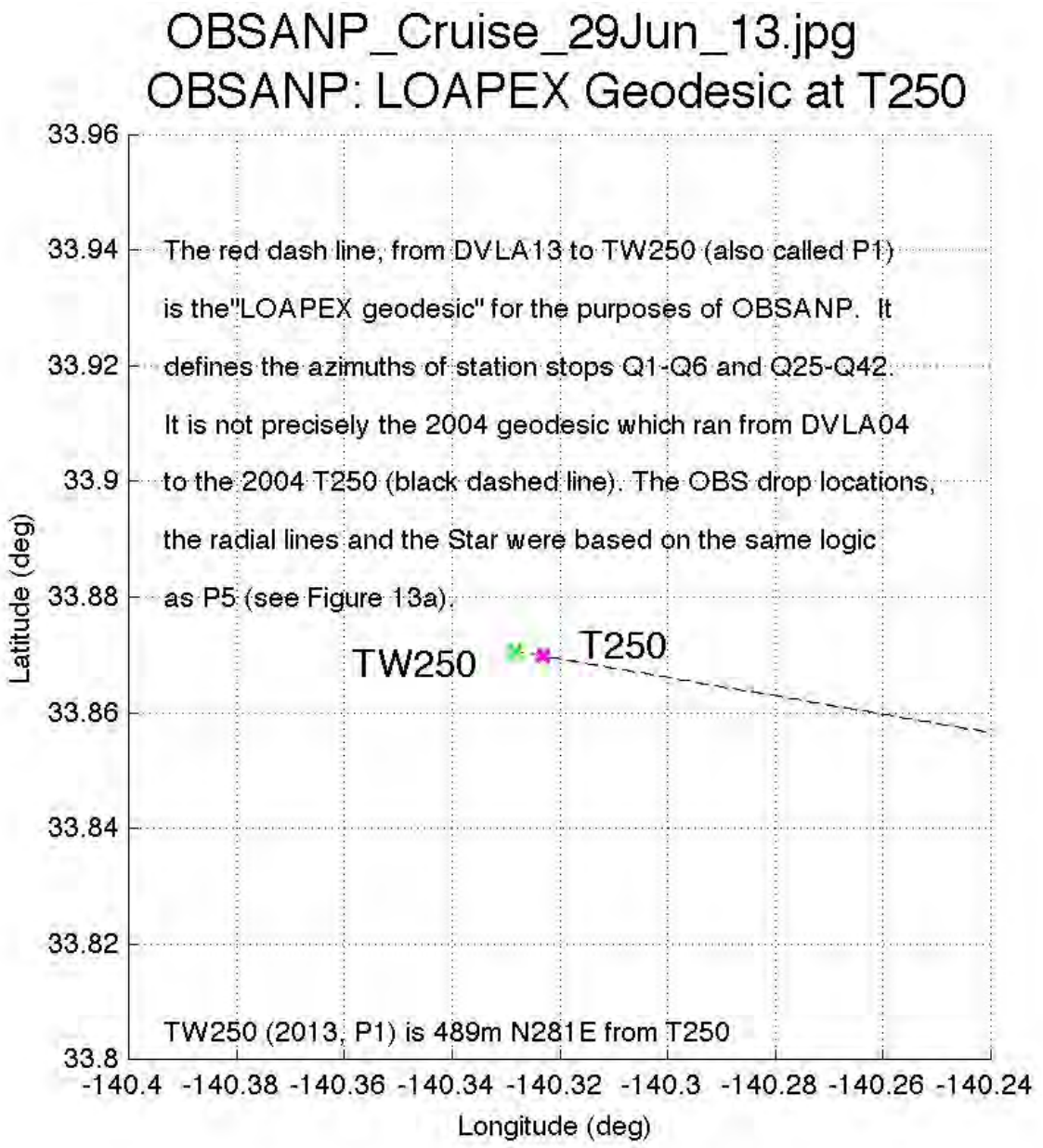

Figure 21.7: TW250 (2013) and T250 (2004) Comparison

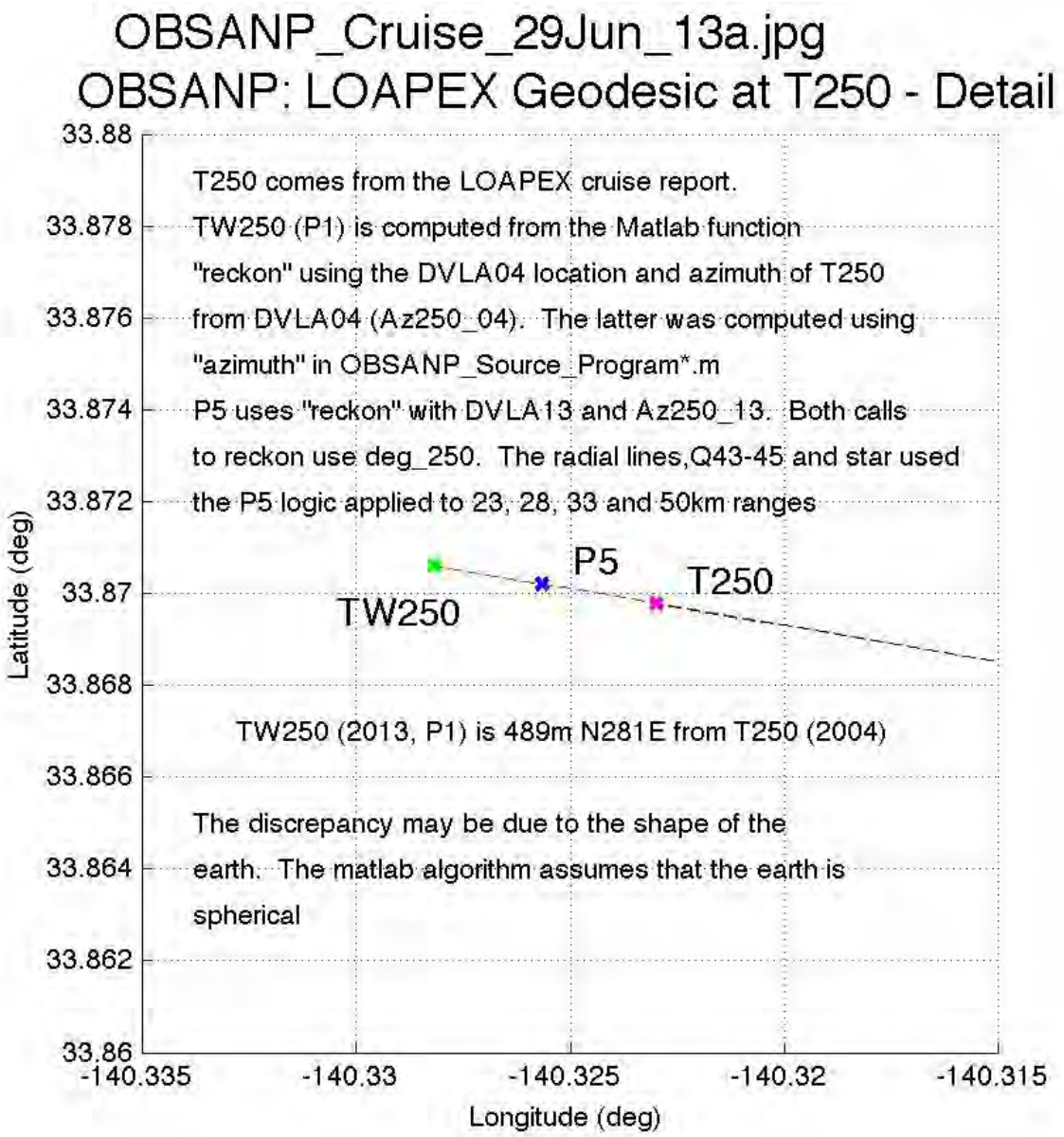

Figure 21.8: T250 Detail

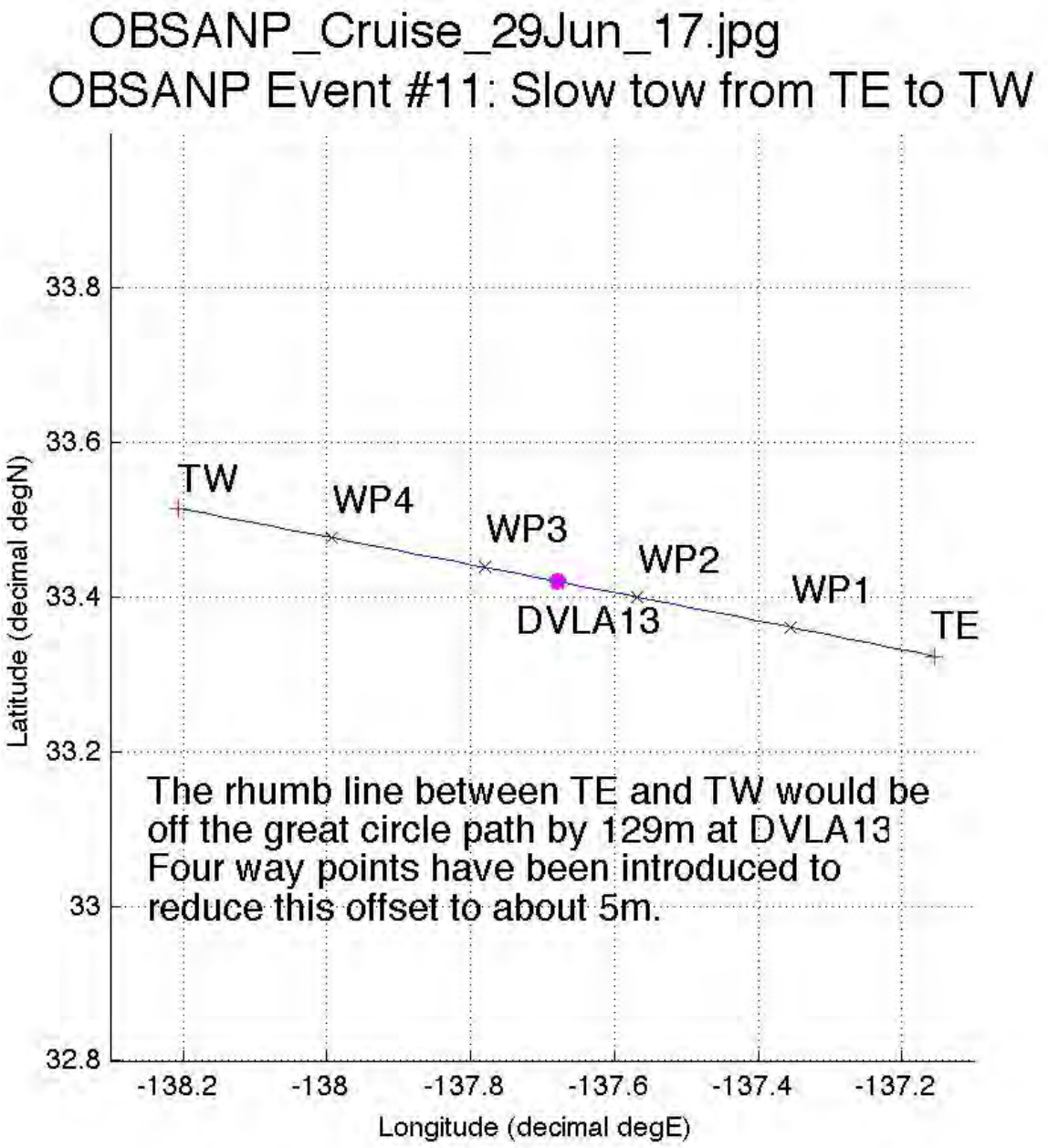

Figure 21.9: Rhumb Line Versus Geodesic for TE to TW

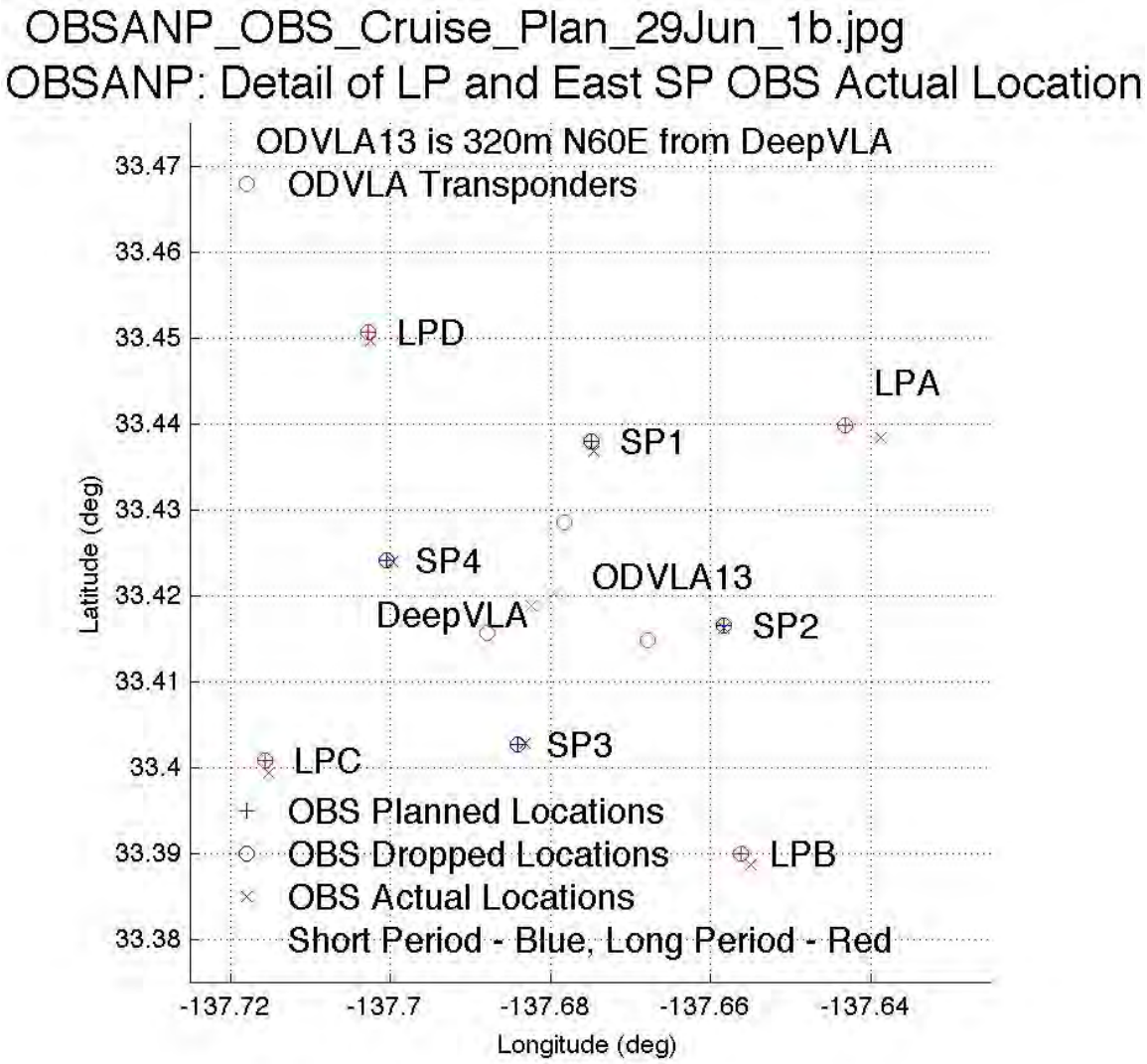

Figure 21.10: Drop Versus Actual OBS Locations (East Half)

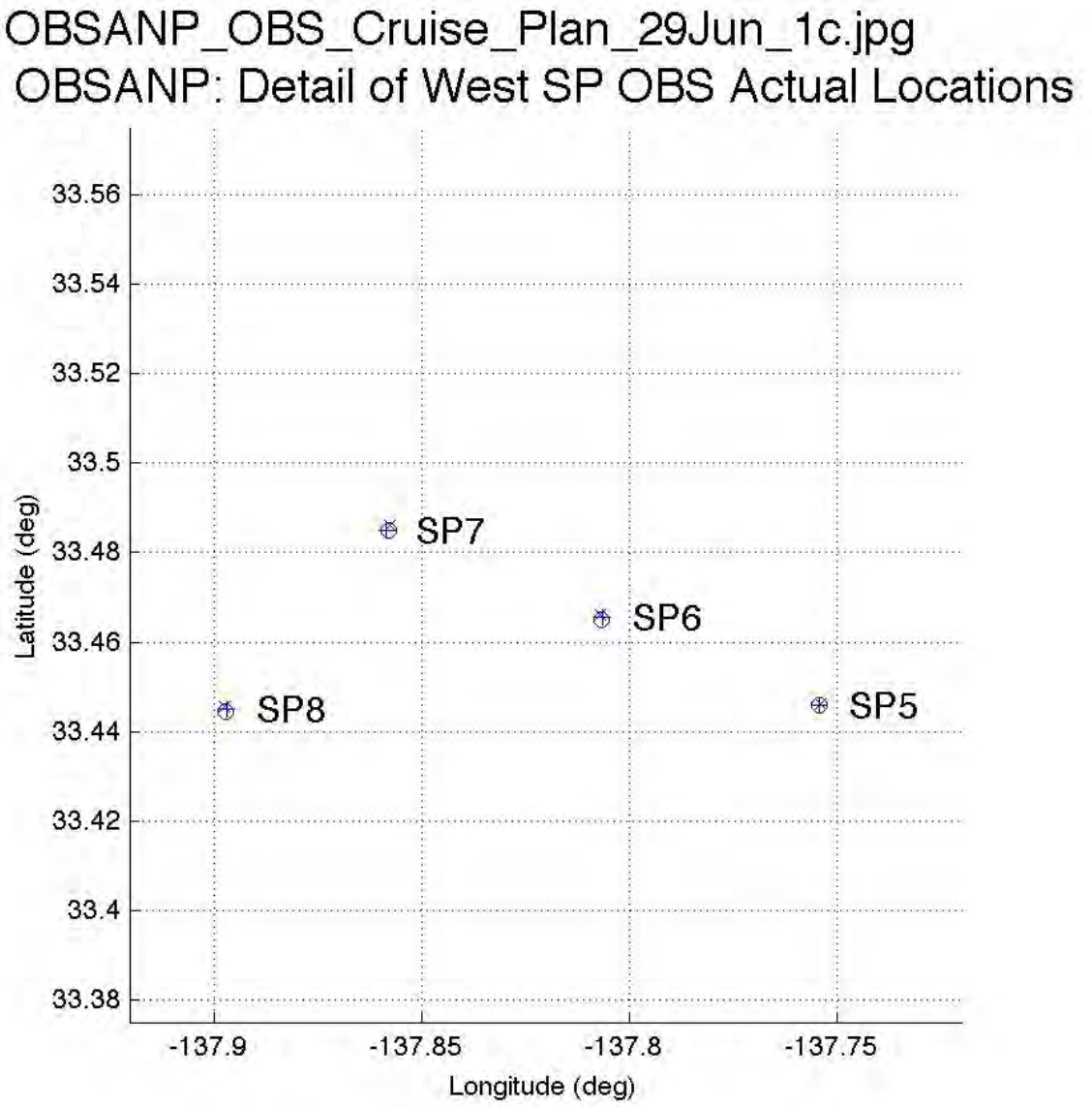

Figure 21.11: Drop Versus Actual OBS Locations (West Half)

22 Appendix K. J15-3 Transmission Notes

22.1 Pre-Cruise Tests (R.Stephen)

On March 25, 2013 Sean McPeak started doing tank tests at WHOI/CRL. I reviewed the 2011 transmission formats in preparation for the tests.

Three things:

1) There was a note in some of the 2011 At sea files of changes made by Peter Worcester on April 19, 2011 to sg_RAS.m. It was recommended that we use sg_RAS_1.m which had
   a) the white noise removed,
   b) the hydrophone sensitivity removed,
   c) the anti-aliasing and anti-strum filters removed, and
   d) clip and quantize removed.

2) There was also a note that Richard Campbell had a better routine for upsampling the M-sequences prior to sending them to the DAQ. This is done in generate_m_sequence.m which was created on the Revelle in Kaohsiung on April 27, 2013. We did a test by comparing a newly created file (using Richard's m-file) with the mat file Richard generated for us in 2011. There are three ways now to get files to input to the DAQ:
   a) use sg_RAS_1 and matlab's "resample"
   b) load mseqs_4000_generated - created by Richard on the Revelle in 2011
   c) use Richard's generate_m_sequence.m directly.

For all three options, code exists to apply tapers but the code is not used.

22.2 Corrupt Files (Ilya Udovydchenkov)

During the experiment Ilya noticed that a sample was missing in the 77.5Hz M-sequence.

List of corrupt files:
1) File OBSANP Primary_Sea_04_ 4K.sio has the sample #422400 set to 0 instead of 0.152395668354392. This occurs at time t=105.59975 sec. This is the last sample in the 4-periods long 77.5 Hz m-sequence. (Figure 1)
2) File OBSANP Primary Sea_06a_ 4K.sio is missing last sample point #3907200 and the null-data gap of 43.2 seconds at the end. The file duration of the file is 976.8-1/4000 seconds instead of 1020 seconds. (Figure 2)
3) File OBSANP Primary Sea_06c_ 4K.sio has the sample #4480000 set to 0 instead of 0.345376569525292. This occurs at time 1119.9975 sec. This is the last sample in the 37- periods long 204.6 Hz m-sequence
4) Consequently, file OBSANP Primary Sea_06T_ 4K.sio has 2 one sample point errors:
sample #3907200 is equal to zero, but should be 0.152395668354392; and
sample #11680000 is equal to zero, but should be 0.345376569525292.

(Note that the sequence "c" starts at the sample 7200000 within the sequence "T", and also note

that 7200000+4480000=11680000) (Figure 3)

22.2.1 Corrupt files used during the experiment:
The error was discovered on or around 6/20/2013 (around 171:21:00:00 UTC). At that time all transmission schedules were changed to the newly created file 6TX, which did not contain these errors. The errors were fixed in all files. Files mentioned above were not used after 171:21:00:00 UTC. All files mentioned above were used at least once prior to 171:21:00:00.

22.2.2 Mitigation:
We do not expect these errors to cause serious problems during data analysis. All errors are incorrect amplitudes (falsely set to 0) of the last sampling point of the last m-sequence sampled at 4 kHz.

[All of Ilya's codes used for M-sequence tests are in the folder ../At_Sea_Archival/Ilyas_codes.]

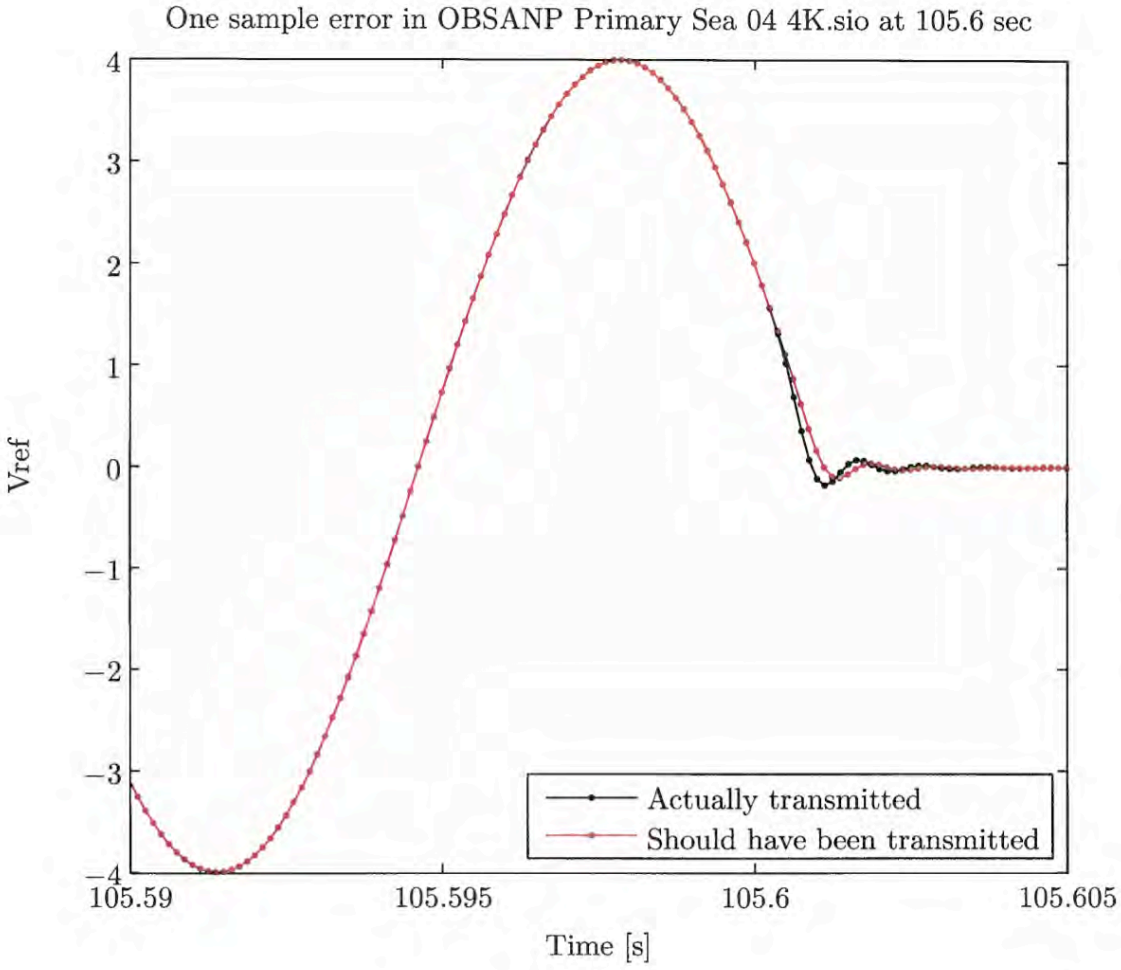

Figure 22.1: Missing Sample Example #1
First example of a missing sample in OBSANP_Primary_sea_04_4K.sio.
[...OBSANP_Cruise_Report/For_Tom_CCH/OBSANP_Missing_Sample/Fig_1]

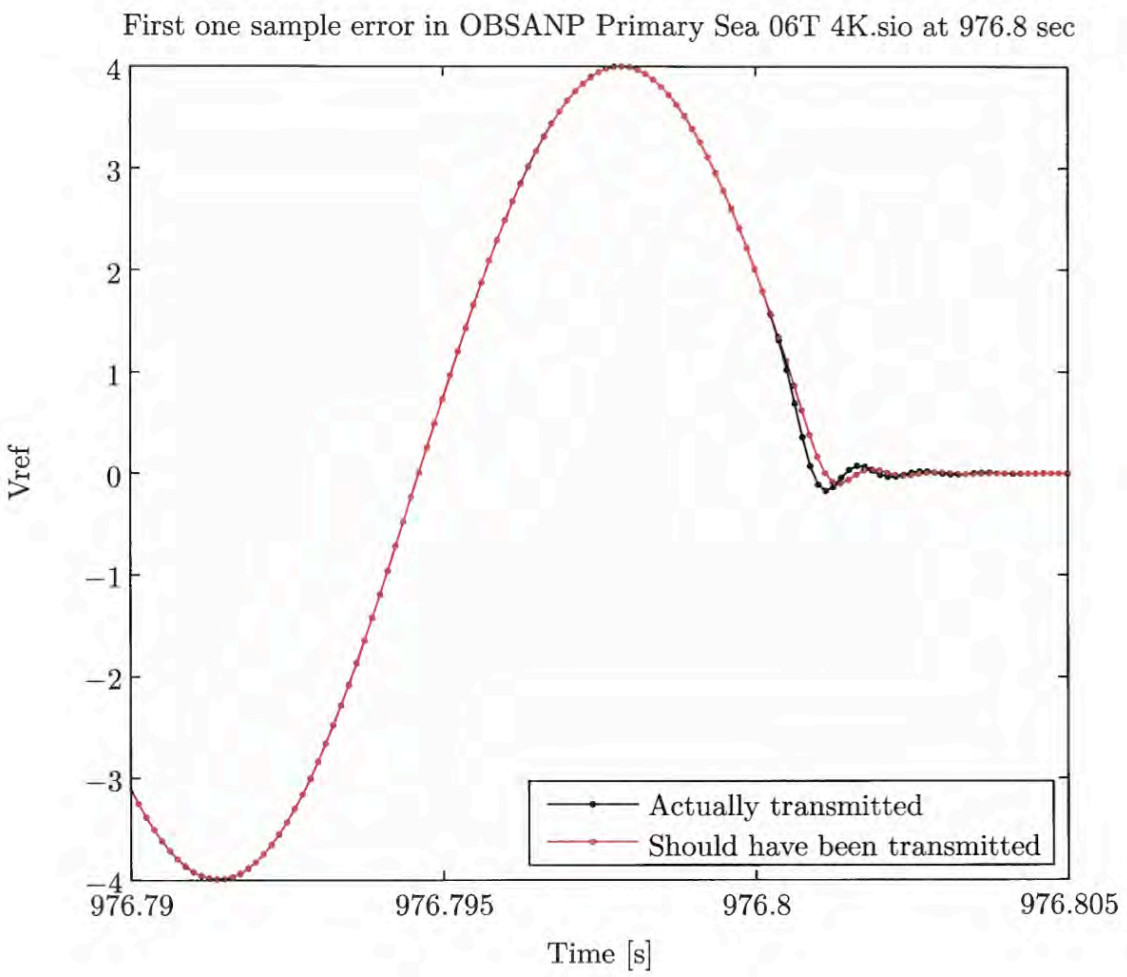

Figure 22.2: Missing Sample Example #2

Second example of a missing sample in OBSANP_Primary_Sea_06T_4K.sio.
[...OBSANP_Cruise_Report/For_Tom_CCH/OBSANP_Missing_Sample/Fig_2]

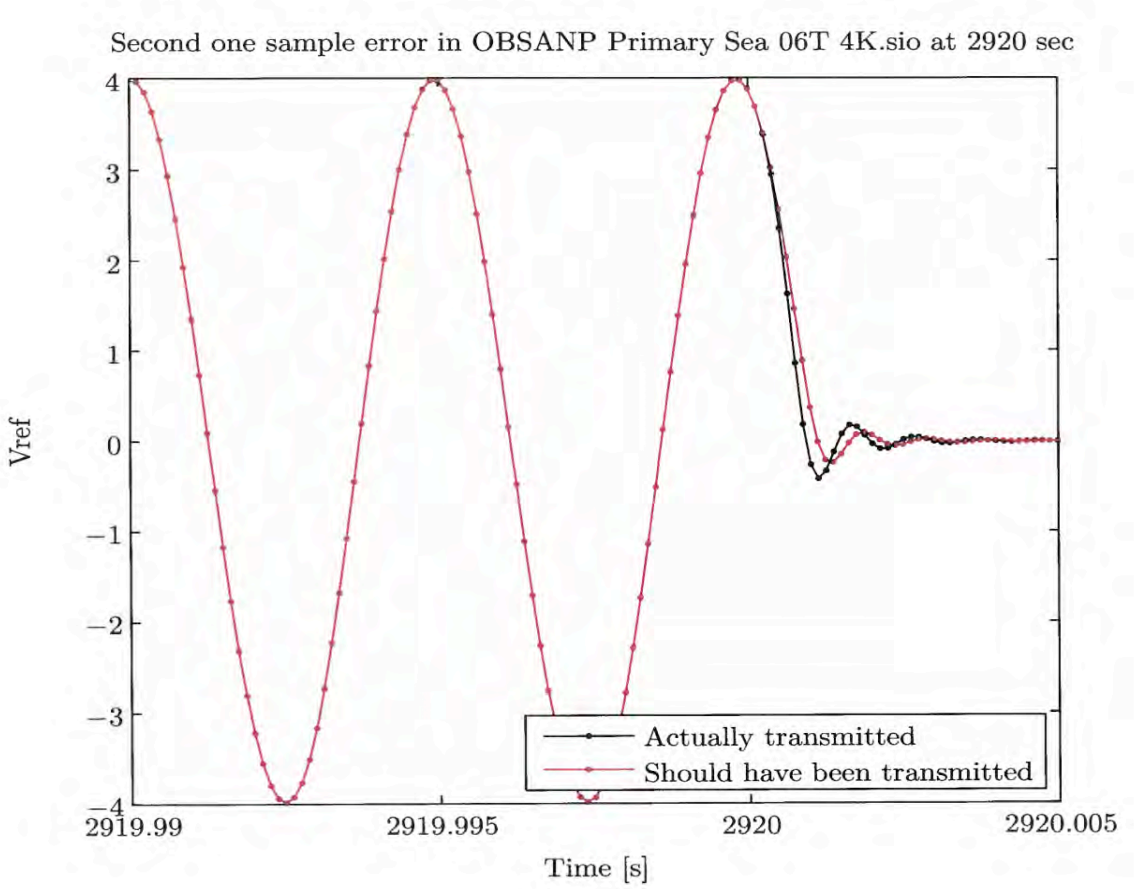

Figure 22.3: Missing Sample Example #3

Third example of a missing sample in OBSANP_Primary_sea_06T_4K.sio.
[...OBSANP_Cruise_Report/For_Tom_CCH/OBSANP_Missing_Sample/Fig_3]

22.3 M-sequence File Summary (Ralph Stephen)

This series of tests was run during the OBSANP cruise. On June 19, Ilya and Sean noticed that program 6a did not have a 43.2sec gap at the end of transmitting 37 77.5Hz m-sequences as specified in the documentation ((37 x 26.4 = 976.8) + 43.2 = 1020sec = 17min). There are a lot of different files with similar names in various folders so confusion is possible.

The files I gave Sean for transmitting from the DAQ were put on a memory stick "EMAILWHOI". The filenames were:

OBSANP_Primary_Sea_04_4K.sio
OBSANP_Primary_Sea_05_4K.sio
OBSANP_Primary_Sea_06a_4K.sio
OBSANP_Primary_Sea_06b_4K.sio
OBSANP_Primary_Sea_06c_4K.sio
OBSANP_Primary_Sea_06T_4K.sio
OBSANP_Primary_Sea_CW_1_4K.sio

I believe these were taken from '/Volumes/RAS_Archive/OBSAPS_Archive/OBSAPS_11/M-sequences/At_Sea/Sources' which had the OBSAPS files. I did not recreate these I believe I just changed the names by replacing OBSAPS with OBSANP. [In retrospect this was a risky thing to do. It would have been better to recreate sequences from the m-files or at least to have used the files from the March 2013 tests.]

All these files need to be checked both as given to Sean for the DAQ and after being acquired on the H91. I will start with a review of the 6a format.

22.3.1 A. OBSANP_Primary_Sea_06a_4K.sio

This file lives in three places:

1) The root directory of RAS_Archive with a date of March 26, 2013.
2) '/Volumes/RAS_Archive/OBSAPS_Archive/OBSAPS_11/M-sequences/At_Sea/Sources_2013' . This folder was created for testing on June 19 and the file was copied to it from the memory stick (since this is what I gave to Sean).
3) The memory stick EMAILWHOI .

On June 19, using sioread, I checked the length of the files in 2) and 3) (which are the same file). the length was one sample short of 976.8 sec (976.8*4000-1 = 3907199. The size of this file is 15.6MB and it has a date of 26 March, 2013. This is the same info as in 1) so all three files look to be the same.

Now in the DAQ Sean repeats the sequence when it comes to the end so the 4080000th sample would equal the first sample. Not optimal but maybe OK. When interpreting time compressions of received data the user should look for a series of at least 37 arrivals. The first would be

incomplete and the 37th may be incomplete so use the 35 sequences (#2-#36) for stacking. The system would continue to transmit m-sequences until the operator stopped the transmissions manually. These additional transmissions could be used as available.

These are the only files with this name on the system. There is a file, OBSANP_Test_06a_4K.sio, under March_tests that has the same date and size. I could have just copied this over and replaced "Test" with "Primary_Sea". We could check the H91 files from the March test to confirm this.

A grep for OBSANP_Primary_Sea in OBSANP_Cruise only returns OBSANP_13/M-sequences/Cruise_sequences/Primary_CW/OBSANP_Primary_4_Sea_CW.m so the CW files, OBSANP_Primary_Sea_CW_1_4K.*, seem to be the only ones created directly. The rest were obtained by changing file names.

In Sources_2013 there are four .sio files. OBSANP_Primary_Sea_06a_4K_save.sio and OBSANP_Primary_Sea_06a_4K.sio are the same. I created the former in case the latter got clobbered. OBSAPS_Primary_06a_p_4K.sio and OBSAPS_Primary_Sea_06a_3_4K.sio were regenerated on June 19 from OBSAPS_Primary_6a_Sea.m and OBSAPS_Primary_6a_Sea_3.m respectively. They are 16.3MB files and have the correct number of points (4080000) for a 17minute transmission with the 43.2sec gap.

22.3.2 B. OBSANP_Primary_Sea_04_4K.sio

This was copied to Sources_2013 on June 20. This has the correct number of samples for 5 minutes, so it includes all three frequencies with gaps.

22.3.3 C. OBSANP_Primary_Sea_05_4K.sio

This was copied to Sources_2013 on June 20. This has one sample less than the correct number of samples for 11 minutes, not good !!!!!

22.3.4 D. OBSANP_Primary_Sea_06b_4K.sio

This was copied to Sources_2013 on June 20. This has the correct number of samples for 13 minutes, so it includes all three frequencies with gaps.

22.3.5 E. OBSANP_Primary_Sea_06c_4K.sio

This was copied to Sources_2013 on June 20. This has the correct number of samples for 19 minutes, so it includes all three frequencies with gaps.

22.3.6 F. OBSANP_Primary_Sea_06T_4K.sio

This was copied to Sources_2013 on June 20. This has the correct number of samples for 49 minutes, so it includes all three frequencies with gaps.

********** RESOLVE **********

Go back to '/Users/ralph/OBSANP_Cruise/OBSANP_13/M-sequences/March_tests'. This has all of the m-sequences and the m-files that created them. Check the file sizes and formats. If necessary rerun the m-files to get correct sizes. Change the names to something simple and put them in Cruise_sequences.

In March_tests_June-20-2013:

OBSANP_Test_04_4K.sio - OK. Has correct number of samples for 5 minutes with gaps.

OBSANP_Test_05_4K.sio - N/G. Has one less sample than the correct number of samples for 11 minutes.

OBSANP_Test_06a_4K.sio - N/G. Has one less sample than the number of samples for 976.8sec when it should be 1020sec (17 minutes).

OBSANP_Test_06b_4K.sio - OK. Has correct number of samples for 13 minutes with gaps.

OBSANP_Test_06c_4K.sio - OK. Has correct number of samples for 19 minutes with gaps.

OBSANP_Test_06T_4K.sio - OK. Has correct number of samples for 49 minutes with gaps.

Back in the Sources_2013 directory on the archive:

OBSAPS_Primary_Sea_05_3_4K.sio - Has correct number of samples for 11 minutes (no gaps are programmed).

OBSAPS_Primary_Sea_06a_3_4K.sio - Has correct number of samples for 17 minutes with gaps.

So we could rename these with OBSANP replacing OBSAPS and use them as is. So let'e rename as follows

OBSANP_Test_04_4K.sio - OBSANP_Sea_04.sio

OBSAPS_Primary_Sea_05_3_4K.sio - OBSANP_Sea_05.sio

OBSAPS_Primary_Sea_06a_3_4K.sio - OBSANP_Sea_06a.sio

OBSANP_Test_06b_4K.sio - OBSANP_Sea_06b.sio

OBSANP_Test_06c_4K.sio - OBSANP_Sea_06c.sio

OBSANP_Test_06T_4K.sio - OBSANP_Sea_06T.sio

and put them in the directory.

Modified June 20, 2013 to make 6Tx a complete 1hour file that could be run continuously and start at hh:52

[These two folders, ../At_Sea_Archival/OBSANP_sioFileUsedAtSea and ../At_Sea_Archival/OBSANP_Program7, were copied from Sean's Labview PC on July 4, 2013 on the R/V Melville. They contain all the files that were transmitted on the OBSANP experiment. There was some confusion between files created by Ilya and by Ralph.

Program 7 was a folder prepared by Ilya for transmission tests at Q1 and Q43 at the end of the experiment. They contain the usual M-sequences (77.5 to 310Hz), MSK M-sequences, and low frequency CW and M-sequences (20-77.5Hz).]

23 Appendix L. OBSANP AB-logger Information from Jeff Babcock

Revised: April 23, 2014

OBSANP AB-logger Generalized Response and Calibration Factor

These calculations are for the generalized case and assume the signal is in the sensor frequency range giving a flat response. Frequency response ranges are indicated.

SENSOR RESPONSE INFO:

For the custom High-Tech Hydrophone (HTI-90-U) the manufacturer calibration files give a sensitivity of -182.7 dB re 1V/µPa. This hydrophone loses ~2 dB in sensitivity per ~6000m in depth (10,000 psi) so for typical ocean depth around 3km we correct ~1 dB and use -183.7 dB re 1V/µPa. Using amplitude spectra throughout (e.g. X[db] =20*log10[X/Xref]), this gives S(hyd-HTI) = 10**(-183.7/20) * 1V/µPa = .653 mV/Pa (@ 3000m water depth). Thus:

S(hyd-HTI) = 0.653 mV/Pa *flat response: 0.05 Hz to 7.5 kHz (@ 3000m depth)*

For the custom SAIC-VLN Hydrophone the provided calibration sheets from the manufacturer indicate a sensor sensitivity of ~-185.5 dB re 1V/µPa. This signal is then fed through a custom hydrophone preamplifier, the combined sensor system gives a sensitivity of ~-158.9 dB re 1V/µPa. This gives s S(hyd-SAIC) = 10**(-158.9/20) * 1V/µPa = 11.35 mV/Pa. Calibration is only provided @ 10 Hz.

S(hyd-SAIC) = 11.35 mV/Pa *response is only calibrated @ 10 Hz*

For the DPG sensitivity:
Calibration of the DPG's (Jim Sari at JHU/APL with a 1 psi sensor) gives -186 dB re 1V/microPa, (a 1psi Bell Jar gave ~1 mV/Pa with a variability of a factor of 2), using the same calculation as the hydrophone:

S(DPG) = 0.501 mV/Pa *flat response: 0.002 Hz (500 sec) to ~30+ Hz*

For the L28LB seismometer sensitivity:
transduction constant --> 1.57 * sqrt(R-coil) V/m/s with R-coil = 630 ohm nominally this gives 39.53 V/m/s. SIO used 55% coil current damping, R-shunt = (7860+51) ohm which gives:

S(l28) = 36.61 V/m/s *flat response: ~4.5 Hz and above*

For the Trillium-240 seismometer sensitivity:
the manufacturer quotes 1200 V*s/m over +/-20V for a full differential signal. SIO-AB uses only a single-sided input to the A/D, effectively halving the sensitivity, thus:

S(T240-ss) = 600 V/m/s *flat response: 0.004167 Hz (240 sec) to 35 Hz*

24 Appendix M. Notes on HM Responses from Matt Dzieciuch

From Matt Dzieciuch on April 18, 2014:

I have attached a program that should help you account for the decreased HTI-90 sensitivity with depth. It Also accounts for the variable sensitivity due to the preamp and other electronic considerations.

An attached plot shows the hydrophone sensitivity with frequency and depth.

I assume you can read in the sample values from the netcdf files. Call those rcv.

To convert from counts to volts at the A/D input use:

```
bits2volts=2.5/2^23;       % A/D full scale is 5 Vpeak-peak or 2.5 Vpeak
rcvx=bits2volts*rcv;       %Convert bits to volts
```

The simple-minded conversion to input pressure, in uPa, (which doesn't account for depth or frequency) is just a scale factor:

```
ampgain=10^(12/20);
hysens=10^(-168/20);
pres=rcvx/ampgain/hysens;   % Convert volts to input pressure (uPa)
```

A better conversion (which accounts for the depth, frequency dependence) is to first convert to A/D input volts and then do a power estimate in the frequency domain. I find pwelch works well in matlab, it gives power/Hz, if you specify the sampling frequency. Then I apply the conversion factor G, to convert to input power in uPa^2/Hz.

```
bits2volts=2.5/2^23;       % A/D full scale is 5 Vpeak-peak or 2.5 Vpeak
rcvx=bits2volts*rcv;       %Convert bits to volts
[Pf, fax]=pwelch( rcvx, wnd, ovrlp, nfft, fs);
G=hycal(fax, hydep);
Pf=10*log10(Pf) - G;
```

The function hycal.m, which I have also attached, produces the correct conversion factor G, as a function of frequency, fax in Hz, and depth, hydep in meters. Note that this procedure does not account for any phase deviations.

I hope that this helps.
Matt

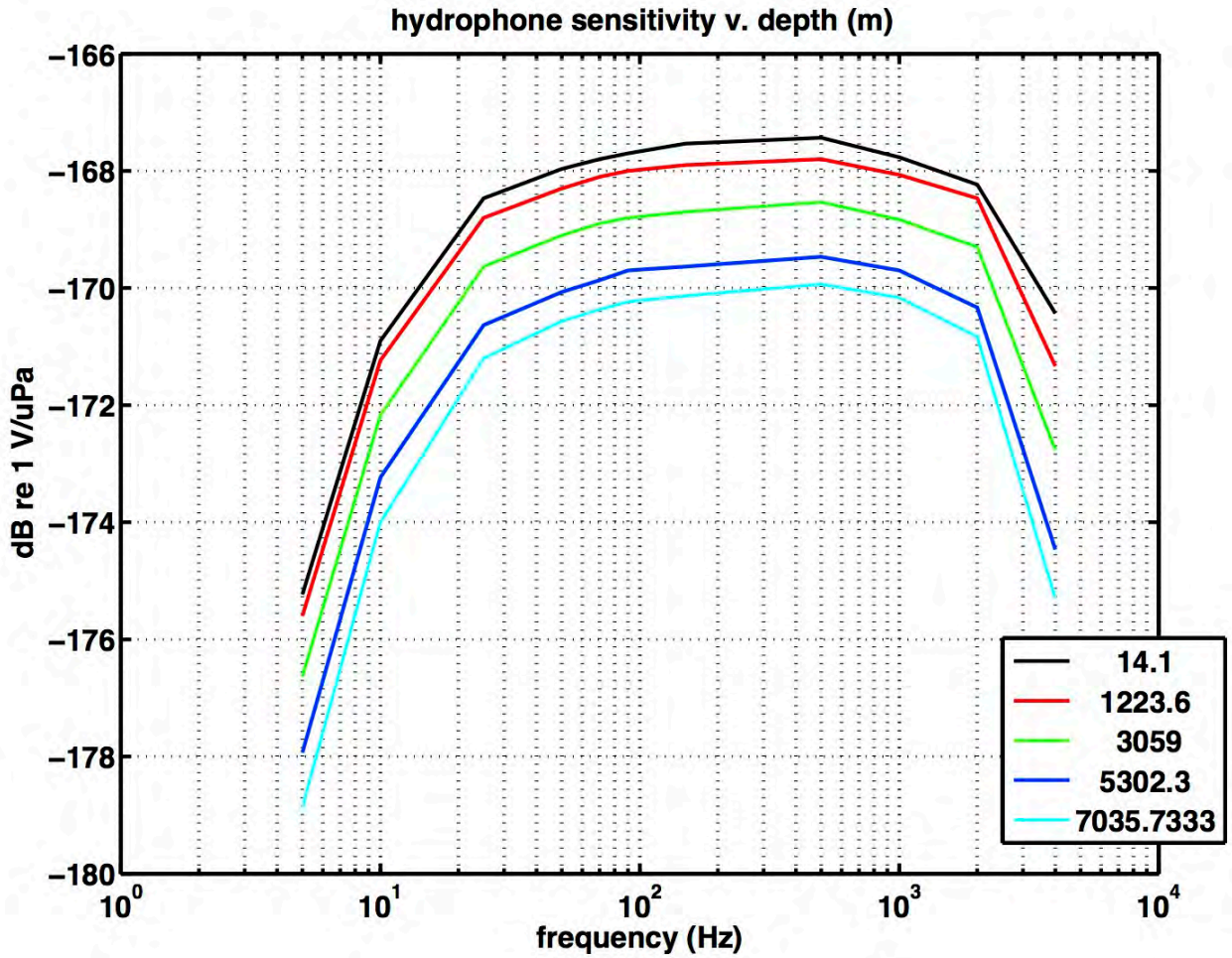

Figure 24.1 Hydrophone sensitivity with frequency and depth

24.1 Matlab Function hycal.m produces correct conversion factor G

```
function Gz=hycal(fax, hz)

hzcf=[ 0.998691744123403; 0.000002249973788];

%hydrophone sensitivity -184 dBV re 1 uPa
M=10^(-184/20); %%measured hydrophone sensitivity

wax=2*pi*logspace(-3,4, 200);
wax=2*pi*fax;

%%%%%%%%%%%%%%%%%%%%%%%%%%%%%%%%%%%%%%%%%%%%%%%%%%%%%%%%%%%%%%%%%%%%%%%%%%%%%%%%
%%%%%%%%%%%%%%%%%%%%%%%%%%%%%%%%%%%%%%%%%%%%%%%%%%%%%%%%%%%%%%%%%%%%%%%%%%%%%%%%
%input coupling
Ch=693e-12; %hydrophone capacitance
C1=0.1e-6;
C2=47e-6;
C6=33e-6;
R1=100e3;
R2=100e3;
R3=100e6;

x=j*wax*R3*C1;
H11=x./(1+x);

Zb=1./(1/R2 + j*wax*C2 + 1./(R1+1./j*wax*C6));
x=j*wax.*(R3+Zb)*C1;
H1=x./(1+x);

%%%%%%%%%%%%%%%%%%%%%%%%%%%%%%%%%%%%%%%%%%%%%%%%%%%%%%%%%%%%%%%%%%%%%%%%%%%%%%%%
%%%%%%%%%%%%%%%%%%%%%%%%%%%%%%%%%%%%%%%%%%%%%%%%%%%%%%%%%%%%%%%%%%%%%%%%%%%%%%%%
%hydrophone preamp response
R5=17400;
C4=390e-12;
R4=499;
C3=33e-6;

Z1=R4 + 1./(j*wax*C3);
Z2=R5./(1+j*wax*R5*C4);
H2=1+Z2./Z1;

%%%%%%%%%%%%%%%%%%%%%%%%%%%%%%%%%%%%%%%%%%%%%%%%%%%%%%%%%%%%%%%%%%%%%%%%%%%%%%%%
%%%%%%%%%%%%%%%%%%%%%%%%%%%%%%%%%%%%%%%%%%%%%%%%%%%%%%%%%%%%%%%%%%%%%%%%%%%%%%%%
%hydrophone current driver
R700=442;
R7=2000;
```

```
H3=R700/(R7+R700);

%%%%%%%%%%%%%%%%%%%%%%%%%%%%%%%%%%%%%%%%%%%%%%%%%%%%%%%%%%%%%
%%%%%%%%%%%%%%%%%%%%%%%%%%%%%%%%%%%%%%%%%%%%%%%%%%%%%%%%%%%%%
%low-noise receiver
C701=4.7e-6;
R702=4420;
C704=2200e-12;
R703=18000;

ZI=R702 + 1./(j*wax*C701);
ZF=R703./(1+j*wax*R703*C704);
H4=-ZF./ZI;
%%%%%%%%%%%%%%%%%%%%%%%%%%%%%%%%%%%%%%%%%%%%%%%%%%%%%%%%%%%%%
%%%%%%%%%%%%%%%%%%%%%%%%%%%%%%%%%%%%%%%%%%%%%%%%%%%%%%%%%%%%%
%total transfer function
H=M*H1.*H2.*H3.*H4;
G=20*log10(abs(H));

Gz=hzcf(1)*G+hzcf(2)*hz*G;

%%%%%%%%%%%%%%%%%%%%%%%%%%%%%%%%%%%%%%%%%%%%%%%%%%%%%%%%%%%%%
%%%%%%%%%%%%%%%%%%%%%%%%%%%%%%%%%%%%%%%%%%%%%%%%%%%%%%%%%%%%%
```

50272-101

REPORT DOCUMENTATION PAGE	1. REPORT NO. WHOI-2014-03	2.	3. Recipient's Accession No.

4. Title and Subtitle
Ocean Bottom Seismometer Augmentation in the North Pacific (OBSANP) - Cruise Report

5. Report Date
December 2014

6.

7. Author(s) Stephen, R.A., Worcester, P.F., Udovydchenkov, I.A., Aaron, E., Bolmer, S.T., Carey, S., McPeak, S.P., Swift, S.A. and Dzieciuch, M.A.

8. Performing Organization Rept. No.

9. Performing Organization Name and Address

Woods Hole Oceanographic Institution
Woods Hole, Massachusetts 02543

10. Project/Task/Work Unit No.

11. Contract(C) or Grant(G) No.
(C) N00014-10-1-0987
(G) N00014-10-1-0510

12. Sponsoring Organization Name and Address

Office of Naval Research

13. Type of Report & Period Covered
Technical Report

14.

15. Supplementary Notes

This report should be cited as: Woods Hole Oceanographic Institution Technical Report, WHOI-2014-03.

16. Abstract (Limit: 200 words)

The Ocean Bottom Seismometer Augmentation in the North Pacific Experiment (OBSANP, June-July, 2013, R/V Melville) addresses the coherence and depth dependence of deep-water ambient noise and signals. During the 2004 NPAL Experiment in the North Pacific Ocean, in addition to predicted ocean acoustic arrivals and deep shadow zone arrivals, we observed "deep seafloor arrivals" (DSFA) that were dominant on the seafloor Ocean Bottom Seismometer (OBS) (at about 5000m depth) but were absent or very weak on the Distributed Vertical Line Array (DVLA) (above 4250m depth). At least a subset of these arrivals correspond to bottom-diffracted surface-reflected (BDSR) paths from an out-of-plane seamount. BDSR arrivals are present throughout the water column, but at depths above the conjugate depth are obscured by ambient noise and PE predicted arrivals. On the 2004 NPAL/LOAPEX experiment BDSR paths yielded the largest amplitude seafloor arrivals for ranges from 500 to 3200km. The OBSANP experiment tests the hypothesis that BDSR paths contribute to the arrival structure on the deep seafloor even at short ranges (from near zero to 4-1/2CZ). The OBSANP cruise had three major research goals: a) identification and analysis of DSFA and BDSR arrivals occurring at short (1/2CZ) ranges in the 50 to 400Hz band, b) analysis of deep sea ambient noise in the band 0.03 to 80Hz, and c) analysis of the frequency dependence of BR and SRBR paths. On OBSANP we deployed a 32 element VLA from 12 to 1000m above the seafloor, eight short-period OBSs and four long-period OBSs and carried out a 15day transmission program using a J15-3 acoustic source.

17. Document Analysis a. Descriptors

bottom interacting ocean acoustics
long range ocean acoustic propagation
North Pacific Acoustic Laboratory

b. Identifiers/Open-Ended Terms

c. COSATI Field/Group

18. Availability Statement

Approved for public release; distribution unlimited.

19. Security Class (This Report)

20. Security Class (This Page)

21. No. of Pages
240

22. Price

(See ANSI-Z39.18) *See Instructions on Reverse*

OPTIONAL FORM 272 (4-77)
(Formerly NTIS-35)
Department of Commerce